EPA600/R-19/011
May 2019

Technical Support Document for the All Ages Lead Model (AALM) – Parameters, Equations, and Evaluations

Office of Research and Development

U.S. Environmental Protection Agency

Washington, DC 20460

Disclaimer

This document is an external review draft. This document does not represent and should not be construed to represent any Agency determination or policy. Mention of trade names or commercial products does not constitute endorsement or recommendation for use. This document and the work described in it was conducted under contracts EP-W-17-008, EP-W-09-031, EP-BPA-11-C-018, EP-13-H-000037, EP-08-H-000055, and EP-C-14-001.

CONTENTS

LIST OF TABLES

LIST OF FIGURES

ACRONYMS AND ABBREVIATIONS

AALM	All Ages Lead Model
AALM-LE	ACSL implementation of Leggett model
AALM-OF	ACSL implementation of O'Flaherty model
ABLOOD	amount of Pb in blood
ABONE	amount of Pb in bone
ACSL	Advanced Continuous Simulation Language
AF	absorption fraction
AKIDNEY	amount of Pb in kidney
ALIVER	amount of Pb in liver
ALM	Adult Lead Methodology
ASOFT	amount of Pb in soft tissue
ATSDR	Agency for Toxic Substances and Disease Registry
AMTBLD	Leggett model blood volume
BLDHCT	age-dependent hematocrit
BLL	blood lead level
CB	O'Flaherty model blood Pb concentration
CF	AALM adjustment factor for Pb deposition into RBCs
CIIIAR	AALM fraction of inhaled Pb trasnfered to stomach
CSFII	continuing survey of food intakes
CSV	comma-delimited text file
DF	deposition fractions
EFH	Exposure Factors Handbook
EPA	Environmental Protection Agency
EVF	extravascular fluid
FRX	O'Flaherty model Pb excretory clearance
GI	gastrointestinal
GIT	gastrointestinal tract
GFR	glomerular filtration rate
GM	geometric mean
GSD	geometric standard deviation
HCTA	adult hematocrit
HRTM	Human Respiratory Tract Model
ICR	Information Collection Request
ICRP	International Commission on Radiological Protection
IEUBK	Integrated Exposure Uptake Biokinetics
IVBA	validated in vitro bioaccessibility
LFM	Leggett Fortran Model
LLIC	lower large intestine contents
NCEA	National Center for Environmental Assessment
NHANES	National Health and Nutrition Examination Survey
NHEXAS	National Human Exposure Assessment Survey
NSLAH	National Survey of Lead and Allergens
NTIS	National Technical Information Service
OCSPP	Office of Chemical Safety and Pollution Prevention
OEHHA	Office of Environmental Health Hazard Assessment
OLEM	Office of Land and Emergency Management
OPPT	Office of Pollution Prevention and Toxics
ORD	Office of Research and Development
OSWER	Office of Solid Waste and Emergency Response

Pb	lead
PK	O'Flaherty model plasma-kidney partition coefficient
PL	O'Flaherty model plasma-liver partition coefficient
PP	O'Flaherty model plasma-poorly perfused tissue partition coefficient
PW	O'Flaherty model plasma-well perfused tissue partition coefficient
RBA	relative bioavailability
RBC	red blood cell
RBCONC	red blood cell Pb concentration
RRBC	rate transfer of Pb from red blood cells to diffusible plasma
RT	respiratory tract
SAB	Science Advisory Board
SOF	Other Soft Tissues
SSC	standardized sensitivity coefficient
ST	soft tissue
ULIC	upper large intestine contents
VBLC	blood volume fraction of body weight
VBONE	bone volume
VK	kidney volume
VL	liver volume
VR	ventilation rate
XRF	X-ray fluorescence
WBODY	body weight
WBONE	bone weight

CHAPTER 1. INTRODUCTION AND HISTORY OF ALL AGES LEAD MODEL

1.1. INTRODUCTION

The All Ages Lead Model (AALM) is a tool for quantitatively relating lead (Pb) exposures from environmental media that occur over the life time to Pb levels and concentrations in blood, other body tissues, and excreta. The primary intended use of the model is for computational Pb toxicology and risk assessment. The AALM represents an extension of research and regulatory models previously developed by EPA such as the Integrated Exposure Uptake Biokinetics (IEUBK) Model for Pb in Children which simulates exposure-blood Pb concentration relationships occurring from birth to age 7 years (Hogan et al., 1998; White et al., 1998; Zaragoza and Hogan, 1998). The AALM also incorporates Pb modeling concepts explored in models developed in other research efforts, including those of Leggett (Pounds and Leggett, 1998; Leggett, 1993; Leggett et al., 1993), O'Flaherty (O'Flaherty et al., 1998; O'Flaherty, 1998, 1995, 1993, 1991a, b, c) and others (U.S. EPA, 2006; Maddaloni et al., 2005).

As discussed in Section 1.2, the AALM has been implemented in several platforms over the course of its development. The AALM was first developed and implemented in Visual C+ (AALM.C) by U.S. EPA's Office of Research and Development (ORD). Subsequently, ORD implemented the AALM in Advance Continuous Simulation Language, ACSL®, a.k.a. acslX, (AALM.CLS) to further develop and evaluate the model. In a parallel effort, EPA's Office of Chemical Safety and Pollution Prevention (OCSPP) was developing a biokinetic Fortran model (ICRPv005.FOR) with similar capabilities to the AALM.CLS being developed by ORD. Since 2015, EPA's ORD and OCSPP have coordinated efforts to advance Pb biokinetic modeling and produced the current version of the AALM software implemented in Fortran (AALM.FOR) with a Microsoft Excel user interface.

This document, in Chapter 2, describes in detail the conceptual and computational structure of the current Fortran version of the AALM (AALM.FOR), including an inventory and explanation of all parameters, variables, and expressions used in the model to calculate Pb intakes and Pb tissue and excreta levels and/or concentrations. Chapter 2 has two primary subsections. The initial primary section (exposure model) describes components of the AALM.FOR that relate environmental and diet Pb exposures to rates of Pb intake. This is followed by a section that provides a detailed description of model components that relate Pb intakes to Pb levels and concentrations in body tissues and excreta. Appendices A and B provide a complete listing of equations and parameters used in the model, respectively, that are directly pertinent to calculations of Pb intakes and Pb levels and concentrations in body tissues and excreta. Appendices C and D provide a complete list of parameter names and default values used in the model.

Chapter 3 describes the development and evaluation of AALM.FOR. This chapter describes the process of harmonizing two model versions [AALM.CLS and OCSPP's biokinetic model in Fortran (ICRPv005.FOR)], evaluating the differing biokinetics for the two versions against available human data, and selection of final model parameters for use in AALM.FOR. The side-by-side comparisons of AALM.CLS and AALM.FOR provided a quality assurance opportunity to ensure code was implemented and operating as expected, i.e., the mathematical relationships posited by the model were correctly translated into computer code and its operation was free of numerical errors. Model parameter optimization and sensitivity analyses discussed in Chapter 4 provides the basis for parameters in AALM.CLS that were ultimately used in AALM.FOR. These analyses were not repeated using AALM.FOR since it provides identical predictions to AALM.CLS. Model evaluations in Chapter 3

compare AALM.CLS and AALM.FOR against the same datasets used in Chapter 4 as well as some additional datasets for striking workers and children.

Chapter 4 describes the ORD development and evaluation of AALM.CLS. The AALM.CLS version implemented both the Leggett model (Leggett, 1993) and O'Flaherty model (O'Flaherty, 1995, 1993). The chapter begins with a comparison of the Leggett and O'Flaherty model structures and then provides a comparison of predicted blood and bone concentrations of Pb between the models. Sensitivity analyses are subsequently provided that were utilized to determine the most influential biokinetic parameters in the models. An evaluation and optimization biokinetics models against observations is provided. A biokinetic parameter controlling Pb binding to red blood cells Pb concentrations was adjusted to align the AALM.CLS results more closely with the IEUBK model for children without adversely affecting the good model agreement and predictive capability for infants or adults.

1.1.1. Quality Assurance and Peer Review

The use of quality assurance (QA) and peer review helps ensure that EPA conducts high-quality science that can be used to inform policymakers, industry, and the public. Quality assurance activities performed by EPA ensure that the Agency's environmental data are of sufficient quantity and quality to support the Agency's intended use. Detailed QA Project Plans (QAPPs) have been developed as a requirement for contracted technical support during the development of the AALM. The AALM is classified as providing Influential Scientific Information (ISI), which is defined by the Office of Management and Budget (OMB) as scientific information the agency reasonably can determine will have or does have a clear and substantial impact on important public policies or private sector decisions (OMB, 2004). OMB requires the Agency to subject ISI to be peer review prior to dissemination. To meet this requirement, EPA often engages the Scientific Advisory Board (SAB) as an independent federal advisory committee to conduct peer reviews. The SAB released a call for peer review panel nominations on November 1, 2018 (83FR54923). Panel members were chosen to create a balanced review panel based on factors such as technical expertise, knowledge, experience, and absence of any real or perceived conflicts of interest. Both peer review comments provided by the SAB panel and public comments submitted to the panel during their deliberations about the external review draft will be considered in the development of a final version of the AALM.

1.2. HISTORY OF THE AALM

The AALM was developed as a computational tool for predicting blood Pb concentrations associated with multimedia exposures to Pb that occur from birth through adulthood. The model is a substantial conceptual extension of an earlier IEUBK model developed by EPA to predict blood Pb concentrations in children, the IEUBK model (Hogan et al., 1998; White et al., 1998; Zaragoza and Hogan, 1998; U.S. EPA, 1994a, c, 1989). The IEUBK model has been widely used at Superfund sites to develop remedial objectives.

1.2.1. AALM.C

Development of the AALM implemented in Visual C (AALM.C) by the EPA National Center for Environmental Assessment (NCEA) began in 1999 to extend Pb exposure and biokinetics modeling capability of the IEUBK model to address a wider range of model applications in computational Pb toxicology and risk assessment; these include:

- Simulation of Pb biokinetics associated with multimedia exposures occurring within any age range from birth through adulthood (the IEUBK model is limited to birth to age 84 months);
- Simulation of Pb biokinetics in blood, bone, soft tissues, and excreta (in the IEUBK model, Pb levels in tissues and excreta are intermediary variables used to support the blood Pb simulation, and are not output variables);
- Simulation of Pb biokinetics in response to changes in Pb exposure that occur over periods of days (the IEUBK model exposure averaging time is typically ≥1 year and predicts quasi-steady state blood Pb concentrations); and
- Expansion of the exposure model to include multiple sources of exposure from air, drinking water, food, and indoor dust and soil.

Over the intervening years between initiation of the development of the IEUBK model in 1989 and its release for regulatory (U.S. EPA, 1994b), several modeling approaches were reported for simulating Pb biokinetics of ages extending beyond early childhood. Two models in particular were influential in developing the structure of the AALM. The first was the Leggett model (Pounds and Leggett, 1998; Leggett, 1993), based on a biokinetic model originally developed for the International Commission on Radiological Protection (ICRP) that calculated radiation doses from environmentally important bone-seeking radionuclides, including radioisotopes of Pb (Leggett, 1992a, b, 1985). The original model was used to develop cancer risk coefficients for internal radiation exposures to Pb and other alkaline earth elements that have biokinetics similar to those of calcium (U.S. EPA, 1998; ICRP, 1993). The compartment structure, Pb transfer coefficients, and numerical integration method of the Leggett model were adopted in the early versions of the AALM. The second model was the O'Flaherty model that simulates Pb exposure, uptake, and disposition in humans, from birth through adulthood (O'Flaherty, 2000; O'Flaherty et al., 1998; O'Flaherty, 1998, 1995, 1993, 1991a, b, c). Important features that distinguish the O'Flaherty model from the Leggett model are simulation of growth (the Leggett model simulates growth of blood volume only), bone formation, and resorption (the Leggett model simulates the "effects" of bone growth and resorption on Pb kinetics, but does not simulate bone growth and resorption explicitly). Uptake and release of Pb from trabecular bone and metabolically active cortical bone are functions of bone formation and resorption rates, respectively, and are simulated in the O'Flaherty model; this establishes a relationship between the age-dependence and the Pb kinetics in and out of bone, and allows for explicit simulation of the effects of bone formation (e.g., growth and loss, changes in bone volume, and bone maturation) on Pb uptake and release from bone. In contrast, the Leggett model represents age-dependence of bone Pb kinetics as age-dependent rate coefficients for transfer of Pb into and out of bone. Although the O'Flaherty model had a more physiologically accurate representation of bone growth and resorption, the Leggett model configuration for growth of the blood volume and bone Pb kinetics was used for early versions of the AALM.

In October of 2005, the EPA Science Advisory Board (SAB) reviewed a Visual C implementation of the AALM (AALMv1.05.C) and highlighted the need for expanded documentation and further evaluation of the model (U.S. EPA, 2007). The SAB also identified a number of deficiencies, and suggested potential improvements. EPA expanded the documentation and evaluation of the AALM to include the following: (1) a Guidance Manual for the AALM that describes the conceptual basis and structure of the model (including all equations, parameters, and parameter values) (SRC, 2008); (2) review and evaluation of evidence supporting further extension and/or refinement of the model (SRC, 2009a); and (3) a comparative review of alternative modeling approaches (SRC, 2009b).

1.2.2. AALM.CSL

Research initiated by EPA NCEA in early 2013 expanded the AALM further to address deficiencies identified by the SAB and re-evaluated performance of the model. The AALM was migrated to acslX which removed the need to develop and maintain computer code for the numerical integration solution of the AALM biokinetics model, and made use of existing acslX code to implement the Leggett and O'Flaherty models (Lorenzana et al., 2005). An exposure model was developed in Excel which removed the need to develop *de novo* computer code for the exposure model, and allowed development of exposure scenarios in Excel without the requirement for a license or knowledge of acslX. Development of the acslX version of the AALM is described in Chapter 4. The latest version of the model is AALMv4.2.CSL (July 2015).

AALM.CSL included the user option to link the exposure model to either the Leggett or O'Flaherty biokinetics models. It also introduced several changes to both the Leggett and O'Flaherty biokinetics models including some new parameters and as well as revised parameter values. Some of these data used in the optimization were not available at the time the original models were developed. Optimization against a common set of data resulted in general convergence of AALM-LG.CSL and AALM-OF.CSL predictions for blood, bone, and soft tissue, and agreement with blood Pb predictions for children from the IEUBK model (Chapter 4).

1.2.3. AALM.FOR

In 2014, the EPA Office of Pollution Prevention and Toxics (OPPT) developed an implementation of the Leggett model (Pounds and Leggett, 1998; Leggett, 1993) biokinetics model to support the Agency's *Approach for Estimating Exposures and Incremental Health Effects from Lead Due to Renovation, Repair, and Painting Activities in Public and Commercial Buildings* (U.S. EPA, 2014b). The latest released version of the model, ICRPv005.FOR, has the capability of simulating Pb levels in body tissues (e.g., blood, bone, brain) and excreta at resulting from acute or chronic exposures to inorganic Pb that occur from birth through adulthood.

In developing ICRPv005.FOR, several changes were made to Leggett biokinetics model (see Table 3-1 in Chapter 3); however, up to ICRPv004.FOR, the biokinetics model was unchanged from Leggett (1993). The major changes included (1) age-dependent blood and tissue masses, adjustments to RBC uptake parameters, and adjustment of bone-to-plasma transfer rates. Collectively, updates made to ICRPv004.FOR to create ICRPv005.FOR resulted in lower predicted blood Pb concentrations for a given Pb intake in children, that more closely agreed with predictions from the IEUBK model (see Figure M-4 in, U.S. EPA, 2014a); and lower blood and bone Pb concentrations in adults (see Figure M-6 in, U.S. EPA, 2014a). ICRPv005.FOR was evaluated against data on blood and bone Pb levels in occupationally exposed adults reported in Nie et al. (2005), although some of these data have not been published. The conclusion from these evaluations was that the model tended to predict lower cortical bone Pb concentrations than observed and higher blood Pb concentrations (see Figures M-5 and M-6 in, U.S. EPA, 2014a).

External peer review of the Approach for Estimating Exposures and Incremental Health Effects from Lead Due to Renovation, Repair, and Painting Activities in Public and Commercial Buildings (U.S. EPA, 2014b) resulted in several recommendations (Post-Meeting Peer Review Summary Report, Versar, 2015), including the need for further evaluation of ICRPv005.FOR. Based on these evaluations, ICRPv005.FOR

was revised and parameter values updated to create AALM.FOR (Chapter 3). In the development of AALM.FOR, the model was evaluated with a larger set of observations in children and adults, including some data that had not been used in previous evaluations of ICRPv005.FOR, including all datasets used in the evaluation and development of the AALM.CSL (Chapter 4). AALM.FOR utilizes the same exposure and biokinetic parameter values as the AALM.CSL and, as a result, both models predict the same blood and tissue Pb levels when the same exposure inputs are used in both models. Similar to the AALM.CSL, AALM.FOR utilizes a spreadsheet graphical user interface for setting exposure and biokinetics parameter model inputs and processing output. The major difference between the general architecture of the two models is that the biokinetics model of the AALM.FOR is implemented in Fortran, whereas, the biokinetics model of the AALM.CSL is implemented in acslX.

CHAPTER 2. THEORETICAL FRAMEWORK, PARAMETERS, AND EQUATIONS

2.1. OVERVIEW OF AALM.FOR STRUCTURE

The AALM.FOR consists of two major submodels that simulate Pb exposure and Pb biokinetics, respectively. The exposure model described in Section 2.2 calculates rates of Pb intake (µg Pb/day) from ingestion or inhalation based on inputs for exposure concentrations in air, indoor dust, soil and water; and Pb intakes (µg/day) from food or other sources. The exposure model simulates a hypothetical individual (subject), defined in terms of age, sex and rates of contact with environmental media (e.g., drinking water or indoor dust or soil ingestion rates).

The AALM.FOR biokinetics model described in Section 2.3 simulates kinetics of absorption of Pb into a central (diffusible blood plasma) compartment, transfers of Pb between the central compartment and various tissues, and transfers of Pb to excreta. Absorption of Pb from the respiratory tract is simulated as a first-order process governed by rate coefficients (d^{-1}) for absorption from each of four respiratory tract compartments. Absorption from the gastrointestinal tract is simulated as a first-order process governed by age-dependent absorption fractions and first-order rate coefficients for transfers of Pb within the gastrointestinal tract. Rates of absorption from inhaled and ingested Pb are summed to yield a total rate of transfer (µg Pb/day) to the central plasma compartment; these rates include Pb absorbed from intakes from exposures as well as Pb transferred to the gastrointestinal tract from the respiratory tract (i.e., mucocilliary clearance), and from the liver (i.e., biliary secretion). Biokinetics model output variables are tissue Pb masses and concentrations, and Pb masses in excreta corresponding to the exposure and absorption scenarios constructed in the exposure and absorption models. Tissues represented in the model include red blood cells and blood plasma (including a pool of Pb in plasma that is bound to proteins), brain, cortical and trabecular bone, kidney, liver, and other soft tissues. Distinct excretory pathways represented in the model include feces, urine, sweat, and other routes (e.g., hair and nails, exfoliated skin). Transfers of Pb between compartments are simulated as first-order processes governed by first-order rate coefficients (d^{-1}) that are scaled for age.

The AALM.FOR architecture consists of two components: (1) a macro-enabled Excel workbook (*AALM Fortan.xlsm)* that implements the exposure model and provides user access to all exposure and biokinetics parameters in the AALM.FOR; (2) a Fortran program that implements the biokinetics model. Input parameter values are selected by the user in *AALM Fortran.xlsm*. Macros in the *AALM Fortran.xlsm* file pass the input parameter values to a comma-delimited (CSV) text file (*AALM_LG_INPUTDATA.DAT*) which are imported into the AALM Fortran program. Output variables from the simulation are passed to a CSV file (*AALM_LG_OUTPUTDATA.DAT*) and are read into the *AALM.Fortran.xlsm* file with Excel macros.

AALM.FOR inputs and outputs are controlled and recorded in *AALM Fortan.xlsm* workbook. This workbook has several functions: (1) allows setting of input parameter values for AALM.FOR simulations; (2) macros in this workbook are used to pass data to and from Fortran; (3) allows plotting of AALM.FOR output data; and (4) provides a complete record of input values and results of each AALM.FOR simulation. Worksheets in *AALM Fortran.xlsm* allow the user to set exposure scenarios for Pb in air (*Air*), food (*Food*), indoor dust, (*Dust*), soil (*Soil*), drinking water (*Water*), and/or other ingestion intakes (*other*). Exposures can be discrete (i.e., a series of exposures at selected ages), and/or pulsed in a repeating frequency (e.g., 2 days/week for 3 months/year, for a selected age range). The AALM.FOR

uses inputs from all exposure media when it creates biokinetics simulations. This allows construction of complex multi-pathway exposure scenarios having varying temporal patterns. Worksheets in *AALM Fortran.xlsm* also allow the user to set values for parameters that control Pb absorption and relative bioavailability in individual exposure media (*RBA*), and biokinetics (*Lung*, *Systemic*, *Sex*). All settings are recorded in the *AALM Fortran.xlsm* workbook and can be recalled to re-run the simulation.

2.2. EXPOSURE MODEL

2.2.1. General Structure of the Exposure Model

The exposure model of the AALM.FOR calculates rates of Pb intake from ingestion and inhalation pathways, for a hypothetical individual (subject) based on inputs for exposure to Pb in air, food, indoor dust, soil, water, and from miscellaneous ingestion intakes (designated in the model as *other*). Intakes (µg Pb/day) derived from the exposure model are passed to the biokinetics model and provide the bases for calculating Pb masses in tissues and excreta for each age day simulated. Calculations of Pb intakes are controlled by model parameters that can specify two major categories of exposure parameters: (1) parameters that define the individual (e.g., age, sex); and (2) parameters that define Pb intake rates. A list of all equations used in the AALM.FOR to calculate Pb intakes as they appear in the AALM.FOR code is provided in Appendix A of this chapter, and parameters used in these equations are defined in Appendix C.

An AALM.FOR simulation progresses through a series of exposure time steps representing age-days. A simulation begins at birth and progresses to a terminal age for the simulation (e.g., 32,850 days for a simulation of approximately 90 years). As a simulation progresses, Pb intakes (µg Pb/day) are calculated for each day based on values specified for Pb concentrations in exposure media (e.g., µg Pb/g dust) and rates of media intakes (e.g., µg dust ingested/day); or based on inputted Pb intake rates (µg Pb/day) for ingestion of Pb in food or in *other* media. The exposure time step of one day is independent of the numerical integration time step described in Section 2.3.1 (setting one has no effect on the other). Lead intakes passed to the biokinetics model are in units of µg/day and are adjusted (along with other time-dependent parameters and variables) in biokinetics differential equations to agree with the integration time step used at every point in the simulation. Lead intakes calculated from the exposure model are accessible as output to the *AALM Fortran.xlsm* file.

Lead intakes resulting from exposures to Pb in air, indoor dust, soil, or water are calculated from inputs of Pb concentrations. The general form of the equations for calculating Pb intakes from Pb concentrations is given in Equation 2.2-1:

$$INmedium = \sum_{i=1}^{n}(Pbmedium_i \cdot fmedium_i) \cdot IRmedium \cdot RBAmedium \qquad \text{Eq. (2.2-1)}$$

where *INmedium* is the Pb intake rate (µg Pb/day) for a specific environmental medium (e.g., water), $Pbmedium_i$ is the exposure concentration (e.g., µg Pb/L water) in that medium for a given exposure setting *i*, $fmedium_i$ is the fraction of total intake of the medium that occurs in setting *i*, *IRmedium* is the intake rate of the medium (e.g., L water/day), and *RBAmedium* is the relative bioavailability of Pb in the exposure medium (relative to completely water-soluble Pb). Parameter values in Equation 2.2-1 representing exposure concentrations, media intakes, and fractional media intakes for each setting can be

assigned age-dependent values; whereas, the value assigned to RBA represents the entire age range simulated. The application of RBA as an adjustment to Pb intake rather than an adjustment to the gastrointestinal absorption fraction is a simplification that results in an underprediction of fecal excretion of unabsorbed Pb and negative mass balance (intake>body burden + excreted) when RBA <1.

Lead intakes resulting from exposures to Pb in food and *other* media are calculated from inputs of Pb intake rate (e.g. µg Pb/day) using equations of the following general form (Equation 2.2-2):

$$INmedium = \sum_{i=1}^{n}(Pbintake_i) \cdot RBAmedium \qquad \text{Eq. (2.2-2)}$$

where $Pbintake_i$ is the rate of Pb intake (µg/day) entered for the medium for exposure setting *i*.

Lead exposure concentrations (air, indoor dust, soil, water) or intakes (food, *other*) can be entered into the AALM.FOR as discrete values representing specific ages, or as pulse trains in which the exposure Pb concentration or Pb intake is turned on or off at specific ages. The AALM User Guide should be consulted for specific examples of how this functionality is implemented in the Excel User Interface. Pulse train intakes or exposure concentrations are fixed as constant over periods specified by users. Users can select whether discrete exposure concentrations or intakes are constant (stepwise) or interpolated between ages specified in the discrete time series. Selection of stepwise or interpolation will be applied to all discrete media concentrations or intakes. In the discrete mode, exposure settings for each exposure medium are simulated as a time (age-day) series of exposure concentrations (air, indoor dust, soil, water) or Pb intakes (food, *other*) and weighting factors for exposure concentrations that represent the percentage of exposure contributed by each setting, each day, at each age. The exposure setting functions allow the user to simulate exposure scenarios in which exposure to a Pb in a specific medium may occur from different sources, or at different locations (e.g., home, school, work) within a day. Concentrations of Pb in air, water, indoor dust or soil, at each specified age, are calculated as the weighted average of contributions from all exposure settings represented in the simulation that contribute to that particular exposure medium (Equation 2.2-3).

$$Pbmedium_{weighted} = \sum_{i=1}^{n}(Pbmedium_i \cdot fmedium_i) \qquad \text{Eq. (2.2-3)}$$

where $fmedium_i$ is the fraction contributed by exposure setting *i*. Intakes of Pb in food and *other* at each specified age are calculated as the sum intakes for exposure settings represented in the simulation that contribute to that particular exposure medium (Equation 2.2-4).

$$INmedium_{sum} = \sum_{i=1}^{n}(INmedium_i) \qquad \text{Eq. (2.2-4)}$$

The exposure model allows inputs of up to three different exposure settings for each medium (n = 3 in Equations 2.2-3 and 2.2-4) and setting discrete exposures for up to 50 ages.

The pulse train functions can be used to represent episodic exposures or intakes that occur at fixed frequency (pulse period) and duration (pulse width) schedule (e.g., 2 days per 7 days), over a given age range (pulse start, pulse stop) above a user-inputted baseline Pb concentration or intake. The exposure model allows the user to specify up to two overlapping pulse trains, which can be used to simulate more complex intermittent exposure patterns (e.g., 2 days per 7 days; 3 months per 12 months). A combination of discrete and pulsed exposures can be simulated by assigning a value of <1 to the parameter f_{pulse}. This parameter apportions the relative contributions of the discrete and pulsed Pb intakes according to the fraction of total assigned to the pulse (Equation 2.2-5)

$$INmedium_{Total} = INmedium_{discrete} \cdot (1 - f_{pulse}) + INmedium_{pulse} \cdot f_{pulse} \qquad \text{Eq. (2.2-5)}$$

Equations used in the AALM.FOR to calculate Pb inhalation and ingestion intakes concentrations in tissues are presented in Tables 2-1 and 2-2 and in Appendix A of this chapter and parameters are defined in Appendix B. The main differences between these two presentations of the equations are that: (1) equations in Appendix A use the exact nomenclature for parameters as they appear in the AALM.FOR code (Appendix B), whereas, nomenclature in Table 2-1 has been modified for simplicity; and (2) the equations in Appendix A are presented in their integrated forms as used in the AALM.FOR numerical integration routine, whereas, the differential equations are shown in Table 2-1. For readability, tables and appendices are provide at the end of this chapter.

2.2.2. Parameters That Define a Hypothetical Individual

Age: Each step in the simulation represents a day of age, beginning at birth (age = 0).

Sex: The sex specification links the subject to an appropriate sex-specific growth algorithm (O'Flaherty, 1995, 1993) described in Section 3.5.2.

Fetal Exposure: The AALM.FOR simulation begins at birth with the neonatal tissue Pb masses assigned values based on the user-designated maternal blood Pb, described in Section 2.3.11.

2.2.3. Exposure Media Intakes and Lead Concentrations

It should be noted that for ingested Pb, the adjustment for RBA is applied to Pb intake rather than an adjustment to the gastrointestinal absorption fraction (Section 2.3.3.2) is a simplification that results in an underprediction of fecal excretion of unabsorbed Pb and negative mass balance (intake > body burden + excreted) when RBA < 1.

2.2.3.1. Air Pb Exposure

Air Pb intakes (µg Pb/day) are calculated as the product of air Pb concentration (µg Pb/m^3) and ventilation rates (m^3 air/day) that are specified for a given age range (Equation 2.2-6).

$$INair = Pbair \cdot VR \qquad \text{Eq. (2.2-6)}$$

where *VR* is the ventilation rate (m^3/day). The values assigned to ventilation rates represent the average daily values for specific age ranges. These values can be modified to represent specific activity levels (e.g., ventilation during periods of rest, moderate activity, strenuous activity, etc.). Values for VR are interpolated between inputted ages. Air Pb intakes (µg Pb/day) are passed to the biokinetics model where they represent values for rates of deposition of Pb in the respiratory tract (see *BRETH* in Section 2.3.3.1).

The discrete mode allows the user to specify exposures to multiple (i.e., $n = 3$) sources; for example, indoor air, outdoor air, or air at different locations (e.g., home, school, work). In the discrete mode, the *PbAir* term in Equation 2.2-6 is the weighted average from all exposure settings (Equation 2.2-7):

$$Pbair_{discrete\ weighted} = \sum_{i=1}^{n}(Pbair_i \cdot fair_i) \quad \text{Eq. (2.2-7)}$$

where $Pbair_i$ is the air concentration for exposure setting *i* at a given age and $fair_i$ is the fraction of total daily exposure assigned to setting *i*.

The pulse mode allows the user to represent episodic exposures to air Pb that occur at fixed frequency (pulse period) and duration (pulse width) schedule. In the pulse mode, air Pb concentration is specified with values for a baseline concentration (µg Pb/m^3), a pulsed concentration, the start and ending ages of the pulse train (day), the width of each pulse (days) and the period of each pulse (the number of days between pulses). During each pulse, air Pb concentration is calculated as the sum of the baseline and pulsed concentrations (Equation 2.2-8):

$$Pbair_{pulse\ sum} = Pbair_{baseline} + Pbair_{pulse} \quad \text{Eq. (2.2-8)}$$

Air Pb intakes calculated for discrete and pulse train inputs are summed to calculate total Pb intake associated with exposures to Pb in air (Equation 2.2-9):

$$INair_{Total} = INair_{discrete} \cdot (1 - F_{pulse}) + INair_{pulse} \cdot F_{pulse} \quad \text{Eq. (2.2-9)}$$

2.2.3.2. Indoor Dust Pb Exposure

Ingestion intakes resulting from contact with Pb in indoor dusts (e.g., adherence on hand-to-mouth) from all sources are simulated by specifying values for dust exposure parameters. Dust Pb intakes (µg Pb/day) are calculated as the product of Pb concentration (µg Pb/g) and ingestion rate (g dust/day, Equation 2.2-10):

$$INdust = Pbdust \cdot IRdust \cdot RBAdust \quad \text{Eq. (2.2-10)}$$

where *INdust* is the intake of dust Pb (µg Pb/day), *Pbdust* is the Pb concentration in dust (µg Pb/g), *IRdust* is the intake rate of dust from all sources (g dust/day) and *RBAdust* is the relative bioavailability of Pb in dust, relative to water-soluble Pb. Values for *IRdust* are interpolated between inputted ages. The model accepts a single inputted value for RBA which represents dust from all sources, in all exposure settings. Dust Pb intakes (µg Pb/day) are summed with other ingestion intakes (i.e., soil, food, water, *other*) and passed to the biokinetics model as rates of intake Pb to the stomach compartment of the gastrointestinal tract (see Section 2.3.3.2).

The discrete mode allows the user to specify exposures to multiple (i.e., $n = 3$) sources; for example, indoor dusts at different locations (e.g., home, school, playground). In the discreet mode, the *Pbdust* term in Equation 2.2-10 is the weighted concentration for all exposure settings (Equation 2.2-11):

$$Pbdust_{discrete\ weighted} = \sum_{i=1}^{n}(Pbdust_i \cdot fdust_i) \quad \text{Eq. (2.2-11)}$$

where $Pbdust_i$ is the soil or dust Pb concentration for exposure setting *i* at a given age and $fdust_i$ is the fraction of total daily exposure assigned to setting *i*.

The pulse mode allows the user to simulate episodic exposures to dust Pb that occur at fixed frequency (pulse period) and duration (pulse width) schedule. In the pulse mode, dust Pb concentration is specified with values for a baseline concentration (µg Pb/g), a pulsed concentration, the start and ending ages of the pulse train (day), the width of each pulse (days) and the period of each pulse (the number of days between pulses). During each pulse, dust Pb concentration is calculated as the sum of the baseline and pulsed concentrations (Equation 2.2-12):

$$Pbdust_{pulse\ sum} = Pbdust_{baseline} + Pbdust_{pulse} \quad \text{Eq. (2.2-12)}$$

Dust Pb intakes calculated for discrete and pulse train inputs are summed to calculate total Pb intake associated with exposures to Pb in dust (Equation 2.2-13):

$$INdust_{Total} = INdust_{discrete} \cdot (1 - f_{pulse}) + INdust_{pulse} \cdot f_{pulse} \quad \text{Eq. (2.2-13)}$$

2.2.3.3. Soil Pb Exposure

Ingestion intakes resulting from contact with Pb in soil (e.g., adherence on hand-to-mouth) from all sources are simulated by specifying values for soil exposure parameters. Exposure to soil could include hand-to-mouth contact with soil transported from surficial soil to other surfaces (e.g., indoor), or direct hand-to-mouth contact with surficial soil. Ingestion of bulk soil (e.g. pica) can also be simulated as a pathway separate from dust (i.e., *other*). The main consideration for including exposures to soil in the soil pathway rather than simulating the soil exposures in the *other* pathway is the determination of

whether or not parameter values for soil ingestion rate (*IRsoil*, Equation 2.2-14) apply to the soil exposure.

Soil Pb intakes (µg Pb/day) are calculated as the product of Pb concentration (µg Pb/g) and ingestion rate (g dust/day, Equation 2.2-14):

$$INsoil = Pbsoil \cdot IRsoil \cdot RBAsoil \quad \text{Eq. (2.2-14)}$$

where *INsoil* is the intake of soil Pb (µg Pb/day), *Pbsoil* is the Pb concentration in soil (µg Pb/g), *IRsoil* is the intake rate of soil from all sources (g soil/day) and *RBAsoil* is the relative bioavailability of Pb in soil, relative to water-soluble Pb. Values for *IRsoil* are interpolated between inputted ages. The model accepts a single inputted value for RBA which represents soil from all sources, in all exposure settings. Soil Pb intakes (µg Pb/day) are summed with other ingestion intakes (i.e., dust, food, water, *other*) and passed to the biokinetics model as rates of intake Pb to the stomach compartment of the gastrointestinal tract (see Section 2.3.3.2).

The discrete mode allows the user to specify exposures to multiple (i.e., $n = 3$) sources; for example, soils at different locations (e.g., home, school, playground). In the discreet mode, the *Pbsoil* term in Equation 2.2-14 is the weighted concentration for all exposure settings (Equation 2.2-15):

$$Pbsoil_{discrete\ weighted} = \sum_{i=1}^{n}(Pbsoil_i \cdot fsoil_i) \quad \text{Eq. (2.2-15)}$$

where $Pbsoil_i$ is the soil or soil Pb concentration for exposure setting *i* at a given age and $fsoil_i$ is the fraction of total daily exposure assigned to setting *i*.

The pulse mode allows the user to simulate episodic exposures to soil Pb that occur at fixed frequency (pulse period) and duration (pulse width) schedule. In the pulse mode, soil Pb concentration is specified with values for a baseline concentration (µg Pb/g), a pulsed concentration, the start and ending ages of the pulse train (day), the width of each pulse (days) and the period of each pulse (the number of days between pulses). During each pulse, soil Pb concentration is calculated as the sum of the baseline and pulsed concentrations (Equation 2.2-16):

$$Pbsoil_{pulse\ sum} = Pbsoil_{baseline} + Pbsoil_{pulse} \quad \text{Eq. (2.2-16)}$$

Soil Pb intakes calculated for discrete and pulse train inputs are summed to calculate total Pb intake associated with exposures to Pb in soil (Equation 2.2-17):

$$INsoil_{Total} = INsoil_{discrete} \cdot (1 - f_{pulse}) + INsoil_{pulse} \cdot f_{pulse} \quad \text{Eq. (2.2-17)}$$

2.2.3.4. Water Pb Exposure

Lead intakes from ingestion of water (µg Pb/day) are calculated as the product of Pb concentration (µg Pb/L) and ingestion rate (L/day, Equation 2.2-18):

$$INwater = Pbwater \cdot IRwater \cdot RBAwater \quad \text{Eq. (2.2-18)}$$

where *INwater* is the intake of Pb in water (µg Pb/day), *Pbwater* is the Pb concentration in water (µg Pb/L), *IRwater* is the rate ingestion of water (L/day) and *RBAwater* is the relative bioavailability of Pb in water and dust, relative to water-soluble Pb. Values for *IRwater* are interpolated between inputted ages. The model accepts a single inputted value for RBA which represents both water, in all exposure settings. Lead dissolved in water would, by definition, have RBA = 1; however, the RBA parameter could be used in scenarios in which ingestion exposures include Pb-bearing particulates suspended in water for which the RBA may be <1. Water Pb intakes (µg Pb/day) are summed with other ingestion intakes (i.e., food, dust, soil, *other*) and passed to the biokinetics model as rates of intake Pb to the stomach compartment of the gastrointestinal tract (see Section 2.3.3.2).

The discrete mode allows the user to specify exposures to multiple (i.e., $n = 3$) sources of water Pb; for example, first-draw, flushed, bottled; or water consumed different locations (e.g., home, school, work). In the discreet mode, the *Pbwater* term in Equation 2.2-18 is the weighted concentration for all exposure settings (Equation 2.2-19):

$$Pbwater_{weighted} = \sum_{i=1}^{n}(Pbwater_i \cdot fwater_i) \quad \text{Eq. (2.2-19)}$$

where $Pbwater_i$ is the water Pb concentration for exposure setting *i* at a given age and $fwater_i$ is the fraction of total daily exposure assigned to setting *i*.

The pulse mode allows the user to simulate episodic exposure to water Pb that occur at fixed frequency (pulse period) and duration (pulse width) schedule. In the pulse mode, water Pb concentration is specified with values for a baseline concentration (µg Pb/L), a pulsed concentration, the start and ending ages of the pulse train (day), the width of each pulse (days) and the period of each pulse (the number of days between pulses). During each pulse, dust Pb concentration is calculated as the sum of the baseline and pulsed concentrations (Equation 2.2-20):

$$Pbwater_{pulse\ sum} = Pbwater_{baseline} + Pbwater_{pulse} \quad \text{Eq. (2.2-20)}$$

Intakes assigned to discrete and pulse train inputs are summed to calculate total Pb intake associated with exposures to Pb in water (Equation 2.2-21):

$$INwater_{Total} = INwater_{discrete} \cdot (1 - f_{pulse}) + INwater_{pulse} \cdot f_{pulse} \quad \text{Eq. (2.2-21)}$$

2.2.3.5. Food Pb Exposure

Food Pb exposures are inputted as Pb intakes from ingestion of food (µg Pb/day) and are adjusted by RBA (Equation 2.2-22):

$$INfood = INfood_{input} \cdot RBAfood \quad \text{Eq. (2.2-22)}$$

Inputted food Pb intakes represent the total Pb intakes from all foods consumed and included in the simulation. The model does not calculate food Pb intakes from inputted data on Pb concentrations in foods and food consumption rates. Lead intakes from food are summed with other ingestion intakes (i.e., water, dust, soil, *other*) and passed to the biokinetics model as rates of Pb transferred to the stomach compartment of the gastrointestinal tract (see Section 2.3.3.2).

The discrete mode allows the user to specify exposures to multiple (i.e., $n = 3$) sources of food Pb (e.g. market basket, home grown produce, local fish or game). In the discrete mode, the $Pbfood_{input}$ term in Equation 2.2-22 is the sum of Pb intakes from all exposure settings (Equation 2.2-23):

$$INfood_{discete\ sum} = \sum_{i=1}^{n}(INfood_i) \cdot RBAfood \quad \text{Eq. (2.2-23)}$$

where $INfood_i$ is the food Pb intake for exposure setting i at a given age, and $RBAfood$ is the relative bioavailability of Pb in food, relative to water-soluble Pb. The model accepts a single inputted value for RBA which represents food in all exposure settings.

The pulse mode allows the user to simulate episodic food Pb intakes that occur at fixed frequency (pulse period) and duration (pulse width) schedule. In the pulse mode, food intake is specified with values for a baseline Pb intake (µg/day), a pulsed Pb intake (µg/day), the start and ending ages of the pulse train (day), the width of each pulse (days) and the period of each pulse (the number of days between pulses). During each pulse, Pb intake is calculated as the sum of the baseline and pulsed intakes (Equation 2.2-24):

$$INfood_{pulse\ sum} = INfood_{baseline} + INfood_{pulse} \quad \text{Eq. (2.2-24)}$$

Intakes assigned to discrete and pulse train inputs are summed to calculate total Pb intake from ingestion of food (Equation 2.2-25):

$$INfood_{Total} = INfood_{discrete} \cdot (1 - f_{pulse}) + INfood_{pulse} \cdot f_{pulse} \quad \text{Eq. (2.2-25)}$$

2.2.3.6. Other Exposure Media

The *other* ingestion category is a placeholder for miscellaneous exposures that are not accounted for by other media (e.g., paint, pica). The *other* ingestion category may also be used to establish a baseline blood Pb concentration such as based on National Health and Nutrition Examination Survey (NHANES) above which the contribution from soil or other media may be determined. *Other* Pb exposures are inputted as Pb intakes (µg Pb/day) and are adjusted by RBA (Equation 2.2-26):

$$INother = INother_{input} \cdot RBAother \quad \text{Eq. (2.2-26)}$$

Other Pb intakes are summed with other ingestion intakes (i.e., water, dust, soil, water) and passed to the biokinetics model as rates of Pb transferred to the stomach compartment of the gastrointestinal tract (see Section 2.3.3.2).

The discrete mode allows the user to specify exposures to multiple (i.e., $n = 3$) sources of other Pb (e.g. home, school, work). In the discrete mode, the $INother_{input}$ term in Equation 2.2-26 is the sum of Pb intakes from all exposure settings (Equation 2.2-27):

$$INother_{sum} = \sum_{i=1}^{n}(INother_i) \cdot RBAother \quad \text{Eq. (2.2-27)}$$

where $INother_i$ is the Pb intake for exposure setting i at a given age, Fi is the fraction of total daily *other* Pb intake assigned to setting i, and *RBAother* is the relative bioavailability of Pb in the *other* medium, relative to water-soluble Pb. The model accepts a single inputted value for *RBAother* which represents Pb in all *other* exposure settings.

The pulse mode allows the user to simulate episodic *other* Pb intakes that occur at fixed frequency (pulse period) and duration (pulse width) schedule. In the pulse mode, *othe*r intake is specified with values for a baseline Pb intake (µg/day), a pulsed Pb intake (µg/day), the start and ending ages of the pulse train (day), the width of each pulse (days) and the period of each pulse (the number of days between pulses). During each pulse, Pb intake is calculated as the sum of the baseline and pulsed intakes (Equation 2.2-28):

$$INother_{pulse\ sum} = INother_{baseline} + INother_{pulse} \quad \text{Eq. (2.2-28)}$$

Intakes assigned to discrete and pulse train inputs are summed to calculate total Pb intake (Equation 2.2-29):

$$INother_{Total} = INother_{discrete} \cdot (1 - f_{pulse}) + INother_{pulse} \cdot f_{pulse} \quad \text{Eq. (2.2-29)}$$

2.3. BIOKINETICS

2.3.1. Computational Structure of the Aalm.For Biokinetics Model

The AALM.FOR computes Pb masses (µg) in tissues and excreta for each age day simulated (e.g., assuming 365 days/year, a simulation extending to age 90 years would include 32,850 days). These masses are used to calculate secondary variables such as blood Pb concentration. Lead masses calculated for each age day are based on Pb intake rates (µg Pb/day) calculated in the exposure model and passed to the biokinetics model. Lead intakes contribute to rates of entry of Pb into the central plasma compartment (i.e., Pb absorption, µg Pb/day), along with transfers to the central compartment resulting from Pb exchanges with other tissues. Lead masses in each biokinetics compartment are computed by numerical integration applied to a series of differential equations that represent the rate of change in Pb mass in each compartment. The general form of the differential equations used in the biokinetics model is as follows (Equation 2.3-1):

$$\frac{dY_j}{dt} = -R_j \cdot Y_j + P_j \qquad \text{Eq. (2.3-1)}$$

where dY_j/dt is the change in Pb mass (µg) in compartment j over time t, R_j is the rate coefficient for transfer of Pb out of compartment j over time t (t^{-1}), and P_j is the rate of transfer of Pb into compartment j (µg Pb/t). Starting values for compartment Pb masses are inputs to the model, allowing the user to start simulations with pre-existing Pb masses (*starting values for compartment Pb masses are set to zero in the current version of AALM.FOR and can be modified in the Fortran input file, POUNDS_GUI.DAT*). The fundamental unit of time in the biokinetics model is day (i.e., rates used in differential equations are in units of µg Pb/day or d^{-1}). Equation 2.3-2 is solved for each state variable (e.g., compartment) using the following numerical approximation for small time steps, Δt (Leggett, 1993; Leggett et al., 1993) as follows (Equations 2.3-2 to 2.3-4):

$$Y_{t+\Delta t} = \left(Y_t - \frac{P_t}{R_t}\right) \cdot e^{-R_t \Delta t} + \frac{P_t}{R_t} \qquad \text{Eq. (2.3-2)}$$

where $Y_{t+\Delta t}$ is the Pb mass at the end of each integration time step. The time-integrated Pb mass in each compartment (*YINT*) at each time step is computed as follows (Equation 2.3-3):

$$YINT_{t+\Delta t} = \left(Y_t - \frac{P_t}{R_t}\right) \cdot \frac{1-e^{-R_t \Delta t}}{R_t} + \frac{P_t \circ \Delta t}{R_t} \qquad \text{Eq. (2.3-3)}$$

The rate of inflow of Pb into each compartment is a function of the time-integrated Pb masses in contributing compartments (Equation 2.3-4):

$$P_j = \frac{R_{i\to j} \cdot YINT_i}{\Delta t} \quad \text{Eq. (2.3-4)}$$

where, P_j is the inflow rate of Pb into compartment j, $R_{i\to j}$ is the rate coefficient for transfer of Pb from compartment i to j, and $YINT_i$ is the time-integrated Pb mass in compartment i. The above numerical integration approach can be expected to achieve numerical integration errors that do not exceed a 0.5% if the integration step size (10^{-N}) is selected such that (Equation 2.3-5):

$$10^{-(N+1)} < \frac{ln(2)}{R_{max}} \quad \text{Eq. (2.3-5)}$$

where R_{max} is largest rate coefficient in the model, and N is an integer value (Leggett et al., 1993). In the AALM.FOR, the largest rate coefficient is 1000 d^{-1}, for transfer of Pb from the plasma to the extravascular compartment and the corresponding integration step size (10^{-N}) that satisfies Equation 2.3-5 is 0.001 day (i.e., N = 3). At a fixed time step, integration error will be more pronounced in the early parts of a simulation, when Pb masses are changing in compartments with fast turnover rates (high R values), and will decrease as the simulation progresses and steady states are achieved in these compartments. In the AALM.FOR, the integration time step can be varied during the simulation by assigning values to the step length at different points in the simulation. This allows for relatively short time steps in the early phases of the simulation to minimize error in integration of fast compartments, and use of longer steps (requiring less computation time) in later phases of the simulation. An integration scheme recommended by Leggett et al. (1993) to minimize error in the early phases of the simulation and achieve computational speed in the later phases is as follows:

Step Length (day)	Integration Cycles	Simulation Day
0.001	1–1000	0–1
0.01	1000–1900	1–10
0.1	1900–2800	10–100
1	>2800	>100

In this scheme, the first 1000 integration cycles (an integration cycle is completed when all state variables have been integrated over a given time step) are computed using a step length of 0.001 day, at the conclusion of which the first age day of the simulation is concluded. The next 900 cycles are computed using a step length of 0.01 days, concluding at age day 10. The next 900 cycles are computed using a step length of 0.1 day, and the remaining cycles are computed with a step length of 1 day. While step length is a user-defined model input, the recommended step length for AALM.FOR is a constant step length of 0.1 to 1 days, which should result in acceptable integration error for anticipated applications of the model, including intermittent exposures. Adequacy of the step length can be determined by evaluating the sensitivity of the output to changes in step length. When using the pulse train function for a brief exposure (e.g., 1-2 days), it is recommended that a step length of ≤0.01 day be used. Varying the step within a simulation (i.e., using different lengths at different times) is not recommended.

2.3.2. Compartment Structure of the AALM.FOR Biokinetics Model

The structure of the AALM.FOR biokinetics model is based on the Leggett (1993) model. The model includes a central exchange compartment, 15 peripheral body compartments, and 3 elimination pools (Figure 2-1). The central exchange compartment is the *diffusible* Pb in plasma distinguished from a *bound* pool in plasma representing Pb bound to plasma proteins. Lead is absorbed from the gastrointestinal tract, respiratory tract into the diffusible plasma compartment. Lead in diffusible plasma exchanges with Pb in bone, brain, kidney, liver, red blood cells (RBC), and other soft tissues. Absorbed Pb is excreted in urine, sweat, and in a combined pathway representing hair, nails, and exfoliated skin. Unabsorbed ingested Pb is excreted in feces along with a fraction of absorbed Pb transferred to the gastrointestinal tract from diffusible plasma and liver (i.e., bile pathway). The application of RBA as an adjustment to Pb intake rather than an adjustment to the gastrointestinal absorption fraction is a simplification that results in an underprediction of fecal excretion of unabsorbed Pb and negative mass balance (intake>body burden + excreted) when RBA <1.

Transfers of Pb between compartments are assumed to follow first-order kinetics governed by rate coefficients (d^{-1}), where each rate coefficient represents a fraction of Pb mass (µg) in the compartment that is transferred per day. Lead masses (µg) in compartments are computed by numerical integration of linear differential equations representing the rates of change of Pb mass in each compartment (see section 2.3.1). The computed Pb masses in tissues and tissue masses (g) and/or volumes (dL) are used to calculate Pb concentrations in tissues. A conceptual representation of equations used in the AALM.FOR to calculate Pb masses and concentrations in tissues are presented in Table 2-2. A more comprehensive and accurate presentation of the equations as they appear in the AALM.FOR code is presented in Appendix A of this chapter and parameters are defined in Appendix B. The main differences between these two presentations of the equations are that: (1) equations in Appendix A use the exact nomenclature for parameters as they appear in the AALM.FOR code (Appendix B), whereas, nomenclature in Table 2-2 has been modified for simplicity; and (2) the equations in Appendix A are presented in their integrated forms as used in the AALM.FOR numerical integration routine, whereas, the differential equations are shown in Table 2-2. General concepts that underlie equations used in the AALM.FOR for calculating Pb masses and concentrations are presented in the sections that follow. For readability, tables and appendixes are provide at the end of this chapter.

2.3.2.1. Rate Equations for Pb Transfers

Transfers of Pb between compartments are assumed to follow first-order kinetics governed by rate coefficients (d^{-1}) and described by first-order rate equations having the following general form (Equations 2.3-6 to 2.3-8):

$$\frac{dY_j}{dt} = INFLOW_j - OUTFLOW_j \qquad \text{Eq. (2.3-6)}$$

$$INFLOW_j = \sum_{i=1}^{n}(R_{i\to j} \cdot Y_i) \qquad \text{Eq. (2.3-7)}$$

$$OUTFLOW_j = \sum_{i=1}^{n}(-R_{j\to i} \cdot Y_j) \qquad \text{Eq. (2.3-8)}$$

where dY_j/dt is the change in Pb mass in compartment j over time t, $INFLOW_l$ is the sum of all transfers into compartment j (Equation 2.3-7), $OUTFLOW_j$ is the sum of all transfers out of compartment j (Equation 2.3-8), $R_{j\rightarrow i}$ is the rate coefficient for transfer of Pb out of compartment j to compartment i over time t (t^{-1}), Y_j is the Pb mass in compartment j (µg), $R_{i\rightarrow j}$ is the rate coefficient for transfer of Pb from compartment i to compartment j, and Y_i is the Pb mass in compartment i. The current version of the AALM.FOR uses values for rate coefficients that are based on Leggett (1993) and updated based on more recent evaluations of the model (Chapter 3); these values are presented in Table 2-3 located at the end of this chapter.

The AALM.FOR uses two approaches to assigning values to INFLOW and OUTFLOW rate coefficients: (1) rate coefficients representing transfers of Pb out of individual compartments are assigned values for specific, user-designated, age ranges in the simulation and are designated in rate equations with the prefix *R* (e.g., *RLV1* for the rate coefficient for transfer of Pb from liver compartment 1 to diffusible plasma); (2) rate coefficients representing transfers of Pb from the diffusible plasma compartment to tissues are variables computed from expressions relating deposition fractions to each tissue and a rate coefficient for transfer of Pb from the diffusible plasma compartment to all receiving compartments. Deposition fractions are designated with the prefix *T* (e.g., *TLVR1* for the deposition fraction from diffusible plasma to liver compartment 1). Deposition fractions represent the instantaneous fractional outflow of Pb from diffusible plasma and are used in the AALM.FOR to establish corresponding rate coefficients.

2.3.2.2. Deposition Fractions

As a means to ensure mass balance of transfers between tissues and the diffusible plasma compartment, transfer rates from the central compartment are expressed as fractions of the combined rate of transfer from the central compartment to all compartments (Equation 2.3-9):

$$R_{PLAS\rightarrow j} = T_{PLAS\rightarrow j} \cdot RPLAS \qquad \text{Eq. (2.3-9)}$$

where $R_{PLAS\rightarrow j}$ is the rate coefficient for transfer of Pb from diffusible plasma to compartment j (d^{-1}), $T_{PLAS\rightarrow j}$ is the deposition fraction for transfer of Pb from diffusible plasma to compartment j, and *RPLAS* is the rate coefficient for transfer of Pb from diffusible plasma to all receiving compartments (2000 d^{-1}). The sum of all deposition fractions from diffusible plasma must equal one to ensure mass balance. The product of the sum of all age-adjusted deposition fractions and the Pb mass in the diffusible plasma compartment is the rate of Pb transfer out of the diffusible plasma to all receiving compartments, and is designated in the AALM.FOR as *BTEMP* (Equations 2.3-10 and 2.3-11):

$$RPLS = \sum_j^n T_{PLAS\rightarrow j} \cdot RPLAS \qquad \text{Eq. (2.3-10)}$$

$$BTEMP = RPLS \cdot YPLS \qquad \text{Eq. (2.3-11)}$$

where *RPLS* is the age-adjusted rate coefficient for or transfer of Pb from the diffusible plasma to all receiving compartments (d^{-1}), and *YPLS* is the mass of Pb (µg) in the diffusible plasma compartment.

2.3.2.3. Scaling of Rate Coefficients and Deposition Fractions

Values for deposition fractions and rate coefficients are age-dependent and are assigned values for specific ages. Values between ages are interpolated. The input values for deposition fractions from diffusible plasma (designated with the prefix TO; e.g., TOBONE) are scaled in the biokinetics model to account for two factors: (1) growth of bone surface area and resulting age-dependence of deposition of Pb to bone surface, which changes the deposition fractions to other tissues; and (2) non-linear uptake of Pb from diffusible plasma to RBCs, which changes the RBC deposition fraction as the RBC Pb concentration increases. Scaled deposition fractions designated with the prefix *T* (e.g., TBONE). The scaling adjustment for bone surface takes the form (Equations 2.3-12 and 2.3-13):

$$AGESCL = \frac{1-TEVF-TBONE}{1-TEVF-TBONEL} \quad \text{Eq. (2.3-12)}$$

$$T_{PLAS\rightarrow j} = AGESCL \cdot TO_{PLAS\rightarrow j} \quad \text{Eq. (2.3-13)}$$

where *TEVF* is the deposition fraction to the extravascular fluid (see description of central compartment and bone Pb kinetics), *TBONE* is the deposition fraction to bone surface, *TBONEL* is the limiting adult value for the bone deposition fraction, and $TO_{PLAS\rightarrow j}$ is the input value for the deposition fraction from diffusible plasma to compartment *j*, before adjustment for bone surface area.

Uptake of Pb into RBCs is simulated as a capacity-limited process, in which the deposition fraction to RBCs (*TRBC*) decreases with increasing RBC Pb concentration above a limiting threshold (see description of RBC compartment in Section 2.3.4.3). The decrease in RBC deposition fraction as the RBC concentration approaches the limiting value results in greater Pb available for deposition to other tissues. This change is accounted for in the model by adjusting the deposition fractions to other tissues by the factor *CF* (Equation 2.3-14):

$$CF = \frac{1-TOORBC}{1-TRBC} \quad \text{Eq. (2.3-14)}$$

where TRBC is the deposition fraction to RBCs below the limiting RBC Pb concentration, and TOORBC is the deposition fraction to RBCs above the limiting RBC Pb concentration. The adjustment factor, CF, increases as the RBC Pb concentration approaches saturation, and deposition fractions to other tissues (TOPLAS→j) are proportionately increased.

Equations 2.3-9 to 2.3-14 yield rate equations for the change in Pb mass with time (i.e., integration time step) of the following typical form, for example for liver compartment 1 (Equation 2.3-15):

$$\frac{dy_{LVR1}}{dt} = TLVR1 \cdot CF \cdot BTEMP - RLVR1 \cdot YLVR1 \quad \text{Eq. (2.3-15)}$$

2.3.2.4. Growth of Blood and Tissues for Calculation of Pb Concentrations

The AALM.FOR biokinetics equations are used to compute Pb masses in each tissue compartment. Concentrations of Pb in selected tissues are calculated as the quotient of Pb mass and tissue volumes (e.g., dL blood) or masses (e.g., g kidney, cortical bone, trabecular bone, skeleton). Tissue volumes and masses are calculated based on growth equations and parameters from O'Flaherty's studies (O'Flaherty, 1995, 1993) (see Table 2-2 Equations N1–N17). Tissue volumes and masses are functions of body weight (Equation 2.3-16):

$$WBODY = WBIRTH + \frac{WCHILD \cdot AGEYEAR}{HALF + AGEYEAR} + \frac{WADULT}{1 + KAPPA \cdot e^{-LAMBDA \cdot WADULT \cdot AGEYEAR}} \quad \text{Eq. (2.3-16)}$$

In the AALM.FOR code, the variable *AGEYEAR* in Equation 2.3-16 is replaced with the variable *HOWOLD*. Equation 2.3-16 calculates body weight as the sum of three growth phases: (1) pre-natal which achieves birth weight; (2) rapid (hyperbolic) post-natal growth that occurs before age 10 years; and (3) logistic growth beginning at puberty and continuing into early adulthood. *WBODY* is the body weight at any given age (*AGEYEAR*), *WBIRTH* is the body weight at birth, *WCHILD* is the maximum body weight achieved during early hyperbolic growth phase, *HALF* is the age at which body weight is one half of *WCHILD*, *WADULT* is the maximum adult body weight, and *KAPPA* and *LAMBDA* are empirically derived logistic parameters. The body weight parameters enable simulation of different growth patterns, including distinct patterns for males and females. The current default growth simulations are show in in Figure 2-2.

Volume growth of blood (*AMTBLD*) is a linear function of body weight (Equation 2.3-17):

$$AMTBLD = VBLC \cdot WBODY \cdot 10 \quad \text{Eq. (2.3-17)}$$

where *VBLC* is the blood volume expressed as a fraction of body weight (*WBODY*). Plasma and RBC volumes are functions of blood volume and age-dependent hematocrit (*BLDHCT*), which increases during the first 4 days post-natal from approximately 0.52 to 0.66 (default value), and then decreases to 0.46 (default value) by age 1 year (Equations 2.3-18 and 2.3-19):

$$BLDHCT_{AGEYEAR \le 0.01} = 0.52 + AGEYEAR \cdot 14 \quad \text{Eq. (2.3-18)}$$

$$BLDHCT_{AGEYEAR > 0.01} = HCTA \cdot (1 + (0.66 - HCTA) \cdot e^{-(AGEYEAR - 0.01) \cdot 13.9}) \quad \text{Eq. (2.3-19)}$$

where HCTA is the adult hematocrit (default = 0.46).

Volume growth of kidney (*VK*) and liver (*VL*) are power functions of body weight (Equations 2.3-20 and 2.3-21).

$$VK = 1000 \cdot VKC \cdot (WBIRTH + WADULT + WCHILD) \cdot \left(\frac{WBODY}{WBIRTH + WADULT + WCHILD} \right)^{0.84}$$

Eq. (2.3-20)

$$VL = 1000 \cdot VLC \cdot (WBIRTH + WADULT + WCHILD) \cdot \left(\frac{WBODY}{WBIRTH + WADULT + WCHILD} \right)^{0.85}$$

Eq. (2.3-21)

where *VKC* and *VLC* are fractions of body weight (*WBODY*). Kidney and liver are weights (*KIDWT*, *LIVWT*) are calculated form tissue density (Equations 2.3-22 and 2.3-23):

$$KIDWT = VK \cdot 1.05$$ Eq. (2.3-22)

$$LIVWT = VL \cdot 1.05$$ Eq. (2.3-23)

The growth of bone volume (*VBONE)* and weight (WBONE) are calculated as a power functions of body weight, with cortical bone volume (*CVBONE*) assigned 0.8 of total bone volume (VBONE, Equations 2.3-24 to 2.3-26):

$$WBONE = 1000 \cdot 0.0290 \cdot WBODY^{1.21}$$ Eq. (2.3-24)

$$VBONE = 1000 \cdot 0.0168 \cdot WBODY^{1.188}$$ Eq. (2.3-25)

$$CVBONE = 0.8 \cdot VBOONE$$ Eq. (2.3-26)

2.3.2.5. Age Dependencies of Parameter Values

Biokinetics parameters that are assumed to change with age are assigned values for specific ages. These assignments are made as arrays of parameter values and corresponding ages (year), beginning with birth (age = 0 years). Parameter values between age designations are calculated by linear interpolation.

2.3.3. Absorption

The AALM.FOR model simulates Pb absorption from inhalation, ingestion, or dermal contact with surface dust. In the AALM.FOR, absorption represents the transfer of Pb intake (µg Pb intake/day), computed in the exposure model, to a rate of entry of Pb into the diffusible plasma compartment of the

biokinetics model (µg Pb absorbed/day). Absorption from each exposure pathway is simulated as a first-order processes governed by absorption fractions and/or first-order rate coefficients (d^{-1}).

2.3.3.1. Absorption from the Respiratory Tract

In the AALM.FOR, the respiratory tract is simulated as four compartments into which inhaled Pb (IN_{AIR}, µg Pb/day) is deposited and from which Pb is absorbed into the diffusible plasma compartment. Division of the respiratory tract into four compartments provides a means for simulating multi-phase absorption kinetics of inhaled Pb observed in studies of human exposures to Pb particulates (Leggett, 1993). The four compartments are intended to represent the intrathoracic, bronchiolar, bronchiole, and alveolar regions of the respiratory tract. In the current version of the AALM.FOR, Pb deposition and absorption are assigned the following values (half-times, $t_{1/2}$, are estimated as ln(2)/BR):

Compartment	**1**	**2**	**3**	**4**
Deposition Fraction (R)	0.08	0.14	0.14	0.04
Rate Coefficient (BR, day^{-1})	16.6	5.4	1.66	0.347
$t_{1/2}$ (hour)	1	3	10	40

The above deposition fractions correspond to the regional distribution of deposited Pb from the Leggett (1993) model partitioned to have 40% total deposition of inhaled Pb in the respiratory tract. Of the total amount of Pb initially deposited, 4% (0.016 of deposited Pb, i.e., 0.04×0.4) is transferred to the stomach (i.e., mucociliary clearance). The above parameter values reflect the data on which the model was based, which were derived from studies in which human subjects inhaled submicron Pb-bearing particles (Morrow et al., 1980; Chamberlain et al., 1978; Wells et al., 1977; Hursh and Mercer, 1970; Hursh et al., 1969). These assumptions would not necessarily apply for exposures to larger or less soluble airborne particles.

Rate equations describing the rates of change of Pb mass (µg) in the respiratory tract are presented in Table 2-2 (Equations C1–C10). In these equations, the parameter *BRETH* (Equation G1 in Table 2-1) represents the total intake of Pb from exposure to Pb in air (µg Pb/day, equivalent to $INAIR_{TOTAL}$ from Equation A4 in Table 2-1). The mucociliary clearance fraction, designated *CIILAR*, appears in the rate equations for diffusible plasma (Table 2-2, Equation E2), in which the rates for transfer of Pb from all respiratory tract compartments to diffusible plasma are factored by the value 1-*CILIAR* (e.g., Equation 2.3-27):

$$UPTAKERT = (1 - CILIAR) \cdot \sum_{i=1}^{4}(BR_i \cdot YR_i) \qquad \text{Eq. (2.3-27)}$$

where *UPTAKERT* is the rate of absorptive transfer of Pb from the respiratory tract to diffusible plasma, *CILIAR* is the fraction of inhaled Pb transferred to the stomach, BR_i is the fraction of inhaled Pb deposited in respiratory tract compartment *i*, and YR_i is the Pb mass (µg) in respiratory tract compartment *i*.

2.3.3.2. Absorption from the Gastrointestinal Tract

In the AALM.FOR, the gastrointestinal tract contents (i.e., Pb masses in the lumen of the gastrointestinal tract) is simulated as four compartments representing: (1) stomach contents (STMC); (2) small intestine contents (SIC); (3) upper large intestine contents (ULIC); and (4) lower large intestine contents (LLIC). Total intake of Pb from ingestion (see Equation G2 in Table 2-1) enters the stomach and is passed, in series, to the small intestine, upper large intestine, lower large intestine, and feces at rates represented by first-order rate coefficients. Absorption of Pb from the gastrointestinal tract is assumed to occur in the small intestine, and is represented by an absorption fraction (*AF1*), representing the fraction of Pb mass in the small intestine that is transferred to the diffusible plasma compartment. The absorption fraction given by Equation 2.3-28 is age-dependent, and calculated based on an expression from O'Flaherty's studies (O'Flaherty, 1995, 1993):

$$AF_{AGEYEAR} = AF_{C1} - \frac{AF_{C2}}{1+30*e^{-AGEYEAR}} \quad \text{Eq. (2.3-28)}$$

Values for AF_{C1} and AF_{C2} were assigned values of 0.4 and 0.28, respectively based on fitting simulations to data on blood Pb concentration in children (Sherlock and Quinn, 1986; Ryu et al., 1983) and adults (Rabinowitz et al., 1976) who ingested Pb in formula or food, respectively, as described in Chapter 4. These parameter values produce a decrease in the absorption fraction from a value of 0.39 at birth to a value of 0.12 at age 8 years (Figure 2-3), which aligns with the fractional gastrointestinal tract absorption for adults in the Adult Lead Methodology (U.S. EPA, 2003). This age pattern of higher absorption fraction in infants and children is generally consistent with observations made in mass balance studies in infants and children (Ziegler et al., 1978; Alexander et al., 1974) and in isotope studies of Pb absorption in adults (Watson et al., 1986; James et al., 1985; Heard and Chamberlain, 1982; Rabinowitz et al., 1980).

Rate equations describing the rates of change of Pb mass (µg) in gastrointestinal tract contents are presented in Table 2-2 (Equations D1–D10). Values of rate coefficients for movement of Pb through the gastrointestinal tract are derived from Leggett (1993); the approximate half-times in adults are assumed to be 0.69, 2.8, 9.0, and 17 hours, respectively. These rate coefficients are scaled for age (GSCAL), relative to adult values:

AGE	**0**	**100 d**	**1 yr**	**5 yr**	**10 yr**	**15**	**≥25**
GSCAL	1.67	1.67	1.67	1.67	1.33	1.33	1.00

In addition to intake of Pb from ingestion of environmental media, the stomach also receives Pb from the respiratory tract (i.e., mucociliary clearance). The rate equation describing stomach inflow of Pb to stomach contents (Table 2-2 Equation D1) includes this mucociliary contribution (Equation 2.3-29):

$$IN_{STMC} = EATCRN + CILIAR \cdot \sum_{i=1}^{4}(BR_i \cdot YR_i) \quad \text{Eq. (2.3-29)}$$

where *EATCRN* is the sum of Pb intakes from all ingestion pathways (µg/day), *CILIAR* is the fraction of inhaled Pb transferred to the stomach, BR_i is the fraction of inhaled Pb deposited in respiratory tract compartment *i*, and YR_i is the Pb mass (µg) in respiratory tract compartment *i*.

The small intestine receives Pb from the stomach as well as from liver (i.e., biliary secretion) and diffusible plasma (Table 2-2 Equation D3). Transfer from the liver to the small intestine is represented in Equation D3 as (Equation 2.3-30):

$$IN_{LVR1\rightarrow SIC} = H1TOSI \cdot RLVR1 \cdot YLVR1 \quad \text{Eq. (2.3-30)}$$

where *H1TOSI* is the fraction of Pb in liver compartment 1 (LVR1) that goes to the small intestine, *RLVR1* is the rate coefficient for transfer of Pb out of liver compartment 1 (d^{-1}), and *YLVR1* is the Pb mass in the fast liver compartment (µg).

Transfer of Pb from the diffusible plasma to the small intestine is represented as (Equation 2.3-31):

$$IN_{PLAS\rightarrow SIC} = TFECE \cdot CF \cdot BTEMP \quad \text{Eq. (2.3-31)}$$

where *TFECE* is the scaled deposition fraction from plasma to small intestine; *CF* is an adjustment factor for deposition fractions from diffusible plasma to account for non-linear uptake of Pb into RBCs (Equation 2.3-14) and *BTEMP* is the rate transfer of Pb from plasma to all receiving compartments (µg Pb/day, Equation 2.3-11).

Although absorption occurs from the small intestine, it is accounted for in the equations for inflow of Pb to the upper large intestine (Table 2-2 Equation D6) and into diffusible plasma (Table 2-2, Equation E1 and E2). All inflows of Pb to the small intestine, including from liver and diffusible plasma, are subject to absorption; as a result, inflow of Pb to the upper large intestine is equivalent to the 1-*AF1* fraction (where *AF1* is the absorption fraction) of the total rate of transfer from the small intestine (Equation 2.3-32), and inflow from the small intestine to the diffusible plasma includes the corresponding *AF1* fraction (Equation 2.3-33):

$$IN_{SIC\rightarrow ULIC} = (1 - AF1) \cdot GSCAL \cdot RSIC \cdot YSIC \quad \text{Eq. (2.3-32)}$$

$$IN_{SIC\rightarrow PLAS} = AF1 \cdot GSCAL \cdot RSIC \cdot YSIC \quad \text{Eq. (2.3-33)}$$

where $IN_{SIC\rightarrow PLAS}$ is the absorption rate (*ABSORBGI*), *AF1* is the absorption fraction, *GSCAL* is the age adjustment factor for movement of Pb through the gastrointestinal tract, *RSIC i*s the rate coefficient for transfer of Pb from small intestine contents to upper large intestine contents (d^{-1}), and *YSIC* is the Pb mass in the small intestine contents (µg). Relative bioavailability (RBA) of ingested Pb (e.g., in

dust) is considered in the exposure model (see Sections 2.2.1 and 2.2.3). The application of RBA as an adjustment to Pb intake rather than an adjustment to the gastrointestinal absorption fraction is a simplification that results in an underprediction of fecal excretion of unabsorbed Pb and negative mass balance (intake>body burden + excreted) when RBA <1.

2.3.4. Vascular and Extravascular Fluid

2.3.4.1. Diffusible Plasma

The AALM.FOR represents Pb in the vasculature as three compartments: (1) diffusible plasma; (2) bound plasma; and (3) RBCs. The diffusible plasma compartment receives Pb from all absorption pathways and exchanges with Pb bound to plasma protein, Pb in RBCs, Pb in an extravascular fluid compartment, and Pb in extravascular tissues (bone, brain, kidney, liver, and other soft tissues). Lead is also transferred from diffusible plasma to the small intestine, where it can contribute to fecal elimination of absorbed Pb. The rate coefficient for transfer of Pb from diffusible plasma to all receiving compartments (*RPLS*) is 2000 day^{-1} ($t_{1/2}$≈0.5 min; ln(2)/rate constant). This rate constant is subdivided into deposition fractions that represent the fractions of the total transfer assigned to each receiving compartment. Deposition fractions appear in all rate equations that include inflows of Pb from diffusible plasma to any compartment, and appear as the product of the deposition fraction (TC_i), an adjustment factor for variable deposition fraction to RBCs (*CF,* from Equation 2.3-14), and the rate of total outflow of Pb from diffusible plasma (*BTEMP*, from Equations 2.3-10 and 2.3-11) (Equation 2.3-34):

$$IN_{PLAS \rightarrow C} = TC_i \cdot CF_i \cdot BTEMP \qquad \text{Eq. (2.3-34)}$$

Values of corresponding rate coefficients for transfers from diffusible plasma to receiving compartments (i.e., TC_i * *RPLS*), based on Leggett (1993), are presented in Table 2-2. The highest rates are for transfers to the extravascular fluid compartment, RBCs, and bone surface.

2.3.4.2. Bound Pb in Plasma

Lead in the bound plasma compartment represents Pb reversibly bound to plasma proteins. Bound Pb in plasma is confined to the vascular fluid. Reversible binding is simulated as first-order transfers between compartments, with no maximum capacity for binding (Table 2-2, Equation E8). The transfer rate ratio establishes the equilibrium for binding. Based on Leggett (1993), these values for adults are 0.8 day^{-1} ($t_{1/2}$ = 0.9 day) for transfer to the bound compartment and 0.139 day^{-1} ($t_{1/2}$ = 5.0 day) for transfer from the bound compartment, providing an equilibrium ratio (bound/free) of approximately 6. Values for children are similar, but transfer to the bound compartment is slightly slower.

2.3.4.3. Red Blood Cells

Lead in diffusible plasma exchanges with Pb in RBCs (Table 2-2, Equation E13) and is governed by a deposition fraction and corresponding rate coefficient for uptake (*TOORBC*) and return from the RBC (*RRBC*). Uptake of Pb in RBCs is assumed to be limited by a maximum capacity, represented in the AALM.FOR by a maximum Pb concentration in RBCs (*SATRAT*, µg Pb/dL RBC volume). Above a threshold concentration in red blood cells (*RBCNL,* µg Pb/dL RBC volume), the deposition fraction (and corresponding rate coefficient) for transfer from diffusible plasma to RBCs (*TOORBC*) declines

(Equation 2.3-35) and deposition fractions to all other tissues increase proportionally by the factor *CF* (from Equation 2.3-14).

$$TOORBC = 1\text{-}\left(\frac{RBCONC\text{-}RBCNL}{SATRAT\text{-}RBCNL}\right)^{1.5} \quad \text{Eq. (2.3-35)}$$

Values for rate coefficients for transfer in and out of the RBC, *SATRAT* (350 µg Pb/dL RBC) and *RBCNL* (20 µg Pb/dL RBC) result in rapid uptake of Pb into RBCs (adult $t_{1/2}$≈2 min in adults, 2-3 min in children) and replicate the non-linear relationship between plasma and red blood observed in adults (Smith et al., 2002; Manton et al., 2001; Bergdahl et al., 1999; Bergdahl et al., 1998; Bergdahl et al., 1997). The values for *RBCNL* and *RRBC* in Equations D-12 and 13 of Table 2-2 were adjusted upward from the values assigned in Leggett (1993) to provide improved fit to plasma-whole blood Pb relationships in adults and to harmonize blood Pb predictions in young children with the IEUBK model at the ages of 1, 5, and 10 years (see Chapter 4).

2.3.4.4. Extravascular Fluid

Lead in diffusible plasma exchanges with Pb in an extravascular fluid (EVF) compartment (Table 2-2 Equation F1). The conceptual basis for including the EVF compartment is to allow simulation of the dynamics of Pb in plasma of efflux of Pb from plasma and return to the plasma during the first minutes following intravenous injection of Pb that has been observed following intravenous injection of Pb, as summarized in Leggett (1993) based on various experimental studies (Heard and Chamberlain, 1984; Booker et al., 1969; Hursh and Suomela, 1968; Stover, 1959). Efflux of Pb from the plasma is assumed to occur immediately after its entrance into plasma and prior to binding of binding of Pb to plasma proteins ($t_{1/2}$≈1 day, adults) and uptake into RBCs (adult $t_{1/2}$≈2 min, adults). Uptake of Pb into RBCs subsequently provides a driving force for return of Pb to the plasma. These dynamics are simulated as rapid exchanges of Pb between the diffusible plasma and EVF compartments. For all ages, rate coefficients for transfers to and from the EVF, based on Leggett (1993), are 1000 day^{-1} ($t_{1/2}$≈1 min) and 333 day^{-1} ($t_{1/2}$≈3 min). These values produce a rapid efflux of Pb to the EVF compartment and return to diffusible plasma, with an equilibrium ratio for EVF/diffusible plasma Pb mass of approximately 3. The corresponding volume of distribution for the rapidly exchanging EVF compartment of three times diffusible plasma is consistent with observations made for the distribution of calcium, summarized in Leggett (1993) based on Harrison et al. (1967) and (Hart and Spencer, 1976).

2.3.5. Skeleton

2.3.5.1. General Structure of Bone Model

A major concept underlying the AALM.FOR simulation of bone Pb kinetics is that Pb kinetics behavior in bone is similar to that of calcium and other bone accumulating elements that mimic calcium (e.g., strontium). Observations that formed the bases for the Leggett (1993) bone Pb model included experimental studies of the kinetics of Pb, calcium, and strontium in humans, non-human primates, and dogs (e.g., Heard and Chamberlain, 1984; Lloyd et al., 1975; Cohen et al., 1970). The AALM.FOR simulates Pb biokinetics in bone as a combination of three processes: (1) relatively rapid exchange of Pb between diffusible plasma and surfaces of cortical and trabecular bone; (2) slower exchange of Pb at bone surfaces with an *exchangeable* Pb pool in bone volume; and (3) slow transfer of a portion of Pb in bone

volume to a *non-exchangeable* pool that is released from bone to diffusible plasma only when bone is resorbed (Figure 2-4). These features are represented in the AALM.FOR as six bone subcompartments; three separate compartments for cortical and trabecular bone, each, representing bone surface, exchangeable Pb in bone volume, and non-exchangeable Pb in bone volume. Cortical and trabecular bone volume are assumed to account for 80% and 20% of total bone volume, respectively (Leggett, 1993). Transfers of Pb in and out of the bone surface compartment are assumed to be relatively rapid: values for $t_{1/2}$ are approximately 0.01 day for transfer from plasma-to-bone surface; and 1.4 days for return from bone surface to plasma and transfer from bone surface to exchangeable bone volume (Leggett, 1993). Transfer from bone surface is faster in children ($t_{1/2} \approx 1.1$ days). Return of Pb from the exchangeable bone volume to bone surface is slower ($t_{1/2} \approx 37$ days); however, the dominant transfer processes determining long-term accrual of bone Pb burden (≈90% of body burden) are the slower rate coefficients for transfer of Pb from the non-exchangeable compartments of trabecular and cortical bone to diffusible plasma (adult $t_{1/2} \approx 1.9$ and 12 years, respectively). Bone transfer coefficients vary with age (faster in children) to reflect age-dependence of bone turnover. The slow, non-exchangeable, bone volume compartment is assumed to be much more labile in infants and children than in adults (e.g., cortical $t_{1/2} \approx 42$ days at birth, 677 days at 15 years, and 4220 days at ≥25 years; trabecular $t_{1/2} \approx 42$ days at birth, 363 days at 15 years, and 703 days at ≥25 years). Other physiological states that affect bone turnover and, therefore, bone Pb kinetics, such as pregnancy and menopause, could be accommodated with adjustments to tissue (e.g., bone) transfer coefficients.

2.3.5.2. Cortical and Trabecular Bone Surface

Cortical and trabecular bone surfaces exchange Pb with diffusible plasma and the exchangeable compartment of bone volume (Table 2-2, Equations G5 and G11). Bone *surfaces*, in this context, represent surfaces of bone in contact with the plasma (e.g., Haversian and Volkmann canals) and/or involved in bone production and resorption (e.g., endosteal and periosteal surfaces for cortical bone, resorption cavities, surfaces of trabecular bone). Deposition of Pb in bone surface is considered to reflect (and be in proportion to) rates of incorporation of calcium in bone that occur during growth, modeling, and remodeling of bone. Rates change with age, reflecting periods of more intense growth (e.g., infancy, pre-adolescence). In the AALM.FOR, bone Pb kinetics have the following three general characteristics. First, transfers are relatively rapid: adult $t_{1/2} \approx 0.01$ day for plasma-to-bone surface, adult $t_{1/2} \approx 1.4$ days for bone surface to plasma. Second, rates of transfer are age-dependent with highest rates during infancy (0–1 years) and adolescence (10–15 years), during periods of rapid bone growth. In infancy, transfer of Pb to bone surface accounts for approximately 24% of total flow of Pb out of the diffusible plasma (8% in adults). And third, relative fractions of transfer from diffusible plasma to cortical and trabecular bone is also age-dependent, decreasing from 80% of total transfer going to cortical bone during infancy, to approximately 44% in adults.

2.3.5.3. Cortical and Trabecular Bone Volume

Bone volume compartments are subdivided into cortical (80%) and trabecular bone (20%), with each further subdivided into *exchangeable* and *non-exchangeable* subcompartments (Table 2-2, Equations G7, G9, G13, and G15). Exchangeable and non-exchangeable compartments represent Pb pools in bone volume having different rates and mechanisms of turnover. Lead in the exchangeable compartment is assumed to be subject to heteroionic exchange with other bone minerals (e.g., calcium) and/or diffusion of Pb into osteons (Leggett, 1993). Lead that enters the non-exchangeable compartment remains there,

unless subject to bone resorption. Turnover of Pb in the non-exchangeable compartment reflects bone turnover rates.

Lead enters bone volume from bone surface. In the AALM.FOR, exchanges of Pb between bone surface and bone volume have the following three characteristics. First, the transfer to bone volume is faster (adult $t_{1/2}$≈1.4 days) compared to return to bone surface (adult $t_{1/2}$≈37 days), resulting in accumulation of Pb in bone volume, relative to bone surface. Second, transfer rates from bone surface to bone volume are constant ($t_{1/2}$≈2 days) up through adolescence, and slower than in adults ($t_{1/2}$≈1.4 days). And third, transfer rates between bone volume and bone surface are assumed to be similar for cortical and trabecular bone.

A portion of the Pb that enters bone from bone surface becomes associated with deep bone mineral deposits that can be mobilized during periods of bone resorption (including that which occurs during bone modeling associated with growth). In the AALM.FOR, kinetics of Pb in this non-exchangeable pool have the following six characteristics. First, transfer of Pb from the exchangeable compartment to the non-exchangeable compartment is relatively faster ($t_{1/2}$≈30 days) than transfer to surface bone ($t_{1/2}$≈37 days). Second, the transfer rate to the non-exchangeable compartment is independent of age. Third, transfer to the non-exchangeable compartments of cortical and trabecular bone occur at the same rates. Fourth, transfer of Pb out of the non-exchangeable compartment returns Pb directly to the diffusible plasma. Fifth, rates of transfer from the non-exchangeable compartment reflect bone turnover rate and are relatively slow (adult $t_{1/2}$≈12 years for cortical bone, adult $t_{1/2}$≈1.9 years for trabecular bone) compared to rates of removal of Pb from the exchangeable compartment. And sixth, age-dependent changes in bone turnover rates give rise to movement of Pb out of the non-exchangeable compartments that declines with increasing age:

AGE	**100 d**	**1 yr**	**5 yr**	**10 yr**	**15 yr**	**≥25**
Cortical $t_{1/2}$ (yr)	0.12	0.33	0.62	1.1	1.9	12
Trabecular $t_{1/2}$ (yr)	0.12	0.33	0.52	0.72	1.0	1.9

Discussed in Chapter 4, values for *RCORT* and *RTRAB* in Equations G9 and G15 of Table 2-2, and *FLONG* (Equation G1-G4) were adjusted to improve agreement between predicted and observed elimination kinetics of Pb from bone in adults (Nilsson et al., 1991).

2.3.6. Liver

The AALM.FOR simulates Pb kinetics in liver as the combination of three properties. First, there is relatively rapid exchange between Pb in diffusible plasma and a *fast* compartment in liver (LVR1). Second, slower transfer of Pb from the *fast* liver compartment to a *slow* compartment in liver (LVR2), which can release Pb to the diffusible plasma. And third, there is transfer of Pb from the fast liver compartment to the small intestine (i.e., biliary secretion). This configuration gives rise to Pb kinetics following a single absorbed dose that result in a relatively rapid initial uptake of Pb in liver, followed by a slow decline in liver Pb burden, consistent with experimental studies conducted in humans, non-human primate, and dogs (Leggett, 1993), based on several studies (Heard and Chamberlain, 1984; Lloyd et al.,

1975; Cohen et al., 1970). With chronic dosing, liver Pb levels increase to approximately 10% of total body burden in early childhood and decline to 2% by age 40 years.

Rate equations for transfers of Pb in and out of liver are presented in Table 2-2 (Equations J1 and J3). In the AALM.FOR, kinetics of Pb in liver have the following four general characteristics. First, transfer to the fast liver compartment (LRV1) from diffusible plasma is relatively rapid (adult $t_{1/2}$≈0.01 day) and accounts for approximately 4% of total transfer of Pb from diffusible plasma. Second, transfers from the LVR1 to diffusible plasma and to the small intestine are assumed to occur at approximately the same rate ($t_{1/2}$≈22 days) and is slower than uptake from diffusible plasma, resulting in Pb accumulates in the fast pool. Third, Pb in the fast liver compartment is slowly transferred to the slow liver pool (LVR2, $t_{1/2}$≈100 day). Fourth, rates of return of Pb from the slow compartment to diffusible plasma are age-dependent, with half-times decreasing from $t_{1/2}$≈1000 days at birth to 500 days at age 5 years, increasing to approximately 1200 days at age ≥10 years. This results in increasing rate of accumulation of Pb in the slow compartment with age, with chronic dosing. As discussed in Chapter 4, the value for *RLIV2* in Equation J3 of Table 2-2 was adjusted from the value reported in Leggett (1993) to improve agreement between predicted and observed soft tissue-bone Pb ratios (Barry, 1975).

Biliary secretion of Pb is simulated as transfer of Pb from the fast liver compartment (LVR1) to the small intestine (Table 2-2, Equation D3). The biliary contribution to the small intestine Pb contents is given by Equation 2.3-36:

$$IN_{LVR1\rightarrow SIC} = H1TOSI \cdot RLVR1 \cdot YLVR1 \qquad \text{Eq. (2.3-36)}$$

where *H1TOSI* is the fraction of Pb in LVR1 that goes to the small intestine, *RLVR1* is the rate coefficient for transfer of Pb out of LVR1 (day^{-1}), and *YLVR1* is the Pb mass in LVR1 (μg). A value of 0.45 is assumed for *H1TOSI*. This value is the rate constant from LVR1 to the small intestine divided by the sum of rate constants for movement from LVR1 to the small intestine, plasma, and LVR2 (Leggett, 1993).

2.3.7. Kidney

Similar to liver, kidney Pb kinetics exhibit multiple components that include an initial phase of rapid uptake of Pb following a single dose of Pb, followed by a slow decline in kidney Pb burden, with long-term retention of <1% of the body burden during chronic dosing. The AALM.FOR simulates Pb kinetics in kidney as the combination of two parallel processes: (1) relatively rapid transfer between Pb from diffusible plasma to a *fast* compartment in kidney (KDN1), a portion of which is excreted in urine (*urinary path*); and (2) slower exchange Pb between diffusible plasma and a *slow* compartment in kidney (KDN2). This configuration gives rise to Pb kinetics following a single absorbed dose that result in a relatively rapid initial uptake of Pb in kidney, followed by a slow decline in kidney Pb burden. With chronic dosing, kidney Pb levels increase to approximately 2% of total body burden in early childhood and decline progressively 0.2–0.3% after age 40 years.

Rate equations for transfers of Pb in and out of kidney are presented in Table 2-2 (Equations I1 and I3). In the AALM.FOR, kinetics of Pb in kidney have the following four general characteristics. First, transfer from the diffusible plasma to the fast (urinary path) kidney compartment (KDN1) is relatively

rapid ($t_{1/2}$≈0.02 day) and accounts for approximately 2.5% of total transfer of Pb from diffusible plasma. Second, transfer from the fast compartment of kidney (KDN1) to bladder urine is slower than uptake from diffusible plasma ($t_{1/2}$≈5 days). As a result, Pb accumulates in the fast compartment. Third, transfer of Pb from diffusible plasma to the slow kidney compartment (KDN2) is approximately 100 times slower than that to the fast compartment (adult $t_{1/2}$≈2 days), receiving approximately 0.04% of the total transfer out of the diffusible plasma). and fourth, rates of return of Pb from the slow compartment (KDN2) to diffusible plasma are age-dependent, with half-times increasing from $t_{1/2}$≈1000 days until age 5 years and to 3648 days at age ≥10 years. This results in increasing rate of accumulation of Pb in the slow compartment with age, with chronic dosing.

The value for *TKDN1* in Equation I1 of Table 2-2 was adjusted (see Chapter 4) from the value reported in Leggett (1993) to improve agreement between predicted and observed plasma-to-urine clearance in adults (Araki et al., 1986; Manton and Cook, 1984; Manton and Malloy, 1983; Chamberlain et al., 1978). The value for *RKDN2* in Equation I3 of Table 2-2 was adjusted (see Chapter 4) from the value reported in Leggett (1993) to improve agreement between predicted and observed soft tissue-bone Pb ratios reported by Barry (1975).

2.3.8. Brain

In the AALM.FOR, the brain is treated as a homogenous compartment (Table 2-2, Equations H1, H2). This assumption is a gross simplification of more complex, non-uniform distribution of Pb in brain tissues. Nevertheless, the simplification has little consequence of overall kinetics of Pb, since brain constitutes a relatively small site of deposition. In the AALM.FOR, the brain is assumed to receive approximately 0.05% total outflow of Pb from the diffusible plasma up to age 1 year and 0.015% at ages ≥5 years. Transfer rates into brain (adult $t_{1/2}$≈2.3 day) and from brain to diffusible plasma ($t_{1/2}$≈730 day) result in brain Pb burdens that are 0.1–0.2% of body burden, with chronic dosing. Transfer rates into brain are age-dependent, and are highest during the first year ($t_{1/2}$≈1 day) and decrease ($t_{1/2}$≈2–3 days) at ages ≥5 years. The age-dependence in transfer rates contribute to a peak in the Pb mass in brain (≈0.8% of body burden) between ages 3–4 years, with chronic exposure.

2.3.9. Other Soft Tissues

In the AALM.FOR, soft tissues not explicitly simulated as distinct compartments (e.g., muscle, skin, etc.) are lumped into a single compartment (Other Soft Tissue, SOF). This compartment is assumed to comprise three subcompartments that are characterized with relatively *fast*, *intermediate*, or *slow* exchange kinetics with diffusible plasma (Table 2-2, Equations K1, K3, and K5), and no exchanges between subcompartments. The fast compartment (*SOF0*) receives approximately 8-9% of the outflow of Pb from diffusible plasma (adult $t_{1/2}$≈0.004 day, child $t_{1/2}$ 0.5-1 day), with slower return of Pb to the diffusible plasma ($t_{1/2}$≈0.33 day). The intermediate compartment (*SOF1*) receives approximately 0.5-1% of the outflow form diffusible plasma (adult $t_{1/2}$≈0.07 day, child $t_{1/2}$ 0.04-0.06 day), with slower return kinetics (adult $t_{1/2}$≈167 day). The slow compartment (*SOF2*) receives approximately 0.1% of the total outflow of Pb from diffusible plasma (adult $t_{1/2}$≈0.35 day, child $t_{1/2}$ 0.400.6 day), with slower return ($t_{1/2}$≈1800 day). This configuration results in approximately 9% of the Pb body burden residing in the combined subcompartments that comprise the other soft tissue compartment during early childhood followed by a decrease to approximately 3% by age 40 years. A pathway for elimination of Pb to hair,

nails, and exfoliated skin is assigned to the intermediate soft tissue compartment (Table 2-2, Equation L9).

2.3.10. Excretion

The AALM.FOR simulates excretion of absorbed Pb as five separate pathways representing urine, secretion from liver to small intestine (e.g., biliary), secretion from diffusible plasma to small intestine, sweat, and other routes (e.g., hair, nails, exfoliated skin as described in Section 2.3.9). The urinary pathway includes excretion of Pb deposited from the diffusible plasma into the fast kidney compartment (KDN1, Table 2-2, Equation L1). This pathway contributes approximately 2.5% of total outflow of Pb from the diffusible plasma. The corresponding plasma clearance (L plasma/day) is approximately 2.4 L/day at age 1 year and 20 L/day at age ≥25 years, and blood clearance (L blood/day) is approximately 0.05 L/day at age 1 year and 0.07 L/day at age ≥25 years. The urinary pathway contributes approximately 45% of total excretion of absorbed Pb in adults and approximately 80% up at ages ≤ 12 years. The AALM.FOR also includes rate coefficient for direct transfer of Pb from plasma to urine (*TURIN* in Equation L1 of Table 2-2). Improved agreement between predicted and observed plasma-to-urine clearance in adults was achieved with adjustments to the parameter *TKDN1* (Equation I1 of Table 2-2). Because values assigned to *TURIN* did not improve the fit to observations, the direct excretion pathway was nulled by setting *TURIN* to zero.

The fecal excretion pathway in the AALM.FOR includes the unabsorbed fraction of Pb that enters the small intestine from three sources (Table 2-2 Equation L5): (1) ingestion; (2) transfer from the liver (biliary secretion, Table 2-2 Equation D3); and (3) transfer from diffusible plasma. Biliary secretion contributes approximately 32% of total excretion of absorbed Pb in adults (55% up to age 12 years) and transfer from plasma contributes approximately 11% (18% at age ≤12 years).

Sweat is simulated as a direct transfer out of diffusible plasma and accounts for approximately 6% in of total excretion of absorbed Pb in adults and approximately 11% at ages ≤12 years (Table 2-2, Equation L7). All other pathways of Pb excretion, not simulated with specific pathways, are accounted for in transfer of Pb from the intermediate soft tissue compartment (SOF1; Table 2-2 Equation L9). These pathways include losses to hair, nails, and exfoliated skin and, combined, account for approximately 6% of total excretion of absorbed Pb in adults and 12% at ages ≤12 years.

2.3.11. Fetus

Lead masses in all compartments at birth are assigned values based on a value for maternal blood Pb concentration (Table 2-2, Equations A1–A7). The general equation for the fetal distribution of Pb masses is in the form (Equation 2.3-37):

$$Y_i = \frac{YF_i \cdot PbB_M \cdot PbB_{F/M} \cdot 3}{YF_{RBC}} \qquad \text{Eq. (2.3-37)}$$

where Yi is the Pb mass (µg) in tissue i at birth, YF_i is the fraction of total body burden in tissue i at birth, PbB_M is the maternal blood Pb concentration (µg/dL), $PbB_{F/M}$ is the fetal/maternal blood Pb concentration ratio, YF_{RBC} is the fraction of body burden in RBCs at birth and Y_{blood} is the blood volume at birth (assumed to be 3 liters). The value 3 in the numerator represents the assumed blood volume(dL) at

birth. Tissue compartments assigned values at birth include: brain, kidney (*KDN2*), liver (*LVR2*), RBC, soft tissue (*SOF0*), and non-exchangeable bone volume (80% cortical, 20% trabecular).

2.3.12. Chelation

The AALM.FOR includes parameters to simulate of the effect of chelation therapy on internal Pb kinetics. The chelation simulation decreases transfer of Pb from diffusible plasma and increases transfer from diffusible plasm to urine. Chelation parameters include the beginning and end age (days) of chelation (*CHEL1*, *CHEL2*) and a parameter that adjusts the deposition fractions of Pb transfer from diffusible plasma to tissues (*CHLEFE*). The adjustment of the deposition fraction takes the following general form (Equation 2.3-38):

$$TBONE = (1 - CHLEFE) \cdot TBONE \quad \text{Eq. (2.3-38)}$$

where *TBONE* is the deposition fraction for transfer from diffusible plasma to bone. The same adjustment is made to the deposition fractions for all tissue and excretory compartments, except urine (*TURIN*). During the chelation period, the deposition fraction from diffusible plasma to urine is calculated as follows (Equation 2.3-39):

$$TURIN = \sum_{i=1}^{n}(1 - T_i) \quad \text{Eq. (2.3-39)}$$

where T_i represents the deposition fraction for a given tissue.

TABLE 2-1. EXPOSURE EQUATIONS OF AALM.FOR

No.		Equation
A		**Pb Intakes from Inhaled Air**
A	1	$INair = PbAir \cdot VR$
A	2	$PbAir_{discrete\ weighted} = \sum_{i=1}^{n}(PbAir_i \cdot f_i)$
A	3	$PbAir_{pulse\ sum} = PbAir_{baseline} + PbAir_{pulse}$
A	4	$INair_{Total} = INair_{discrete} \cdot (1 - f_{pulse}) + INair_{pulse} \cdot f_{pulse}$
B		**Pb Intakes from Ingested Indoor Dust**
B	1	$INdust = PbDust \cdot IRdust \cdot RBA$
B	2	$IRdust = IR_{SD} \cdot f_{IR_{soil}}$
B	3	$PbDust_{discrete\ weighted} = \sum_{i=1}^{n}(PbDust_i \cdot f)$
B	4	$PbDust_{pulse\ sum} = PbDust_{baseline} + PbDust_{pulse}$
B	5	$INdust_{Total} = INdust_{discrete} \cdot (1 - f_{pulse}) + INdust_{pulse} \cdot f_{pulse}$
C		**Pb Intakes from Ingested Soil**
C	1	$INsoil = PbSoil \cdot IRsoil \cdot RBA$
C	2	$IRsoil = IR_{SD} \cdot (1 - f_{IR_{soil}})$
C	3	$PbSoil_{discrete\ weighted} = \sum_{i=1}^{n}(Pbsoil_i \cdot f)$
C	4	$PbSoil\backslash_{pulse\ sum} = PbSoil_{baseline} + PbSoil_{pulse}$
C	5	$INsoil_{Total} = INsoil_{discrete} \cdot (1 - f_{pulse}) + Isoil_{pulse} \cdot f_{pulse}$
D		**Pb Intakes from Ingested Water**
D	1	$INwater = PbWater \cdot IRwater \cdot RBA$
D	2	$PbWater_{discrete\ weighted} = \sum_{i=1}^{n}(PbWater_i \cdot f)$
D	3	$PbWater_{pulse\ sum} = PbWater_{baseline} + PbWater_{pulse}$
D	4	$INwater_{Total} = INwater_{discrete} \cdot (1 - f_{pulse}) + INwater_{pulse} \cdot f_{pulse}$
E		**Pb Intakes from Ingested Food**
E	1	$INfood = INfood_{\ input} \cdot RBA$
E	2	$INfood_{discrete\ sum} = \sum_{i=1}^{n}(INfood_i) \cdot RBA$
E	3	$INfood_{pulse\ sum} = INfood_{baseline} + INfood_{pulse}$
E	4	$INfood_{Total} = INfood_{discrete} \cdot (1 - f_{pulse}) + INfood_{pulse} \cdot f_{pulse}$
F		**Pb Intakes from Ingested Other Media**

No.		Equation
F	1	$INother = INother_{input} \cdot RBA$
F	2	$INother_{discrete\ sum} = \sum_{i=1}^{n}(INother_i) \cdot RBA$
F	3	$INother_{pulse\ sum} = INother_{baseline} + INother_{pulse}$
F	4	$INother_{Total} = INother_{discrete} \cdot (1 - f_{pulse}) + INother_{pulse} \cdot f_{pulse}$
G		**Pb Intakes from All Exposure Pathways**
G	1	$BRETH = INair_{total}$
G	2	$IN_{ingestion_{total}} = IN_{water} + IN_{dust} + IN_{food} + IN_{other}$
G	3	$EAT = IN_{ingestion_{total}}$

See text (Section 2.2.1) for explanation of parameter names. The prefix *IN* refers to Pb intake (µg/day) and the prefix *Pb* refers to Pb concentration (e.g. µg/L, µg/g).

1

TABLE 2-2. BIOKINETICS EQUATIONS OF AALM.FOR

No.		Equation
A		**Pb Masses at Birth**
A	1	$YBRAN = \frac{BRANIN \cdot BLDMOT \cdot BRATIO \cdot 3}{RBCIN}$
A	2	$YCVOL = \frac{0.8 \cdot BONIN \cdot BLDMOT \cdot BRATIO \cdot 3}{RBCIN}$
A	3	$YKDN2 = \frac{RENIN \cdot BLDMOT \cdot BRATIO \cdot 3}{RBCIN}$
A	4	$YLVR2 = \frac{HEPIN \cdot BLDMOT \cdot BRATIO \cdot 3}{RBCIN}$
A	5	$YRBC = \frac{RBCIN \cdot BLDMOT \cdot BRATIO \cdot 3}{RBCIN}$
A	6	$YSOF = \frac{SOFIN \cdot BLDMOT \cdot BRATIO \cdot 3}{RBCIN}$
A	7	$YTVOL = \frac{0.2 \cdot BONIN \cdot BLDMOT \cdot BRATIO \cdot 3}{RBCIN}$
B		**Age-scaling of Diffusible Plasma-to-tissue Deposition Fractions**
B	1	$AGSCL = \frac{1 - TEVF - TBONE}{1 - TEVF - TBONEL}$
B	2	$TBRAN = AGESCL \cdot TOBRAN$
B	3	$TFECE = AGESCL \cdot TOFECE$
B	4	$TKDN1 = AGESCL \cdot TOKDN1$
B	5	$TKDN2 = AGESCL \cdot TOKDN2$
B	6	$TLVR1 = AGESCL \cdot TOLVR1$
B	7	$TPROT = AGESCL \cdot TOPROT$
B	8	$TRBC = AGESCL \cdot TORBC$
B	9	$TSOF0 = AGESCL \cdot TOSOF0$
B	10	$TSOF1 = AGESCL \cdot TOSOF1$
B	12	$TSOF2 = AGESCL \cdot TOSOF2$
B	13	$TSWET = AGESCL \cdot TOSWET$
B	14	$TURIN = AGESCL \cdot TOURIN$

No.		Equation
C		**Respiratory Tract (RT)**
C	1	$\frac{dR1}{dt} = R1 \cdot BRTCRN - BR1 \cdot YR1$
C	2	$YR1 = \int_0^T \frac{dR1}{dt} dt$
C	3	$\frac{dR2}{dt} = R2 \cdot INHALE - BR2 \cdot YR2$
C	4	$YR2 = \int_0^T \frac{dR2}{dt} dt$
C	5	$\frac{dR3}{dt} = R3 \cdot INHALE - BR3 \cdot YR3$
C	6	$YR3 = \int_0^T \frac{dR3}{dt} dt$
C	7	$\frac{dR4}{dt} = R4 \cdot INHALE - BR4 \cdot YR4$
C	8	$YR4 = \int_0^T \frac{dR4}{dt} dt$
C	9	$YLUNG = YR1 + YR2 + YR3 + YR4$
C		**Rate of Pb Absorption from RI**
C	10	$UPTAKERI = \frac{(1 - CILIAR) \cdot (BR1 \cdot YR1 \cdot BR2 \cdot YR2 \cdot BR2 \cdot YR3 \cdot BR4 \cdot YR4)}{dt}$
D		**Gastrointestinal Tract (GIT) – Stomach (STMC)**
D	1	$\frac{dSTMC}{dt} = EATCRN \cdot CILIAR \cdot (BR1 \cdot YR1 + BR2 \cdot YR2 + BR3 \cdot YR3 + BR4 \cdot YR4) - GSCAL \cdot RSTMC \cdot YSTMC$
D	2	$YSTMC = \int_0^T \frac{dSTMC}{dt} dt$
D		**Gastrointestinal Tract (GIT) – Small Intestine (SI)**
D	3	$\frac{dSIC}{dt} = GSCAL \cdot RSTMC \cdot YSTMC + H1TOSI \cdot RLVR1 \cdot YLVR1 + TFECE \cdot CF \cdot BTEMP - GSCAL \cdot RSIC \cdot YSIC$

No.		Equation
D	4	$YSIC = \int_0^T \frac{dSIC}{dt} dt$
D		**Gastrointestinal Tract (GIT) – Upper Large Intestine (ULI)**
D	5	$F_1 = AF_{C1} - \frac{AF_{C2}}{1 + 30 * e^{-AGEYEAR}}$
D	6	$\frac{dULIC}{dt} = (1 - F1) \cdot GSCAL \cdot RSIC \cdot YSIC - GSCAL \cdot RULI \cdot YULIC$
D	7	$YULIC = \int_0^T \frac{dULIC}{dt} dt$
D		**Gastrointestinal Tract (GIT) – Lower Large Intestine (LLI)**
D	8	$\frac{dLLIC}{dt} = GSCAL \cdot RULI \cdot YULIC - GSCAL \cdot RLLI \cdot YLLIC$
D	9	$YLLIC = \int_0^T \frac{dLLIC}{dt} dt$
D		**Rate of Absorption from Gastrointestinal Tract (GI)**
D	10	$UPTAKEGI = \frac{F1 \cdot GSCALE \cdot RSIC \cdot YSIC}{dt}$
E		**Blood – Plasma (Diffusible)**
E	1	$PP1 = RPROT \cdot YPROT + RRBC \cdot YRBC + \cdot REVF \cdot YEVF + RSOF0 \cdot YSOF0 +$ $(1 - S2HAIR) \cdot RSOF1 \cdot YSOF1 + RSOF2 \cdot YSOF2 + H1TOBL \cdot RLVR1 \cdot YLVR1 +$ $RLVR2 \cdot YLVR2 + RKDN2 \cdot YKDN2 + RCS2B \cdot YCSUR + RTS2B \cdot YTSUR +$ $RCORT \cdot YCVOL + RTRAB \cdot YTVOL + RBRAN \cdot YBRAN + F1 \cdot GSCAL \cdot RSIC \cdot YSIC$
E	2	$\frac{dPLS}{dt} = PP1 + (1 - CILIAR) \cdot (BR1 \cdot YR1 + BR2 \cdot YR2 + BR3 \cdot YR3 + BR4 \cdot YR4) -$ $RPLS \cdot YPLS$
E	3	$YPLS = \int_0^T \frac{dPLS}{dt} dt$
E	4	$RPLS = TSUM \cdot RPLAS$
E	5	$TSUM = TOORBC + TEVF + TPROT + TBONE + TURIN + TFECE + TSWET +$ $TLIVR1 + TKDN1 + TKDN2 + TSOF0 + TSOF1 + TSOF2 + TBRAN$
E	6	$BTEMP = RPLS \cdot YPLS$

No.		Equation
E	7	$CF = \frac{1 - TOORBC}{1 - TRBC}$
E		**Blood – Plasma – Protein Bound**
E	8	$\frac{dPROT}{dt} = TPROT \cdot CF \cdot BTEMP - RPROT \cdot YPROT$
E	9	$YPROT = \int_0^T \frac{dPROT}{dt} dt$
E		**Blood – Total Pb in Plasma (Diffusible, Protein Bound)**
E	10	$YPLAS = YPLS + YPROT$
E		**Blood – Red Blood Cell (RBC)**
E	11	$RBCONC \le RBCNL$: $TOORBC = TRBC$
E	12	$RBCONC > RBCNL$: $TOORBC = TRBC \cdot \left(1 - \frac{RBCONC - RBCNL}{SATRAT - RBCNL}\right)^{1.5}$
E	13	$\frac{dRBC}{dt} = TOORBC \cdot BTEMP - RRBC \cdot YRBC$
E	14	$YRBC = \int_0^T \frac{dRBC}{dt} dt$
E		**Blood – Total Pb in Blood**
E	15	$YBLUD = YPLAS + YRBC$
E		**Blood – Concentrations and Clearance**
E	16	$BLCONC = \frac{YBLUD}{AMTBLD}$
E	17	$RBCONC = \frac{YRBC}{BLDHCT \cdot AMTBLD}$
E	18	$PCENT = \frac{100 \cdot YPLAS}{YBLUD}$
E	19	$CLEAR = \frac{100 \cdot URIN}{DELT \cdot YPLAS}$
E	20	$BCLEAR = \frac{100 \cdot URIN}{DELT \cdot YBLUD}$

No.		Equation
F		**Extravascular Fluid**
F	1	$\frac{dEVF}{dt} = TEVF \cdot CF \cdot BTEMP - REVF \cdot YEVF$
F	2	$REVF = TEVF \cdot \frac{RPLS}{SIZEVF}$
F	3	$YEVF = \int_0^T \frac{dEVF}{dt} dt$
G		**Bone – Transfer Rates within Bone**
G	1	$RDF2CS = (1 - FLONG) \cdot RDIFF$
G	2	$RDF2TS = (1 - FLONG) \cdot RDIFF$
G	3	$RDF2DC = (FLONG) \cdot RDIFF$
G	4	$RDF2DT = (FLONG) \cdot RDIFF$
G		**Bone – Cortical Bone Surface**
G	5	$\frac{dCSUR}{dt} = TBONE \cdot (1 - TFRAC) \cdot CF \cdot BTEMP + RDF2CS \cdot YCDIF -$ $(RCS2B + RCS2DF) \cdot YCSUR$
G	6	$YCSUR = \int_0^T \frac{dCSUR}{dt} dt$
G		**Bone – Exchangeable Cortical Bone**
G	7	$\frac{dCDIF}{dt} = RCS2DF \cdot YCSUR - (RDF2CS + RDF2DC) \cdot YCDIF$
G	8	$YCDIF = \int_0^T \frac{dCDIF}{dt} dt$
G		**Bone – Non-Exchangeable Cortical Bone Volume**
G	9	$\frac{dCVOL}{dt} = RDF2DC \cdot YCDIF - RCORT \cdot YCVOL$
G	10	$YCVOL = \int_0^T \frac{dCVOL}{dt} dt$
G		**Bone – Trabecular Bone Surface**
G	11	$\frac{dTSUR}{dt} = TBONE \cdot TFRAC \cdot CF \cdot BTEMP + RDF2TS \cdot YTDIF -$ $(RTS2B + RTS2DF) \cdot YTSUR$

No.		Equation
G	12	$YTSUR = \int_0^T \frac{dTSUR}{dt} dt$
G		**Bone – Exchangeable Trabecular Bone**
G	13	$\frac{dTDIF}{dt} = RTS2DF \cdot YTSUR - (RDF2TS + RDF2DT) \cdot YTDIF$
G	14	$YTDIF = \int_0^T \frac{dTDIF}{dt} dt$
G		**Bone – Non-Exchangeable Trabecular Bone**
G	15	$\frac{dTVOL}{dt} = RDF2DT \cdot YTDIF - RTRAB \cdot YTVOL$
G	16	$YTVOL = \int_0^T \frac{dTVOL}{dt} dt$
G		**Total Pb in Cortical, Trabecular, and Total Bone**
G	17	$YCORT = YCVOL + YCDIF + YCSUR$
G	18	$YTRAB = YTVOL + YTDIF + YTSUR$
G	19	$YSKEL = YCVOL + YTVOL + YCDIF + YTDIF + YCSUR + YTSUR$
G		**Bone – Pb Concentration**
G	20	$CRTCON = \frac{YCORT}{CORTWT}$
G	21	$CRTCONBM = \frac{CRTCON}{0.55}$
G	22	$TRBCON = \frac{YTRAB}{TRBWT}$
G	23	$TRBCONBM = \frac{TRABCON}{0.50}$
G	24	$ASHCON = \frac{YSKEL}{TSKELWT}$
H		**Brain**
H	1	$\frac{dBRAN}{dt} = TBRAN \cdot CF \cdot BTEMP - RBRAN \cdot YBRAN$

No.		Equation
H	2	$YBRAN = \int_0^T \frac{dBRAN}{dt} dt$
I		**Kidney – Compartments 1 (fast, urinary path) and 2 (slow)**
I	1	$\frac{dKDN1}{dt} = TKDN1 \cdot CF \cdot BTEMP - RKDN1 \cdot YKDN1$
I	2	$YKDN1 = \int_0^T \frac{dKDN1}{dt} dt$
I	3	$\frac{dKDN2}{dt} = TKDN2 \cdot CF \cdot BTEMP - RKDN2 \cdot YKDN2$
I	4	$YKDN2 = \int_0^T \frac{dKDN2}{dt} dt$
I		**Kidney – Total Pb in Kidney**
I	5	$YKDNE = YKDN1 + YKDN2$
I		**Kidney – Pb Concentration in Kidney**
I	6	$RENCON - \frac{YKDNE}{KIDWT}$
J		**Liver – Fast Compartment 1**
J	1	$\frac{dLVR1}{dt} = TLVR1 \cdot CF \cdot BTEMP - RLVR1 \cdot YLVR1$
J	2	$YLVR1 = \int_0^T \frac{dLVR1}{dt} dt$
J		**Liver – Slow Compartment 2**
J	3	$\frac{dLVR2}{dt} = H1TOH2 \cdot RLVR1 \cdot YLVR1 - RLVR2 \cdot YLVR2$
J	4	$YLVR2 = \int_0^T \frac{dLVR2}{dt} dt$
J		**Liver – Total Pb in Liver**
J	5	$YLIVR = YLVR1 + YLVER2$
J		**Liver – Pb Concentration in Liver**
J	6	$LIVCON - \frac{YLIVR}{LIVWT}$

No.		Equation
K		**Soft Tissue – Compartments 0 (fast), 1 (intermediate), and 2 (slow)**
K	1	$\frac{dSOF0}{dt} = TSOF0 \cdot CF \cdot BTEMP - RSOF0 \cdot YSOF0$
K	2	$YSOF0 = \int_0^T \frac{dSOF0}{dt} dt$
K	3	$\frac{dSOF1}{dt} = TSOF1 \cdot CF \cdot BTEMP - RSOF1 \cdot YSOF1$
K	4	$YSOF1 = \int_0^T \frac{dSOF1}{dt} dt$
K	5	$\frac{dSOF2}{dt} = TSOF2 \cdot CF \cdot BTEMP - RSOF2 \cdot YSOF2$
K	6	$YSOF2 = \int_0^T \frac{dSOF2}{dt} dt$
K		**Soft Tissue – Total Pb in Soft Tissue**
K	7	$YSOFT = YSOF0 + YSOF1 + YSOF2$
L		**Excretion – Urinary Bladder**
L	1	$\frac{dBLAD}{dt} = TURIN \cdot CF \cdot BTEMP + RKDN1 \cdot YKDN1 - RBLAD \cdot YBLAD$
L	2	$YBLAD = \int_0^T \frac{dBLAD}{dt} dt$
L		**Excretion – Urine**
L	3	$\frac{dURIN}{dt} = RBLAD \cdot YBLAD$
L	4	$YURIN = \int_0^T \frac{dURIN}{dt} dt$
L		**Excretion – Feces**
L	5	$\frac{dFECE}{dT} = GSCAL \cdot RLLI \cdot YLLIC$
L	6	$YFECE = \int_0^T \frac{dFECE}{dt} dt$
L		Excretion – Sweat

No.		Equation
L	7	$\frac{dSWET}{dt} = TSWET \cdot CF \cdot BTEMP$
L	8	$YSWET = \int_0^T \frac{dSWET}{dt} dt$
L		**Excretion – Other (e.g., hair, nails, desquamated skin)**
L	9	$\frac{dHAIR}{dt} = S2HAIR \cdot RSOF1 \cdot YSOF1$
L	10	$YHAIR = \int_0^T \frac{dHAIR}{dt} dt$
M		**Lead Body Burden and Distribution**
M	1	$SIGMA = YPLAS + YRBC + YEVF + YSOF0 + YSOF1 + YSOF2 + YBRAN + YCVOL + YTVOL + YCSUR + YTSUR + YCDIF + YTDIF + YKDN1 + YKDN2 + YBLAD + YLVR1 + YLVR2 + YR1 + YR2 + YR3 + YR4 + YSTMC + YSIC + YULIC + YLLIC + YURIN + YFECE + YSWET + YHAIR$
M	2	$TBODY1 = YPLAS + YRBC + YEVF + YSOF0 + YSOF1 + YSOF2 + YBRAN + YCVOL + YTVOL + YCSUR + YTSUR + YCDIF + YTDIF + YKDN1 + YKDN2 + YLVR1 + YLVR2$
M	3	$TBODY2 = YPLAS + YRBC + YEVF + YSOF0 + YSOF1 + YSOF2 + YBRAN + YCVOL + YTVOL + YCSUR + YTSUR + YCDIF + YTDIF + YKDN1 + YKDN2 + YBLAD + YLVR1 + YLVR2 + YR1 + YR2 + YR3 + YR4 + YSTMC + YSIC + YULIC + YLLIC$
M	4	$TSOFTALL = YSOFT + YKDNE + YLIVR + YBRAN + YBLUD + YEVF$
M	5	$BLDFRC = \frac{YBLUD}{TBODY1}$
M	6	$BONFRC = \frac{YSKEL}{TBODY1}$
M	7	$BRNFRC = \frac{YBRAN}{TBODY1}$
M	8	$HEPFRC = \frac{YLIVR}{TBODY1}$
M	9	$RENFRC = \frac{YKDNE}{TBODY1}$

No.		Equation
M	10	$OTHFRC = \frac{YSOFT}{TBODY1}$
N		**Growth and Tissue Volumes and Masses**
N	1	$WBODY = WBIRTH + \frac{WCHILD \cdot AGEYEAR}{HALF + AGEYEAR} + \frac{WADULT}{1 + KAPPA \cdot e^{-LAMBDA \cdot WADULT \cdot AGEYEAR}}$
N	2	$AMTBLD = VBLC \cdot WBODY \cdot 10$
N	3	$PLSVOL = AMTBLD \cdot (1 - BLDHCT)$
N	4	$RBCVOL = AMTBLD \cdot (BLDHCT)$
N	5	$BLDHCT_{AGEYEAR \le 0.01} = 0.52 + AGEYEAR \cdot 14$ $BLDHCT_{AGEYEAR > 0.01} = HCTA \cdot (1 + (0.66 - HCTA) \cdot e^{-(AGEYEAR - 0.01) \cdot 13.9})$
N	6	$VK = 1000 \cdot VKC \cdot (WBIRTH + WADULT + WCHILD) \cdot \left(\frac{WBODY}{WBIRTH + WADULT + WCHILD}\right)^{0.84}$
N	7	$KIDWT = VK \cdot 1.05$
N	8	$VL = 1000 \cdot VLC \cdot (WBIRTH + WADULT + WCHILD) \cdot \left(\frac{WBODY}{WBIRTH + WADULT + WCHILD}\right)^{0.85}$
N	9	$LIVWT = VL \cdot 1.05$
N	10	$VK = 1000 \cdot VKC \cdot (WBIRTH + WADULT + WCHILD) \cdot \left(\frac{WBODY}{WBIRTH + WADULT + WCHILD}\right)^{0.84}$
N	11	$TSKELWT = 1000 \cdot 0.058 \cdot WBODY^{1.21}$
N	12	$WBONE = 1000 \cdot 0.0290 \cdot WBODY^{1.21}$
N	13	$VBONE = 1000 \cdot 0.0168 \cdot WBODY^{1.188}$
N	14	$CVBONE = 0.8 \cdot VBONE$
N	15	$TVBONE = VBONE - CVBONE$
N	16	$CORTWT = \frac{WBONE \cdot CVBONE}{VBONE}$
N	17	$TRABWT = \frac{WBONE \cdot TVBONE}{VBONE}$

No.	Equation

See Appendix B for parameter name definitions and descriptions. Generally, prefix R indicates a rate constant from a compartment, prefix T indicates deposition fractions from plasma into a compartment, and prefix Y indicates mass in a compartment. Also see text (Section 2.3) for discussion of equations.

1

2

3

4

TABLE 2-3. RATE COEFFICIENTS FOR PB TRANSFERS IN AALM

Pathway	100 days	1 year	5 years	10 years	15 years	≥25 years
Plasma-D to EVF	1000	1000	1000	1000	1000	1000
Plasma-D to RBCs	297.1	406.9	425.1	366.9	300.6	480.0
Plasma-D to Plasma-B	0.495	0.678	0.709	0.611	0.501	0.800
Plasma-D to Urinary Bladder	0	0	0	0	0	0
Plasma-D to Small Intestine	7.429	10.171	10.629	9.171	7.514	12.000
Plasma-D to Trab Surf	96.00	57.60	56.83	89.50	132.25	88.96
Plasma-D to Cort Surf	384.0	230.4	199.2	268.5	341.8	71.0
Plasma-D to Liver 1	49.52	67.81	70.86	61.14	50.10	80.00
Plasma-D to Kidney 1	31.0	42.4	44.3	38.2	31.3	50.0
Plasma-D to Kidney 2	0.496	0.678	0.708	0.612	0.500	0.800
Plasma-D to ST0	103.3	141.5	148.4	128.0	104.9	177.5
Plasma-D to ST1	12.38	16.95	17.71	15.29	12.52	10.00
Plasma-D to ST2	1.238	1.695	1.771	1.529	1.252	2.000
Plasma-D to Brain	0.557	0.763	0.266	0.229	0.188	0.300
Plasma-D to Sweat	4.333	5.933	6.200	5.350	4.383	7.000
RBCs to Plasma-D	0.4620	0.7854	0.4986	0.1946	0.1390	0.1390
EVF to Plasma-D	333.3	333.3	333.3	333.3	333.3	333.3
Plasma-B to Plasma-D	0.139	0.139	0.139	0.139	0.139	0.139
Cort Surf to Plasma-D	0.65	0.65	0.65	0.65	0.65	0.50
Trab Surf to Plasma-D	0.65	0.65	0.65	0.65	0.65	0.50
Cort Surf to Exch Vol	0.35	0.35	0.35	0.35	0.35	0.50
Trab Surf to Exch Vol	0.35	0.35	0.35	0.35	0.35	0.50
Cort Exch Vol to Surf	0.0185	0.0185	0.0185	0.0185	0.0185	0.0185
Trab Exch Vol to Surf	0.0185	0.0185	0.0185	0.0185	0.0185	0.0185
Cort Exch Vol to Nonexch Vol	0.02311	0.02311	0.02311	0.02311	0.02311	0.02311
Trab Exch Vol to Nonexch Vol	0.02311	0.02311	0.02311	0.02311	0.02311	0.02311
Cort Nonexch Vol to Plasma-D	0.01644	0.00576	0.00308	0.00178	0.00102	0.00016

Pathway	100 days	1 year	5 years	10 years	15 years	≥25 years
Trab Nonexch Vol to Plasma-D	0.01644	0.00576	0.00362	0.00264	0.00191	0.00099
Liver 1 to Plasma-D	0.0312	0.0312	0.0312	0.0312	0.0312	0.0312
Liver 1 to Small Intestine	0.0312	0.0312	0.0312	0.0312	0.0312	0.0312
Liver 1 to Liver 2	0.00693	0.00693	0.00693	0.00693	0.00693	0.00693
Liver 2 to Plasma-D	0.000693	0.000693	0.001386	0.000570	0.000570	0.000570
Kidney 1 to Urinary Bladder	0.139	0.139	0.139	0.139	0.139	0.139
Kidney 2 to Plasma-D	0.000693	0.000693	0.000693	0.000190	0.000190	0.000190
ST0 to Plasma-D	2.079	2.079	2.079	2.079	2.079	2.079
ST1 to Plasma-D	0.00416	0.00416	0.00416	0.00416	0.00416	0.00416
ST1 to Excreta	0.00277	0.00277	0.00277	0.00277	0.00277	0.00277
ST2 to Plasma-D	0.00038	0.00038	0.00038	0.00038	0.00038	0.00038
Brain to Plasma-D	0.00095	0.00095	0.00095	0.00095	0.00095	0.00095

Coefficients are in units of d^{-1}. Coefficients from diffusible plasma (Plasma-D) are derived from the product of scaled deposition fractions and the rate coefficient for transfer from the diffusible plasma to all receiving compartments (RPLS, 2000 d^{-1}), from Equation 2.3-9.

Cort, cortical bone; Exch, exchangeable; EVF, extravascular fluid; Nonexch, nonexchangeable; Plasma-D, diffusible plasma; Plasma-B, Pb-bound plasma RBC, red blood cell; Surf, surface; ST0, ST1, and ST2, soft tissues with fast, moderate, and slow exchange rates, respectively, Trab, trabecular bone; vol, volume.

1

2

FIGURE 2-1. STRUCTURE OF AALM.FOR BIOKINETICS MODEL.

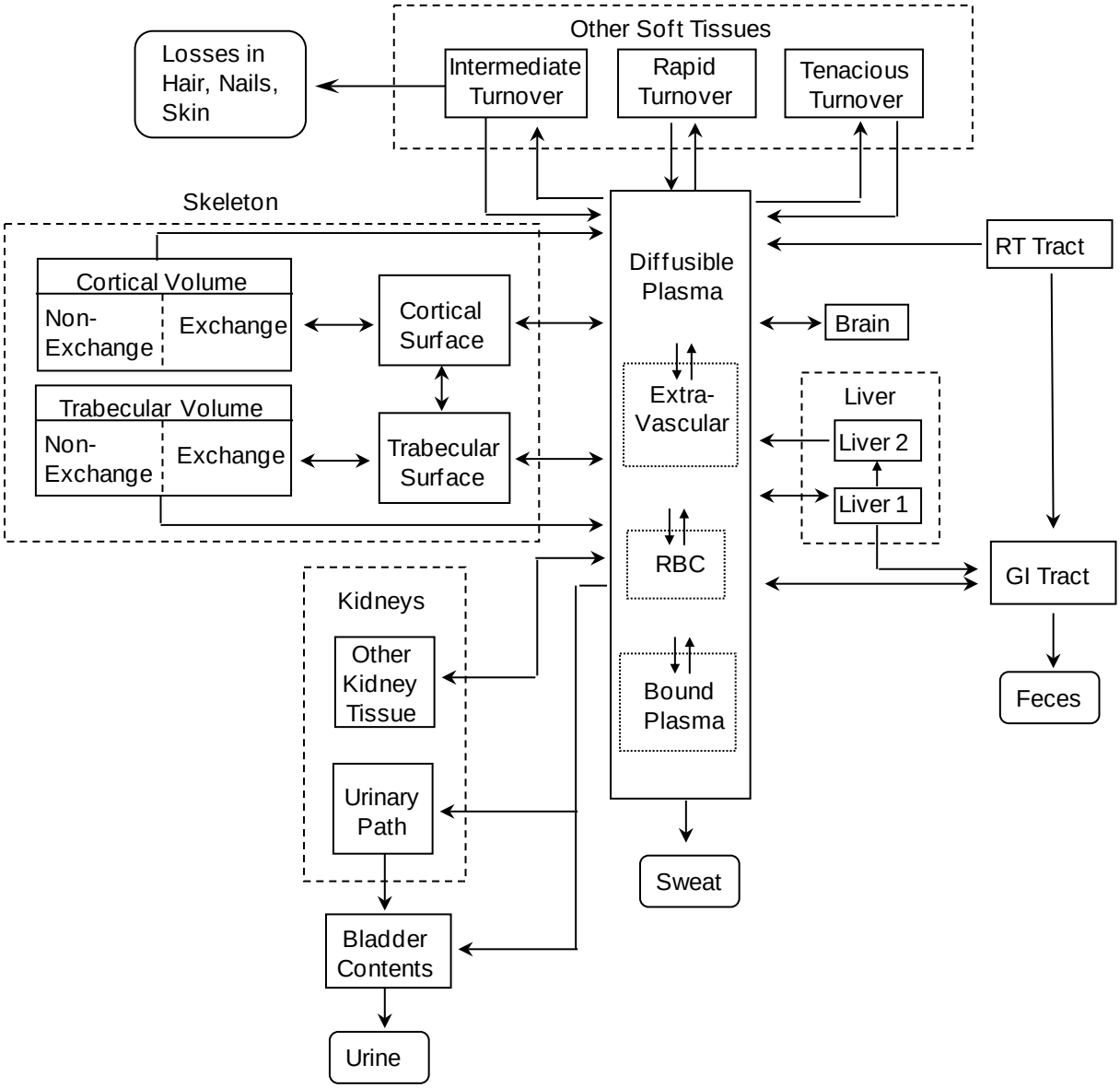

Based on Leggett (1993). Lines with arrows represent Pb transfers.

FIGURE 2-2. BODY AND TISSUE GROWTH IN THE AALM.FOR.

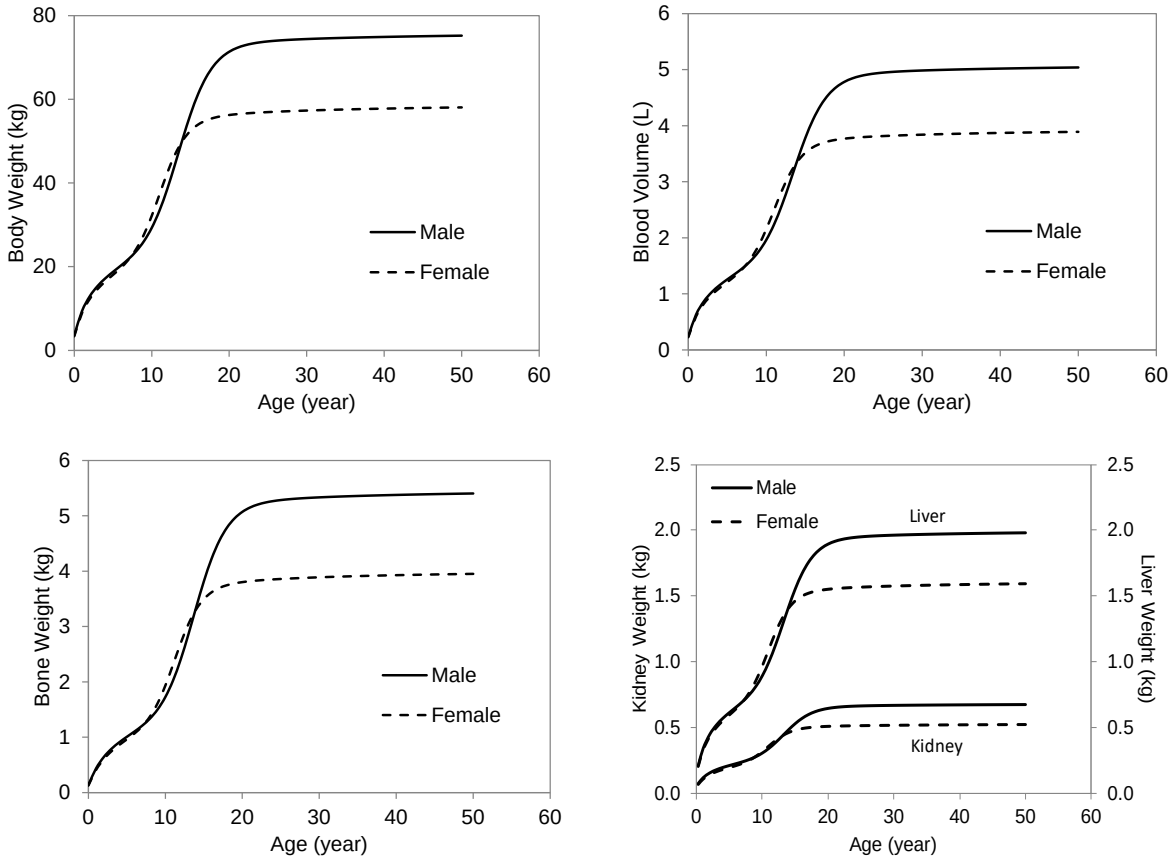

FIGURE 2-3. GASTROINTESTINAL ABSORPTION OF PB AS OPTIMIZED IN AALM.FOR.

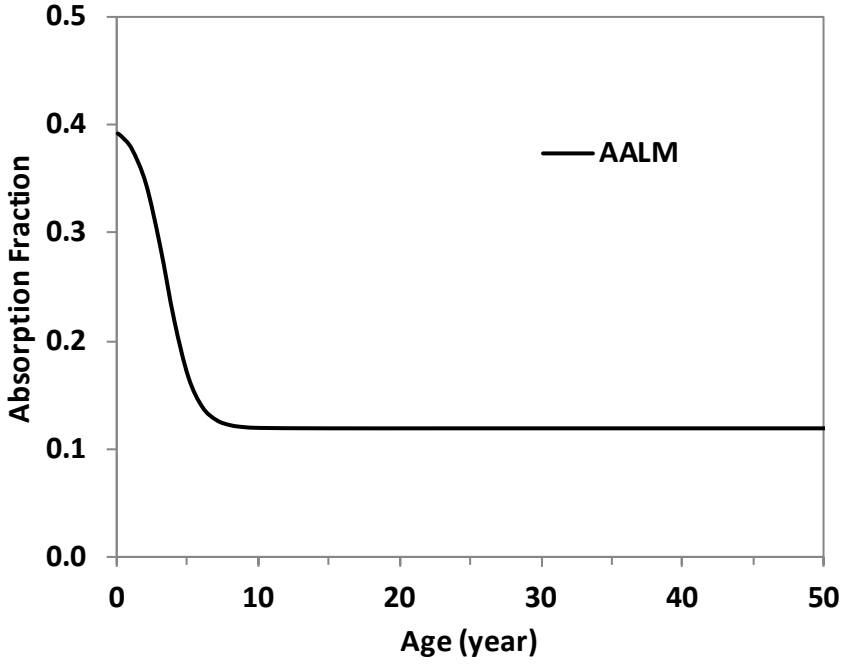

Optimization based on Ryu et al. (1983), Sherlock and Quinn (1986), Rabinowitz et al. (1976) and Maddaloni et al. (2005).

FIGURE 2-4. STRUCTURE OF AALM.FOR BONE MODEL.

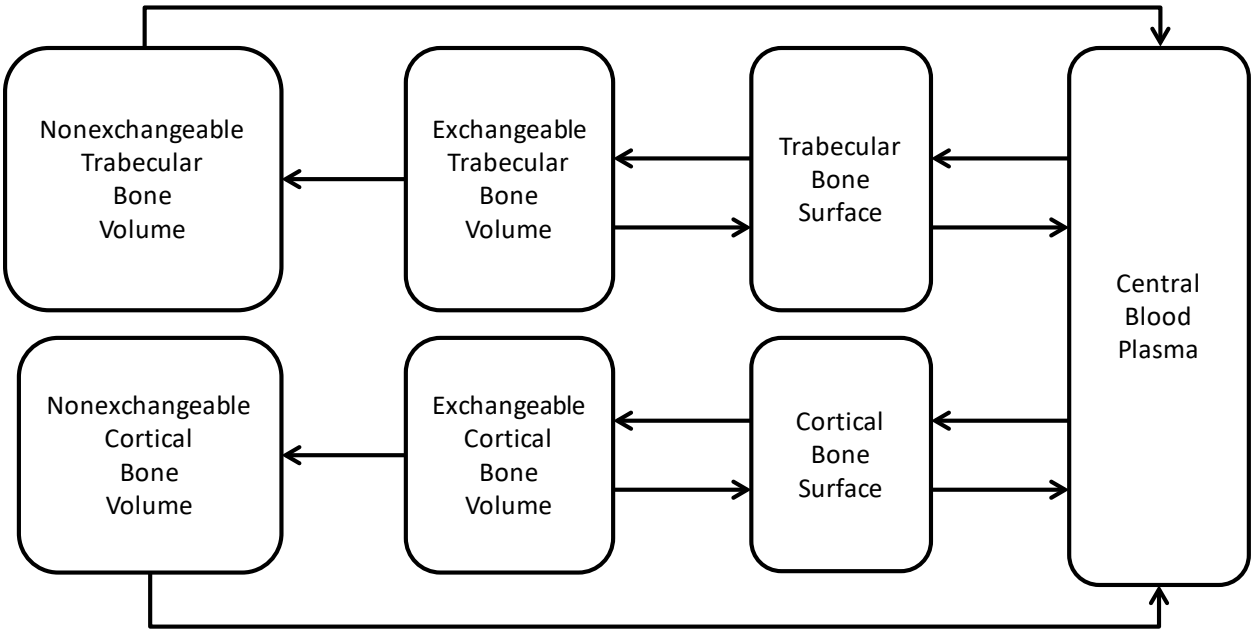

This figure is based on Leggett (1993).

CHAPTER 3. EVALUATION AND DEVELOPMENT OF AALM.FOR

3.1. INTRODUCTION AND OJBECTIVES OF THIS ANALYSIS

In 2014, EPA released the report Framework for Identifying and Evaluating Lead-Based Paint Hazards from Renovation, Repair, and Painting Activities in Public and Commercial Buildings (U.S. EPA, 2014c) which described how EPA could identify and evaluate hazards in public and commercial buildings. The framework report was followed by a more detailed Approach for Estimating Exposures and Incremental Health Effects due to Lead During Renovation, Repair and Painting Activities in Public and Commercial Buildings (U.S. EPA, 2014b) and appendices (U.S. EPA, 2014a). The latter report describes in greater detail an approach to estimating potential environmental concentrations, Pb body burdens, and incremental health effects related to exposure to Pb from renovations of public and commercial buildings. A key element in the approach was a Monte Carlo Analysis of Pb exposure scenarios and predicted blood and bone Pb concentrations in children and adults. Blood and bone Pb were predicted using an implementation of the Leggett (Pounds and Leggett, 1998; Leggett, 1993) biokinetics model (Leggett Fortran Model, LFM). Several modifications were made to the LFM to improve its performance and facilitate the Monte Carlo Analysis. The results of these modifications produced ICRPv005.FOR, also referred to as Leggett Model Version 5 (https://www.epa.gov/lead/approach-estimating-exposures-and-incremental-health-effects-lead-due-renovation-repair-and). In developing ICRPv005.FOR, several changes were made to the Leggett biokinetics model (Table 3-1). ICRPv005.FOR performed well when evaluated using the NHANES data for children and occupational Pb smelter data for adults, indicating good agreement with both these measured data sources and IEUBK model estimates. As part of the response to peer review comments on the approach, EPA undertook the analyses described in another report (Post-Meeting Peer Review Summary Report, Versar, 2015).

In the months following EPA OPPT's release of the Approach for Estimating Exposures and Incremental Health Effects due to Lead During Renovation, Repair and Painting Activities in Public and Commercial Buildings document, EPA ORD NCEA completed a beta test version of the All Ages Lead Model (AALM.CLS; v. 4.2, July 2015) which also implemented an updated and expanded version of the Leggett model (Pounds and Leggett, 1998; Leggett, 1993) in Advanced Continuous Simulation Language (ACSL; a.k.a. acslX). The development of AALM.CSL included calibration and evaluation of model performance that are described in Chapter 4 using several data sets that were of potential value for further evaluations of the ICRPv005.FOR model. EPA was also interested in exploring differences in the structures and predictions of blood and bone Pb from the two models. In part, to determine if one or the other model might offer advantages for applications in predicting Pb body burdens related to public and commercial building renovations as well as other potential research and regulatory applications of the models for predicting exposure-body burden relationships.

This chapter summarizes results of analyses undertaken by EPA to explore differences in the structures and predictions of blood and bone Pb between AALM.CSL and ICRPv005.FOR. The specific objectives of these analyses were as follows:

- Conduct further evaluations of ICRPv005.FOR and AALM.CSL;
- Modify the models as needed, based on the outcome of these evaluations; and
- Harmonize the two models so that the models predict similar blood and bone Pb levels for similar exposure inputs.

A detailed description of the structure of the AALM.FOR is provided in Chapter 2.

Within this chapter, Section 3.2 compares predictions of blood and bone Pb concentrations obtained from the models. Section 3.3 describes the outcomes of comparisons of model predictions to observations. Section 3.4 discusses data needs for potential further refinement and evaluation of the models. Section 3.5 summarizes conclusions from the model comparisons, model harmonization and responses to peer review comments on approaches to blood and bone Pb modeling.

3.2. MODEL PREDICTIONS OF BLOOD AND BONE PB

Differences in the parameter values used in ICRPv005.FOR and AALM.CSL biokinetics models (Table 3-2) resulted in different predictions of blood and tissue Pb levels for similar Pb exposure assumptions. Ultimately it was decided to harmonize the two models and a Fortran version (AALM.FOR) of AALM.CSL was created. Thus, Table 3-2 essentially provides the changes in ICRPv005.FOR that were required to create AALM.FOR. The AALM.FOR and AALM.CSL implementations are structurally identical and have only few differences in parameter values and computational schemes that do not affect simulations of blood and bone Pb concentrations (Table 3-3). The most important changes made to ICRPv005.FOR to create AALM.FOR include the following: (1) Growth parameters from O'Flaherty (1995, 1993) were adopted in AALM.FOR, this results in identical age profiles for blood volumes and tissue masses between the models (see Chapter 2, Figure 2-2); and (2) GI absorption parameters from AALM.CSL were adopted in AALM.FOR (see Section 4.7.1 and Figure 4-13). The GI absorption fraction is 0.39 at birth and decreases to 0.12 at age 8 years (Figure 3-1). All other parameter values (e.g. transfer rates and deposition fractions) from AALM.CSL were adopted in AALM.FOR.

Two types of comparisons were made of ICRPv005.FOR and AALM: (1) age profiles for blood and tissue Pb levels following an exposure to a constant Pb intake (µg/day) were simulated and compared; and (2) dose-response relationships between ingested dose and Pb levels were compared by simulating a series of increasing Pb intakes. In either type of simulation, parameters that control Pb absorption and growth were set to the same values, so that differences in blood and tissue Pb levels could be attributed entirely to differences in the simulation of systemic (post-absorption) biokinetics.

3.2.1. Constant Pb Intake

Figures 3-2 and 3-3 show simulations of the accrual and elimination of Pb in blood and bone, respectively, in children and adults. Exposures were simulated as a constant baseline Pb intake (5 µg/day) with a period of elevated intake (40 µg/day in children and 105 µg/day in adults). This exposure results in predicted blood Pb concentrations ≤5 µg/dL, which is well below the concentration at which saturation of uptake into RBCs significantly affects blood Pb levels. Several differences are evident from these comparisons:

- The harmonized AALM.FOR and AALM.CSL produce identical predictions of blood and bone Pb concentrations.
- The AALM predicts higher blood and bone Pb concentrations than ICRPv005.FOR. The difference is more pronounced in the adult simulation (Figure 3-2).
- The AALM predicts a slower approach to a quasi-state state blood Pb concentration than ICRPv005.FOR and slower elimination and return to baseline (Figure 3-2). The difference is

more pronounced in the adult simulation. The AALM predicts a return to baseline over a period of decades in adults; whereas, ICRPv005.FOR predicts a return to baseline within one year.

- The pattern of decline in blood Pb concentration following an abrupt decrease in Pb intake is also different in the AALM and ICRPv005.FOR. Both models predict multi-phasic elimination of Pb from blood in children (Figure 3-2A); however, the AALM predicts an early rapid phase, followed by a slower phase; whereas, ICRPv005.FOR predicts a slower early phase, followed by more rapid phase.
- The AALM predicts similar cortical and trabecular bone Pb concentrations in children; whereas, ICRPv005.FOR predicts trabecular bone Pb concentrations that are approximately 25% of cortical bone (Figure 3-3A, 8C).
- The AALM and ICRPv005.FOR predict higher Pb concentrations in adult trabecular bone, compared to cortical bone, and slower accrual and elimination kinetics in cortical bone (Figure 3-3 B, D).
- The AALM predicts faster elimination of Pb from adult cortical bone compared to ICRPv005.FOR (Figure 3-3B).

3.2.2. Dose-Response for Blood and Bone Pb

Although both the AALM and ICRPv005.FOR model are mathematically linear models (i.e., all compartment Pb masses are defined with linear differential equations), they predict curvilinear dose-response relationships for blood Pb resulting from a saturable capacity of RBCs to take up Pb. Dose-response relationships predicted from AALM.CSL, AALM.FOR and ICRPv005.FOR are shown in Figures 3-4 for blood and 3-5 for bone, in children (age 2 years) and adults (age 30 years). In the AALM, curvature in the intake-blood Pb relationship is negligible at blood Pb concentrations <10 µg/dL. Both models predict linear dose-response relationships for bone Pb.

3.3. COMPARISONS OF MODEL PREDICTIONS TO OBSERVATIONS

Peer reviewers of Approach for Estimating Exposures and Incremental Health Effects due to Lead During Renovation, Repair and Painting Activities in Public and Commercial Buildings (U.S. EPA, 2014b) suggested that data be used to evaluate blood and bone Pb predictions in adults from Hattis (1981) and Nie et al. (2005), including additional unpublished Nie et al. data.

Data that were available from the Nie study consisted of three longitudinal blood and bone XRF measurements for 209 adult Pb workers. The measurements were made in 1991, 1999 and 2008. This period included a nine-month strike (July 1990 to May 1991), during which exposures at the plant were interrupted. The available data also included birth dates and dates of hire. There were no data on actual exposures at the plant. Although attempts were made to reconstruct exposures so that blood and bone Pb concentrations could be predicted and compared to observations, ultimately, it was concluded that the data were not suitable for model evaluations because of the uncertainty in the exposures that preceded the blood and bone Pb measurements and that occurred during the measurement period. Exposures prior to 1991, including the period of the strike, had to be reconstructed with no basis for verification other than the observed blood and bone Pb measurements. In one reconstruction attempted, each subject was assumed to have an age-intake profile that predicted an age-blood Pb profile that was similar to the

central estimates from the NHANES survey that corresponded to the subject's age date. Added to this background intake was a constant occupational intake (except during the strike) that was calibrated to achieve a good fit to the weighted MSE for observed bone Pb (tibia and calcaneus) and blood Pb (relative weights: cortical bone 3, trabecular bone 2, blood 1). This fitting procedure resulted in good agreement between cortical and trabecular bone Pb predicted from ICRPv005.FOR and corresponding observations ($r^2 > 0.8$). However, a good fit to the observations could be expected for a wide range biokinetics parameter settings; therefore, these data would not allow a determination of whether ICRPv005.FOR or the AALM would perform better at predicting the observations.

Data that were available from the Hattis study were much more suitable for model evaluation. These data included blood Pb concentrations in 57 workers at hire and prior to and following a nine-month strike. Although pre-hire exposures were unknown, it was possible to calibrate the post-hire and pre-strike exposures to achieve agreement with blood Pb concentrations at the time of hire and just prior to the strike, and then predict without further calibration the post-strike blood Pb. Agreement between post-strike observations and predictions would be sensitive to biokinetics parameter settings that control blood Pb elimination rates. Therefore, these data were used to compare performance of ICRPv005.FOR and AALM. The outcome of this comparison indicated that the AALM performed better at predicting the Hattis observations than ICRPv005.FOR (described in detail in Section 3.3.1). Based on these evaluations, a Fortran version of the AALM (AALM.FOR) was developed and additional evaluations of AALM.FOR and AALM.CSL were conducted. These evaluations are described in Sections 3.3.2 to 3.3-10.

Goodness of fit of model predictions to observations were evaluated three approaches: (1) visual inspection of observed and predicted values; (2) inspection of standardized residuals (Equation 3-1); and (3) r^2 for the least-squares linear regression of observed and predicted values.

$$Standardized\ Residual = \frac{Predicted - Observed}{Standard\ Deviation\ of\ Observed\ Mean} \qquad \text{Eq. (3-1)}$$

Standardized residuals $\leq \pm 2$ and $r^2 > 0.70$ were considered acceptable fit to the observations.

3.3.1. Pb Elimination Kinetics in Workers with Dose Reconstruction (Hattis Data)

The Hattis data set used in this analysis included the following data on 57 adult Pb workers: (1) duration of employment prior to strike (Days_prestrike); (2) blood Pb concentration prior to start of employment (BLL_start); (3) blood Pb just prior to a nine-month strike (BLL_prestrike); and (4) blood Pb on return to work, following strike (BLL_poststrike). The 57 subjects comprised a subset of the 66 subjects in the dataset described in Hattis (1981). Subjects were excluded from the analysis if pre-strike blood Pb was >75 µg/dL, post-strike blood Pb was < blood Pb at date of hire, or post-strike blood Pb was > pre-strike blood Pb. In the absence of information on pre-employment Pb exposures, pre-hire Pb intake was simulated as a constant ingestion intake (µg/day/kg body weight) that would result in a predicted blood Pb concentration at age 20 years that was similar to BLL_start (±1 µg/dL). Pre-strike occupational exposure was simulated as a constant ingestion intake (µg/day) that would result in a predicted blood Pb concentration at age = (20 years + duration of strike) that was similar to BLL_start (±1 µg/dL). During the strike (assumed to be 270 days in duration), ingestion intake reverted to the pre-hire Pb intake.

An example of a simulation for a single subject from the Hattis data is shown in Figure 3-6 for AALM.CSL. In this simulation, the pre-hire Pb intake and pre-strike exposure intake were calibrated to

predict blood Pb concentrations similar to the observations made at the time of hire and at the start of the strike. In this case, the predicted post-strike blood Pb concentration (18.5 µg/dL) was within 10% of the observed (17.0 /dL). A pseudo first-order elimination rate (d^{-1}) and $t_{1/2}$ were estimated from the observed blood Pb concentrations at the beginning and end of the strike as follows (Equations 3-2 and 3-3):

$$k = \ln\left(\frac{BLL\ pre-strike}{BLL\ post-strike}\right)/270 \qquad \text{Eq. (3-2)}$$

$$t_{1/2} = \frac{\ln(2)}{k} \qquad \text{Eq. (3-3)}$$

The $t_{1/2}$ calculated from the blood Pb concentrations predicted from the model and observations were 371 days and 320 days, respectively. The calculated values for $t_{1/2}$ do not reflect the actual elimination kinetics of Pb from blood in this subject, or predicted from the AALM, because both would be expected to be multi-phasic over the 270-day interval. However, it serves as a convenient metric for comparing model performance when applied to the entire set of 57 subjects.

Both ICRPv005.FOR and AALM.CSL were successfully calibrated to the blood Pb concentrations measured at time of hire and just prior to the strike (r^2 = 1.0). Predicted and observed post-strike blood Pb concentrations were also correlated, but showed substantially more variability that could not be accounted for by the models, as expected for model predictions (r^2 = 0.47; Figure 3-7).

Figure 3-8 shows the distribution of calculated $t_{1/2}$ values for the Hattis subjects. Summary statistics for the evaluation are presented in Table 3-4. The median $t_{1/2}$ predicted from the observations was 633 days (GSD 2.4). The median from AALM.CSL was 483 days (GSD 1.6) and the median from ICRPv005.FOR was 274 days (GSD 1.6). The average difference between the individual observed and predicted $t_{1/2}$ values was -5% for AALM.CSL and -37% for ICRPv005.FOR. AALM.FOR predicted $t_{1/2}$ (median 465 days, GSD 1.6; percent difference -8%) that were similar to AALM.CSL prediction.

3.3.2. Pb Elimination Kinetics in Workers with Dose Reconstruction (Nilsson et al., 1991)

Nilsson et al. (1991) reported longitudinal data on blood and finger bone Pb concentrations in 14 Pb workers for period ranging from 8–18 years following cessation of their occupational exposures. The median blood Pb concentration at the end of exposure was approximately 45 µg/dL. The decline in bone Pb concentration was described by a first-order model with a single rate constant. Estimates of elimination half-times for each individual were reported. The group median was 16 years (95% CI: 12, 23). The decline in blood Pb was described by a tri-exponential model with the following parameters.

Parameter	Unit	C1 (95% CI)	C2 (95% CI)	C3 (95% CI)
$t_{1/2}$	year	34 day (29, 41)	1.2 year (0.85, 1.8)	13 year (10, 18)
C	µg/dL	10.2	12.6	22.8

AALM simulations were run for a constant Pb intake from birth to age 60 years, to achieve a terminal blood Pb concentration of approximately 45 µg/dL (2000 µg/day), followed by 20 years without exposure. A first-order exponential rate was estimated for the decline in cortical bone Pb concentrations predicted for 20 years following cessation of exposure. Figure 3-9 compares rates of elimination of Pb from bone and blood with the corresponding empirical models derived for the Pb workers (Nilsson et al., 1991). Elimination rates of Pb from bone predicted from the optimized models are within the 95% CI of the empirical model and yield standardized residuals that range within the -2, 2, criteria ($r^2 = 0.99$). Elimination half-times predicted for bone Pb (16 years) were identical to estimates from Nilsson et al. (1991). Although elimination rates from blood predicted by the optimized models are approximately at the confidence limits of the empirical model, the initial model divergence is due largely to the slower elimination kinetics observed during the first 5 years following cessation of exposure; after which the models converge on the empirical model ($r^2 = 0.96$). Half-times predicted for the period 5 to 20 years after exposure were 1.25 years, similar to values predicted for C2 (1.2 year) from Nilsson et al. (1991).

3.3.3. Blood Pb Accrual and Elimination Kinetics in Adults with Known Pb Doses (Rabinowitz et al., 1976)

Rabinowitz et al. (1976) conducted a pharmacokinetics study in which four adults ingested daily doses of [207Pb] nitrate for periods up to 124 days. Concentrations of 207Pb in blood, urine, and feces were then monitored during and following cessation of exposure, and data on daily intakes and blood concentrations for each subject were reported. Absorption fractions for Pb were estimated for each individual based on mass balance in feces.

Figure 3-10 compares observed and predicted blood 207Pb concentrations from AALM.FOR and AALM.CSL. Gastrointestinal absorption fractions were set in both models to the estimates for each individual reported in Rabinowitz et al. (1976). No other changes were made to parameter values. Both models predicted the rise and decline in blood Pb concentrations in temporal patterns that agreed with observations. Values for r^2 for AALM predictions are 0.99, 0.98, 0.92, and 0.97 for Subjects A, B, D, and E, respectively.

3.3.4. Post-mortem Soft Tissue-to-Bone Pb Ratio (Barry, 1975)

Four studies provide data for measurements of post-mortem soft tissue and bone Pb concentrations (Gerhardsson et al., 1995; Barry, 1981, 1975; Gross et al., 1975). Gerhardsson et al. (1995) reported only soft tissue Pb concentrations; whereas, the other three studies reported soft tissue and bone Pb concentrations that can be used to estimate the ratios. Barry (1981, 1975) reported data for children and adults in age brackets, so the data from Barry (1975) was used as the primary source to optimize parameters for kidney/bone and liver/bone Pb ratios as a function of age. Barry (1975) reported data on tibia Pb concentrations that are simulated as cortical bone concentrations in the AALM models. Since Barry (1975) reported group mean tissue concentrations (not ratios in autopsy cases), the mean tissue-to-bone ratios were approximated from the group means. Figure 3-11 compares predicted and observed kidney/bone and liver/bone Pb ratios in adults. Values for r^2 for kidney/bone predictions (of average of male and female ratios) were 0.95. Values for r^2 for liver/bone predictions were 0.96 and 0.93 for AALM, respectively.

3.3.5. Plasma-to-Bone Pb Ratio in Workers (Hernandez-Avila et al., 1998; Cake et al., 1996)

Two studies provide data to evaluate the relationship between plasma or serum blood Pb and bone Pb concentrations (Hernandez-Avila et al., 1998; Cake et al., 1996). Cake et al. (1996) measured paired serum, tibia, and calcaneus Pb concentrations in 49 adult male Pb workers, and reported corresponding linear regression parameters. Hernandez-Avila et al. (1998) measured paired plasma, tibia and patella Pb concentrations in 26 adults (20 female) who had no known occupational exposures to Pb. These data can be used to derive corresponding linear regression parameters for the log-transformed plasma Pb. Individual subject data were digitized from Figure 1 of Hernandez-Avila et al. (1998), and linear regression parameters derived for the untransformed plasma Pb concentrations, in order to compare these with the linear regression parameters from Cake et al. (1996).

Bone Pb/plasma Pb slopes at age 50 years were predicted from the AALM for a series of simulations in which Pb intake was varied from 1 to 1000 µg/day. Table 3-5 and Figure 3-12 compare predicted and observed slopes based on data from Cake et al. (1996) and Hernandez-Avila et al. (1998). The bone/plasma ratios predicted from the AALM were within the 95% CI of the Cake et al. (1996) estimates and were also within the 95% CI of the Hernandez-Avila et al. (1998) for tibia.

3.3.6. Plasma Pb – Blood Pb Relationship (Meta-data)

Six studies provided data on individual human subjects that can be used to evaluate the relationship between plasma Pb and blood Pb concentrations. Measurements of plasma Pb were made using either inductively coupled plasma mass spectrometry (Smith et al., 2002; Bergdahl et al., 1999; Bergdahl et al., 1998; Hernandez-Avila et al., 1998; Bergdahl et al., 1997; Schutz et al., 1996) or stable isotope dilution with thermal ionization mass spectrometry (Manton et al., 2001). In all of these studies, methods were employed to control for sample contamination, which is of particular importance in measurements of the low Pb levels found in plasma. Taken together, the observations from these reports varied over a wide range of blood Pb (approximately 0.34–94.8 µg/dL) and plasma Pb (approximately 0.0014–1.92 µg/dL) levels. These studies provided 406 individual measurements of plasma Pb and blood Pb, in adult workers as well as individuals with no known history of occupational exposure to Pb (SRC, 2003). Only one study provides similar data in children (Bergdahl et al., 1999). The observations in children do not appear to differ substantially from those for adults.

A best fit (least-squares) model for combined data from the above six studies was identified, and is presented in Equation 3-4:

$$Blood\ Pb = 87.0 \cdot Plasma\ Pb^{0.5} - 3.89 \quad (r^2=0.90) \qquad \text{Eq. (3-4)}$$

Figures 3-13 compares the observed and predicted plasma-whole blood Pb relationship in adults. Standardized residuals for the optimized models are within acceptable limits (-2, 2). The r^2 values for predictions are 0.99 and 0.98.

3.3.7. Blood Pb Elimination Kinetics in Infants with Known Doses (Sherlock and Quinn, 1986; Ryu et al., 1983)

Only two studies provide data on the relationships between Pb dose and blood Pb concentration in infants (Sherlock and Quinn, 1986; Ryu et al., 1983). In the Ryu et al. (1983) study, blood Pb concentrations were monitored in 25 formula-fed infants. From birth to age 111 days, infants were fed formula

(packaged in cartons) that had a Pb concentration of approximately 20 µg/L. From age 112 to 195 days, a subset of the infants (n = 7) were switched to formula (packaged in cans) that had a Pb concentration of approximately 57 µg/L. Formula intakes were measured, and provided estimates of Pb intakes in each subject. Ryu et al. (1983) reported a table of individual Pb intakes, and presented a figure illustrating group mean blood Pb concentrations at various ages (these data were digitized for use in this analysis). Standard errors (or deviations) of mean blood Pb concentrations were not reported; however, as discussed below, based on Sherlock and Quinn (1986), standard errors may have been approximately 10% of the means. The parameter for maternal blood Pb concentration was set at 10 µg/dL, the reported maternal mean for the study. Lead absorption was not quantified in Ryu et al. (1983); therefore, the gastrointestinal absorption fraction during infancy was set to 40%, based on estimates from mass balance studies (Ziegler et al., 1978). No other changes were made to parameter values. Figure 3-14 compares predicted and observed blood Pb concentrations for the two exposure regimens (carton formula or carton followed by canned formula). Simulations are shown for the mean intake (12–20 µg/day) and ± 1 SD (10–18 µg/day, 15–22 µg/day). AALM.CSL and AALM.FOR simulations encompass most of the observations within ±1 SD of the mean intakes. If standard errors of mean blood Pb concentrations were 10% of the mean, standardized residuals for AALM predictions ranged from -3.7 to 0.15 for carton exposures (mean -1.2). The AALM captures the increase in blood Pb concentration associated with the switch the higher Pb intakes for canned formula and the overall temporal trends in the observations; r^2 for predictions were 0.85.

Sherlock and Quinn (1986) measured blood Pb concentration in 131 infants at age 13 weeks and estimated dietary intake of Pb for each infant based on Pb measurements made in duplicate diet samples collected daily during week 13. Sherlock and Quinn (1986) provided a plot of blood Pb means and standard errors for group mean dietary Pb intakes (these data were digitized for use in this analysis). The parameter for maternal blood Pb concentration was set at 18 µg/dL, the reported maternal geometric mean. The gastrointestinal absorption fraction was set at 40% for infants; the same value used in simulations of Ryu et al. (1983). Figure 3-15 compares predicted and observed blood Pb concentrations for the range of Pb intakes in the study. AALM.CSL and AALM.FOR models reproduce the general shape of the observed curvilinear dose-blood Pb relationship; the apparent plateau observed at the higher end of the dose range, however, it is achieved at higher doses in the models (>800 µg/day). Although the model results for the plateau contributed to high residuals at the highest Pb intake (>200 µg/day), standardized residuals for lower Pb doses ranged from -4.8 to 1.5 (mean -2.3). The overall dynamics of increasing blood Pb with increasing Pb dose was predicted with $r^2 = 0.95$. One possible explanation for the higher plateaus in the dose-blood Pb relationship predicted from both models is that the models may estimate higher saturation levels of Pb in RBCs than actually occurred in the infants in the Sherlock and Quinn (1986) study. Parameter values for RBC uptake are based on data collected on adults, and have not been optimized for infants due to an absence of good supporting data (see Section 3.3.6).

3.3.8. Blood Pb Elimination Kinetics in Infants with Dose Reconstruction (ATSDR)

Agency for Toxic Substances and Disease Registry (ATSDR) made available for this analysis longitudinal blood Pb data in children following intervention in response to measurement of an elevated blood Pb concentration. The data included dates of birth and dates and results of repeated Pb measurements in 12 females and 12 males. Interventions included interruption of the exposure which allows an evaluation of elimination kinetics of blood Pb. However, other interventions may have also been conducted but were not documented in the data made available for this analysis. Intervention is

likely to have included chelation therapy in children whose blood Pb concentration exceeded 45 µg/dL. Chelation would be expected to have affected rates of decline in blood Pb concentration during the first 1-3 weeks following the diagnosis of elevated blood Pb. The longitudinal blood Pb data available for longer periods would reflect post-chelation kinetics and are suitable for evaluating model predictions of blood Pb elimination kinetics.

Since actual exposures to Pb were unknown for each child, the exposures leading up to the first blood Pb measurements were reconstructed as a constant baseline Pb intake (µg/day) that resulted in a blood Pb concentration of 5 µg/dL at age 6 months. Selection of 5 µg/dL as the target for the baseline simulation is supported by the observations that that average terminal blood Pb concentration was 5.5 µg/dL (±2.4 SD, n = 24). Some children had blood Pb concentrations reported prior to an episode of elevated blood Pb concentrations; the mean was 5.3 µg/dL (±2.4 SD, n = 4). Another uncertainty is the reconstruction of the level and duration of the elevated exposure that occurred prior to the detection of the elevated blood Pb. Since there was no information about the exposure level or duration, these were parameters were calibrated to the blood Pb observations to achieve optimal residuals and r^2 for the predictions. Examples of successful exposure constructions are shown in Figures 3-16 to 3-18. Although, there is considerable uncertainty about the reconstructed exposures, in each case, the AALM simulated the blood Pb elimination kinetics from observations well beyond the expected period of chelation. Figure 3-18 shows one of the few cases in which a baseline blood Pb measurement was available prior to the elevated exposure. The timing of this baseline measurement considerably decreases the uncertainty about the duration of the elevated exposure. Since the baseline measurement was made at age 450 days and first elevated blood Pb was measured at age 810 days, the duration was likely to have been no more than 360 days. The optimized duration (age day 600 – 800) and exposure level (13,000 ppm Pb in dust) provided a good fit to the observed elimination kinetics (r^2 0.81). The simulations shown in Figures 3-16 to 3-18 are examples of one approach to reconstructing the Pb exposures that occurred prior to the blood Pb observations.

3.3.9. Comparison to IEUBK Model for Pb in Children

Figure 3-19 compares predictions of the AALM and the IEUBK model for a continuous dust Pb intake of 10 µg/day. In both models, the relative bioavailability (RBA) for Pb in dust was assumed to be 60%. This corresponds to an absolute bioavailability of approximately 20% at age 2 years in the AALM and 30% in the IEUBK model. At age 2 years the IEUBK model predicts a blood Pb concentration of 1.18 µg/dL; the AALM predicts 1.25 µg/dL.

3.3.10. Comparison to Adult Lead Methodology

Figure 3-20 and Table 3-6 compare predictions of adult blood Pb concentrations from the Adult Lead Methodology and AALM, for an exposure to 1000 ppm. In both models, the RBA for Pb in dust was assumed to be 60%. This corresponds to an absolute bioavailability of approximately 4.8% in the AALM and 12% in the Adult Lead Methodology. The Adult Lead Methodology predicts a blood Pb concentration of 2.9 µg/dL; the AALM predicts 3.1 µg/dL at age 30 years (mid-point for age range in the Adult Lead Methodology, 17-45 years).

3.4. DATA NEEDS FOR FURTHER REFINEMENT OF THE AALM

The AALM.FOR model discussed in this report demonstrates the considerable advancements that have been made since a development of ICRPv005.FOR in terms of its capability and evaluation predictions of Pb body burdens, including blood Pb concentrations in children and blood and bone Pb concentrations in adults. Blood Pb concentrations in adults predicted from the AALM are very similar to predictions from the EPA Adult Lead Methodology (ALM) for the same soil Pb concentrations. Predictions for infants are similar between the AALM and the IEUBK. Work done to date has been responsive to comments received on both models from peer reviews conducted in 2005 and 2014 (see Section 3.5).

Recommendations for data to reduce uncertainty in the predictions obtained from AALM.FOR and AALM.CSL, and improve the consistency among all model predictions include the following:

- *Further verify AALM predictions.* Additional observations in humans should be identified that can serve to evaluate the performance of the optimized AALM (and that were not used in the optimization). Ideally, these would be blood and/or bone Pb measurements in people for whom Pb intakes are known with reasonable certainty. Ethical concerns typically preclude Pb dosing experiments; therefore, Pb doses must be estimated with accurate tools such as duplicate diet surveys or dietary recalls and information on Pb levels in diet and other relevant exposure media. Types of data that would be valuable for model validation include: (1) blood soft tissue or bone Pb levels in children or adults for whom Pb dosage is known or can be reliable estimated from exposure data; (2) changes in blood, soft tissue or bone Pb levels in children or adults following and abrupt change (increase or decrease) in Pb exposure; (3) steady state (or quasi-steady state) blood/soft tissue blood/bone Pb ratios in children or adults; (4) urinary Pb clearance from blood or plasma in children or adults; and (5) plasma/whole blood concentration ratios in children.

- *Evaluate and document the empirical basis for exposure model parameters.* Most of the exposure parameter values currently in the AALM serve as placeholders and should, in the future, be replaced with default values for specific receptor populations for which an empirical basis can be provided.

- *Further refine the gastrointestinal tract model*. AALM.FOR allows the user to input values for RBA of Pb in exposure media. This is important for risk assessment applications because the absorption fraction Pb is known to vary with the environmental medium in which it is contained (e.g. Pb in soil can have a lower absorption fraction than Pb dissolved in water). However, in the current version of AALM.FOR, the RBA adjustment is applied to the media-specific Pb intake rather than to the absorption fraction (*F1*) in the small intestine (see Section 2.2.3). In this configuration, Pb that is not absorbed when RBA is <1 does not appear in feces. This will result in an underestimation of fecal Pb excretion and a negative mass balance (excretion < intake). A model that adjusts the absorption fraction by RBA would provide a more accurate representation of medium-specific absorption and excretion of Pb. This would be similar to the modeling approach to RBA that is contained in AALM.CSL.

- *Further refine the respiratory tract (RT) model*. The current version of AALM.FOR uses a 4-compartment RT model from the Leggett (1993) model in which Pb intake to the RT represents the deposited dose (µg Pb deposited in the RT per day), which must be calculated outside of AALM.FOR for a given set of assumptions regarding the air Pb concentration (µg/m^3), inhaled

particle size and minute (day) and volume day volume (m^3/day). A model that would use inputs of air Pb concentration, particle size and Pb species would be more useful for applications to simulating air Pb exposures. This could be similar to the simplified version of the ICRP (1994) model that was implemented in the beta test version of AALM.CSL (v. 4.2, July 2015).

- *Refinement of the bone mineral model*. The AALM includes calculations for converting concentrations of Pb in bone wet weight to concentration per g bone mineral by dividing the wet weight concentration by the ash fraction of bone. This conversion is important for comparing model predictions of bone Pb concentrations with bone X-ray fluorescence (XRF) data, which is typically reported in units of Pb per g bone mineral. In AALM.CSL, bone ash fractions were assumed to be 0.55 and 0.50 for cortical and trabecular bone, respectively (ICRP, 1981). In ICRPv005.FOR, the bone ash fractions were assumed to be 0.55 for cortical bone and 0.18 for trabecular bone. AALM.CSL values have been adopted for AALM.FOR and the different values for trabecular bone have not been reconciled. Further research that could provide a stronger empirical basis for these values would improve confidence in simulations of XRF observations.

3.5. CONCLUSIONS AND IMPLICATIONS FOR MODELING LEAD BODY BURDENS

The current version of AALM.FOR represents a substantial update to ICRPv005.FOR used in the Approach for Estimating Exposures and Incremental Health Effects due to Lead During Renovation, Repair and Painting Activities in Public and Commercial Buildings (U.S. EPA, 2014b) and appendices (U.S. EPA, 2014a) . The updates include new parameters for simulating physiological growth and gastrointestinal absorption, as well as updated parameters that govern rates of exchange of Pb between plasma, RBCs, bone, kidney and liver (Table 3-2). AALM.FOR predicts blood, bone and soft tissue Pb levels that are identical AALM.CSL and provides an alternative Fortran platform to acslX, which is no longer commercially supported, for implementing the AALM.

3.5.1. Evaluation of AALM.FOR Performance

AALM.FOR was evaluated with a larger set of observations in children and adults, including some data that had not been used in previous evaluations of ICRPv005.FOR. Data on Pb dose-blood Pb relationships is limited to a three studies; one of adults in which five male subjects were administered known doses of a stable Pb isotope for periods of 2 to 6 months (Rabinowitz et al., 1976) and two studies of infants in which Pb ingestion doses were estimated from dietary (formula) Pb measurements and exposures were for approximately 3 months (Ryu et al., 1983, n = 25); (Sherlock and Quinn, 1986, n = 131). No data were available on dose-blood Pb concentration relationships in older children or adolescents for whom Pb ingestion doses were known with certainty. Several studies have reconstructed Pb intakes in children from exposure models supported by measurements of environmental exposure concentrations (Dixon et al., 2009; TerraGraphics Environmental Engineering, 2004; Malcoe et al., 2002; Hogan et al., 1998; Lanphear et al., 1998; Bornschein et al., 1985). However, these studies were not considered in the current evaluations of AALM.FOR and may be useful for future efforts to validate a version of the AALM that combines the biokinetics model (AALM.FOR) with a multimedia exposure model.

Although limited in size, these evaluations suggest that AALM.FOR can provide an accurate prediction of dose-blood Pb relationships when actual doses are known or can be calculated with certainty. In general, AALM.FOR predicted the observed blood Pb concentrations and dynamics in infants and adults in

response to changing Pb dosing (see Figures 3-10, 3-14). AALM.FOR also predicted quasi-steady state blood Pb concentrations in infants across a range of ingestion doses of Pb (Figures 3-15). The model predicted a higher plateau for the dose-blood Pb relationship than was observed in infants (Figure 3-15), however, this difference would be of quantitative significance only at intakes resulting in blood Pb concentrations >30 µg/dL. These evaluations show that the model reliably predicts both quasi-steady state blood Pb concentrations as well the rates of change Pb that occur with a change in exposure.

AALM.FOR also predicted the observed relationships between plasma and whole blood Pb concentrations in adults (Figure 3-13). Transfer out of RBCs in AALM.FOR is age-dependent and faster in children than in adults. The validity of the age-dependence was not rigorously explored in this analysis. What little data there are on plasma-blood Pb relationships in children does not suggest an appreciable difference in the relationship for children and adults (Bergdahl et al., 1999). Since the age-dependence could not be rigorously evaluated it is retained in AALM.FOR. AALM.FOR also predicted the observed relationships between plasma and bone Pb concentrations in adults (Figure 3-12) and between kidney, liver and bone Pb concentrations in children and adults based on post-mortem data (Figure 3-11). This suggests that the model accurately predicts the ratios of the exchange kinetics (rates into tissue and out to plasma) that give rise to the age-dependent distribution of Pb between bone and soft tissue.

AALM.FOR predicted the observed changes in blood Pb concentrations in children and adults for reconstructed exposures estimated based on observed blood Pb measurements (Figures 3-8, 3-9, 3-16 to 3-18). These evaluations indicate that the model accurately predicts observed elimination kinetics of Pb from blood in children and adults, and bone in adults. AALM.FOR predicts more rapid elimination of Pb from bone in children compared to adults (Figure 3-3). This is consistent with more active bone growth and turnover of bone mineral during childhood which should contribute to more volatile bone Pb stores (O'Flaherty, 1995; Leggett, 1993). However, the kinetics of bone Pb in children predicted by the model have not been quantitatively verified as no data were available on kinetics of elimination of Pb from bone in children.

Collectively, the above observations provide added confidence for applications of AALM.FOR for predicting Pb body burdens associated with long-term steady state exposures or short-term intermittent exposures, such as those associated with public and commercial building renovations.

3.5.2. Response to Peer Review of ICRPv005.FOR

The updates made to ICRPv005.FOR and further evaluations of ICRPv005.FOR and AALM.FOR address several comments made by peer reviewers of the *Approach for Estimating Exposures and Incremental Health Effects due to Lead During Renovation, Repair and Painting Activities in Public and Commercial Buildings* (Versar, 2015; U.S. EPA, 2014b). These are summarized below.

Rationale for selecting the Leggett model over the O'Flaherty model. Peer reviewers suggested that performance of the Leggett and O'Flaherty models be evaluated and that a stronger rationale be provided for selecting the Leggett model for applications to public and commercial renovation assessments. This report does not specifically address performance of the O'Flaherty model; however, the model was extensively evaluated Chapter 4. The latter report described the development and evaluation of AALM.CSL which includes modules that implement biokinetics models based on either the Leggett model (AALM-LG.CSL) or O'Flaherty model (AALM-OF.CSL). A conclusion of the latter report was

that AALM-LG.CSL provided superior agreement to the Rabinowitz et al. (1976) observations compared to AALM-OF.CSL. This conclusion supports selection of the Leggett model as the basis for AALM.FOR and for applications of AALM.FOR, rather than the O'Flaherty model, to assessments of public and commercial building renovations. Additional considerations that support use of AALM.FOR were: (1) the need for Monte Carlo applications of the model which require sufficient computational speed afforded by the Fortran code; and (2) limited future availability of an acslX program to run AALM.CSL, because acslX is no longer being commercially supported.

Accounting for sex differences in biokinetics. The peer reviewers suggested that the model should simulate sex differences in Pb biokinetics. The analyses described in this report could not evaluate sex differences in biokinetics because there are no data on dose-body burden relationships in humans that would allow such evaluations. ICRPv005.FOR was updated in creating AALM.FOR to include algorithms that control growth of the body, volumes of plasma and blood and masses of bone and soft tissues AALM.FOR includes parameters to simulate male or female growth. AALM.FOR was shown to predict elimination kinetics of Pb from blood in male and female children when exposures were reconstructed (Figure 3-16 to 3-17), and soft tissue-bone Pb relationships in males and females (Figure 3-11).

Evaluation of relationship between plasma-whole blood Pb concentrations. The peer reviewers suggested that the model should be evaluated for accurately predicting the plasma-blood Pb concentration ratio. A meta-dataset of observations of plasma-blood Pb concentrations in children and adults was assembled for evaluation of model performance. In all of these studies, methods were employed to control for sample contamination, which is of particular importance in measurements of the low Pb levels found in plasma. The dataset used in the evaluation included paired observations of plasma and whole blood Pb concentration for 409 adults (Smith et al., 2002; Bergdahl et al., 1999; Bergdahl et al., 1998; Hernandez-Avila et al., 1998; Bergdahl et al., 1997; Schutz et al., 1996). The relationship between plasma and whole blood Pb concentrations predicted from AALM.FOR agreed with observations (Figure 3-13). Only one study provides similar data in children (Bergdahl et al., 1999). Based on these data, the plasma-blood relationships in children and adults do not appear to differ substantially.

Accounting for relative bioavailability (RBA) of ingested Pb. The peer reviewers suggested that RBA of Pb in dust/soil needs to be included as part of the ingestion calculations. This has been included in AALM.FOR. However, by making RBA an adjustment on the ingested dose, rather than the gastrointestinal absorption fraction, the RBA adjustment will result in an underestimation of fecal Pb excretion and a negative mass balance (excretion < intake) if RBA is <1 (see Sections 2.2.3). An error in the Pb intake-excretion mass balance will not affect the simulation internal kinetics of Pb or body burdens (e.g., blood or bone concentrations), although, it may be noteworthy for some research applications. Further refinement of the model at some point in the future to make the RBA an adjustment to the absorption fraction in the small intestine is discussed in Section 3.4.

Revaluation of model predictions of blood Pb kinetics in the Rabinowitz et al. (1976) study. The peer reviewers suggested that the model should be revaluated with the Rabinowitz et al. (1976) data to ensure that changes made to the model in creating ICRPv005.FOR did not degrade performance of the model to accurately simulate these observations. AALM.FOR predicted blood Pb concentrations and the temporal pattern of the rise and decline in blood Pb concentrations observed in the Rabinowitz et al. (1976) subjects (Figure 3-10).

Evaluation of model performance for Hattis data. The peer reviewers suggested that the model be evaluated for predicting blood Pb concentrations in a cohort of workers described in Hattis (1981). These data included blood Pb concentrations in workers measured at the date of hire and prior to and following a nine-month strike. Although pre-hire exposures were unknown, it was possible to calibrate the post-hire and pre-strike exposures to achieve agreement with blood Pb concentrations at the time of hire and just prior to the strike, and then predict without further calibration the post-strike blood Pb. After calibration to the blood Pb concentrations measured at time of hire and just prior to the strike ($r^2 = 1.0$), AALM.FOR predicted rates of decline in blood Pb concentration (pseudo first-order $t_{1/2}$) for individual subjects and for the group median that agreed with the observations (Table 3-4).

Evaluation of model performance for the Nie et al. data. The peer reviewers suggested that the model be evaluated for predicting blood and bone Pb concentrations in a cohort of workers described in Nie et al. (2005) including use of some unpublished Nie et al. data. These data were used in an analyses of an implementation of the Leggett model developed by California EPA (CalEPA, 2013). There were no data on actual exposures experienced by the workers in this cohort. As described in Section 3.3, the Nie et al. data were reviewed and evaluated. Although attempts were made to reconstruct exposures so that blood and bone Pb concentrations could be predicted and compared to observations, ultimately, it was concluded that the data were not suitable for model evaluations because of the uncertainty in the exposures that preceded the blood and bone Pb measurements and that occurred during the measurement period.

Evaluation of model performance for intermittent exposures. Renovations of public and commercial building renovations can result in elevated Pb exposures that may persist for several days to several months. Therefore, assessment methods applied to renovation-related exposure scenarios must be able to predict blood and bone Pb levels that might occur as a result of short-term or intermittent exposures to children or adults. Several evaluations described in this report suggest that AALM.FOR can be expected to reliably predict blood Pb kinetics associated with short-term or intermittent exposures. (1) AALM.FOR predicted the rate of accrual and elimination of Pb from blood in adult subjects who were exposed to Pb over periods of 2-6 months (Figure 3-10). (2) The model predicted the increase in blood Pb that was observed in infants who were abruptly switched to a higher Pb level diet following approximately 100 days of ingesting a lower Pb level diet (Figure 3-14). (3) The model predicted the rate of decline in blood Pb that was observed following interventions to decrease elevated exposures that occurred over periods of 200 – 400 days (Figures 3-16 to 3-18). (4) The model predicted the decrease in blood Pb concentrations that occurred in Pb workers following a nine-month strike (Table 3-4).

3.5.3. Summary

Collectively, the updates made to ICRPv005.FOR to create AALM.FOR and evaluations of AALM.FOR provide increased confidence in applying a biokinetics modeling approach to support estimations of Pb body burdens following a variety of potential Pb exposure scenarios. AALM.FOR offers an improved modeling tool for predicting exposure-body burden relationships for intermittent as well as chronic Pb exposures.

TABLE 3-1. CHANGES MADE TO ICRPV004.FOR TO CREATE ICRPV005.FOR

ICRPv004.FOR[a]	ICRPv005.FOR	Output/Functionality Affected
Adult kidney mass	Age-dependent kidney mass based on ICRP (2002)	Age-dependent kidney Pb concentrations
Adult bone mass	Age-dependent bone mass based on ICRP (2002)	Age-dependent bone Pb concentrations
Constant hematocrit	Age-dependent hematocrit based on ICRP (2002)	Age-dependent RBC and plasma volumes
Constant trabecular bone fraction (20%)	Age-dependent trabecular bone fraction from Table M-1 of U.S. EPA (2014a)	Age-dependent cortical and trabecular bone Pb concentrations
RBC Pb saturation threshold (25 µg/dL blood) and maximum (350 µg/dL RBC)	RBC Pb saturation threshold (0 µg/dL blood) and maximum (270 µg/dL RBC)	Pb uptake– blood Pb relationship
Transfer rate from (d^{-1}) plasma to RBC birth–10 years: • birth: 0.462 • 0.27 y: 0.462 • 1 y: 0.462 • 5 y: 0.277 • 10 y: 0.139	Transfer rate from (d^{-1}) plasma to RBC birth–10 years: • birth: 0.562 • 0.27 y: 0.562 • 1 y: 0.562 • 5 y: 0.277 • 10 y: 0.277	Plasma– RBC Pb relationship in children
Depostion fraction from RBC to diffusible plasma (0.24)	Deposition fraction from RBC to diffusible plasma: • birth: 0.20 • 0.27 y: 0.20 • 1 y: 0.20 • 5 y: 0.21 • 10 y: 0.22 • ≥15 y: 0.22	Plasma– RBC Pb relationship in children
Transfer rate (d^{-1}) from non-exchangeable cortical bone to diffusible plasma: • birth: 0.00822 • 0.27 y: 0.00822 • 1 y: 0.00288 • 5 y: 0.00154 • 10 y: 0.00089 • 15 y: 0.000512 • ≥25 y: 0.000082	Transfer rate (d^{-1}) from non-exchangeable cortical bone to diffusible plasma: • birth: 0.0102 • 0.27 y: 0.00822 • 1 y: 0.00288 • 5 y: 0.00154 • 10 y: 0.00089 • 15 y: 0.000512 • 18 y: 0.000370 • 24 y: 0.000082 • ≥30 y: 0.000041	Bone to plasma Pb kinetics, in late adolescence (age 15–19 years) and adults (≥30 years)

ICRPv004.FOR[a]	ICRPv005.FOR	Output/Functionality Affected
Transfer rate (d^{-1}) from non-exchangeable trabecular bone to diffusible plasma: • birth: 0.00822 • 0.27 y: 0.00822 • 1 y: 0.00288 • 5 y: 0.00181 • 10 y: 0.00132 • 15 y: 0.000956 • ≥25 y: 0.000493	Transfer rate (d^{-1}) from non-exchangeable trabecular bone to diffusible plasma: • birth: 0.0102 • 0.27 y: 0.00822 • 1 y: 0.00288 • 5 y: 0.00181 • 10 y: 0.00132 • 15 y: 0.000956 • 18 y: 0.000781 • 24 y: 0.000493 • 30 y: 0.000247 • 40 y: 0.000247 • 45 y: 0.000274 • 55 y: 0.000301 • 65 y: 0.000329 • 75 y: 0.000356	Bone-to-plasma Pb transfer kinetics (age 15–18 years), adults (≥25 years)

Based on (U.S. EPA, 2014a, b).

[a]ICRPv004.FOR is an implementation of the Leggett (1993) model.

1

2

TABLE 3-2. DIFFERENCES IN ICRPV005.FOR AND AALM.CLS BIOKINETICS

ICRPv005.FOR	AALM.FOR	Output/Functionality Affected
Age-dependent blood and plasma volumes based on ICRP (2002)	Age-dependent blood and plasma volumes based on O'Flaherty (1995, 1993)	Age-dependent blood Pb concentration
Age-dependent bone mass based on ICRP (2002)	Age-dependent bone mass based on O'Flaherty (1995, 1993)	Age-dependent cortical and trabecular bone Pb concentration
Age-dependent trabecular bone fraction based from Table M-1 of U.S. EPA (2014a)	Age-dependent cortical and trabecular bone masses based on O'Flaherty (1995, 1993)	Age-dependent cortical and trabecular bone Pb concentration
Age-dependent kidney mass based on ICRP (2002)	Age-dependent kidney mass based on O'Flaherty (1995, 1993)	Age-dependent kidney Pb concentration
Adult liver mass	Age-dependent liver mass based on O'Flaherty (1995, 1993)	Age-dependent liver Pb concentration
Age-dependent absorption fraction (*F1*): • birth: 0.45 • 0.27 y: 0.45 • 1 y: 0.30 • 5 y: 0.30 • 10 y: 0.30 • 15 y: 0.30 • ≥25 y: 0.15	Age-dependent absorption fraction (*F1*): • birth: 0.39 • 0.27 y: 0.39 • 1 y: 0.38 • 5 y: 0.17 • ≥10 y: 0.12	Absorption fraction for ingested Pb
Absorption fraction for ingested Pb not adjusted for RBA	Media-specific ingestion intakes adjusted for RBA	Intake-fecal mass balance
RBC Pb saturation threshold: 0 µg/dL blood) Maximum: 270 µg/dL RBC	RBC Pb saturation threshold: 20 µg/dL blood) Maximum: 350 µg/dL RBC)	Pb uptake–blood Pb relationship
Transfer rate (d^{-1}) from non-exchangeable cortical bone to diffusible plasma (RCORT): • birth: 0.0102 • 0.27 y: 0.00822 • 1 y: 0.00288 • 5 y: 0.00154 • 10 y: 0.00089 • 15 y: 0.00512 • ≥25 y: 0.0000822	Transfer rate (d^{-1}) from non-exchangeable cortical bone to diffusible plasma (RCORT): • birth: 0.0204 • 0.27 y: 0.01644 • 1 y: 0.00576 • 5 y: 0.00308 • 10 y: 0.00178 • 15 y: 0.00124 • ≥25 y: 0.0001644	Shorter retention of Pb in cortical bone
Transfer rate (d^{-1}) from non-exchangeable trabecular bone to diffusible plasma (RTRAB): • birth: 0.0102	Transfer rate (d^{-1}) from non-exchangeable trabecular bone to diffusible plasma (RTRAB): • birth: 0.0204	Shorter retention of Pb on trabecular bone

ICRPv005.FOR	AALM.FOR	Output/Functionality Affected
• 0.27 y: 0.00822 • 1 y: 0.00288 • 5 y: 0.00181 • 10 y: 0.00132 • 15 y: 0.000956 • ≥25 y: 0.000493	• 0.27 y: 0.01644 • 1 y: 0.00576 • 5 y: 0.00362 • 10 y: 0.00264 • 15 y: 0.001912 • ≥25 y: 0.000986	
Fraction of total transfer from the exchangeable bone directed to non-exchangeable bone (FLONG): 0.2	Fraction of total transfer from the exchangeable bone directed to non-exchangeable bone (FLONG): 0.6	Longer retention of Pb in cortical and trabecular bone
Transfer rate (d^{-1}) from liver compartment 2 to diffusible plasma (RLVR2): • birth: 0.00693 • 0.27 y: 0.00693 • 1 y: 0.00693 • 5 y: 0.00693 • 10 y: 0.00190 • 15 y: 0.00190 • ≥25 y: 0.00190	Transfer rate (d^{-1}) from liver compartment 2 to diffusible plasma (RLVR2): • birth: 0.000693 • 0.27 y: 0.000693 • 1 y: 0.000693 • 5 y: 0.001386 • 10 y: 0.000570 • 15 y: 0.000570 • 25 y: 0.000570 • 30 y: 0.001425 • 40 y: 0.003040 • 60 y: 0.003420 • 90 y: 0.00380	Longer retention of Pb in liver
Transfer rate (d^{-1}) from kidney compartment 2 to diffusible plasma (RKDN2): • birth: 0.00693 • 0.27 y: 0.00693 • 1 y: 0.00693 • 5 y: 0.00693 • 10 y: 0.00190 • 15 y: 0.00190 • ≥25 y: 0.00190	Transfer rate (d^{-1}) from kidney compartment 2 to diffusible plasma (RKDN2): • birth: 0.000693 • 0.27 y: 0.000693 • 1 y: 0.000693 • 5 y: 0.000693 • 10 y: 0.000190 • 15 y: 0.000190 • 25 y: 0.000190 • 30 y: 0.000950 • ≥40 y: 0.00190	Longer retention of Pb in kidney
Deposition fraction from diffusible plasma to kidney compartment 2 (TKDN2): 0.0002	Transfer rate (d^{-1}) from kidney compartment 2 to diffusible plasma (TKDN2): 0.0004	Faster transfer from diffusible plasma to kidney at all ages
Deposition fraction from diffusible plasma to kidney compartment 1 (TKDN1): 0.02	Deposition fraction from diffusible plasma to kidney compartment 1 (TKDN1): 0.025	Faster transfer from diffusible plasma to kidney at all ages

ICRPv005.FOR	AALM.FOR	Output/Functionality Affected
Deposition fraction from diffusible plasma to urine (TOURIN): 0.015	Deposition fraction from diffusible plasma to urine (TOURIN): 0	All urinary excretion occurs from kidney

1

TABLE 3-3. DIFFERENCES BETWEEN AALM.FOR AND AALM.CSL

AALM.FOR	AALM.CSL	Output/Functionality Affected
Numerical integration time steps controlled by user input	Numerical integration time steps controlled by user Gear (1971) algorithm	Numerical integration error
Media-specific ingestion intakes adjusted for RBA	GI tract absorption fraction adjusted for media-specific RBA	Fecal Pb mass balance
4-compartment RT model that requires user inputs for deposition rate (µg/day)	12-compartment model that accepts user inputs for air concentration, particle size and absorption class	Simulations of Pb deposition and absorption of inhaled Pb

TABLE 3-4. BLOOD LEAD PREDICTIONS FROM THE AALM FOR 57 SUBJECTS IN THE HATTIS DATASET

		Hattis		ICRPv005		AALM.CSL		AALM.FOR	
		Mean	SD	Mean	SD	Mean	SD	Mean	SD
BLL at hire	µg/dL	20	7	20	7	20	7	20	7
BLL at strike	µg/dL	48	11	49	13	48	11	48	11
BLL after strike	µg/dL	33	9	23	7	31	7	31	7
BLL half-time	days	1027	1433	312	184	553	370	523	314
BLL half-time delta				-0.37	0.59	-0.05	0.54	-0.08	0.52

		Hattis		ICRPv005		AALM.CSL		AALM.FOR	
		GM	GSD	GM	GSD	GM	GSD	GM	GSD
BLL half-time	days	633	2.4	274	1.6	483	1.6	465	1.6

	Hattis		ICRPv005.FOR		AALM.CSL		AALM.FOR	
	Mean	SD	Mean	SD	Mean	SD	Mean	SD
BLL at hire (µg/dL)	20	7	20	7	20	7	20	7
BLL at strike (µg/dL)	48	11	49	13	48	11	48	11
BLL after strike (µg/dL)	33	9	23	7	31	7	31	7
BLL half-time (d)	1027	1433	312	184	553	370	523	314
BLL half-time delta (d)			-0.37	0.59	-0.05	0.54	-0.08	0.52

	Hattis		ICRPv005.FOR		AALM.CSL		AALM.FOR	
	GM	GSD	GM	GSD	GM	GSD	GM	GSD
BLL half-time (d)	633	2.4	274	1.6	483	1.6	465	1.6

TABLE 3-5. COMPARISON OF PREDICTED AND OBSERVED PLASMA PB/BONE PB SLOPES

Model	Study	Bone	Predicted Slope	Observed Slope	SE	95%CL	Residual
AALM	CA96	Cortical	0.037	0.052	0.013	0.027, 0.077	-1.16
AALM	CA96	Trabecular	0.040	0.041	0.007	0.027, 0.054	-0.16
AALM	HE98	Cortical	0.037	0.036	0.011	0.014, 0.058	0.12
AALM	HE98	Trabecular	0.040	0.025	0.004	0.017, 0.033	3.67

CA96, Cake et al. (1996); HE98, Hernandez-Avila et al. (1998)

TABLE 3-6. COMPARISON OF ALM AND AALM PREDICTIONS OF BLOOD PB CONCENTRATIONS IN ADULTS

Parameter	Description	Units	ALM	AALM
PbS	Soil lead concentration	µg/g or ppm	1000	1000
BKSF	Biokinetic Slope Factor	µg/dL per µg/day	0.4	NA
PbB_0	Baseline Blood Pb	µg/dL	1.5	1.5
IR_S	Soil Ingestion Rate	g/day	0.050	0.05
$AF_{S, D}$	Absorption Fraction	--	0.12	0.072
$EF_{S, D}$	Exposure Frequency	days/yr	219	219
$AT_{S, D}$	Averaging Time	days/yr	365	365
PbB_{adult}	Blood Pb Concentration	µg/dL	2.9	2.9

ALM, Adult Lead Methodology. See Figure 3-20 for AALM input parameter values.

FIGURE 3-1. GASTROINTESTINAL ABSORPTION OF PB IN THE (LEGGETT, 1993) MODEL AND AALM, OPTIMIZED TO (RYU ET AL., 1983).

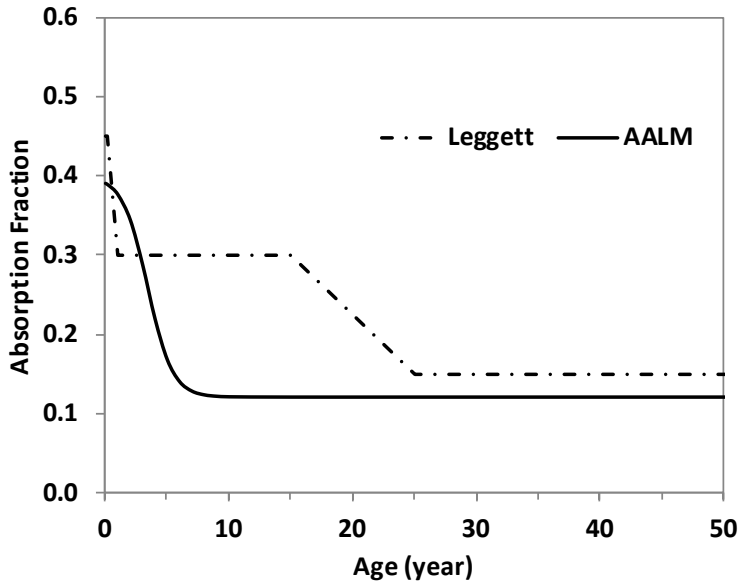

FIGURE 3-2. COMPARISON OF ACCRUAL AND ELIMINATION KINETICS OF BLOOD PB IN CHILDREN (A) AND ADULTS (B) PREDICTED FROM AALM.CSL, AALM.FOR AND ICRPV005.FOR.

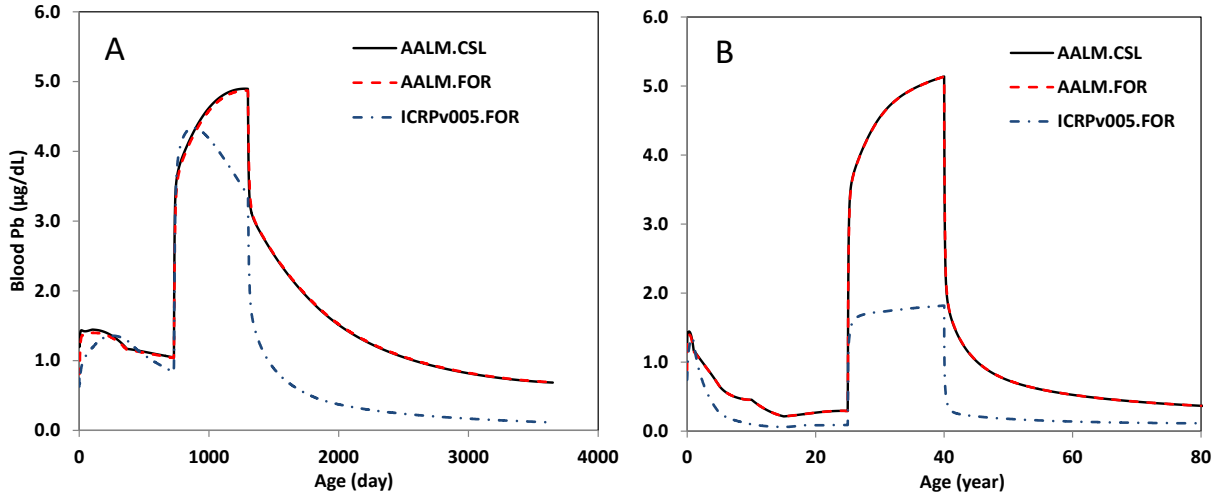

The simulated Pb exposure was a constant baseline intake (5 µg/day) beginning at birth. In the child simulation, a period of elevated intake of (40 µg/day) began on day 720 and ended on day 1300. In the adult simulation, a period of elevated intake of (105 µg/day) began at age 25 years and ended at age 40 years.

FIGURE 3-3. COMPARISON OF ACCRUAL AND ELIMINATION KINETICS OF CORTICAL BONE (A, B) AND TRABECULAR BONE (C, D) PB IN CHILDREN (A, C) AND ADULTS (B, D) PREDICTED FROM AALM.CSL, AALM.FOR AND ICRPV005.FOR.

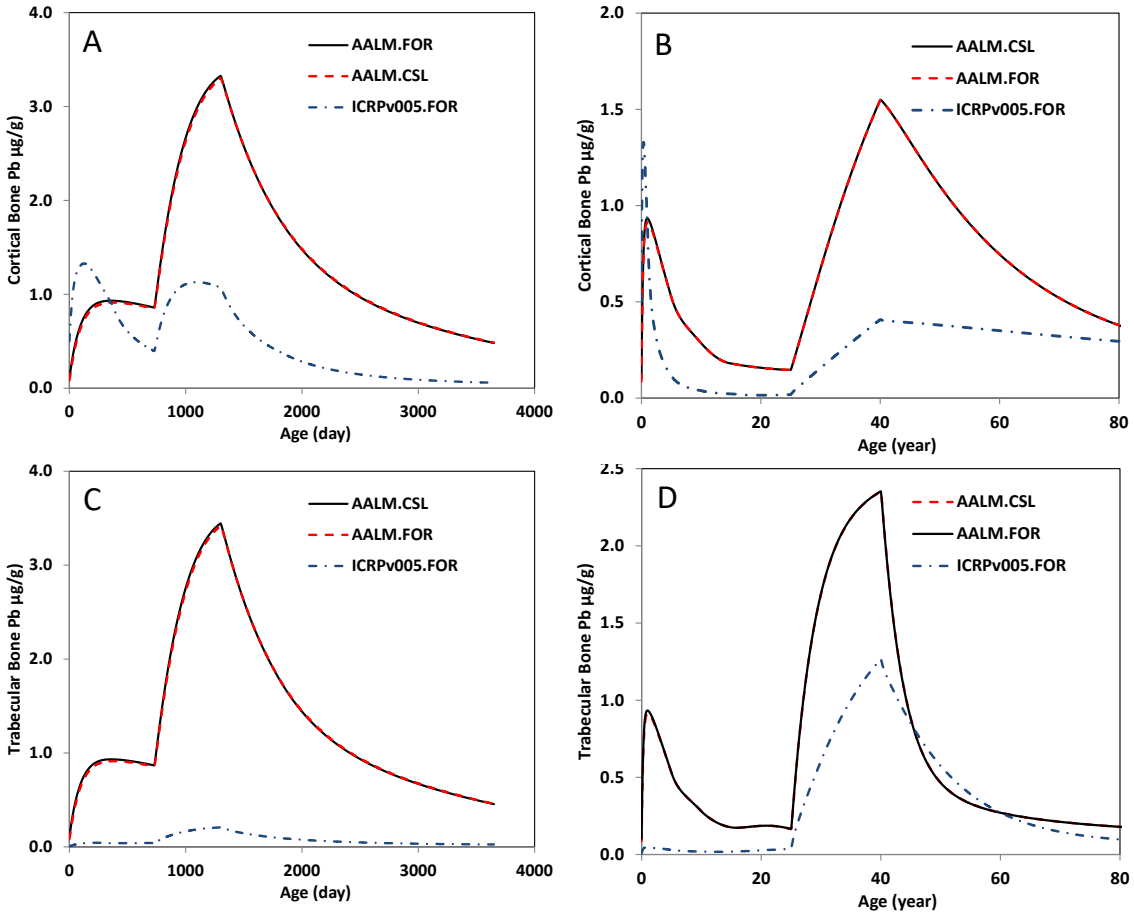

The simulated Pb exposure was a constant baseline intake (5 µg/day) beginning at birth. In the child simulation, a period of elevated intake of (40 µg/day) began on day 720 and ended on day 1300. In the adult simulation, a period of elevated intake of (105 µg/day) began at age 25 years and ended at age 40 years.

FIGURE 3-4. COMPARISON OF RELATIONSHIPS BETWEEN PB INTAKE (G/DAY) AND BLOOD PB IN CHILDREN (A) AND ADULTS (B) PREDICTED FROM AALM.CSL, AALM.FOR AND ICRPV005.FOR.

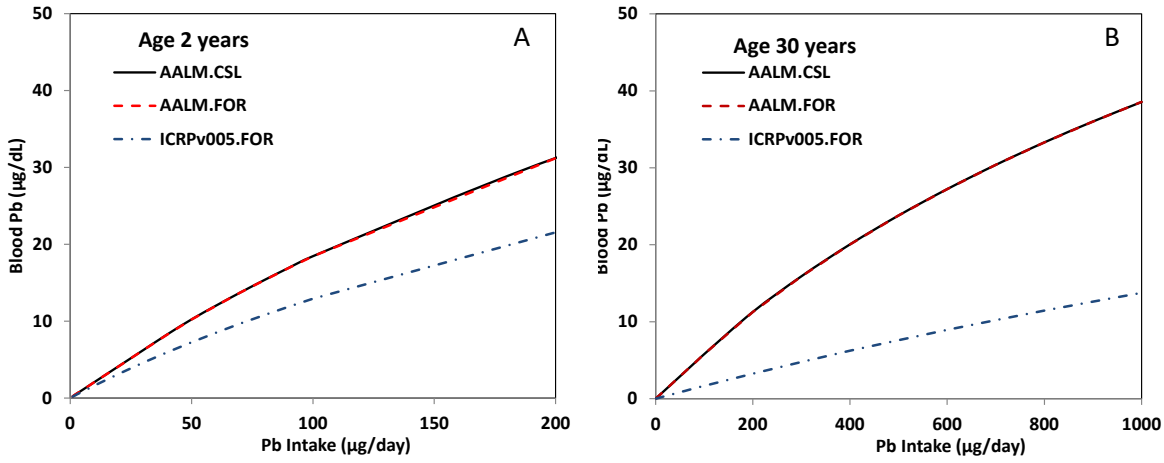

FIGURE 3-5. COMPARISON OF RELATIONSHIPS BETWEEN PB INTAKE (G/DAY) AND CORTICAL (A, B) AND TRABECULAR (C, D) BONE PB IN CHILDREN (A, C) AND ADULTS (B, D) PREDICTED FROM AALM.CSL, AALM.FOR AND ICRPV005.FOR.

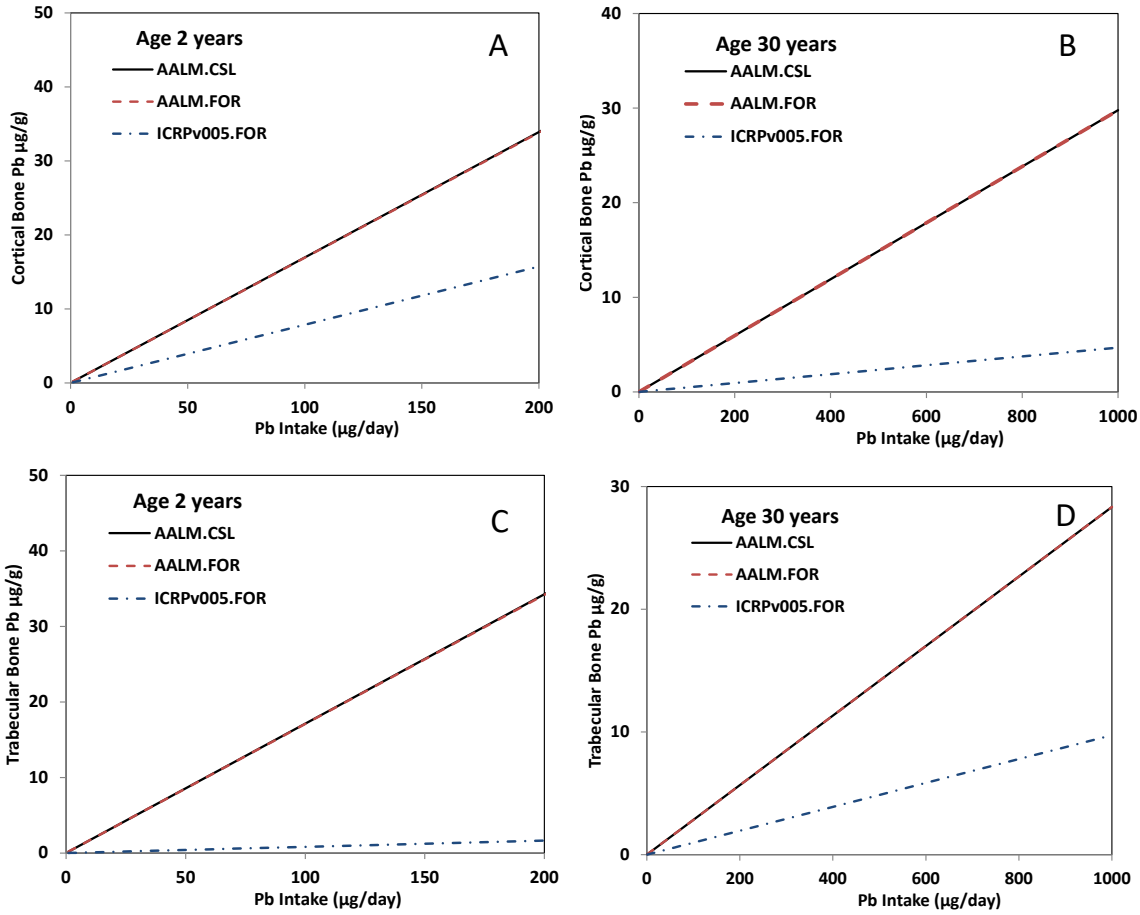

FIGURE 3-6. AALM.CLS SIMULATION OF OBSERVATIONS FOR HATTIS COHORT SUBJECT 5.

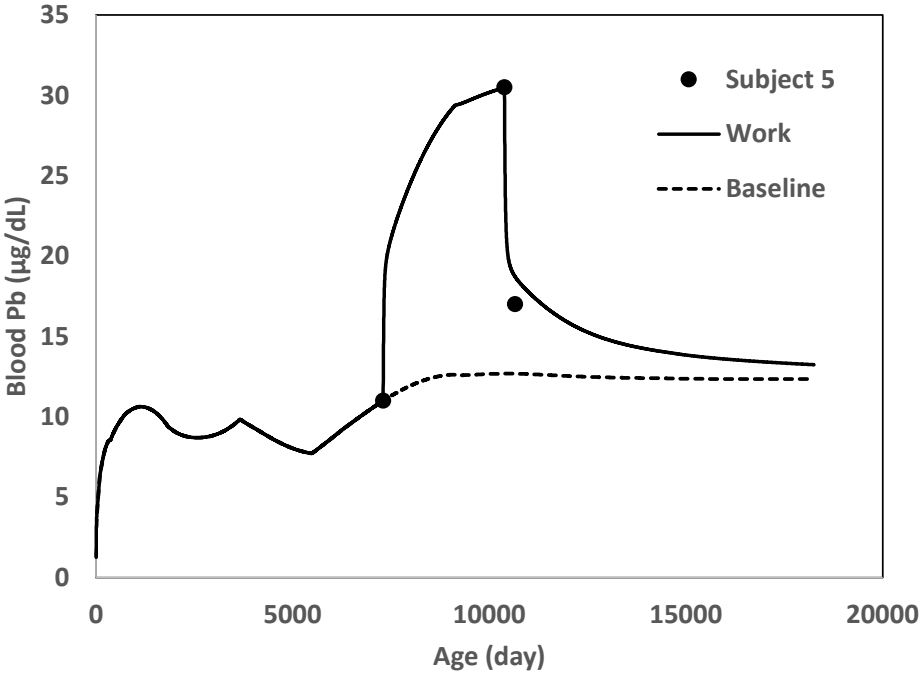

Age		AALM BLL (µg/dL)	Observed BLL (µg/dL)	Ratio (Pred./Obs.)
7300	days	10.6	11.0	0.96
10384	days	30.6	30.5	1.00
10654	days	18.5	17.0	1.09
k	day^{-1}	0.00187	0.00216	0.86
$t_{1/2}$	day	372	320	1.16

The subject (unknown age and sex) experience an occupational exposure that was interrupted by 9-month strike. Pre-strike exposures were reconstructed as a constant Pb ingestion (µg/kg/day) that resulted in a pre-hire blood Pb that was within 1 µg/dL of the reported pre-hire blood Pb (11 µg/dL) for the subject. Pre-strike exposures were reconstructed as a constant Pb ingestion (µg/day), for the reported pre-strike employment durations (3084 days), that resulted in a pre-strike blood Pb that was within 1 µg/dL of the reported pre-strike blood Pb (30.5 µg/dL) for the subject. During the 9-month strike (assumed to be 270 days), exposure reverted to the per/kg baseline level. The elimination half-time from blood was calculated from pre-strike and post-strike blood Pb concentrations, assuming a first-order elimination. The elimination half-time predicted from the observed blood Pb data is 320 days. The half-time predicted from the AALM.CLS is 372 days.

FIGURE 3-7. COMPARISON OF ICRPV005.FOR (TOP) AND AALM.FOR (BOTTOM) PREDICTIONS AND OBSERVED BLOOD PB CONCENTRATIONS AFTER THE STRIKE FOR 57 SUBJECTS IN THE HATTIS COHORT.

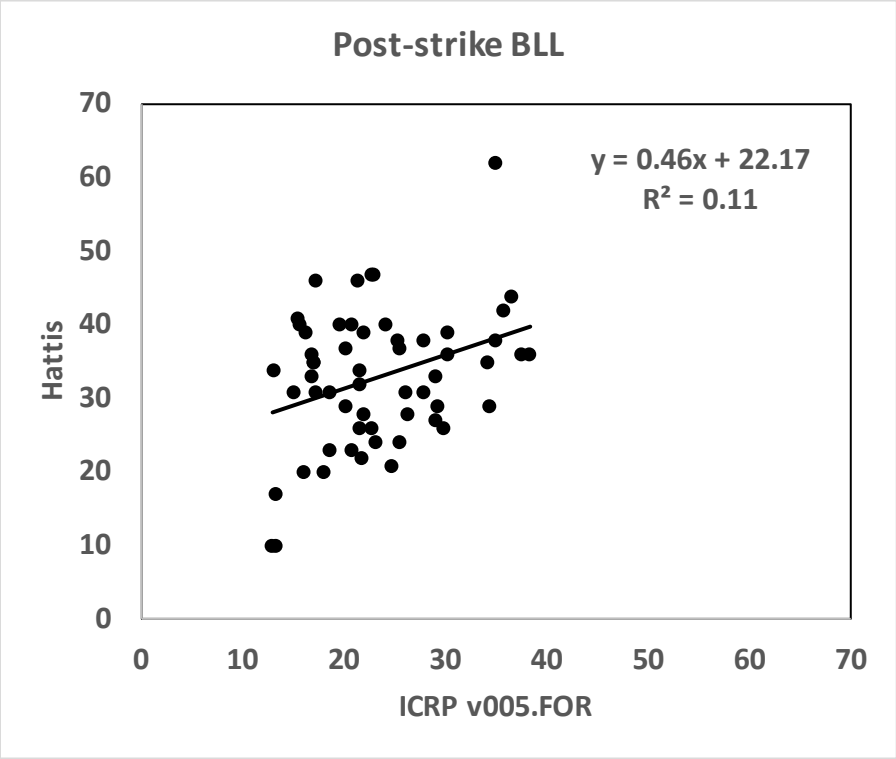

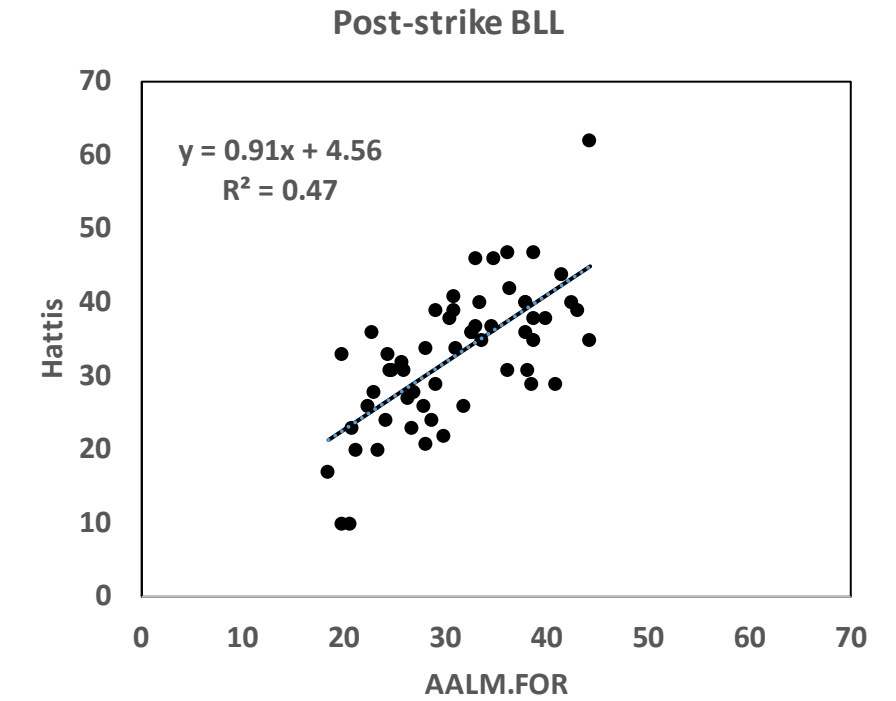

FIGURE 3-8. AALM.CSL, AALM.FOR AND ICRPV005.FOR SIMULATIONS OF BLOOD PB ELIMINATION HALF-TIME FOR 57 SUBJECTS IN THE HATTIS COHORT.

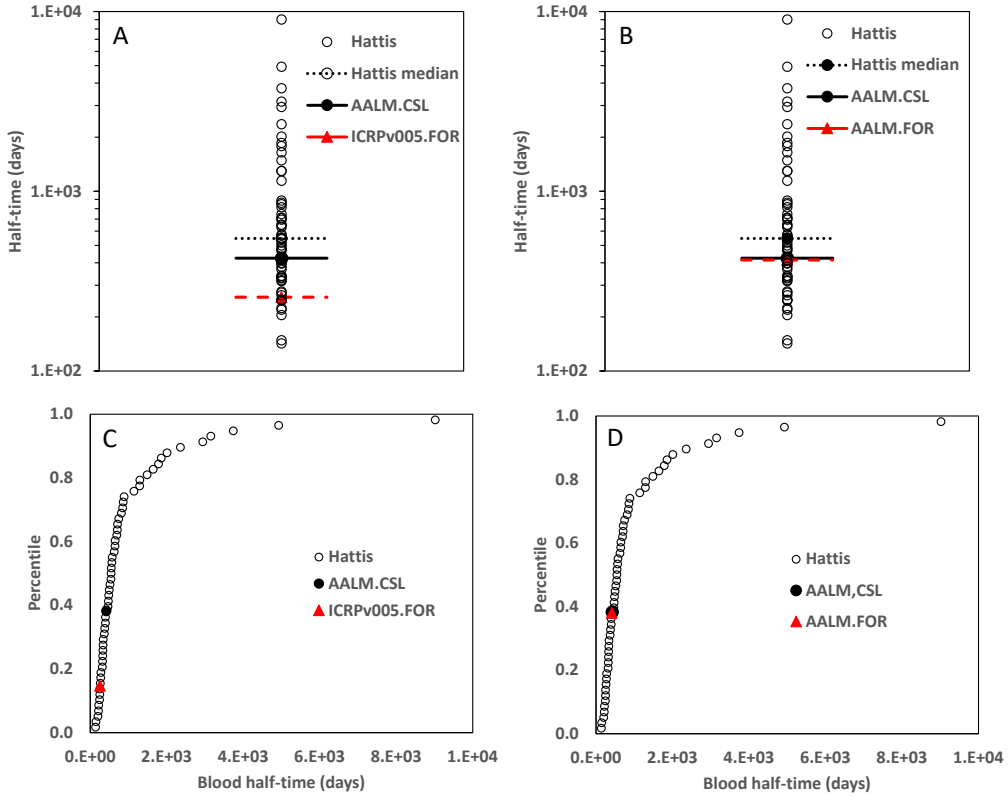

Panel A compares the half-times predicted for the observations with medians predicted from the AALM.CSL and ICRPv005.FOR. Panel C displays the same data as percentiles of the half-times predicted from the observations for AALM.CSL and ICRPv005.FOR. Panels B and D display the corresponding plots comparing AALM.CSL and AALM.FOR. Half-times were calculated as follows: half-time = ln(2)/[ln(pre-strike/post-strike)/270].

FIGURE 3-9. AALM.CSL AND AALM.FOR SIMULATIONS OF ELIMINATION KINETICS OF PB FROM BLOOD (A) AND BONE (B).

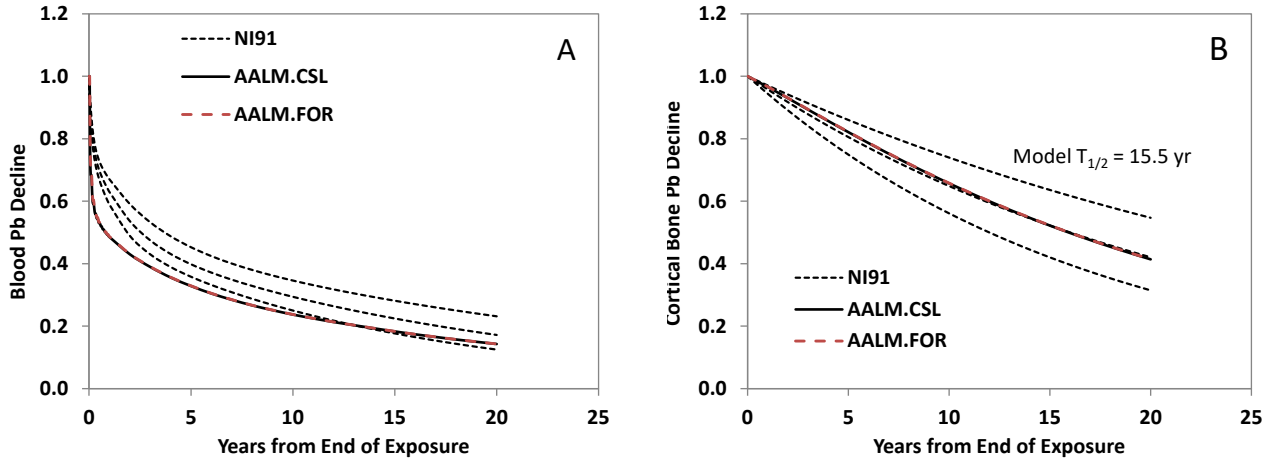

Dotted lines show the elimination from based on the median and upper and lower 95% confidence limits of the tri-exponential model retired Pb workers (n = 14, median age 60 years at time of retirement) reported in Nilsson et al. (1991).

FIGURE 3-10. AALM.CSL AND AALM.FOR SIMULATIONS OF BLOOD PB CONCENTRATIONS IN INDIVIDUALS WHO RECEIVED INGESTION DOSES OF [^{202}PB]-NITRATE (RABINOWITZ ET AL., 1976).

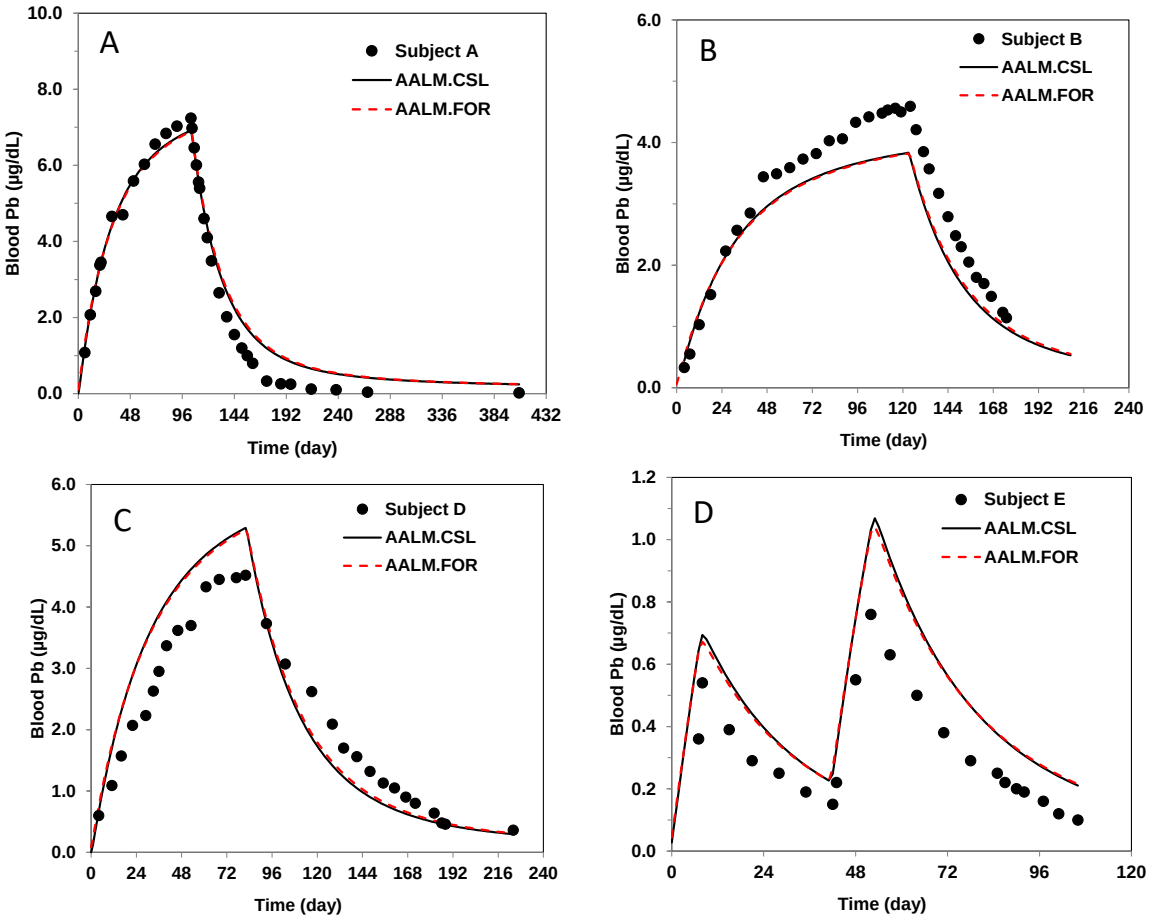

Subject A received 204 µg/day for 104 days, Subject B received 185 µg/day for 124 days, Subject D received 105 µg/day for 83 days, and Subject E received 99 µg/day for on days 1–8 and days 42–51. Estimated absorption fractions were 8.5% for Subject A, 6.5% for Subject B, 10.9% for Subject D and 9.1% for Subject E.

FIGURE 3-11. AALM AND LFM SIMULATIONS OF POST-MORTEM SOFT TISSUE/TIBIA PB RATIOS.

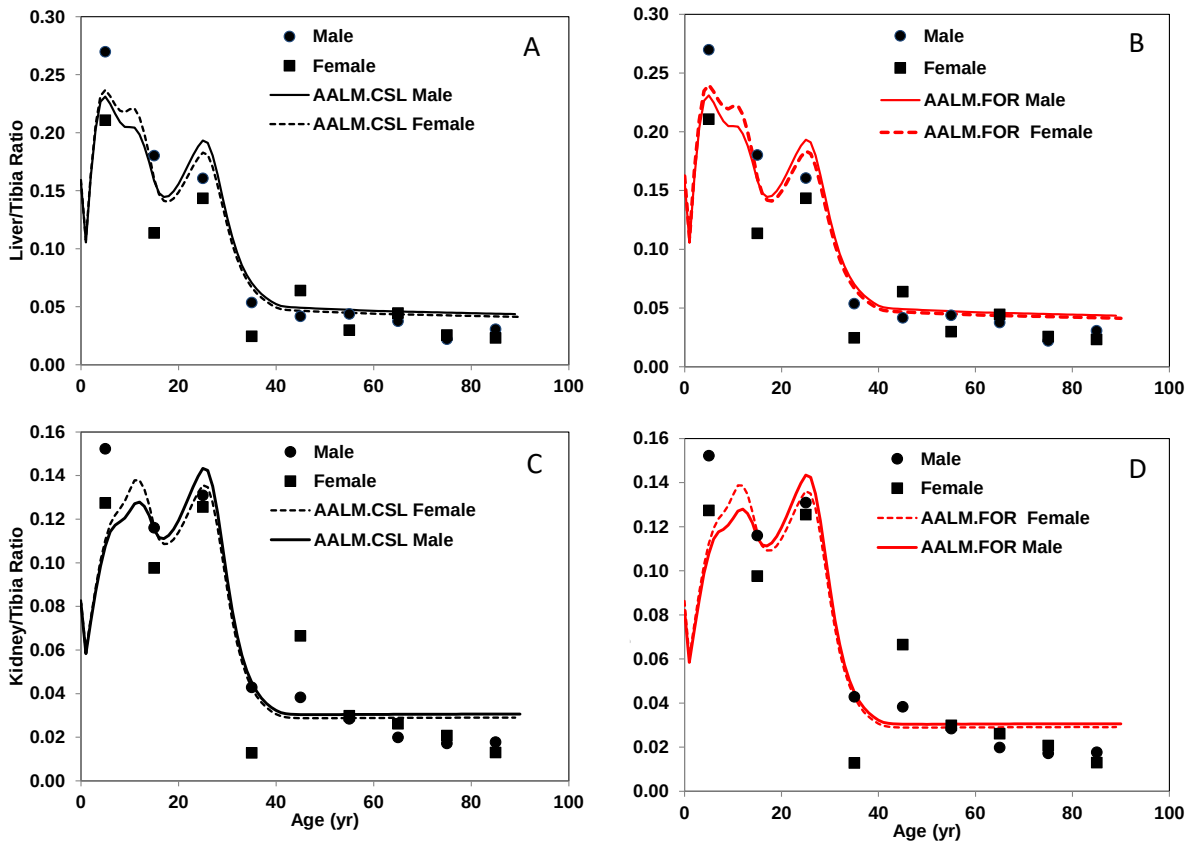

Shown are means for 9 (liver, A and B) and 8 (kidney, C and D) individual predicted from the AALM.CSL (A, C) or AALM.FOR (B, D), based on Barry (1975).

FIGURE 3-12. AALM.CSL AND AALM.FOR SIMULATIONS OF PLASMA PB/BONE PB RATIO IN ADULTS.

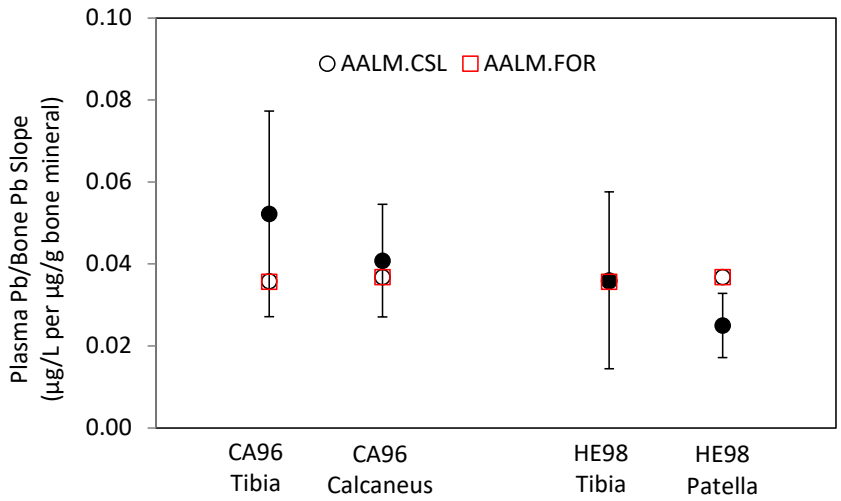

Observations are means and 95% CIs, based on CA96, Cake et al. (1996); HE98, Hernandez-Avila et al. (1998).

FIGURE 3-13. SIMULATION OF WHOLE BLOOD AND PLASMA PB IN ADULTS.

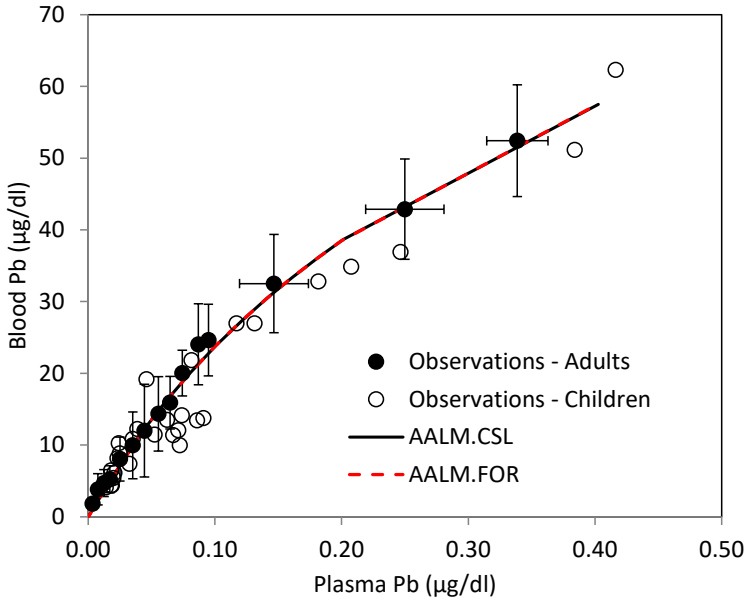

Combined data for adult individuals (N = 406) from all studies were quantized into ranges of plasma Pb; shown are mean and standard deviations for ranges (Smith et al., 2002; Bergdahl et al., 1999; Bergdahl et al., 1998; Hernandez-Avila et al., 1998; Bergdahl et al., 1997; Schutz et al., 1996). The r^2 for predictions and observatiosn was 0.99. Data for children (n = 29) are are overlayed on the adult data (Bergdahl et al., 1999).

FIGURE 3-14. AALM.CSL (A) AND AALM.FOR (B) SIMULATIONS OF FORMULA-FED INFANTS FROM (RYU ET AL., 1983).

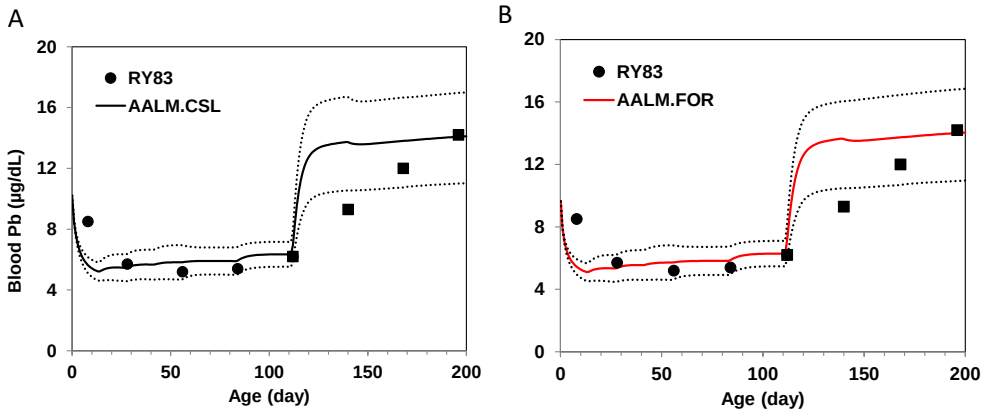

Data (RY83) are from infants fed formula from cartons (12–20 µg/day) from age 8–196 days (closed circles, n=25) and then a subset (closed squares, n = 7) that were switched to formula from cans at age 112 days (60–63 µg/day). Solid lines show simulations of the mean Pb intakes; dotted lines show simulations of ±1 SD of mean intakes.

FIGURE 3-15. AALM.CSL AND AALM.FOR SIMULATIONS OF FORMULA-FED INFANTS.

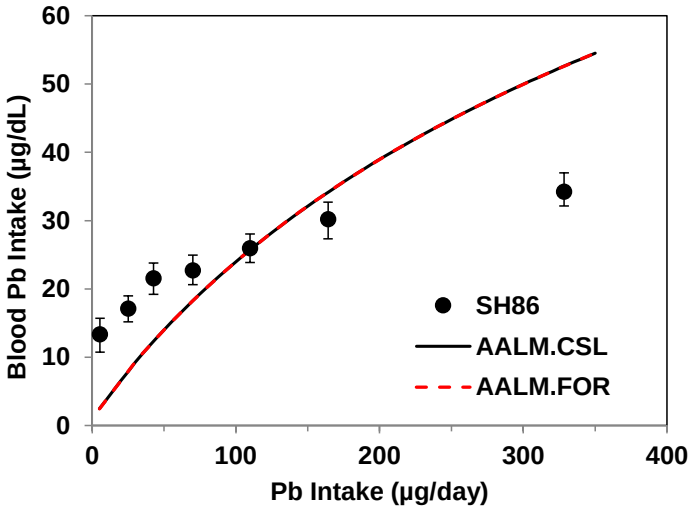

Data are for 131 infants, age 91 days from Sherlock and Quinn (1986).

FIGURE 3-16. AALM SIMULATION OF SUBJECT 48490 (FEMALE).

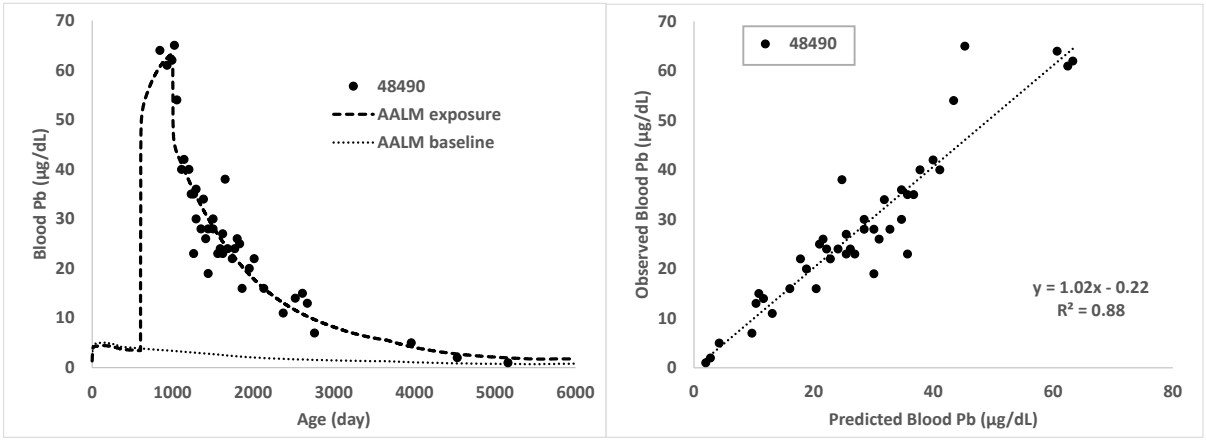

Baseline (15 µg/day) was set to achieve a 6-month BLL of approximately 5 µg/dL, consistent with data for other subjects. Exposure to 22,000 ppm dust Pb (RBA = 0.6) began on age day 600 and continued to age day 1000. Data provided by ATSDR.

FIGURE 3-17. AALM SIMULATION OF SUBJECT 3030 (MALE).

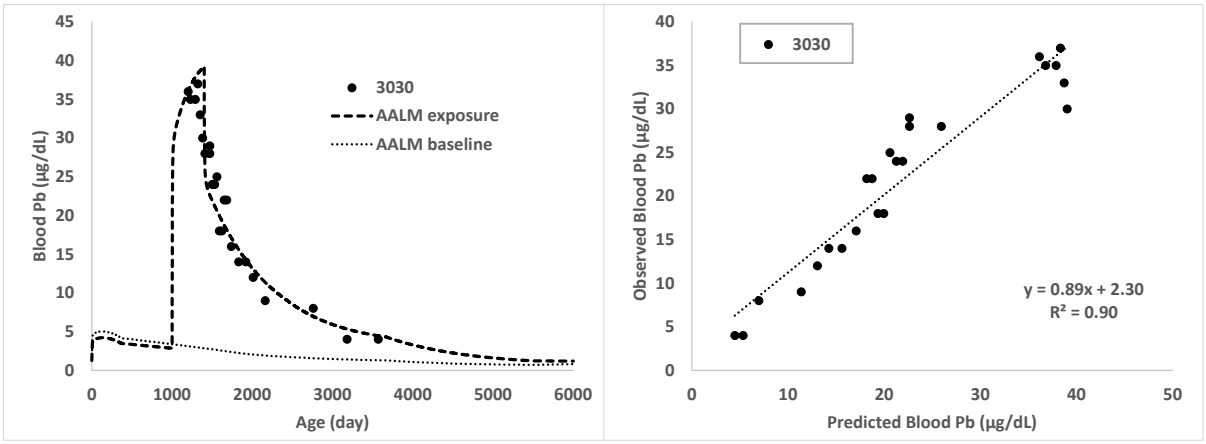

Baseline (15 µg/day) was set to achieve a 6-month BLL of approximately 5 µg/dL, consistent with data for other subjects. Exposure to 11,000 ppm dust Pb (RBA = 0.6) began on age day 1000 and continued to age day 1400. Data provided by ATSDR.

FIGURE 3-18. AALM SIMULATION OF SUBJECT 87350 (FEMALE).

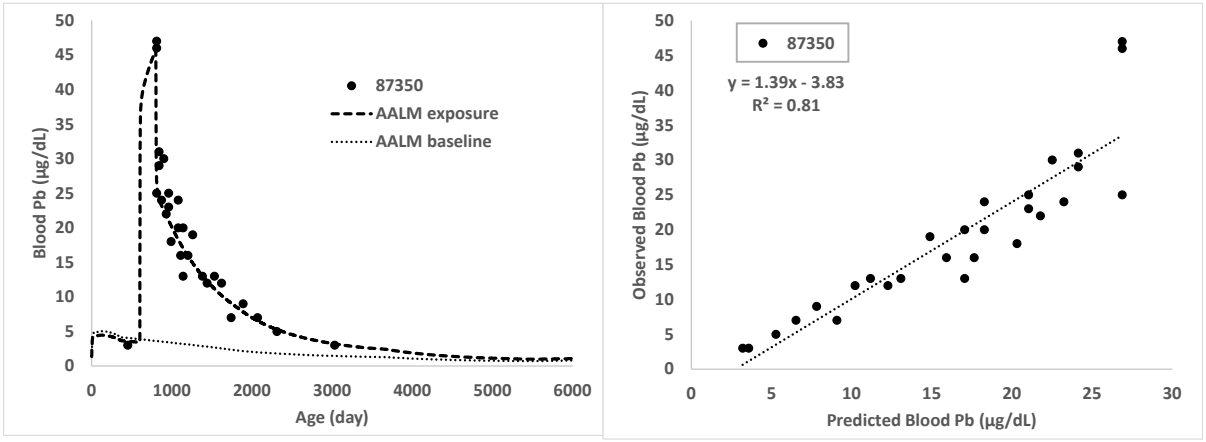

Baseline (15 µg/day) was set to achieve a 6-month BLL of approximately 5 µg/dL, consistent with data for other subjects. Exposure to 13,000 ppm dust Pb (RBA = 0.6) began on age day 600 and continued to age day 800. Data provided by ATSDR.

FIGURE 3-19. COMPARISON OF BLOOD PB PREDICTIONS OF AALM AND IEUBK MODEL.

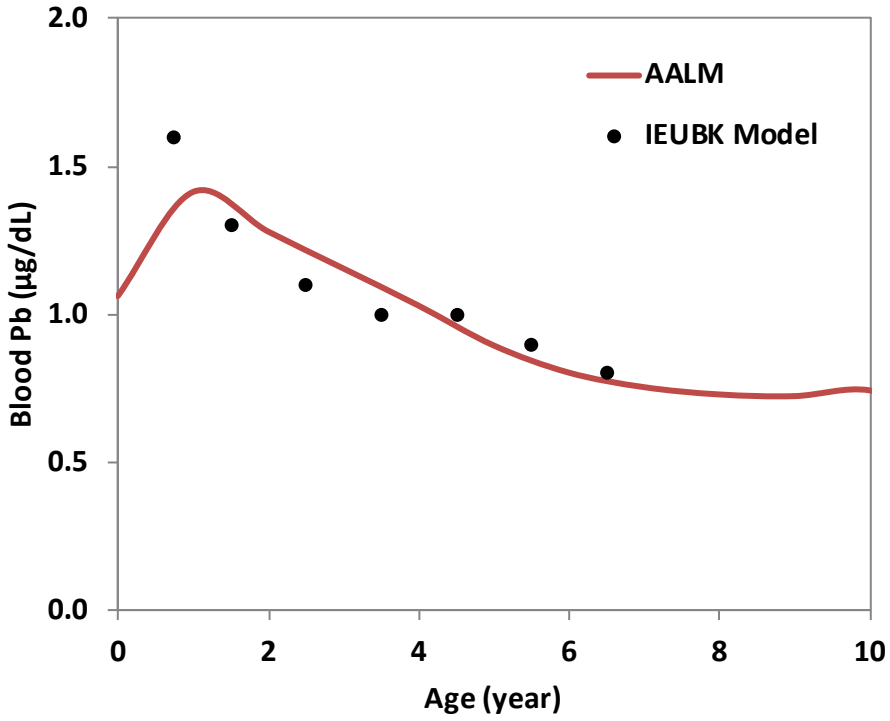

Maternal blood Pb was assumed to be 1 µg/dL. Exposure was to Pb in soil (RBA = 0.6) at a constant intake (10 µg/day). Absorption parameters were: AF1 C1=0.40 (AF1=0.39 at birth), AF1 C2=0.28 (AF1=0.12 at age ≥10 years). The average AF1 for age 0-7 years was 0.26.

FIGURE 3-20. COMPARISON OF BLOOD PB PREDICTIONS OF AALM AND ALM.

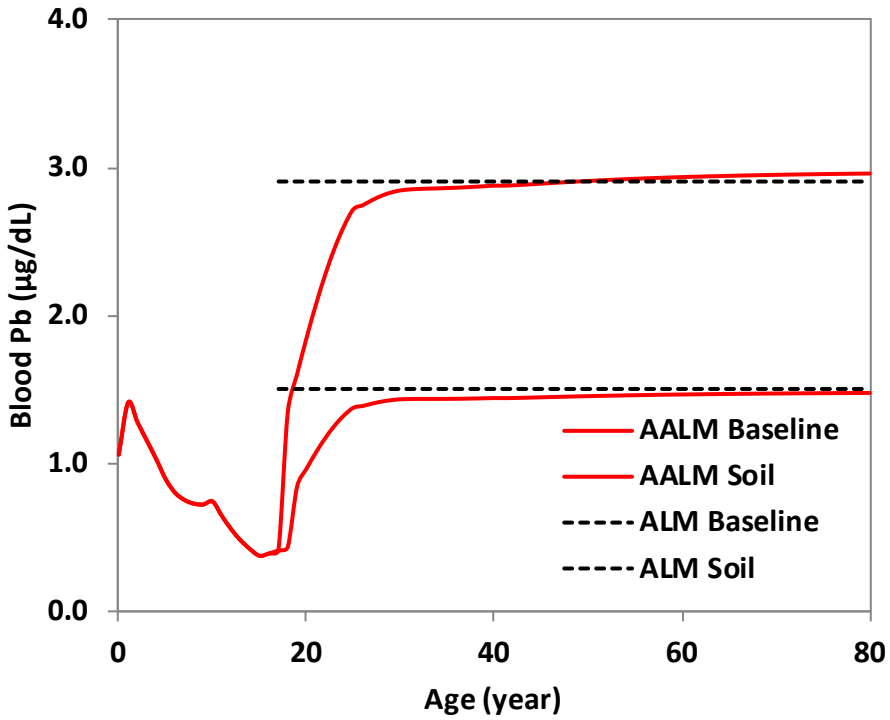

AALM input parameters:

OTHER Baseline Pb=6 µg/day

OTHER Pulse Pb=12 µg/day

OTHER Pulse start= 6205 day (17 years)

OTHER RBA = 1

SOIL baseline Pn = 0 µg/day

SOIL Pulse Pb=600 µg/g (1000*219/365)

SOIL IRs = 0.05 at age ≥15 years

SOIL RBA = 0.6

AF1 C1=0.40 (AF1=0.39 at birth), AF1 C2=0.28 (AF1=0.12 at age ≥10 years)

CHAPTER 4. EVALUATION AND DEVELOPMENT OF AALM.CLS

4.1. INTRODUCTION

This chapter summarizes developments in the AALM that were initiated in early 2013 by EPA's Office of Research and Development (ORD)/National Center for Environmental Assessment (NCEA). Six major objectives have been realized in this most recent effort, and are described in this report including: (1) recoding of the AALM biokinetics models from Visual C to the more robust kinetic model development software, Advance Continuous Simulation Language, ACSL® (acslX); (2) addition of a user friendly, flexible, and transparent exposure model interface implemented in Microsoft Excel®(Excel); (3) capability to run either the Leggett (AALM-LG) or O'Flaherty (AALM-OF) biokinetics models from the same exposure model interface, and with the same exposure and absorption conditions; (4) a more realistic RT model representation in both the Leggett and O'Flaherty biokinetics models compared with earlier versions; (5) accessible and transparent output for easy comparison of the predictions from the Leggett and O'Flaherty biokinetics models; and (6) an evaluation and optimization of the Leggett and O'Flaherty biokinetics models against a common set of observations that lead to the version of the AALM in acslX (AALM.CLS v.4.2, July 2015).

Section 4.2 provides a brief overview the functional structure of AALM.CLS. Section 4.3 compares the structures of the two biokinetics models contained in the AALM.CLS (AALM-LG, AALM-OF). Section 4.4 describes the outcomes of model runs that compare predictions of blood and tissue Pb levels obtained from the AALM-LG and AALM-OF. Section 4.5 presents the results of sensitivity analyses coefficients (SSCs) conducted from the AALM.CLS biokinetics models. Section 4.6 presents the conclusions from the model comparison. Section 4.7 presents results of an empirical evaluation and optimization of the AALM-LG and AALM-OF. Section 4.8 provides conclusions and discusses implications of performance of the optimized models for model applications. Section 4.9 discusses differences between the AALM.CLS model output and the IEUBK model for similar exposures, identifies AALM model parameter changes that resolve the differences, and provides a rationale for changes in the parameter values. Section 4.10 outlines the next steps to be taken, and the data needed to further develop and evaluate the AALM.CLS.

4.2. OVERVIEW OF AALM.CLS STRUCTURE

The AALM predicts blood and tissue Pb masses (µg) and concentrations (µg/g) resulting from exposures to Pb in air, drinking water, surface dust, food, or miscellaneous Pb ingestion pathways. The AALM exposure module allows the user to simulate multi-pathway exposures that are constant or that vary in time increments as small as one day; and that occur at any age from birth to 90 years. The user can select to run a Pb biokinetics simulation based on either the Leggett (AALM-LG) or O'Flaherty (AALM-OF) biokinetics models. The ICRP Human Respiratory Tract Model (HRTM; ICRP, 1994) deposition and absorption parameters are used in both the AALM-LG and AALM-OF. The user can select gastrointestinal absorption fractions for any age values as well as values for relative bioavailability (RBA) of Pb from all ingestion pathways.

The AALM software architecture consists of three components: (1) a macro-enabled Excel workbook (INPUT&OUTPUT.xlsm) that implements the exposure model and provides user access to all exposure and biokinetics parameters in the AALM; (2) an acslX program that implements a Leggett-based

biokinetics model (AALM-LG.csl); and (3) an acslX program that implements an O'Flaherty-based biokinetics model (AALM-OF.csl).

The data flow for AALM simulations is shown in Figure 4-1. The AALM simulation is implemented in acslX with AALM_LG.csl (or AALM_OF.csl). Input parameter values are selected by the user in a macro-enabled INPUT&OUTPUT Excel file (.xlsm). Macros in the INPUT&OUTPUT Excel file pass the input parameter values to a comma-delimited (CSV) text file (INPUT.DAT). Data in INPUT.DAT are imported into the AALM acslX program with acslX m-file scripts. Output variables from the simulation are passed from acslX to a CSV file (OUTPUT.DAT) and are read into the INPUT&OUTPUT Excel file with Excel macros.

AALM inputs and outputs are controlled and recorded in the *INPUT&OUTPUT.xlsm* workbook. This workbook has several functions: (1) allows setting of input parameter values for AALM simulations; (2) macros in this workbook are used to pass data to and from acslX; (3) allows plotting of AALM output data; and (4) provides a complete record of input values and results of each AALM simulation.

Worksheets in *INPUT&OUTPUT.xlsm* allow the user to set exposure scenarios for Pb in air (*Air*), surface dust, (*Dust*), drinking water (*Water*), food (*Food*) and/or other ingestion intakes (*Other*). Exposures can be discrete (i.e., a series of exposures at selected ages), and/or pulsed in a repeating frequency (e.g., 2 days/week for 3 months/year, for a selected age range). The AALM uses inputs from all exposure media when it creates biokinetics simulations. This allows construction of complex multi-pathway exposure scenarios having varying temporal patterns. Worksheets in *INPUT&OUTPUT.xlsm* also allow the user to set values for parameters that control Pb absorption and relative bioavailability in each medium (*RBA*), and biokinetics (*Lung*, *Systemic*, *Sex*). All settings are recorded in the *INPUT&OUTPUT.xlsm* workbook and can be recalled to re-run the simulation.

The two biokinetics models in the AALM have been modified from the originally reported Leggett (1993) and O'Flaherty (1995, 1993) models. The important modifications include: (1) removal of all exposure components (moved to the Excel implementation); (2) implementation of a simplified version of the ICRP HRTM (ICRP, 1994) in both biokinetics models; (3) implementation of the O'Flaherty model growth algorithms in both biokinetics models to enable output of Pb concentrations in tissues in both models, and to unify blood and tissue volumes; and (4) implementation of relative bioavailability factors for ingested Pb from each exposure medium.

4.3. COMPARISON OF STRUCTURES OF AALM-LG AND AALM-OF BIOKINETICS MODELS

The AALM has two systemic biokinetics modules, one that is based on the Leggett (1993) model (AALM-LG) and the other based on the O'Flaherty (1995, 1993) model (AALM-OF). Figures 4-2 and 4-3 show the structures of both models. Table 4-1 summarizes some of the major differences between the two modules. The most important difference is the way each model simulates Pb kinetics in bone. Both models represent kinetics of Pb in bone that are influenced by changes in the rates of bone turnover (bone formation and resorption). In general, the major features of bone Pb kinetics in both models are as follows: (1) relatively rapid transfers of Pb between plasma and bone forming surfaces; (2) increased bone Pb uptake during periods of bone growth; (3) incorporation of Pb into bone matrix and release of Pb from bone matrix during bone resorption; (4) maturation of bone associated with lower rates of bone turnover and related decreased mobility of Pb in bone matrix; and (5) more rapid turnover of trabecular

bone Pb, relative to mature cortical bone. However, these processes are parameterized very differently in the two models.

AALM-LG simulates bone as a multi (6)-compartment system (see Figure 4-4) consisting of 3 cortical and 3 trabecular compartments that are distinguished by different Pb transfer rates: (1) relatively rapid exchange of Pb between diffusible plasma and surfaces of cortical and trabecular bone; (2) slower exchange of Pb at bone surfaces with an exchangeable Pb pool in bone volume; and (3) slow transfer of a portion of Pb in bone volume to a non-exchangeable pool that is released from bone to diffusible plasma only when bone is resorbed. Bone growth and maturation are simulated by age-dependent adjustments in rate coefficients for Pb transfers from plasma-to-bone surfaces, and from bone matrix to plasma. This approach simulates outcomes of the bone formation and resorption with bone Pb kinetics parameters, rather than simulating the underlying physiology of bone formation and resorption directly with parameters that govern formation and resorption.

AALM-OF simulates bone formation, resorption, and maturation of bone explicitly, and links these processes to uptake and release of Pb from bone (see Figure 4-5). In AALM-OF, bone turnover in cortical and trabecular bone is simulated with parameters that govern age-dependent bone formation and resorption of bone. Two phases of bone turnover are simulated. In juvenile bone, formation and resorption rates in cortical and trabecular bone are relatively high (high bone turnover) and formation dominates, resulting in bone growth, which ceases at age 25 years. In mature bone, formation and resorption rates are slower and bone formation rate equals resorption rate, resulting in remodeling, but no net growth of bone. Transfers of Pb into and out of trabecular bone are governed by age-dependent rates of bone formation and resorption, respectively. Cortical bone is assumed to consist of two regions: (1) metabolically active cortical bone in which Pb transfers are governed solely by rates of bone formation and resorption; and (2) mature cortical bone in which Pb undergoes exchange with bone calcium. The later process is simulated as bidirectional radial diffusion of Pb in between eight concentric shells of cortical bone.

The approach to modeling bone in AALM-OF (i.e., bone Pb kinetics as a function of bone physiological parameters) offers two major advantages: (1) inclusion of parameters that control bone physiology (e.g., growth, volume, maturation) supports simulation of changes to bone mineral metabolism that might affect bone production, growth, or maturation (e.g., disease, nutrition, menopause, weightlessness), and predictions of the effects that these changes might have on bone Pb kinetics. An analogous simulation in the AALM-LG requires direct knowledge (or assumptions) of the effects of these changes on bone Pb transfer coefficients; and (2) advances in the knowledge of bone physiology (e.g., metabolism, growth, resorption, disease) and of bone kinetics for other elements (e.g., calcium, strontium) can be incorporated into the model to improve the parameterization and parameter values of the model, and its capability to simulate and predict bone growth, volume, and maturation. In contrast, specialized studies for all the different age related scenarios would be needed to improve values for the less physiologically representation of bone Pb kinetics in the AALM-LG model based on compartment transfer rates that change with age.

4.4. COMPARISON OF AALM-LG AND AALM-OF PREDICTIONS OF BLOOD AND TISSUE PB

Differences in the structures of the Leggett and O'Flaherty biokinetics models would be expected to result in different predictions of blood and tissue Pb levels for similar Pb exposure assumptions (Maddaloni et al., 2005). The revised AALM provides a convenient platform for comparing the models, because it

allows both to be run using the same exposure and absorption settings. Two types of comparisons were made of AALM-LG and AALM-OF: (1) age profiles for blood and tissue Pb levels following an exposure to a constant Pb intake (µg/day) were simulated and compared; and (2) dose-response relationships between ingested dose and Pb levels were compared by simulating a series of increasing Pb intakes. In either type of simulation, parameters that control Pb absorption and growth were set to the same values (defaults for AALM-OF), so that differences in blood and tissue Pb levels could be attributed entirely to differences in the simulation of systemic (post-absorption) biokinetics.

4.4.1. Comparison of Model Predictions for Constant Pb Intake

Figures 4-6 thru 4-9 show results of the simulations for a constant ingestion of 5 µg Pb/day beginning at birth and extending to age 30 years. This exposure results in predicted blood Pb concentrations less than 5 µg/dL, which is well below the concentration at which saturation of uptake into RBCs significantly affects blood Pb levels. Figure 4-6 shows the age profiles for selected output variables (µg Pb in blood, bone, soft tissue and total body). Figure 4-7 shows the differences expressed relative to the AALM-LG (arbitrarily selected as the reference for presentation of the results). A negative value in Figure 4-7 indicates that the prediction from AALM-OF is less than that from AALM-LG. For example, -0.65 in Figure 4-7 indicates that the AALM-OF blood Pb prediction is less than the AALM-LG prediction, and the magnitude of the difference is 65% relative to the AALM-LG value. Figure 4-8 compares predicted cumulative urinary and fecal Pb excretion. Figure 4-9 compares elimination rates following cessation of exposure.

Several differences between the models are evident from these comparisons.

- AALM-OF predicts lower blood Pb levels prior to age 10 years (64–65%), after which, the models begin to converge on similar blood Pb levels, with adult predictions from the AALM-OF exceeding AALM-LG by approximately 20%.
- AALM-OF predicts lower bone Pb levels in children prior to age 10 years (63–68%), after which, the models begin to converge on similar bone Pb levels, with adult predictions from the AALM-OF exceeding AALM-LG by approximately 18%.
- AALM-OF predicts lower soft tissue Pb levels (all tissues combined, excluding bone) at all ages (59–92%).
- Both models predict similar accumulation of Pb over the lifetime, reflected in similar total body burdens (agreement is within 10%).
- With cessation of exposure, both models predict rapid declines of Pb in blood ($t_{1/2}$ = 30–50 days) and soft tissue, with a slower decline in bone Pb ($t_{1/2}$ 10–20 years).
- Both models predict multiple rates of decline in blood Pb. In adults, the half-time for the first 50 days following cessation of exposure is approximately 36 days in AALM-LG and 46 days in AALM-OF. The half-time for the period 5–20 years following cessation of exposure is 12.7 years in AALM-LG, and 10.9 years in AALM-OF. The slow phase results from transfer of bone Pb to blood.

- Both models predict a more rapid decline in bone Pb in children compared to adults following cessation of exposure. The two models predicted similar half-times for bone Pb elimination in children ($t_{1/2}$ = 3.00 [AALM-LG], 2.24 years [AALM-OF]).
- Although both models predict slower elimination of Pb from bone in adults, AALM-OF predicts a more rapid decline ($t_{1/2}$ = 12.6 year) than AALM-LG ($t_{1/2}$ = 19.7 year).
- AALM-OF predicts a higher rate of urinary excretion of Pb compared to AALM-LG. Fecal excretion is identical in both models because it is dominated by unabsorbed Pb and gastrointestinal absorption parameters were set to the same values in both models for the comparison simulations.

Amounts of Pb in tissues are converted to Pb concentrations in both models by dividing Pb masses by age-dependent values for tissue weights. The latter are predicted in both models from the body growth and tissue growth models developed by O'Flaherty (1995). The blood and bone Pb concentrations predicted for an exposure to 5 µg Pb/day are shown in Figure 4-10. Differences in the model predictions of tissue Pb masses are reflected in the tissue Pb concentrations. The magnitudes of the differences between models (i.e., ratio AALM-LG/AALM-OF) are the same for Pb masses and concentrations, because both models use the same tissue growth algorithms, which predict the same tissue volumes and weights.

4.4.2. Comparison of Predicted Dose-Response for Blood and Tissue Pb

Although both AALM-LG and AALM-OF are mathematically linear models (i.e., all state variables are defined with linear differential equations), they predict curvilinear dose-response relationships for blood Pb resulting from a saturable capacity of red blood cells (RBC) to take up Pb. Dose-response relationships predicted from AALM-LG and AALM-OF are shown in Figures 4-11 and 4-12, for children (age 5 years) and adults (age 30 years), respectively. Although curvature of the dose-response relationship for blood derives from saturation of uptake of Pb in RBCs, the two models use different computational approaches to model the saturable uptake. AALM-LG simulates binding of Pb in red blood cells with rate coefficients for transfer of Pb from plasma to RBCs (child and adult, $t_{1/2}$ = 0.0014 days), and from RBCs to plasma (child $t_{1/2}$ = 2.5 days, adult $t_{1/2}$ = 5 days). This results in a rapid uptake, slower release, and accumulation of RBC Pb. The plasma-blood concentration ratio is governed, in part, by the ratio of these transfer coefficients (plasma to RBC/RBC to plasma). The higher ratio in children (i.e., exit rate is faster) results in higher plasma-RBC concentration ratios in children. Above a non-linear, threshold Pb concentration in red blood cells (60 µg/L), the rate constant for transfer into RBCs declines with increasing intracellular concentration, approaching zero (no uptake) at a saturating concentration of 350 µg/dL RBC (see Equation 4-1).

$$TOORBC = TORBC \cdot [1 - \left(\frac{RBCCONC - RBCNL}{SATRAT - RBCNL}\right)]^{1.5} \quad \text{Eq. (4-1)}$$

where *TOORBC* is the deposition fraction from diffusible plasma to red blood cells; TORBC the age-scaled deposition fraction from diffusible plasma to red blood cells below non-linear threshold; *RBCCONC* the red blood cell Pb concentration (µg/dL RBC volume); *RBCNL* the non-linear uptake kinetics threshold concentration (µg Pb/dL RBC volume); and *SATRAT* the maximum capacity of the red blood cell compartment (µg Pb/dL RBC volume).

AALM-OF simulates a binding equilibrium (rather than kinetics) in which Pb in plasma achieves instantaneous equilibrium with unbound Pb in RBCs, which is in equilibrium with bound Pb. Binding parameters include a maximum capacity (270 µg Pb/dL RBC) and half-saturation concentration (0.75 µg/dL RBC), with the relationship represented as follows (see Equation 4-2):

$$CB = (1 - HCT) \cdot CP + HCT \cdot CP \cdot \left\{G + \frac{BIND}{KBIND + CP}\right\} \quad \text{Eq. (4-2)}$$

where *CB* is the blood Pb concentration (µg/dL), *CP* the plasma Pb concentration (µg/dL); *HCT* is the hematocrit; *G* the ratio of unbound RBC Pb to plasma Pb; *BIND* the maximum capacity of RBC binding (µg/dL); and *KBIND* the half-saturation coefficient (µg/dL). One advantage of this approach is that the parameters BIND and KBIND have a direct empirical basis, as they have been estimated from data on Pb concentrations in plasma and RBCs (e.g., Bergdahl et al., 1998; O'Flaherty, 1993). However, a disadvantage is that it represents plasma-RBC kinetics as essentially being instantaneous; whereas, observations made following injection of radiolead suggest that kinetics may be slower and more complex [see Leggett (1993) for discussion of these observations].

The different parameterizations of RBC saturation are evident in the relationships between plasma and blood Pb predicted from the two models. In both models, the plasma-blood concentration ratio increases with increasing blood Pb concentration, as the RBC approaches saturation. In AALM-OF, the plasma-blood Pb ratio below saturation remains nearly constant with age (0.007); whereas, in AALM-LG, the plasma:blood ratios are higher in children compared to adults. AALM-LG predicts a plasma-blood ratio that declines from 0.01 at age 1 year to 0.003 at ages beyond 10 years (below saturation).

Both models predict linear dose-response relationships for bone Pb, and for all other tissue Pb. The predicted dose-response relationships for bone are more similar in adults, whereas, AALM-LG predicts a steeper dose-response relationship for bone in children. The steeper dose-response relationship for bone Pb in children occurs in AALM-LG even though the elimination rates from bone are similar in both models. This suggests that the differences between model results for bone Pb is related to the rates of deposition of Pb in bone, rather than to differences in rates of bone Pb elimination.

4.5. SENSITIVITY ANALYSIS OF AALM-LG AND AALM-OF

Relative to the AALM-LG, AALM-OF predicts lower amounts and concentrations of Pb in blood in children, higher amounts and concentrations of Pb in blood in adults, and lower amounts and concentrations of Pb in soft tissues in at all ages. Numerous individual parameters or combinations of parameters could contribute to these differences. AALM-LG has 39 parameters and AALM-OF has 35 parameters that collectively determine the biokinetics of absorbed Pb in each model to varying degrees. These parameters and their nominal values are presented in Tables 4-2 (AALM-LG) and 4-3 (AALM-OF). A univariate sensitivity analysis was conducted to determine the effect of each parameter on predictions of Pb in blood, bone, and soft tissues.[1] The sensitivity analysis consisted of running each model before and after perturbing values for single parameters by a factor of 0.01, in the up and down

[1] This approach to sensitivity analysis does not consider potential interactions between parameters. Sensitivity coefficients measured in univariate analyses may be larger or smaller than SSCs measured in multivariate analyses (i.e., when multiple parameters are varied simultaneously).

directions. Parameter sensitivities were assessed by comparing standardized sensitivity coefficients (see Equation 4-3):

$$SSC = f'(x) = \frac{ABS[f(x+\Delta x) - f(x-\Delta)]}{2\Delta x} \cdot \frac{x}{f(x)} \qquad \text{Eq. (4-3)}$$

where *SSC* is the standardized sensitivity coefficient; *f(x)* the output variable (e.g., blood Pb) at parameter value *x*; and Δ the perturbation of *x* (e.g., 0.01x). Values for SSC were determined for blood, bone, and soft tissue Pb at ages selected to represent children (5 years) or adults (30 years).

4.5.1. Sensitivity Analysis of AALM-LG

SSCs were derived for all input parameters to AALM-LG other than those that control Pb absorption or growth. Separate sensitivity analyses were run to determine parameter sensitivity of the total amount of Pb in blood, bone, liver, kidney, or other soft tissues, in children (age 5 years) and adults (age 30 years). SSCs are displayed in order of highest to smallest value for adults in Tables 4-4 thru 4-8. Larger values of SSC indicate larger effects of the parameter on blood Pb. For example, blood Pb is most sensitive to the value of the parameter *TEVF*, the deposition fraction for Pb transfer from diffusible plasma to the extravascular fluid (see Table 4-4). The value 8.38 indicates that a 1% change in *TEVF* results in an 8.38% change in blood Pb. Influential parameters have SSCs that exceed 0.1 (>0.1% change in tissue Pb per 1% change in the input parameter).

In the discussion that follows, input parameter values are expressed as their equivalent first-order transfer rates (day^{-1}) shown in Table 4-2 and their corresponding approximate first-order half-times ($t_{1/2}$, day). In AALM-LG, the central distribution compartment is diffusible plasma, which exchanges Pb with other tissue compartments. Input parameters that control transfers of Pb from tissues to diffusible plasma are expressed as first-order rates. Input parameters that control transfers from diffusible plasma to tissues are expressed as deposition fractions. Deposition fractions represent the fractional apportionment of the total outflow of Pb from diffusible plasma (Leggett, 1993). First-order rates are derived in the AALM-LG as the product of deposition fraction and total outflow of Pb from the diffusible plasma compartment (*RPLAS*, see Equation 4-4).

$$REFV = TEFV \cdot RPLAS \qquad \text{Eq. (4-4)}$$

where *REFV* is the transfer rate from diffusible plasma to the extravascular fluid (day^{-1}); *TEFV* the deposition fraction for transfer to the extravascular fluid; and *RPLAS* the total rate of transfer of Pb to all tissues (day^{-1}). The nominal value for *RPLAS* is 2000 day^{-1}. If the deposition fraction for *TEFV* is 0.5, the corresponding transfer rate for *TEFV* is 1000 day^{-1} (0.5×2000 day^{-1}). Values for transfer rates corresponding to deposition fractions are presented in Table 4-2, so that they can be directly compared to the return transfer rates from tissue to diffusible plasma. The values for the corresponding depositions fractions can be calculated from Equation 4-4.

4.5.1.1. Influential Parameters Common to All Tissues

Several parameters had relatively large influences (SSC > 0.1) across all or most of the tissues that were included in the sensitivity analysis and dominate Pb biokinetics in the AALM-LG. These parameters are *TEVF*, *TORBC*, *TOSOF0*, *TOLVR1*, *H1TOBL*, and *TBONE*.

The parameter *TEVF* controls the rate of transfer of Pb from diffusible (non-bound) plasma to the extravascular space. The nominal value for the rate is 1000 day^{-1} ($t_{1/2}$ = 1.0 min) or approximately one half of the total transfer rate out of diffusible plasma to all tissues (2000 day^{-1}). The return rate to diffusible plasma is 333 day^{-1} ($t_{1/2}$ = 3.0 min). This results in a rapid exchange of Pb in diffusible plasma with the extravascular fluid, with an equilibrium ratio in which the extravascular fluid contains approximately 3 times the amount of Pb in diffusible plasma. The extravascular fluid serves as a rapid exchange reservoir that contributes to plasma Pb. Increasing or decreasing the value of *TEVF* increases or decreases, respectively, the amount of Pb in plasma and, thereby, blood Pb and the amount of Pb available for distribution to other tissues. The prominence of *TEVF* in the SSCs for all tissues may also result from its use in age-scaling of deposition fractions in the model. Deposition fractions for all tissues other than bone are scaled as function of *TEVF* and *TBONE* (the deposition fraction to bone surfaces) (see Equation 4-5).

$$AGESCL = \frac{1-TEVF-TBONE(t)}{1-TEVF-TBONEL} \quad \text{Eq. (4-5)}$$

where *TBONEL* is the terminal value for *TBONE* on the last day of the simulation. The *AGESCL* variable adjusts the deposition fractions (and total outflow) from diffusible plasma to soft tissues so that their sum does not exceed total outflow (*TEFV*), while outflow to bone (*TBONE*) varies with age. As a result of its use to age scale deposition fractions, changes to *TEVF* affects Pb kinetics of RBC, kidney, liver, and other soft tissues.

The parameters *TORBC* and *RRBC* control the transfer rates of Pb into and out of RBCs, respectively. The nominal values in adults are 480 day^{-1} ($t_{1/2}$ = 2.1 min) and 0.139 day^{-1} ($t_{1/2}$ = 5.0 day). The equilibrium ratio (*TORBC/RRBC*) is approximately 3450, which results in accumulation of Pb in the RBC, relative to plasma, and Pb in red blood cells being the dominant contributor to blood Pb. Increasing the transfer rate into red blood cells (*TORBC*), without a change in the return rate (*RRBC*) increases blood Pb, whereas, increasing the transfer rate out of red blood cells (*RRBC*), makes more Pb available to the diffusible plasma compartment for distribution to other tissues, and decreases blood Pb.

AALM-LG has three soft tissue compartments, representing fast (*SOF0*), moderate (*SOF1*), and slow (*SOF2*) kinetic pools of Pb in soft tissues other than blood, kidney, or liver. The parameter *TOSOF0* controls the rate of transfer from diffusible plasma to the fast compartment. The nominal value in adults is 178 day^{-1} ($t_{1/2}$ = 5.6 min) and the return rate is 2.08 day^{-1} ($t_{1/2}$ = 8.0 hours). Similar to the extravascular fluid, this soft tissue compartment provides an exchange reservoir to support plasma and blood Pb, as well as Pb available for distribution to other tissues.

The parameters *TOLVR1* and *H1TOBL* control the transfer of Pb from diffusible plasma to liver and the return to plasma, respectively. Nominal values are 80 day^{-1} ($t_{1/2}$ = 12.5 min) for transfer to liver and 0.03 day^{-1} ($t_{1/2}$ = 23.1 day) for return. Similar to the rapid exchange soft tissue compartment, this liver compartment provides a reservoir to support plasma and blood Pb.

The parameter *TBONE* controls the transfer rate from diffusible plasma to surface bone, the only pathway for entrance of Pb into bone where it can be sequestered into slower kinetic pools of bone volume. The nominal values are 89 day^{-1} and 71 day^{-1} ($t_{1/2}$ = 11.2 min, 14.1 min) for trabecular and cortical bone, respectively. The return value from both types of bone is 0.5 day^{-1} (14 day). More than 90% of the Pb body burden resides in bone, as a result, the transfer to bone affects Pb levels in all other tissues. The terminal value of *TBONE* (*TBONEL*) is also used in the age-scaling of deposition fractions to all tissues

other than bone (see Equation 4-5). This is reason why it shows up as an influential parameter across all tissues.

4.5.1.2. Sensitivity Analysis of AALM-LG Blood Pb Predictions

AALM-LG SSCs for blood Pb (*ABLOOD*) are shown in Table 4-4. The most influential parameters on blood Pb (SSCs > 0.1) are *TEFV*, *TORBC*, *TOSOF0*, *RRBC*, *TOLVR1*, *H1TOBL*, and *TBONE*. These parameters have SSCs > 0.1 across all tissues (see Section 4.5.1.1).

4.5.1.3. Sensitivity Analysis of AALM-LG Bone Pb Predictions

AALM-LG SSCs for bone Pb (*ABONE*) are shown in Table 4-5. The most influential parameters on bone Pb (SSCs > 0.1) are *TEFV*, *TORBC*, *TBONE*, *TOSOF0*, *FLONG*, *RCS2DF*, *TOLVR1*, *H1TOBL*, and *RTS2DF*. The bone model in AALM-LG includes three sub-compartments for cortical and trabecular bone that represent fast (surface bone), moderate (exchangeable), and slow (non-exchangeable) Pb pools (see Figure 4-4). The slow compartment contains most (>90%) of the Pb in bone and, therefore, is the major determinant of the amount of Pb in bone. The parameter *FLONG* controls the rate of transfer of Pb from the moderate to the slow compartment. Lead enters the moderate and slow bone compartments from surface bone, which is in direct exchange with plasma. The parameter *TBONE* controls the rate of transfer of Pb to bone surfaces; nominal values are 89 day^{-1} and 71 day^{-1} ($t_{1/2}$ = 11.2 min, 14.1 min) for trabecular and cortical bone, respectively. The parameters *RCS2DF* and *RTS2DF* control the rate of return of Pb from bone surface to plasma (0.5 day^{-1}, $t_{1/2}$ = 1.4 day).

4.5.1.4. Sensitivity Analysis of AALM-LG Liver Pb Predictions

The most influential parameters on liver Pb (SSCs > 0.1) are *TEFV*, *TORBC*, *TOSOF0*, *TOLVR1*, *H1TOH2*, *RLVR2*, *H1TOBL*, and *RLVR1* (see Table 4-6). The liver model in AALM-LG includes two sub-compartments representing fast (H1) and slow (H2) pools. Lead in the fast compartment exchanges with plasma and delivers Pb into the slow compartment and to bile. Transfer of Pb into the fast compartments controlled by the parameter *TOLVR1* (80 day^{-1}, $t_{1/2}$ = 11.2 min) and return to plasma is controlled by *RLVR1* (0.0312 day^{-1}, $t_{1/2}$ = 22.2 day). Transfer of Pb from the fast to the slow compartment is controlled by *H1TOH2* (0.00693 day^{-1}, $t_{1/2}$ = 100 day) and transfer to bile is controlled by *H1TOBL* (0.0312day^{-1}, 22.2 day). Return of Pb to plasma is controlled by *RLVR2* (0.0019 day^{-1}, $t_{1/2}$ = 365 day).

4.5.1.5. Sensitivity Analysis of AALM-LG Kidney Pb Predictions

The most influential parameters on kidney Pb (SSCs > 0.1) are *TEFV*, *TORBC*, *TOSOF0*, *RKDN2*, *TOKDN1*, *TOKDN2*, *RKDN2*, *TOLV1*, and *H1TOBL* (see Table 4-7). The kidney model in AALM-LG includes two sub-compartments representing urinary route through the kidney (RK1) and a storage compartment that exchanges with plasma (RK2) pools. Transfer of Pb into kidney is controlled by the parameters *TOKDN1* (40 day^{-1}, $t_{1/2}$ = 25 min) and *TOKDN2* (0.4 day^{-1}, $t_{1/2}$ = 1.7 day). Return of Pb to plasma is controlled by the parameter *RKDN2* (0.0019 day^{-1}, $t_{1/2}$ = 365 day).

4.5.1.6. Sensitivity Analysis of AALM-LG Other Soft Tissue Pb Predictions

The most influential parameters on other soft tissue Pb (SSCs > 0.1) are *TEFV*, *TORBC*, *TOSOF0*, *RSOF2*, *TOSOF2*, *TOLVR1*, *H1TOBL*, *TOSOF1*, and *RSOF1* (see Table 4-8). AALM-LG has three soft tissue compartments, representing fast (SOF0), moderate (SOF1), and slow (SOF2) kinetic pools of Pb in soft tissues other than blood, kidney, or liver. Transfer into each compartment is controlled by parameters TOSOF0 (178 day^{-1}, $t_{1/2}$ = 5.6 min), *TOSOF1* (10 day^{-1}, 1.7 hours), and *TOSOF2* (2 day^{-1}, $t_{1/2}$ = 8.3

hours). Return of Pb to plasma is controlled by parameters *RSOF0* (2.08 day^{-1}, $t_{1/2}$ = 8.0 hours), *RSOF1* (0.00416 day^{-1}, $t_{1/2}$ = 167 day), and *RSOF2* (0.00038 day^{-1}, 1824 day).

4.5.2. Sensitivity Analysis of AALM-OF

SSCs were derived for all input parameters to AALM-OF other than those that control Pb absorption or growth. Separate sensitivity analyses were run to determine parameter sensitivity of the total amount of Pb in blood, bone, liver, kidney, or poorly perfused and well-perfused tissues, in children (age 5 years) and adults (age 30 years). Input parameter values for AALM-OF are presented in Table 4-3. This is a mix of parameters for Pb, and parameters that control bone formation and resorption rates that determine transfer of Pb in and out of deep bone. SSCs for each tissue are displayed in order from highest to smallest value for adults in Tables 4-9 thru 4-14.

4.5.2.1. Influential Parameters Common to All Tissues

Three parameters had large influences (SSC > 0.1) across all, or most, of the tissues that were included in the sensitivity analysis, and dominate Pb kinetics in the AALM-OF. These parameters are C1, C2, and C3. Urinary excretory clearance of Pb from plasma is simulated in AALM-OF as a function of glomerular filtration rate (GFR). The parameters *C1*, *C2*, and *C3* are unitless parameters in the function that simulates GFR as a function of age. Changes to these parameters alter the rate of removal of Pb from plasma to urine and, thereby, the amount of Pb in blood and available for distribution to other tissues.

4.5.2.2. Sensitivity Analysis of AALM-OF Blood Pb Predictions

The most influential parameters on blood Pb (SSCs > 0.1) are *C1*, *C2*, *BIND*, *KBIND*, and *C3* (see Table 4-9). Uptake of Pb into RBCs is simulated in AALM-OF as a binding equilibrium between plasma Pb and RBC Pb (see Section 2.2). The parameters *BIND* (2.7 mg/L) and *KBIND* (0.0075 mg/L) are the maximum binding capacity of the RBCs, and the half-saturation concentration of Pb for binding, respectively. Changing *BIND* or *KBIND* affects the amount of Pb sequestered in RBCs, and the amount of Pb available to the plasma compartment for distribution to other tissues. Increasing *BIND* increases RBC binding, and increases blood Pb. Increasing *KBIND* increases the plasma Pb concentration needed to achieve a given RBC Pb concentration, and decreases blood Pb.

4.5.2.3. Sensitivity Analysis of AALM-OF Bone Pb Predictions

The most influential parameters on bone Pb (SSCs > 0.1) are *C1*, *C2*, *R0*, *RAD8*, *EXPO*, and *C3* (see Table 4-10). The parameter *R0* controls the clearance of Pb from bone into the vascular sites in bone (canaliculi) where exchange with plasma occurs. The nominal value is 5E-7 cm^3/day. Increasing *R0* decreases bone Pb. The parameter *RAD8* is the radius of the deepest (eight of 8) diffusion shells in mature cortical bone. This parameter determines the diffusion volume (2.14E-3 cm) and, thereby, the clearance of Pb from the deepest bone compartment. Increasing *RAD8* decreases bone Pb. The parameter *EXPO* is a unitless exponent constant in the function that simulates the age-dependency of the bone volume participating in adult remodeling. During adult remodeling, bone formation and resorption rates are slower than during child and adolescent growth periods. As a result, exchange of Pb between deep bone deposits and plasma is slower in mature bone than during growth.

4.5.2.4. Sensitivity Analysis of AALM-OF Liver Pb Predictions

The most influential parameters on liver Pb (SSCs > 0.1) are *C1*, *C2*, *PL*, and *C3* (see Table 4-11). Exchange of Pb between plasma and liver is simulated in AALM-OF as a flow-limited process

determined by the liver/plasma partition coefficient and blood flow to the liver. The parameter *PL* is the liver/plasma partition coefficient (*PL* = 50). The nominal value is 50. Increasing *PL* increases liver Pb.

4.5.2.5. Sensitivity Analysis of AALM-OF Kidney Pb Predictions

The most influential parameters on kidney Pb (SSCs > 0.1) are *C1*, *C2*, *PK*, and *C3* (see Table 4-12). Similar to liver, exchange of Pb between plasma and kidney is simulated in AALM-OF as a flow-limited process determined by the kidney/plasma partition coefficient (*PK* = 50) and blood flow to the kidney. Increasing *PK* increases kidney Pb.

4.5.2.6. Sensitivity Analysis of AALM-OF Poorly Perfused Tissue Pb Predictions

The most influential parameters on poorly perfused tissue Pb (SSCs > 0.1) are *C1*, *C2*, *PP*, and *C3* (see Table 4-13). Exchange of Pb between plasma and poorly perfused tissue is simulated in AALM-OF as a flow-limited process determined by the tissue/plasma partition coefficient (*PP* = 2.0) and blood flow to the tissue. Increasing *PP* increases poorly perfused tissue Pb.

4.5.2.7. Sensitivity Analysis of AALM-OF Well-Perfused Tissue Pb Predictions

The most influential parameters on well-perfused tissue Pb (SSCs > 0.1) are *C1*, *C2*, *PW*, and *C3* (see Table 4-14). Exchange of Pb between plasma and well-perfused tissue is simulated in AALM-OF as a flow-limited process determined by the tissue/plasma partition coefficient (*PW* = 50) and blood flow to the tissue. Increasing *PW* increases well-perfused tissue Pb.

4.6. CONCLUSIONS FROM MODEL COMPARISONS AND SENSITIVITY ANALYSES

Table 4-15 lists the dominate parameters causing major differences between predictions from AALM-LG and AALM-OF and corresponding parameter values that had the highest SSCs for each prediction. Data may exist for some of the significant parameters that would allow evaluation and/or optimization of parameter values. AALM-OF parameters *C1* and *C2* control GFR, and thereby, urinary clearance of Pb from plasma. Abundant data exist on rates and age (i.e., body size) dependence of glomerular filtration in humans (e.g., Peters, 2004; Peters et al., 2000). Data on urinary clearance of Pb in humans also exist that may be useful for evaluating model predictions (e.g., Diamond, 1992).

AALM-OF parameters *BIND* and *KBIND* and AALM-LG parameters *TORBC* and *RRBC* control uptake of Pb into RBCs and, thereby, influence plasma Pb and its distribution to tissues. These parameters can be evaluated against data from studies in which levels of Pb in plasma and whole blood (and/or RBCs) have been measured in humans with methods that ensure sampling of plasma Pb without contamination with Pb from lysed red cells (e.g., SRC, 2003).

Direct empirical evaluation of AALM-OF and AALM-LG parameters that control bone Pb may not be feasible because of lack of data to directly estimate parameter values. However, optimization of influential parameters that control bone Pb levels and relationships between blood and bone Pb may be feasible with data from long-term monitoring studies of blood and bone, where exposure to Pb was abruptly changed (e.g., retired Pb workers; see U.S. EPA, 2013).

Similarly, direct empirical evaluation of AALM-OF tissue-plasma partition coefficients, and AALM-LG transfer rates and deposition fractions that control Pb levels in liver, kidney, and other soft tissues may not be feasible because of lack of data to directly estimate parameter values. However, it may be possible to

optimize these parameters against data from cadaver studies in which the distribution of Pb body burden in bone and soft tissue has been measured.

4.7. EVALUATION AND OPTIMIZATION OF THE AALM

Although the sensitivity analyses described in Section 5.0 provide some insight regarding the parameters that contribute to differences in predictions from the two models; a more important objective is to determine what set of parameters provides the most accurate representation of observations of Pb kinetics in humans. Extensive documentation of the development and calibration of the Leggett and O'Flaherty models has been reported (O'Flaherty, 2000; O'Flaherty et al., 1998; O'Flaherty, 1998, 1995; Leggett, 1993; O'Flaherty, 1993). New data have become available since the development of the models (U.S. EPA, 2013). Important objectives for further development of the AALM are: (1) collect and re-examine all available data for utility in model evaluation, optimization, and validation; (2) conduct a comprehensive evaluation of the models against a common set of data; (3) optimize influential parameters identified in Section 5 that can be informed by the observation data sets; and (4) validate the model against a set of observations not utilized in optimization of the models.

Searches for studies of the toxicokinetics of Pb in humans that provide data that might be useful for estimated model parameter values were conducted. Three types of data were of particular interest: (1) blood, tissue, or excreted Pb paired with measured Pb intakes and/or exposures; (2) temporal patterns of blood, tissue, or excreted Pb following an abrupt change in Pb intake or exposure; and (3) paired data for blood and tissues or excreted Pb (e.g., urine/blood or tissue/blood ratios). Based on the available data retrieved and processed from the searches as well as considerations of the results of comparisons of the two models, a stepwise optimization approach was developed, in which specific outputs of the models were evaluated against observations in humans, and key parameters were optimized to achieve agreement with the observations (see Table 4-16).

Optimization was achieved using maximum likelihood (MLE) algorithms available in acslX (e.g., Nelder Mead) or if this was not possible, by visual inspection. Optimizations were evaluated by inspection of residuals (Equation 4-6) and the r^2 for the least-squares linear regression of observed and predicted values.

$$Residual = \frac{Predicted - Observed}{Standard\ Deviation\ of\ Mean} \qquad \text{Eq. (4-6)}$$

The optimization objectives were residuals $\leq \pm 2$ and $r^2 > 0.70$.

Most pertinent to the AALM.FOR model are the changes made to the Leggett (1993) model to create the AALM-LG model, based on the evaluations described below. These changes are summarized in Table 4-22.

4.7.1. Unification of Simulation of GI Absorption and Growth

A goal of the optimization was to determine if AALM-LG and AALM-OF would converge on similar predictions for post-absorption kinetics of blood and tissue Pb concentrations. To remove effects of differences in absorption and growth parameters in the two biokinetics modules, the GI absorption and growth parameters from the O'Flaherty (1995, 1993) model were adopted for both AALM sub-models. The resulting AALM GI absorption model is a continuous function (Equation 4-7) that simulates an age-dependent decline in the absorption fraction (AF_{Age}), from the value in infancy to the value in adults.

$$AF_{Age} = AF_{C1} - \frac{AF_{C2}}{1+30 \cdot e^{-Age}} \quad \text{Eq. (4-7)}$$

The settings (AF_{C1} = 0.60, AF_{C2} = 0.52) result in AF = 0.58 at birth and AF = 0.08 in adults (see Figure 4-13, OF default). As discussed in Section 4.7.8, AF_{C1} was set to 0.40 for infants based on Ryu et al. (1983). An AF_{C2} of 0.28 keeps the AF for adults at 0.12 (see Figure 4-13, AALM), which aligns with the Adult Lead Methodology (U.S. EPA, 2003).

Tissue growth in the AALM is simulated as a function of body weight, which is age-dependent (see Figure 4-14). Tissue Pb concentrations are calculated as the Pb mass (µg) divided by the tissue weight (g). Concentrations of Pb in bone wet weight are converted to concentration per gram bone mineral by dividing the wet weight concentration by the ash fraction of bone. This conversion was used to compare model predictions with bone X-ray fluorescence (XRF) data, which is typically reported in units of Pb per g bone mineral. Bone ash fractions were assumed to be 0.55 and 0.50 for cortical and trabecular bone, respectively (ICRP, 1981).

4.7.2. Optimization of Plasma Pb – Blood Pb Relationship

Six studies provided data on individual human subjects that can be used to evaluate the relationship between plasma Pb and blood Pb concentrations. Measurements of plasma Pb were made using either inductively coupled plasma mass spectrometry (Smith et al., 2002; Bergdahl et al., 1999; Bergdahl et al., 1998; Hernandez-Avila et al., 1998; Bergdahl et al., 1997; Schutz et al., 1996) or stable isotope dilution with thermal ionization mass spectrometry (Manton et al., 2001). In all of these studies, methods were employed to control for sample contamination, which is of particular importance in measurements of the low Pb levels found in plasma. Taken together, the observations from these reports varied over a wide range of blood Pb (approximately 0.34–94.8 µg/dL) and plasma Pb (approximately 0.0014–1.92 µg/dL) levels. These studies provided 406 individual measurements of plasma Pb and blood Pb, in adult workers as well as individuals with no known history of occupational exposure to Pb (SRC, 2003). Only one study provides similar data in children (Bergdahl et al., 1999). The observations in children do not appear to differ substantially from those for adults.

A best fit (least-squares) model for combined data from the above six studies was identified, and is presented in Equation 4-8:

$$Blood\ Pb = 87.0 \cdot Plasma\ Pb^{0.5} - 3.89 \ (r^2 = 0.90) \quad \text{Eq. (4-8)}$$

AALM-OF parameters KBIND and BIND were optimized (Nelder Mead) against this data set in the AALM-OF function relating plasma Pb and blood Pb (Equation 4-9):

$$CB = (1 - HCT) \cdot CP + HCT \cdot CP \cdot \left(\frac{G+BIND)}{KBIND+CP}\right) \quad \text{Eq. (4-9)}$$

AALM-LG parameter RBCNL was optimized by visual inspection (it was not possible to derive an independent expression for the plasma Pb and blood Pb relationship because relevant parameters control rate constants for transfer of Pb between plasma and RBC compartments).

Figures 4-15 compares the observed and predicted whole blood and plasma Pb in adults relationship. Residuals for the optimized models are within acceptable limits (-2, 2). The r^2 values for predictions are 0.99 and 0.98.

4.7.3. Optimization of Plasma-to-Urine Pb Clearance

Four studies provide data to derive estimates of the Pb plasma-to-urine clearance rate (L/day) (Araki et al., 1986; Manton and Cook, 1984; Manton and Malloy, 1983; Chamberlain et al., 1978). Clearance estimates from these studies are reported in Diamond (1992). These estimated clearance rates are based on measurements made in a total of 32 ("normal" subjects). The mean of the estimates from the four studies is 18 L/day ± 4 (SD).

Rentschler et al. (2012) reported individual subject data on urinary excretion of Pb (µg/g creatinine) and plasma Pb concentration in in five cases of Pb poisoning (blood Pb>80 µg/dL). The cases were followed for periods up to 800 days. If assumptions are made about body weight (not reported) and established associations between creatinine excretion and lead body mass, clearance rates can be estimated from these data. The estimated mean plasma clearance was 43 L/day ±13 (SD) (range: 32–64 L/day). Lead poisoning may have been a contributing factor to the relatively high clearances based on Rentschler et al. (2012). Therefore, for the purpose of model optimization, 18 L/day was selected as the representative value for plasma-to-urine clearance.

In AALM-OF, urinary excretion of Pb is an age-dependent fraction of GFR. Parameters for the GFR function were modified to achieve an adult GFR of approximately 170 L/day/1.73m^2 (120 mL/min/1.73 m^2 body surface area (ICRP, 1981), with infant (<1 year) values 30% of the adult value (Dewoskin and Thompson, 2008). AALM-OF parameters C2 and C3 were optimized in a function relating age and total Pb excretory clearance (FRX) as shown in Equation 4-10.

$$FRX = C1 - C2/(1 + C3 \cdot e^{-AGE}) \quad \text{Eq. (4-10)}$$

AALM-LG parameters TKDN1 and TOURIN were optimized by visual inspection.

Figure 4-16 compares predicted and observed urinary clearance in adults. No data are available to evaluate the different age patterns for urinary clearance predicted by AALM-LG and AALM-OF.

4.7.4. Optimization of Soft Tissue-to-Bone Pb Ratio

Four studies provide data for measurements of post-mortem soft tissue and bone Pb concentrations (Gerhardsson et al., 1995; Barry, 1981, 1975; Gross et al., 1975). Gerhardsson et al. (1995) reported only soft tissue Pb concentrations; whereas, the other three studies reported soft tissue and bone Pb concentrations that can be used to estimate the ratios. Barry (1981, 1975) reported data for children and adults in age brackets, so the data from Barry (1975) was used as the primary source to optimize parameters for kidney/bone and liver/bone Pb ratios as a function of age.

Barry (1975) reported data on tibia Pb concentrations that are simulated as cortical bone concentrations in the AALM models. Since Barry (1975) reported group mean tissue concentrations (not ratios in autopsy cases), the mean tissue-to-bone ratios were approximated from the group means.

In AALM-OF, uptake of Pb into kidney, liver, and other well-perfused tissue is assumed to be flow-limited and governed by blood flow and the tissue/plasma partition coefficients, PK, PL, and PW. Attempts to optimize these three parameters failed to accurately simulate the decline in the tissue/bone ratios predicted from the Barry (1975) observations. An improved fit was achieved when the constants PK, PL, and PW were allowed to vary with age according to the function shown in Equation 4-11.

$$PK = PKC \cdot (1 + e^{-PKA \cdot AGE)}) \quad \text{Eq. (4-11)}$$

The parameters PKC and PKA (for kidney), PLC and PLA (for liver), and PWC and PWA (for other well-perfused) were optimized (Nelder Mead) against the tissue/cortical bone ratios derived from the data reported in Barry (1975).

AALM-LG parameters TOKDN2 and RKDN2 (for kidney) and RLVR2 (for liver) were optimized by visual inspection. It was not possible to use acslX parameter estimation functions because RKDN2 and RLVR2 are array variables.

Figure 4-17 compares predicted and observed kidney/bone and liver/bone Pb ratios in adults. Standard deviations of observed means were not available for calculating residuals because they were calculated from group mean tissue concentration reported in Barry (1975). Values for r^2 for kidney/bone predictions (of average of male and female ratios) were 0.95 and 0.77 for AALM-LG and AALM-OF, respectively. Values for r^2 for liver/bone predictions were 0.96 and 0.93 for AALM-LG and AALM-OF, respectively.

4.7.5. Optimization of Blood-to-Bone Pb Ratio

Two studies provide data to evaluate the relationship between plasma or serum blood Pb and bone Pb concentrations (Hernandez-Avila et al., 1998; Cake et al., 1996). Cake et al. (1996) measured paired serum, tibia, and calcaneus Pb concentrations in 49 adult male Pb workers, and reported corresponding linear regression parameters. Hernandez-Avila et al. (1998) measured paired plasma, tibia and patella Pb concentrations in 26 adults (20 female) who had no known occupational exposures to Pb. These data can be used to derive corresponding linear regression parameters for the log-transformed plasma Pb. Individual subject data were digitized from Figure 1 of Hernandez-Avila et al. (1998), and linear regression parameters derived for the untransformed plasma Pb concentrations, in order to compare these with the linear regression parameters from Cake et al. (1996).

Bone Pb/Plasma Pb slopes at age 50 years were predicted from AALM-LG and AALM-OF from a series of simulations in which Pb intake was varied from 1 to 1000 µg/day. Table 4-17 and Figure 4-18 compare predicted and observed slopes based on data from Cake et al. (1996) and Hernandez-Avila et al. (1998). Given the relatively low residuals for cortical bone, which were within the range -2 to 2, no further optimization for either model was needed for the respective parameters.

4.7.6. Optimization of Bone Pb Elimination Kinetics

Nilsson et al. (1991) reported longitudinal data on blood and finger bone Pb concentrations in 14 Pb workers for period ranging from 8–18 years following cessation of their occupational exposures. The median blood Pb concentration at the end of exposure was approximately 45 µg/dL. The decline in bone Pb concentration was described by a first-order model with a single rate constant. Estimates of elimination half-times for each individual were reported. The group median was 16 years (95% CI: 12, 23). The decline in blood Pb was described by a tri-exponential model with the following parameters.

Parameter	Unit	C1 (95% CI)	C2 (95% CI)	C3 (95% CI)
$t_{1/2}$	year	34 day (29, 41)	1.2 year (0.85, 1.8)	13 year (10, 18)
C	µg/dL	10.2	12.6	22.8

AALM-OF simulations were run for a constant Pb intake from birth to age 60 years, to achieve a terminal blood Pb concentration of approximately 45 µg/dL (1000 µg/day), followed by 20 years without exposure. A first-order exponential rate was estimated for the decline in cortical bone Pb concentrations predicted for 20 years following cessation of exposure. The AALM-OF parameter R0 (coefficient for Pb diffusion out of bone mineral into canalicules) was optimized (visual inspection) to achieve an elimination half-time from cortical cone of 16 years, the median value based on the Nilsson et al. (1991) results.

AALM-LG simulations were run for a constant Pb intake from birth to age 60 years, to achieve a terminal blood Pb concentration of approximately 45 µg/dL (2000 µg/day), followed by 20 years without exposure. A first-order exponential rate was estimated for the decline in cortical bone Pb concentrations predicted for 20 years following cessation of exposure. The AALM-LG parameters FLONG (fraction of total transfer from the exchangeable bone directed to non-exchangeable bone) and RCORT (transfer rate from non-exchangeable cortical bone to diffusible plasma) were optimized (visual inspection) to achieve an elimination half-time from cortical bone of 16 years, the median value based on the Nilsson et al. (1991) results. FLONG and RCORT are age-dependent arrays and were varied in the optimization by applying a constant (proportional) adjustment to all elements in the age array. The same adjustment factor was therefore applied to child and adult values, even though the optimization was made against data only for adults. The same adjustment factor was also applied to RTRAB (transfer rate from non-exchangeable cortical bone to diffusible plasma).

Figure 4-19 compares rates of elimination of Pb from bone and blood with the corresponding empirical models derived for Pb workers (Nilsson et al., 1991). Elimination rates of Pb from bone predicted from the optimized models are within the 95% CI of the empirical model and yield residuals that range within the -2, 2, criteria ($r^2 = 0.99$). Elimination half-times predicted for bone Pb (16 years) were identical to estimates from Nilsson et al. (1991). Although elimination rates from blood predicted by the optimized models are approximately at the confidence limits of the empirical model, the initial model divergence is due largely to the slower (AALM-LG) or faster (AALM-OF) elimination kinetics during the first 5 years following cessation of exposure; after which the models converge on the empirical model ($r^2 = 0.96$ AALM-LG; $r^2 = 0.99$ AALM-OF). Half-times predicted for the period 5 to 20 years after exposure were 1.25 years from AALM-LG and 1.06 years from AALM-OF, similar to values predicted for C2 (1.2 year) from Nilsson et al. (1991).

4.7.7. Evaluation of Blood Pb Elimination Kinetics in Adults

Rabinowitz et al. (1976) conducted a pharmacokinetics study in which four adults ingested daily doses of [^{207}Pb] nitrate for periods up to 124 days. Concentrations of ^{207}Pb in blood, urine, and feces were then monitored during and following cessation of exposure, and data on daily intakes and blood concentrations for each subject were reported. Absorption fractions for Pb were estimated for each individual based on mass balance in feces.

Figure 4-20 compares observed and predicted blood ^{207}Pb concentrations for the optimized AALM-LG and AALM-OF. Gastrointestinal absorption fractions were set in both models to the estimates for each individual reported in Rabinowitz et al. (1976). No other changes were made to parameter values. Although both models AALM-LG predict a rise and decline in blood Pb concentrations, AALM-LG predictions are closer to the observations. Values for r^2 for AALM-LG predictions are 0.99, 0.98, 0.92, and 0.97 for Subjects A, B, D, and E, respectively. Values for r^2 for AALM-OF predictions range from

0.08 (Subject E) to 0.24 (Subjects A, B, and D). AALM-OF predicts slower accrual and decline of blood Pb, and lower peak blood Pb concentrations.

4.7.8. Evaluation of Blood Pb Elimination Kinetics in Infants

Only two studies provide data on the relationships between Pb dose and blood Pb concentration in infants (Sherlock and Quinn, 1986; Ryu et al., 1983). In the Ryu et al. (1983) study, blood Pb concentrations were monitored in 25 formula-fed infants. From birth to age 111 days, infants were fed formula (packaged in cartons) that had a Pb concentration of approximately 20 µg/L. From age 112 to 195 days, a subset of the infants (n = 7) were switched to formula (packaged in cans) that had a Pb concentration of approximately 57 µg/L. Formula intakes were measured, and provided estimates of Pb intakes in each subject. Ryu et al. (1983) reported a table of individual Pb intakes, and presented a figure illustrating group mean blood Pb concentrations at various ages (these data were digitized for use in this analysis). Standard errors (or deviations) of mean blood Pb concentrations were not reported; however, as discussed below, based on Sherlock and Quinn (1986), standard errors may have been approximately 10% of the means. The parameter for maternal blood Pb concentration was set at 10 µg/dL, the reported maternal mean for the study. Lead absorption was not quantified in Ryu et al. (1983); therefore, the gastrointestinal absorption fraction during infancy was set to 40%, based on estimates from mass balance studies (Ziegler et al., 1978). No other changes were made to parameter values. Figure 4-21 compares predicted and observed blood Pb concentrations for the two exposure regimens (carton formula or carton followed by canned formula). Simulations are shown for the mean intake (12–20 µg/day) and ± 1 SD (10–18 µg/day, 15–22 µg/day). AALM-LG encompasses most of the observations within ±1 SD of the mean intakes. AALM-OF predictions are higher than observations. If standard errors of mean blood Pb concentrations were 10% of the mean, residuals for AALM-LG predictions ranged from -3.7 to 0.15 for carton exposures (mean -1.2). Residuals for AALM-OF predictions ranged from -3.0 to 4.4 (mean 2.0). Both models capture the increase in blood Pb concentration associated with the switch the higher Pb intakes for canned formula and the overall temporal trends in the observations; r^2 for predictions were 0.85 and 0.76 for AALM-LG and AALM-OF, respectively.

Sherlock and Quinn (1986) measured blood Pb concentration in 131 infants at age 13 weeks and estimated dietary intake of Pb for each infant based on Pb measurements made in duplicate diet samples collected daily during week 13. Sherlock and Quinn (1986) reported a plot of blood Pb means and standard errors for group mean dietary Pb intakes (these data were digitized for use in this analysis). The parameter for maternal blood Pb concentration was set at 18 µg/dL, the reported maternal geometric mean. The gastrointestinal absorption fraction was set at 40% for infants; the same value used in simulations of Ryu et al. (1983). Figure 4-22 compares predicted and observed blood Pb concentrations for the range of Pb intakes in the study. Both models reproduce the general shape of the observed curvilinear dose-blood Pb relationship; the apparent plateau observed at the higher end of the dose range, however, is achieved at higher doses in the models (>800 µg/day AALM-LG, >600 AALM-OF). Although the model results for the plateau contributed to high residuals at the highest Pb intake (>200 µg/day), residuals for lower Pb doses ranged from -4.8 to 1.5 (mean -2.3) for AALM-LG and -4.3 to 2.2 (mean – 1.0) for AALM-OF. The overall dynamics of increasing blood Pb with increasing Pb dose was predicted with r^2 = 0.95 for AALM-LG and 0.98 for AALM-OF. One possible explanation for the higher plateaus in the dose-blood Pb relationship predicted from both models is that the models may estimate higher saturation levels of Pb in RBCs than actually occurred in the infants in the Sherlock and Quinn

(1986) study. Parameter values for RBC uptake are based on data collected on adults, and have not been optimized for infants due to an absence of good supporting data (see Section 4.7.2).

4.8. CONCLUSIONS AND IMPLICATIONS OF PERFORMANCE OF OPTIMIZED MODELS

The initial configuration of the AALM biokinetics model was an acslX implementation of the Leggett (1993) and O'Flaherty (1995, 1993) models. The AALM.CLS (v. 4.2, July 2015) introduced several changes to both models, including new parameters (see Table 4-18), and has optimized parameter values against the same data sets. Some of the data used in the optimization were not available at the time the original models were developed. Optimization against a common set of data resulted in convergence of model predictions for blood, bone, and soft tissue (see Figures 4-23 and 4-24). The optimized AALM-LG and AALM-OF predict similar blood, bone, and soft tissue Pb concentration (see Table 4-19). Evaluation of model predictions of blood Pb relationships at known ingestion doses of Pb was limited to data in a few adult subjects (Rabinowitz et al., 1976), and only two studies in infants (where Pb ingestion doses were estimated from dietary [formula] Pb measurements) (Sherlock and Quinn, 1986; Ryu et al., 1983). No data were available on blood Pb concentrations in children or adolescents, for whom Pb ingestion doses were known with certainty. Several studies have reconstructed Pb intakes in children from exposure models supported by measurements of environmental exposure concentrations (Dixon et al., 2009; TerraGraphics Environmental Engineering, 2004; Malcoe et al., 2002; Hogan et al., 1998; Lanphear et al., 1998; Lanphear and Roghmann, 1997; Bornschein et al., 1985). However, these studies were not considered for evaluation of the AALM biokinetics models since they would introduce exposure uncertainty into the evaluation.

Although limited in scope, these evaluations provide several insights into model performance. In general, the AALM, in both AALM-LG and AALM-OF configurations, predicted-observed blood Pb dynamics in infants and adults, in response to changing Pb dosing (see Figures 4-20 thru 4-22). In infants, observed blood Pb concentrations were on average within ±2 SE of the observed mean (mean residual range -2, 2). AALM-LG and AALM-OF predict similar quasi-steady state blood Pb concentrations in infants (Figures 4-21 and 4-22). Both models predict a higher plateau for the dose-blood Pb relationship than was observed in infants, however, this difference would be of quantitative significance only at intakes resulting in blood Pb concentrations >30 µg/dL.

AALM-OF predicts slower than observed blood Pb kinetics in adults compared to AALM-LG. This resulted in larger differences between predicted and observed blood Pb concentrations in controlled, short-term, exposure studies. More rapid blood Pb kinetics predicted by AALM-LG provided a closer agreement to observations (see Figure 4-20). Although short-term exposure studies revealed important differences in blood Pb kinetics predicted by AALM-LG and AALM-OF, both models predict well the long-term elimination rates of Pb from bone following decades of exposure, and its effect on long-term elimination of Pb from blood, that have been observed in worker populations following cessation of exposure (see Figure 4-19).

Optimization exercises also revealed differences in model structure that are relevant to model applications. Attempts to optimize AALM soft tissue/bone lead ratios solely by adjusting tissue/plasma partition coefficients were unsuccessful. Improved performance was achieved by introducing age-dependence and larger values for partition coefficients. O'Flaherty (1995, 1993) assigned values of 50 to the kidney/plasma and liver/plasma partition coefficients. The optimized values are substantially higher;

approximately 1350 for plasma/kidney, and 1600 for plasma/liver, in infants that progressively decrease with age to adult values of approximately 700 and 800 respectively. It is possible, and likely, that these large adjustments were necessary because the assumption of flow-limited transfer of Pb into and out of soft tissue Pb does not accurately reflect the complexities of age-dependent transport and retention of Pb in soft tissues. In support of this hypothesis, optimization of the bidirectional transfer coefficients that govern uptake and retention of Pb in kidney and liver successfully predicted observations made in infants, children and adults (see Figure 4-17).

AALM-LG and AALM-OF were also successfully optimized to predict observed relationships between plasma and whole blood Pb concentrations in adults even though the two models use very different mathematical approaches to simulating uptake and retention of Pb in RBCs. AALM-OF simulates binding of Pb with RBCs as a saturable instantaneous equilibrium. AALM-LG simulates bidirectional transfer between plasma and RBCs, with saturable transfer into RBCs. Transfer out of RBCs in AALM-LG is age-dependent and faster in children than in adults. The validity of the age-dependence was not rigorously explored in this analysis. What little data there are on plasma-RBC relationships in children does not suggest an appreciable difference in the relationship for children and adults (Bergdahl et al., 1999). Since the age-dependence assumption could not be rigorously evaluated it is retained in AALM-LG.

The most substantial differences in the structures of AALM-LG and AALM-OF are in the simulation of bone Pb kinetics. In AALM-LG, bone Pb kinetics are represented as age-dependent rate coefficients for transfer of Pb into and out of bone. In AALM-OF, bone Pb kinetics are simulated as outcomes of a physiological model of bone formation and resorption. The physiological approach to bone metabolism implemented in AALM-OF allows the model to be used to explore relationships between bone metabolism and Pb kinetics. This is potentially useful for simulating Pb kinetics in various bone metabolism contexts associated with life stages [e.g., pregnancy and menopause, O'Flaherty (2000); diseases (e.g., bone wasting diseases); and environments (e.g., weightlessness)].

Although, at this time, the AALM remains a research model, it possesses several attributes (discussed in the following bullets) that make it attractive in human health risk assessment when estimating Pb internal dosimetry following real or hypothetical environmental exposures.

- Currently, human health risk assessment of Pb is conducted using two separate regulatory models, the IEUBK model for Lead in Children and Adult Lead Methodology. The IEUBK model has a terminal age of 7 years. The Adult Lead Methodology is limited to adults. The AALM provides a single physiological/compartmental model capable of predicting blood Pb concentrations at all ages from birth through adulthood. The AALM would replace or supplement the results of the two separate models, and would provide additional assessment capability for older children and adolescent subpopulations.

- The current regulatory model, the Adult Lead Methodology is a slope factor model in which biokinetics are represented as a single variable relating the linear slope of the change in blood Pb concentration per unit change of absorbed Pb (µg/day). The AALM offers a more mechanistic approach to simulating Pb kinetics that can incorporate information on age, growth, life stage, and other physiological variables that may affect Pb kinetics.

- The AALM can simulate exposures in time steps as small as a single day. This allows predictions of blood Pb concentrations associated with acute or highly intermittent exposures. The IEUBK model and Adult Lead Methodology simulate quasi-steady state blood Pb concentration

associated with exposures that have durations of >3 months. Shorter-term dynamics of blood Pb concentrations expected to occur with exposures that vary over days or weeks cannot be simulated with the IEUBK model or the ALM.

- The AALM can predict concentrations of Pb in bone. This offers the potential for using estimates of bone Pb as an internal dosimeter in assessing health risk from exposure to environmental Pb. Bone Pb may be more suitable than blood Pb when predicting risk for certain effects of Pb such as hypertension (U.S. EPA, 2013).

- The RT model in the AALM provides a more realistic simulation of inhaled aerosols of Pb that incorporates information on air Pb concentrations, air Pb particle size, solubility, receptor activity levels (which determine inhalation volumes), and age. This capability of the AALM is a major improvement over the RT representation in the IEUBK model, which consists only of parameters for inhalation volumes, and a single parameter for the absorption fraction of inhaled Pb (from the lung and GI tract). The Adult Lead Methodology does not represent the RT.

4.9. CALIBRATING THE AALM TO THE IEUBK MODEL

Figure 4-25 compares predictions of the AALM and the IEUBK model for a continuous dust Pb intake of 10 µg/day. In both models, the relative bioavailability (RBA) for Pb in dust was assumed to be 60%. This corresponds to an absolute bioavailability of approximately 20% at age 2 years in the AALM and 30% in the IEUBK model. At age 2-3 years the IEUBK model predicts a blood Pb concentration of 1.1 µg/dL; AALM-LG and AALM-OF predict 2.1 and 2.8 µg/dL, respectively.

Table 4-20 compares predictions of adult blood Pb concentrations from the Adult Lead Methodology and AALM.CLS, for an exposure to 1000 ppm. In both models, the RBA for Pb in dust was assumed to be 60%. This corresponds to an absolute bioavailability of approximately 4.8% in the AALM and 12% in the Adult Lead Methodology. The Adult Lead Methodology predicts a blood Pb concentration of 2.9 µg/dL; AALM-LG and AALM-OF predict 3.1 and 4.6 µg/dL at age 30 years (mid-point for age range in the Adult Lead Methodology, 17-45 years), respectively.

The optimized AALM discussed in Section 4.7 thus predicts blood Pb concentrations in children that are approximately 2-fold higher than the currently established regulatory IEUBK model based on the same Pb intakes. Data available for optimizing and evaluating performance of the Pb biokinetics models are largely limited to data for Pb kinetics in adults. Only two studies have reported data on intake-blood Pb relationships in infants (Sherlock and Quinn, 1986; Ryu et al., 1983), and no data of this type are available for children in the age range 1-7 years, the age range simulated in the IEUBK model. Given the large uncertainties in the available data on intake-blood Pb relationships in children, the model differences in absolute terms are relatively small in the context of model capabilities (e.g., approximately 1–2 µg/dL in children for a dust Pb ingestion rate of 10 µg/day). These small differences in model estimates, however, could have implications to consider in making risk management decisions at contaminated sites, which are typically based on a “not-to-exceed” blood Pb concentration (U.S. EPA, 1994a).

The IEUBK model has a long, established history of use in risk assessment and support for soil clean-up goals at hazardous waste sites. Thus, it was deemed worthwhile to further evaluate the most sensitive AALM parameter values to determine which parameters values could be calibrated against the IEUBK

model output for child blood Pb concentrations relative to Pb intake without altering the AALM model performance in simulating the infant and adult data.

This additional evaluation identified value changes for a single biokinetic parameter, *RRBC*, that were sufficient to align the AALM-LG results more closely with the IEUBK model results. The RRBC parameter controls the rate of return of Pb from RBCs to plasma. Support for adjusting this parameter is based on the following three arguments: (1) sensitivity analyses of the AALM-LG revealed that blood Pb predictions were highly sensitive to parameters controlling plasma-RBC Pb exchange rates (Section 4.5, Table 4-4), (2) the parameter *RRBC* value is derived from an age-dependent array that allows adjustment of the parameter value for children without altering values for infants or adults, precluding degradation of model performance in estimating Pb kinetics for infant and adult subpopulations; and (3) the RRBC parameter value for children remains uncertain and has no data support, however the upward adjustment needed for this parameter (i.e., faster outflow from RBCs) is consistent with assumptions that were made in the early development of the Leggett model, namely that removal half-times of Pb from RBCs are expected to be shorter in young children than in adults (Leggett, 1993). The *RRBC* parameter was adjusted upward until close agreement was achieved between blood Pb predicted by AALM-LG and the IEUBK model for a constant ingestion intake of 10 µg/day Pb in surface dust, and an RBA relative to soluble Pb = 0.60 (compare Figure 4-25 with 4-26).

Using the same rationale, red cell parameters in AALM-OF were adjusted to align the AALM-OF blood Pb predictions in children more closely with the IEUBK model results. Unlike the AALM-LG, which represents Pb exchanges between plasma and RBC with first-order rate coefficients, the AALM-OF represents binding of Pb in RBCs as an instantaneous binding equilibrium with plasma Pb controlled by two parameters, a half-saturation parameter (*KBIND*) and maximum binding capacity (*BIND*), both of which are constants and independent of age. Although, either of the two parameters could be adjusted, the half-saturation parameter (*KBIND*) was selected in order to keep the binding capacity unchanged, which is similar to the strategy used in resolving differences with AALM-LG.

As illustrated in Figure 4-26, adjustments to the RBC parameters in the AALM-LG and AALM-OF resulted in close agreement with child blood Pb profiles in children predicted by the IEUBK model. At age 2-3 years the IEUBK model predicts a blood Pb concentration of 1.1 µg/dL; AALM-LG and AALM-OF predict 1.3 and 1.5 µg/dL, respectively, for a dust Pb intake of 10 µg/dL. Because the parameter adjustments were age-dependent and were restricted to children, the adjustments had no effect on predictions of Pb kinetics in adults, and the revised AALM models performed similarly to the optimized version in predicting observed Pb kinetics in adults. Similarly, the adjustments made to the AALM RBC parameter values for the children subpopulation had minimal effect on the model predictions of blood Pb levels or kinetics in infants (see Figures 4-27 and 4-28). Blood and tissue Pb concentrations predicted by the revised AALM are presented in Table 4-21.

4.10. DATA NEEDS AND FURTHER EVALUATION OF THE AALM

The improvements in the AALM discussed in this report demonstrate the considerable advancements made in the AALM model capability and exposure interface, as well as the optimized parameters that control important model predictions (e.g., plasma/RBC ratios, soft tissue/bone ratios, plasma-to-urine clearance), and that have been optimized against the available data in infants and adults.

Of particular interest to risk assessment applications are predictions of blood and bone Pb, as these two biomarkers have been used extensively to establish dose-response relationships for health effects of Pb in humans (U.S. EPA, 2013). The two models predict long-term accrual of Pb in blood and bone Pb levels in adults (ages >16 years), that differ by less than 20%. This agreement is remarkable, given the very different approaches used to simulate bone Pb, which is the major depot for Pb in the body. This magnitude of difference is less than observed inter-individual variability in blood and bone Pb measurements in humans (CDC, 2013; U.S. EPA, 2013; Hu et al., 2007). The two models also predict similar blood Pb concentrations in children. At an earlier age of 2 years, however, blood Pb concentrations predicted from AALM-LG are approximately 25% lower than predictions from AALM-OF, however, data are limited, and additional data are likely to result in improvements in model performance.

Blood Pb concentrations in adults predicted from the AALM are very similar to predictions from the Adult Lead Methodology for the same soil Pb concentrations. Predictions for infants are similar between the AALM and the IEUBK. With the adjusted RBC parameter value, the AALM and IEUBK model predict similar blood Pb concentrations in children for the same dust Pb intakes and RBA assumptions. Subject to further external peer review and verification of the AALM results, the agreement between the AALM, the IEUBK model, and the ALM supports the potential future use of the AALM in risk assessment applications to supplement or replace the IEUBK model and the ALM in supporting regulatory decisions. At present, however, the IEUBK model and the ALM remain the established methods that will be used for regulatory decisions.

Recommendations for data to reduce uncertainty in the AALM model results, and improve the consistency among all model predictions include the following:

- *Resolve differences between the AALM-LG and AALM-OF predictions of blood Pb kinetics.* AALM-OF predicts slower accrual and elimination of Pb from blood compared to AALM-LG, while AALM-LG more close reproduced blood Pb kinetics observed in the short-term Pb dosing studies of Rabinowitz et al. (1976). Additional data on blood Pb kinetics may serve to improve the optimization of both models, and resolve these differences. This will be important for application of either model to simulating blood Pb dynamics associated with short-term or highly variable exposures.

- *Evaluate and optimize AALM-OF bone metabolism parameters.* A literature search and review of newer data on rates of bone production and resorption may provide a basis for re-optimization of AALM-OF or its extension to include simulations of specific bone metabolism scenarios of interest to toxicology or risk assessment (e.g., pregnancy, osteomalacia).

- *Further verify AALM-LG and AALM-OF predictions.* Additional observations in humans should be identified that can serve to evaluate the performance of the optimized AALM (and that were not used in the optimization). Ideally, these would be blood and/or bone Pb measurements in people for whom Pb intakes are known with reasonable certainty. Ethical concerns typically preclude Pb dosing experiments; therefore, Pb doses must be estimated with accurate tools such as duplicate diet surveys or dietary recalls and information on Pb levels in diet and other relevant exposure media. Types of data that would be valuable for model validation include: (1) blood soft tissue or bone Pb levels in children or adults for whom Pb dosage is known or can be reliable estimated from exposure data; (2) changes in blood, soft tissue or bone Pb levels in children or

adults following and abrupt change (increase or decrease) in Pb exposure; (3) steady state (or quasi-steady state) blood/soft tissue blood/bone Pb ratios in children or adults; (4) urinary Pb clearance from blood or plasma in children or adults; and (5) plasma/whole blood concentration ratios in children.

- *Evaluate and document the empirical basis for exposure model parameters.* Most of the exposure parameter values in the AALM.CLS serve as placeholders and should, in the future, be replaced with default values for specific receptor populations for which an empirical basis can be provided.

- *Further refine the RT model*. The AALM.CLS includes values for inhalation rates and deposition fractions for the general public, as defined by ICRP (1994). These values do not adequately represent many receptor populations of interest who have activity levels that differ from general population assumptions (e.g., workers). Additional parameter value matrices should be developed to represent selected receptor populations of interest.

Finally, the AALM has been developed with a relatively easy to use and versatile exposure interface, access to model parameters and values, and transparency of model code to support stakeholder use and evaluation internally and external to the Agency. It is recommendation of this report that the AALM be made available to the Agency and the research community as a beta test version to facilitate additional case studies, parameter refinements and external evaluation; and to advance the model towards regulatory use and exposure assessment.

TABLE 4-1. SUMMARY OF MAJOR DIFFERENCES BETWEEN STRUCTURES OF AALM-LG AND AALM-OF

Model Component	AALM-LG	AALM-OF
GI tract	Four compartments representing stomach, small intestine, upper and lower large intestine	No GI tract compartment
Absorption from GI tract	First-order transfer from small intestine to blood	First-order transfer of ingested Pb to liver (portal blood)
Plasma	Two compartments representing diffusible (transferable to other tissues) and bound	One compartment in equilibrium with bound Pb in RBC
RBC	Binding represented with first-order rate transfer rates adjusted for saturating concentration	Binding represented with non-linear binding function (i.e., maximum and half-saturating concentration)
Kidney	Two compartments, first-order transfer rates	One compartment with flow-limited transfer
Liver	Two compartments, first-order transfer rates	One compartment with flow-limited transfer
Other soft tissue	Three compartments, first-order transfer rates	None
Poorly perfused tissue	None	One compartment with flow-limited transfer
Well-perfused tissue	None	One compartment with flow-limit transfer
Brain	One compartment, first-order transfer rates	None
Bone	Six compartments representing surface, exchangeable and non-exchangeable cortical and trabecular bone. Pb transfers governed by age-dependent first-order transfer rates	Transfer to and from metabolically active trabecular and cortical bone governed by age-dependent bone formation and resorption rates, respectively; transfer to and from mature cortical bone governed by radial diffusion
Sweat	First-order transfer from plasma to sweat	None
Miscellaneous excretory routes (e.g., hair)	First-order transfer from other soft tissues to other excretory routes	None

TABLE 4-2. AALM-LG INPUT PARAMETERS CONTROLLING POST-ABSORPTION PB KINETICS

No.	Transfer Pathway	Controlling Parameter(s)	Rate at Specified Age (day^{-1})					
			0-100 days	1 year	5 years	10 years	15 years	≥25 years
1	Plasma-D to EVF	TEVF	1.00E+03	1.00E+03	1.00E+03	1.00E+03	1.00E+03	1.00E+03
2	Plasma-D to RBCs	TORBC	2.97E+02	4.07E+02	4.25E+02	3.67E+02	3.01E+02	4.80E+02
3	Plasma-D to Plasma-B	TOPROT	4.95E-01	6.78E-01	7.09E-01	6.11E-01	5.01E-01	8.00E-01
4	Plasma-D to Urinary bladder	TOURIN	1.86E+01	2.54E+01	2.66E+01	2.29E+01	1.88E+01	3.00E+01
5	Plasma-D to Small intestine	TOFECE	7.43E+00	1.02E+01	1.06E+01	9.17E+00	7.51E+00	1.20E+01
6	Plasma-D to Trab surf	TOBONE (TFRAC)	9.60E+01	5.76E+01	5.68E+01	8.95E+01	1.32E+02	8.90E+01
7	Plasma-D to Cort surf	TBONE (1-TFRAC)	3.84E+02	2.30E+02	1.99E+02	2.69E+02	3.42E+02	7.10E+01
8	Plasma-D to Liver 1	TOLVR1	4.95E+01	6.78E+01	7.09E+01	6.11E+01	5.01E+01	8.00E+01
9	Plasma-D to Urinary path	TOKDN1	2.48E+01	3.39E+01	3.54E+01	3.06E+01	2.51E+01	4.00E+01
10	Plasma-D to Other kidney	TOKDN2	2.48E-01	3.39E-01	3.54E-01	3.06E-01	2.50E-01	4.00E-01
11	Plasma-D to ST0	TOSOF0	1.03E+02	1.42E+02	1.48E+02	1.28E+02	1.05E+02	1.78E+02
12	Plasma-D to ST1	TOSOF1	1.24E+01	1.70E+01	1.77E+01	1.53E+01	1.25E+01	1.00E+01
13	Plasma-D to ST2	TOSOF2	1.24E+00	1.70E+00	1.77E+00	1.53E+00	1.25E+00	2.00E+00
14	Plasma-D to Brain	TOBRAN	5.57E-01	7.63E-01	2.66E-01	2.29E-01	1.88E-01	3.00E-01
15	Plasma-D to Sweat	TOWET	4.33E+00	5.93E+00	6.20E+00	5.35E+00	4.38E+00	7.00E+00
16	RBCs to Plasma-D	RRBC	4.62E-01	4.62E-01	2.77E-01	1.39E-01	1.39E-01	1.39E-01
17	EVF to Plasma-D	RPLAS	3.33E+02	3.33E+02	3.33E+02	3.33E+02	3.33E+02	3.33E+02
18	Plasma-B to Plasma-D	RPROT	1.39E-01	1.39E-01	1.39E-01	1.39E-01	1.39E-01	1.39E-01
19	Cort surf to Plasma-D	RCS2DF	6.50E-01	6.50E-01	6.50E-01	6.50E-01	6.50E-01	5.00E-01
20	Trab surf to Plasma-D	RTS2DF	6.50E-01	6.50E-01	6.50E-01	6.50E-01	6.50E-01	5.00E-01

No.	Transfer Pathway	Controlling Parameter(s)	Rate at Specified Age (day^{-1})					
			0-100 days	1 year	5 years	10 years	15 years	≥25 years
21	Cort surf to Exch vol	RCS2B	3.50E-01	3.50E-01	3.50E-01	3.50E-01	3.50E-01	5.00E-01
22	Trab surf to Exch vol	RTS2B	3.50E-01	3.50E-01	3.50E-01	3.50E-01	3.50E-01	5.00E-01
23	Cort exch vol to Surl	RDIFF*(1-FLONG)	1.85E-02	1.85E-02	1.85E-02	1.85E-02	1.85E-02	1.85E-02
24	Trab exch vol to Surf	RDIFF*(1-FLONG)	1.85E-02	1.85E-02	1.85E-02	1.85E-02	1.85E-02	1.85E-02
25	Cort exch vol to Nonexch vol	RDIFF*FLONG	4.62E-03	4.62E-03	4.62E-03	4.62E-03	4.62E-03	4.62E-03
26	Trab exch vol to Nonexcn vol	RDIFF*FLONG	4.62E-03	4.62E-03	4.62E-03	4.62E-03	4.62E-03	4.62E-03
27	Cort nonexch vol to Plasma-D	RCORT	8.22E-03	2.88E-03	1.54E-03	8.90E-04	5.12E-04	8.22E-05
28	Trab nonexch vol to Plasma-D	RCORT	8.22E-03	2.88E-03	1.81E-03	1.32E-03	9.56E-04	4.93E-04
29	Liver 1 to Plasma-D	RLVR1	3.12E-02	3.12E-02	3.12E-02	3.12E-02	3.12E-02	3.12E-02
30	Liver 1 to Small intestine	H1TOSI	3.12E-02	3.12E-02	3.12E-02	3.12E-02	3.12E-02	3.12E-02
31	Liver 1 to Liver 2	H1TOH2	6.93E-03	6.93E-03	6.93E-03	6.93E-03	6.93E-03	6.93E-03
32	Liver 2 to Plasma-D	RLVR2	6.93E-03	6.93E-03	6.93E-03	1.90E-03	1.90E-03	1.90E-03
33	Urinary path to Urinary bladder	RBLAD	1.39E-01	1.39E-01	1.39E-01	1.39E-01	1.39E-01	1.39E-01
34	Other kidney to Plasma-D	RKDN2	6.93E-03	6.93E-03	6.93E-03	1.90E-03	1.90E-03	1.90E-03
35	ST0 to Plasma-D	RSOF0	2.08E+00	2.08E+00	2.08E+00	2.08E+00	2.08E+00	2.08E+00
36	ST1 to Plasma-D	RSOF1	4.16E-03	4.16E-03	4.16E-03	4.16E-03	4.16E-03	4.16E-03
37	ST1 to Excreta	S2HAIR	2.77E-03	2.77E-03	2.77E-03	2.77E-03	2.77E-03	2.77E-03
38	ST2 to Plasma-D	RSOF2	3.80E-04	3.80E-04	3.80E-04	3.80E-04	3.80E-04	3.80E-04
39	Brain to Plasma-D	RBRAN	9.50E-04	9.50E-04	9.50E-04	9.50E-04	9.50E-04	9.50E-04

1

TABLE 4-3. AALM-OF INPUT PARAMETERS CONTROLLING POST-ABSORPTION PB KINETICS

No.	Parameter	Unit	Value	Parameter Description
1	A1	–	4.0	Constant 1 for bone formation rate algorithm
2	A2	–	0.4	Constant 2 for bone formation rate algorithm
3	A3	–	4.0	Constant 3 for bone formation rate algorithm
4	A5	–	0.6	Constant 5 for bone formation rate algorithm
5	AGE0	year	0	Age at which simulation begins
6	BASE	–	0.1	Base bone formation rate in bone growth algorithm
7	BIND	mg/L	2.7	Maximum capacity of sites in red cells to bind Pb
8	C1	–	1.0	Constant 1 for urinary clearance of Pb as a fraction of GFR
9	C2	–	0.9	Constant 2 for urinary clearance of Pb as a fraction of GFR
10	C3	–	50	Constant 3 for urinary clearance of Pb as a fraction of GFR
11	CON	f	0.65	Fraction of bone blood flow to trabecular bone
12	D0	cm^3/day	0.0000005	Diffusion constant
13	EXPO	–	0.6	Exponent constant for bone volume participating in adult-type bone remodeling
14	G	NA	1.2	Linear parameter for unbound lead in red cells
15	KBIND	mg/L	0.0075	Half-saturation concentration of Pb for binding by sites in red cells
16	P0	cm^3/day	0.02	Permeability constant for diffusion from canaliculi to bone
17	PK	f	50	Kidney/plasma partition coefficient
18	PL	f	50	Liver/plasma partition coefficient
19	PP	f	2.0	Poorly perfused/plasma partition coefficient
20	PW	f	50	Well-perfused/plasma partition coefficient
21	QBONEC	f	0.05	Fraction cardiac output going to bone
22	QCC	L/day/kg	340	Cardiac output in the adult
23	QKC	f	0.17	Fraction cardiac output going to kidney
24	QLC	f	0.25	Fraction cardiac output going to liver
25	QWC	f	0.44	Fraction cardiac output going to other well-perfused tissues
26	R0	cm^3/day	0.0000005	Permeability constant for diffusion from bone to canaliculi
27	RAD1	cm	0.000027	Radius of shell 1 of bone in the canalicular diffusion region of deeper bone
28	RAD2	cm	0.000052	Radius of shell 2 of bone in the canalicular diffusion region of deeper bone

No.	Parameter	Unit	Value	Parameter Description
29	RAD3	cm	0.000079	Radius of shell 3 of bone in the canalicular diffusion region of deeper bone
30	RAD4	cm	0.000106	Radius of shell 4 of bone in the canalicular diffusion region of deeper bone
31	RAD5	cm	0.000133	Radius of shell 5 of bone in the canalicular diffusion region of deeper bone
32	RAD6	cm	0.000160	Radius of shell 6 of bone in the canalicular diffusion region of deeper bone
33	RAD7	cm	0.000187	Radius of shell 7 of bone in the canalicular diffusion region of deeper bone
34	RAD8	cm	0.000214	Radius of shell 8 of bone in the canalicular diffusion region of deeper bone
35	S	cm^2/cm	0.000126	Surface area of canaliculi

1

TABLE 4-4. AALM-LG STANDARDIZED SENSITIVITY COEFFICIENTS FOR BLOOD PB IN CHILDREN (5 YEARS) AND ADULTS (30 YEARS)

Variable	Parameter	Child	Adult	Parameter Description
ABLOOD	TEVF	9.16E+00	8.38E+00	Deposition fraction from diffusible plasma to extravascular fluid
ABLOOD	TORBC	5.30E+00	4.93E+00	Deposition fraction from diffusible plasma to RBCs, below non-linear threshold
ABLOOD	TOSOF0	1.50E+00	1.44E+00	Age-scaled deposition fraction from diffusible plasma to soft tissue compartment 0
ABLOOD	TBONEL	1.42E+00	1.30E+00	Terminal value of age-scaled deposition fraction from diffusible plasma to surface bone
ABLOOD	RRBC	1.00E+00	9.98E-01	Age-scaled transfer rate from RBC to diffusible plasma
ABLOOD	TOLVR1	4.90E-01	3.85E-01	Deposition fraction from diffusible plasma to liver compartment 2
ABLOOD	H1TOBL	3.25E-01	2.94E-01	Fraction of transfer out of liver compartment 1 to diffusible plasma
ABLOOD	TBONE	1.05E-01	7.16E-02	Age-scaled deposition fraction from diffusible plasma to surface bone
ABLOOD	TFRAC	8.33E-03	7.10E-02	Bone deposition-scaled fraction of diffusible plasma-to-bone deposition that goes to trabecular surface bone; 1-TFRAC is the fraction that goes to cortical surface bone
ABLOOD	H1TOH2	7.70E-02	6.58E-02	Fraction of transfer out of liver compartment 1 to liver compartment 2
ABLOOD	TOSOF1	1.16E-01	5.52E-02	Age-scaled deposition fraction from diffusible plasma to soft tissue compartment 1
ABLOOD	S2HAIR	7.63E-02	3.63E-02	Deposition fraction from soft tissue compartment 1 to other excreta
ABLOOD	H1TOSI	8.91E-02	2.49E-02	Fraction of transfer out of liver compartment 1 to the small intestine
ABLOOD	TOSOF2	9.31E-03	1.76E-02	Age-scaled deposition fraction from diffusible plasma to soft tissue compartment 2
ABLOOD	RCORT	9.00E-02	1.27E-02	Age-scaled transfer rate from non-exchangeable cortical bone to diffusible plasma
ABLOOD	RTS2B	8.11E-03	1.17E-02	Age-scaled transfer rate from surface trabecular bone to exchangeable trabecular bone
ABLOOD	RTS2DF	7.59E-03	1.17E-02	Age-scaled transfer rate from trabecular bone surface to diffusible plasma
ABLOOD	RTRAB	2.12E-02	1.06E-02	Age-scaled transfer rate from non-exchangeable trabecular bone to diffusible plasma
ABLOOD	RDIFF	6.04E-02	1.04E-02	Age-scaled transfer rate from the exchangeable bone, including transfer to surface and non-exchangeable bone

Variable	Parameter	Child	Adult	Parameter Description
ABLOOD	TOFECE	3.23E-02	9.00E-03	Deposition fraction from diffusible plasma directly to the small intestine (not including the transfer from biliary secretion, specified by RLVR1)
ABLOOD	TOPROT	1.06E-02	8.24E-03	Deposition fraction from diffusible plasma to protein-bound plasma
ABLOOD	TOKDN2	3.81E-03	3.28E-03	Deposition fraction from diffusible plasma to kidney compartment 2
ABLOOD	TOBRAN	5.10E-03	2.62E-03	Age-scaled deposition fraction from diffusible plasma to brain
ABLOOD	RSOF2	8.49E-03	2.40E-03	Transfer rate from soft tissue compartment 2 to diffusible plasma
ABLOOD	RPROT	3.38E-03	1.66E-03	Transfer rate from bound plasma to diffusible plasma
ABLOOD	RCS2DF	2.21E-02	1.57E-03	Age-scaled transfer rate from cortical bone surface to diffusible plasma
ABLOOD	RCS2B	2.42E-02	1.34E-03	Age-scaled transfer rate from cortical bone surface to exchangeable cortical bone
ABLOOD	FLONG	4.12E-02	1.25E-03	Age-scaled fraction of total transfer from the exchangeable bone directed to non-exchangeable bone
ABLOOD	RSOF1	5.63E-03	4.37E-04	Transfer rate from soft tissue compartment 1 to diffusible plasma
ABLOOD	RPLAS	6.95E-04	2.94E-04	Total transfer rate from diffusible plasma to all compartments
ABLOOD	RLVR2	3.70E-03	2.20E-04	Age-scaled transfer rate from the slow liver compartment 2 to diffusible plasma
ABLOOD	RBRAN	1.66E-03	1.76E-04	Age-scaled transfer rate from brain to diffusible plasma
ABLOOD	RLVR1	3.03E-03	1.00E-04	Transfer rate out of the liver compartment 1, including to small intestine and diffusible plasma
ABLOOD	RSOF0	3.74E-04	1.09E-05	Transfer rate from soft tissue compartment 0 to diffusible plasma
ABLOOD	RKDN2	1.93E-04	1.09E-05	Age-scaled transfer rate from kidney compartment 2 to diffusible plasma
ABLOOD	TOKDN1	1.18E-05	5.81E-06	Deposition fraction from diffusible plasma to kidney compartment 1
ABLOOD	TOURIN	8.88E-06	4.35E-06	Deposition fraction from diffusible plasma to urine
ABLOOD	RSTMC	1.42E-05	3.62E-06	Transfer rate from stomach to small intestine
ABLOOD	SIZEVF	6.52E-06	3.27E-06	Relative volume of the EVF compartment compared to plasma (EVF/Plasma)
ABLOOD	GSCAL	2.30E-05	2.63E-06	Age-scaling factor for GIT transfer
ABLOOD	RULI	4.98E-05	1.07E-06	Transfer rate from upper large intestine to lower large intestine

Variable	Parameter	Child	Adult	Parameter Description
ABLOOD	TOSWET	2.18E-06	1.06E-06	Deposition fraction from diffusible plasma to sweat
ABLOOD	RSIC	5.92E-05	7.18E-07	Transfer rate from small intestine to upper large intestine
ABLOOD	RLLI	5.28E-06	1.16E-07	Transfer rate from lower large intestine to feces
ABLOOD	RKDN1	5.83E-10	1.31E-08	Transfer rate from kidney compartment 1 to urinary pathway
ABLOOD	POWER	0.00E+00	0.00E+00	Exponent for RBC deposition
ABLOOD	RBCNL	0.00E+00	0.00E+00	Threshold concentration in RBC for non-linear deposition from diffusible plasma to RBC
ABLOOD	SATRAT	0.00E+00	0.00E+00	Maximum (saturating) concentration of lead in RBC
ABLOOD	RBLAD	0.00E+00	0.00E+00	Age-scaled transfer rate from urinary bladder to urine

1

2

TABLE 4-5. AALM-LG STANDARDIZED SENSITIVITY COEFFICIENTS FOR BONE PB IN CHILDREN (5 YEARS) AND ADULTS (30 YEARS)

Variable	Parameter	Child	Adult	Parameter Description
ABONE	TEVF	8.11E+00	8.12E+00	Deposition fraction from diffusible plasma to extravascular fluid
ABONE	TORBC	3.75E+00	3.71E+00	Deposition fraction from diffusible plasma to RBCs, below non-linear threshold
ABONE	TBONE	1.27E+00	1.42E+00	Age-scaled deposition fraction from diffusible plasma to surface bone
ABONE	TOSOF0	1.31E+00	1.32E+00	Age-scaled deposition fraction from diffusible plasma to soft tissue compartment 0
ABONE	TBONEL	1.07E+00	1.05E+00	Terminal value of age-scaled deposition fraction from diffusible plasma to surface bone
ABONE	FLONG	3.93E-01	6.80E-01	Age-scaled fraction of total transfer from the exchangeable bone directed to non-exchangeable bone
ABONE	RCS2DF	5.33E-01	6.02E-01	Age-scaled transfer rate from cortical bone surface to diffusible plasma
ABONE	TOLVR1	4.44E-01	3.70E-01	Deposition fraction from diffusible plasma to liver compartment 2
ABONE	H1TOBL	2.81E-01	2.78E-01	Fraction of transfer out of liver compartment 1 to diffusible plasma
ABONE	RTS2DF	1.36E-01	1.48E-01	Age-scaled transfer rate from trabecular bone surface to diffusible plasma
ABONE	TOSOF1	9.53E-02	7.79E-02	Age-scaled deposition fraction from diffusible plasma to soft tissue compartment 1
ABONE	H1TOH2	6.29E-02	6.13E-02	Fraction of transfer out of liver compartment 1 to liver compartment 2
ABONE	H1TOSI	9.98E-02	3.06E-02	Fraction of transfer out of liver compartment 1 to the small intestine
ABONE	TOSOF2	5.70E-03	1.94E-02	Age-scaled deposition fraction from diffusible plasma to soft tissue compartment 2
ABONE	TOFECE	3.60E-02	1.11E-02	Deposition fraction from diffusible plasma directly to the small intestine (not including the transfer from biliary secretion, specified by RLVR1)
ABONE	TOPROT	6.28E-03	6.20E-03	Deposition fraction from diffusible plasma to protein-bound plasma
ABONE	TOBRAN	3.68E-03	3.25E-03	Age-scaled deposition fraction from diffusible plasma to brain
ABONE	TOKDN2	3.13E-03	3.05E-03	Deposition fraction from diffusible plasma to kidney compartment 2
ABONE	RLVR2	8.15E-04	6.26E-04	Age-scaled transfer rate from the slow liver compartment 2 to diffusible plasma

Variable	Parameter	Child	Adult	Parameter Description
ABONE	RKDN2	3.09E-05	3.22E-05	Age-scaled transfer rate from kidney compartment 2 to diffusible plasma
ABONE	GSCAL	4.15E-05	1.35E-05	Age-scaling factor for GIT transfer
ABONE	RULI	8.28E-05	6.79E-06	Transfer rate from upper large intestine to lower large intestine
ABONE	RLLI	8.76E-06	7.29E-07	Transfer rate from lower large intestine to feces
ABONE	RKDN1	9.84E-10	8.50E-08	Transfer rate from kidney compartment 1 to urinary pathway
ABONE	POWER	0.00E+00	0.00E+00	Exponent for RBC deposition
ABONE	RBCNL	0.00E+00	0.00E+00	Threshold concentration in RBC for non-linear deposition from diffusible plasma to RBC
ABONE	SATRAT	0.00E+00	0.00E+00	Maximum (saturating) concentration of lead in RBC
ABONE	RBLAD	0.00E+00	0.00E+00	Age-scaled transfer rate from urinary bladder to urine
ABONE	TOSWET	1.38E-08	9.86E-09	Deposition fraction from diffusible plasma to sweat
ABONE	TOURIN	5.72E-08	4.07E-08	Deposition fraction from diffusible plasma to urine
ABONE	TOKDN1	7.63E-08	1.38E-07	Deposition fraction from diffusible plasma to kidney compartment 1
ABONE	RPROT	5.69E-06	3.42E-06	Transfer rate from bound plasma to diffusible plasma
ABONE	RSIC	1.12E-04	8.33E-06	Transfer rate from small intestine to upper large intestine
ABONE	SIZEVF	4.23E-06	2.34E-05	Relative volume of the EVF compartment compared to plasma (EVF/Plasma)
ABONE	RSTMC	1.52E-05	2.48E-05	Transfer rate from stomach to small intestine
ABONE	RPLAS	3.87E-05	3.19E-05	Total transfer rate from diffusible plasma to all compartments
ABONE	RSOF0	7.55E-05	4.18E-05	Transfer rate from soft tissue compartment 0 to diffusible plasma
ABONE	RRBC	1.06E-03	6.84E-05	Age-scaled transfer rate from RBC to diffusible plasma
ABONE	RLVR1	1.51E-04	4.01E-04	Transfer rate out of the liver compartment 1, including to small intestine and diffusible plasma
ABONE	RBRAN	1.82E-03	1.03E-03	Age-scaled transfer rate from brain to diffusible plasma
ABONE	RSOF2	6.31E-03	1.26E-03	Transfer rate from soft tissue compartment 2 to diffusible plasma
ABONE	RSOF1	1.16E-03	2.10E-03	Transfer rate from soft tissue compartment 1 to diffusible plasma
ABONE	S2HAIR	6.27E-02	5.13E-02	Deposition fraction from soft tissue compartment 1 to other excreta

Variable	Parameter	Child	Adult	Parameter Description
ABONE	RDIFF	2.93E-01	8.41E-02	Age-scaled transfer rate from the exchangeable bone, including transfer to surface and non-exchangeable bone
ABONE	RTS2B	1.38E-01	1.48E-01	Age-scaled transfer rate from surface trabecular bone to exchangeable trabecular bone
ABONE	RTRAB	1.17E-01	1.83E-01	Age-scaled transfer rate from non-exchangeable trabecular bone to diffusible plasma
ABONE	TFRAC	1.03E-02	3.00E-01	Bone deposition-scaled fraction of diffusible plasma-to-bone deposition that goes to trabecular surface bone; 1-TFRAC is the fraction that goes to cortical surface bone
ABONE	RCS2B	5.41E-01	6.03E-01	Age-scaled transfer rate from cortical bone surface to exchangeable cortical bone
ABONE	RCORT	4.61E-01	7.07E-01	Age-scaled transfer rate from non-exchangeable cortical bone to diffusible plasma

1

TABLE 4-6. AALM-LG STANDARDIZED SENSITIVITY COEFFICIENTS FOR LIVER PB IN CHILDREN (5 YEARS) AND ADULTS (30 YEARS)

Variable	Parameter	Child	Adult	Parameter Description
ALIVER	TEVF	8.91E+00	8.41E+00	Deposition fraction from diffusible plasma to extravascular fluid
ALIVER	TORBC	4.19E+00	3.94E+00	Deposition fraction from diffusible plasma to RBCs, below non-linear threshold
ALIVER	TOSOF0	1.46E+00	1.45E+00	Age-scaled deposition fraction from diffusible plasma to soft tissue compartment 0
ALIVER	TOLVR1	1.48E+00	1.39E+00	Deposition fraction from diffusible plasma to liver compartment 2
ALIVER	TBONEL	1.39E+00	1.31E+00	Terminal value of age-scaled deposition fraction from diffusible plasma to surface bone
ALIVER	H1TOH2	6.09E-01	8.54E-01	Fraction of transfer out of liver compartment 1 to liver compartment 2
ALIVER	RLVR2	5.99E-01	7.92E-01	Age-scaled transfer rate from the slow liver compartment 2 to diffusible plasma
ALIVER	H1TOBL	3.16E-01	2.95E-01	Fraction of transfer out of liver compartment 1 to diffusible plasma
ALIVER	RLVR1	4.83E-01	2.14E-01	Transfer rate out of the liver compartment 1, including to small intestine and diffusible plasma
ALIVER	TBONE	6.32E-02	7.96E-02	Age-scaled deposition fraction from diffusible plasma to surface bone
ALIVER	TFRAC	7.36E-03	7.60E-02	Bone deposition-scaled fraction of diffusible plasma-to-bone deposition that goes to trabecular surface bone; 1-TFRAC is the fraction that goes to cortical surface bone
ALIVER	TOSOF1	1.12E-01	5.62E-02	Age-scaled deposition fraction from diffusible plasma to soft tissue compartment 1
ALIVER	S2HAIR	7.35E-02	3.69E-02	Deposition fraction from soft tissue compartment 1 to other excreta
ALIVER	H1TOSI	9.28E-02	2.54E-02	Fraction of transfer out of liver compartment 1 to the small intestine
ALIVER	TOSOF2	8.37E-03	1.77E-02	Age-scaled deposition fraction from diffusible plasma to soft tissue compartment 2
ALIVER	RCORT	9.61E-02	1.41E-02	Age-scaled transfer rate from non-exchangeable cortical bone to diffusible plasma
ALIVER	RTS2B	3.07E-03	1.36E-02	Age-scaled transfer rate from surface trabecular bone to exchangeable trabecular bone
ALIVER	RTS2DF	2.66E-03	1.35E-02	Age-scaled transfer rate from trabecular bone surface to diffusible plasma
ALIVER	RDIFF	4.72E-02	1.26E-02	Age-scaled transfer rate from the exchangeable bone, including transfer to surface and non-exchangeable bone

Variable	Parameter	Child	Adult	Parameter Description
ALIVER	TOFECE	3.34E-02	9.08E-03	Deposition fraction from diffusible plasma directly to the small intestine (not including the transfer from biliary secretion, specified by RLVR1)
ALIVER	RTRAB	2.34E-02	8.01E-03	Age-scaled transfer rate from non-exchangeable trabecular bone to diffusible plasma
ALIVER	TOPROT	7.10E-03	6.65E-03	Deposition fraction from diffusible plasma to protein-bound plasma
ALIVER	TOKDN2	3.67E-03	3.29E-03	Deposition fraction from diffusible plasma to kidney compartment 2
ALIVER	TOBRAN	4.79E-03	2.64E-03	Age-scaled deposition fraction from diffusible plasma to brain
ALIVER	RSOF2	7.94E-03	2.61E-03	Transfer rate from soft tissue compartment 2 to diffusible plasma
ALIVER	RCS2DF	5.38E-03	1.75E-03	Age-scaled transfer rate from cortical bone surface to diffusible plasma
ALIVER	RCS2B	7.19E-03	1.48E-03	Age-scaled transfer rate from cortical bone surface to exchangeable cortical bone
ALIVER	FLONG	4.94E-02	7.59E-04	Age-scaled fraction of total transfer from the exchangeable bone directed to non-exchangeable bone
ALIVER	RSOF1	4.17E-03	5.79E-04	Transfer rate from soft tissue compartment 1 to diffusible plasma
ALIVER	RRBC	2.10E-03	2.48E-04	Age-scaled transfer rate from RBC to diffusible plasma
ALIVER	RBRAN	1.76E-03	1.89E-04	Age-scaled transfer rate from brain to diffusible plasma
ALIVER	RSOF0	3.13E-04	1.22E-05	Transfer rate from soft tissue compartment 0 to diffusible plasma
ALIVER	RPLAS	5.46E-05	5.13E-06	Total transfer rate from diffusible plasma to all compartments
ALIVER	GSCAL	2.56E-05	3.35E-06	Age-scaling factor for GIT transfer
ALIVER	RSTMC	2.51E-05	3.23E-06	Transfer rate from stomach to small intestine
ALIVER	SIZEVF	6.72E-06	2.84E-06	Relative volume of the EVF compartment compared to plasma (EVF/Plasma)
ALIVER	RKDN2	1.45E-04	2.69E-06	Age-scaled transfer rate from kidney compartment 2 to diffusible plasma
ALIVER	RULI	5.24E-05	1.17E-06	Transfer rate from upper large intestine to lower large intestine
ALIVER	RPROT	2.25E-05	9.68E-07	Transfer rate from bound plasma to diffusible plasma
ALIVER	RSIC	5.27E-05	2.33E-07	Transfer rate from small intestine to upper large intestine
ALIVER	RLLI	5.56E-06	1.27E-07	Transfer rate from lower large intestine to feces

Variable	Parameter	Child	Adult	Parameter Description
ALIVER	TOKDN1	3.12E-07	3.12E-08	Deposition fraction from diffusible plasma to kidney compartment 1
ALIVER	RKDN1	6.21E-10	1.44E-08	Transfer rate from kidney compartment 1 to urinary pathway
ALIVER	TOURIN	2.34E-07	1.28E-08	Deposition fraction from diffusible plasma to urine
ALIVER	TOSWET	5.69E-08	3.10E-09	Deposition fraction from diffusible plasma to sweat
ALIVER	POWER	0.00E+00	0.00E+00	Exponent for RBC deposition
ALIVER	RBCNL	0.00E+00	0.00E+00	Threshold concentration in RBC for non-linear deposition from diffusible plasma to RBC
ALIVER	SATRAT	0.00E+00	0.00E+00	Maximum (saturating) concentration of lead in RBC
ALIVER	RBLAD	0.00E+00	0.00E+00	Age-scaled transfer rate from urinary bladder to urine

1

TABLE 4-7. AALM-LG STANDARDIZED SENSITIVITY COEFFICIENTS FOR KIDNEY PB IN CHILDREN (5 YEARS) AND ADULTS (30 YEARS)

Variable	Parameter	Child	Adult	Parameter Description
AKIDNEY	TEVF	9.08E+00	8.40E+00	Deposition fraction from diffusible plasma to extravascular fluid
AKIDNEY	TORBC	4.27E+00	3.94E+00	Deposition fraction from diffusible plasma to RBCs, below non-linear threshold
AKIDNEY	TOSOF0	1.48E+00	1.44E+00	Age-scaled deposition fraction from diffusible plasma to soft tissue compartment 0
AKIDNEY	TBONEL	1.41E+00	1.31E+00	Terminal value of age-scaled deposition fraction from diffusible plasma to surface bone
AKIDNEY	RKDN1	8.20E-01	5.76E-01	Transfer rate from kidney compartment 1 to urinary pathway
AKIDNEY	TOKDN1	8.15E-01	5.76E-01	Deposition fraction from diffusible plasma to kidney compartment 1
AKIDNEY	TOKDN2	1.91E-01	4.30E-01	Deposition fraction from diffusible plasma to kidney compartment 2
AKIDNEY	RKDN2	2.08E-01	4.27E-01	Age-scaled transfer rate from kidney compartment 2 to diffusible plasma
AKIDNEY	TOLVR1	4.88E-01	3.87E-01	Deposition fraction from diffusible plasma to liver compartment 2
AKIDNEY	H1TOBL	3.22E-01	2.95E-01	Fraction of transfer out of liver compartment 1 to diffusible plasma
AKIDNEY	TBONE	9.11E-02	7.58E-02	Age-scaled deposition fraction from diffusible plasma to surface bone
AKIDNEY	TFRAC	8.00E-03	7.36E-02	Bone deposition-scaled fraction of diffusible plasma-to-bone deposition that goes to trabecular surface bone; 1-TFRAC is the fraction that goes to cortical surface bone
AKIDNEY	H1TOH2	7.60E-02	6.59E-02	Fraction of transfer out of liver compartment 1 to liver compartment 2
AKIDNEY	TOSOF1	1.15E-01	5.57E-02	Age-scaled deposition fraction from diffusible plasma to soft tissue compartment 1
AKIDNEY	S2HAIR	7.53E-02	3.66E-02	Deposition fraction from soft tissue compartment 1 to other excreta
AKIDNEY	H1TOSI	9.02E-02	2.51E-02	Fraction of transfer out of liver compartment 1 to the small intestine
AKIDNEY	TOSOF2	8.99E-03	1.76E-02	Age-scaled deposition fraction from diffusible plasma to soft tissue compartment 2
AKIDNEY	RCORT	9.20E-02	1.34E-02	Age-scaled transfer rate from non-exchangeable cortical bone to diffusible plasma
AKIDNEY	RTS2B	6.42E-03	1.27E-02	Age-scaled transfer rate from surface trabecular bone to exchangeable trabecular bone

Variable	Parameter	Child	Adult	Parameter Description
AKIDNEY	RTS2DF	5.94E-03	1.26E-02	Age-scaled transfer rate from trabecular bone surface to diffusible plasma
AKIDNEY	RDIFF	5.60E-02	1.16E-02	Age-scaled transfer rate from the exchangeable bone, including transfer to surface and non-exchangeable bone
AKIDNEY	RTRAB	2.21E-02	9.30E-03	Age-scaled transfer rate from non-exchangeable trabecular bone to diffusible plasma
AKIDNEY	TOFECE	3.27E-02	9.04E-03	Deposition fraction from diffusible plasma directly to the small intestine (not including the transfer from biliary secretion, specified by RLVR1)
AKIDNEY	TOPROT	7.16E-03	6.58E-03	Deposition fraction from diffusible plasma to protein-bound plasma
AKIDNEY	TOBRAN	4.99E-03	2.63E-03	Age-scaled deposition fraction from diffusible plasma to brain
AKIDNEY	RSOF2	8.31E-03	2.51E-03	Transfer rate from soft tissue compartment 2 to diffusible plasma
AKIDNEY	RCS2DF	1.65E-02	1.67E-03	Age-scaled transfer rate from cortical bone surface to diffusible plasma
AKIDNEY	RCS2B	1.85E-02	1.41E-03	Age-scaled transfer rate from cortical bone surface to exchangeable cortical bone
AKIDNEY	FLONG	4.39E-02	9.93E-04	Age-scaled fraction of total transfer from the exchangeable bone directed to non-exchangeable bone
AKIDNEY	RSOF1	5.14E-03	5.12E-04	Transfer rate from soft tissue compartment 1 to diffusible plasma
AKIDNEY	RRBC	2.76E-03	2.28E-04	Age-scaled transfer rate from RBC to diffusible plasma
AKIDNEY	RBRAN	1.69E-03	1.83E-04	Age-scaled transfer rate from brain to diffusible plasma
AKIDNEY	RLVR2	3.37E-03	1.32E-04	Age-scaled transfer rate from the slow liver compartment 2 to diffusible plasma
AKIDNEY	RLVR1	2.85E-03	1.07E-04	Transfer rate out of the liver compartment 1, including to small intestine and diffusible plasma
AKIDNEY	RSOF0	3.53E-04	1.16E-05	Transfer rate from soft tissue compartment 0 to diffusible plasma
AKIDNEY	RPLAS	4.93E-05	5.15E-06	Total transfer rate from diffusible plasma to all compartments
AKIDNEY	RSTMC	1.74E-05	3.41E-06	Transfer rate from stomach to small intestine
AKIDNEY	SIZEVF	2.54E-06	3.05E-06	Relative volume of the EVF compartment compared to plasma (EVF/Plasma)
AKIDNEY	GSCAL	2.37E-05	3.01E-06	Age-scaling factor for GIT transfer

Variable	Parameter	Child	Adult	Parameter Description
AKIDNEY	RULI	5.06E-05	1.12E-06	Transfer rate from upper large intestine to lower large intestine
AKIDNEY	RPROT	2.54E-05	9.09E-07	Transfer rate from bound plasma to diffusible plasma
AKIDNEY	RSIC	5.75E-05	2.19E-07	Transfer rate from small intestine to upper large intestine
AKIDNEY	RLLI	5.33E-06	1.21E-07	Transfer rate from lower large intestine to feces
AKIDNEY	TOURIN	2.64E-07	1.21E-08	Deposition fraction from diffusible plasma to urine
AKIDNEY	TOSWET	6.43E-08	2.93E-09	Deposition fraction from diffusible plasma to sweat
AKIDNEY	POWER	0.00E+00	0.00E+00	Exponent for RBC deposition
AKIDNEY	RBCNL	0.00E+00	0.00E+00	Threshold concentration in RBC for non-linear deposition from diffusible plasma to RBC
AKIDNEY	SATRAT	0.00E+00	0.00E+00	Maximum (saturating) concentration of lead in RBC
AKIDNEY	RBLAD	0.00E+00	0.00E+00	Age-scaled transfer rate from urinary bladder to urine

1

TABLE 4-8. AALM-LG STANDARDIZED SENSITIVITY COEFFICIENTS FOR OTHER SOFT TISSUE PB IN CHILDREN (5 YEARS) AND ADULTS (30 YEARS)

Variable	Parameter	Child	Adult	Parameter Description
ASOFT	TEVF	6.63E+00	8.12E+00	Deposition fraction from diffusible plasma to extravascular fluid
ASOFT	TORBC	3.14E+00	3.81E+00	Deposition fraction from diffusible plasma to RBCs, below non-linear threshold
ASOFT	TOSOF0	1.10E+00	1.39E+00	Age-scaled deposition fraction from diffusible plasma to soft tissue compartment 0
ASOFT	TBONEL	1.06E+00	1.27E+00	Terminal value of age-scaled deposition fraction from diffusible plasma to surface bone
ASOFT	RSOF2	2.36E-01	8.95E-01	Transfer rate from soft tissue compartment 2 to diffusible plasma
ASOFT	TOSOF2	4.68E-01	7.90E-01	Age-scaled deposition fraction from diffusible plasma to soft tissue compartment 2
ASOFT	TOLVR1	3.71E-01	3.80E-01	Deposition fraction from diffusible plasma to liver compartment 2
ASOFT	H1TOBL	2.35E-01	2.86E-01	Fraction of transfer out of liver compartment 1 to diffusible plasma
ASOFT	TOSOF1	4.74E-01	2.71E-01	Age-scaled deposition fraction from diffusible plasma to soft tissue compartment 1
ASOFT	RSOF1	4.36E-01	2.04E-01	Transfer rate from soft tissue compartment 1 to diffusible plasma
ASOFT	TFRAC	3.97E-03	6.66E-02	Bone deposition-scaled fraction of diffusible plasma-to-bone deposition that goes to trabecular surface bone; 1-TFRAC is the fraction that goes to cortical surface bone
ASOFT	H1TOH2	5.20E-02	6.32E-02	Fraction of transfer out of liver compartment 1 to liver compartment 2
ASOFT	S2HAIR	5.19E-02	4.28E-02	Deposition fraction from soft tissue compartment 1 to other excreta
ASOFT	TBONE	1.17E-01	3.82E-02	Age-scaled deposition fraction from diffusible plasma to surface bone
ASOFT	H1TOSI	8.38E-02	3.11E-02	Fraction of transfer out of liver compartment 1 to the small intestine
ASOFT	RCORT	9.33E-02	2.72E-02	Age-scaled transfer rate from non-exchangeable cortical bone to diffusible plasma
ASOFT	FLONG	6.62E-02	2.38E-02	Age-scaled fraction of total transfer from the exchangeable bone directed to non-exchangeable bone
ASOFT	RDIFF	1.38E-02	1.85E-02	Age-scaled transfer rate from the exchangeable bone, including transfer to surface and non-exchangeable bone

Variable	Parameter	Child	Adult	Parameter Description
ASOFT	RSOF0	9.54E-03	1.20E-02	Transfer rate from soft tissue compartment 0 to diffusible plasma
ASOFT	TOFECE	2.99E-02	1.12E-02	Deposition fraction from diffusible plasma directly to the small intestine (not including the transfer from biliary secretion, specified by RLVR1)
ASOFT	RCS2DF	5.93E-02	1.07E-02	Age-scaled transfer rate from cortical bone surface to diffusible plasma
ASOFT	RCS2B	5.94E-02	1.02E-02	Age-scaled transfer rate from cortical bone surface to exchangeable cortical bone
ASOFT	TOPROT	5.25E-03	6.37E-03	Deposition fraction from diffusible plasma to protein-bound plasma
ASOFT	RTS2B	1.48E-02	5.37E-03	Age-scaled transfer rate from surface trabecular bone to exchangeable trabecular bone
ASOFT	RTS2DF	1.48E-02	5.23E-03	Age-scaled transfer rate from trabecular bone surface to diffusible plasma
ASOFT	RTRAB	2.34E-02	3.25E-03	Age-scaled transfer rate from non-exchangeable trabecular bone to diffusible plasma
ASOFT	TOKDN2	2.59E-03	3.15E-03	Deposition fraction from diffusible plasma to kidney compartment 2
ASOFT	TOBRAN	3.04E-03	2.83E-03	Age-scaled deposition fraction from diffusible plasma to brain
ASOFT	RLVR2	1.04E-03	6.65E-04	Age-scaled transfer rate from the slow liver compartment 2 to diffusible plasma
ASOFT	RBRAN	1.49E-03	3.24E-04	Age-scaled transfer rate from brain to diffusible plasma
ASOFT	RLVR1	4.97E-04	8.64E-05	Transfer rate out of the liver compartment 1, including to small intestine and diffusible plasma
ASOFT	RRBC	1.51E-03	6.63E-05	Age-scaled transfer rate from RBC to diffusible plasma
ASOFT	RKDN2	4.71E-05	3.31E-05	Age-scaled transfer rate from kidney compartment 2 to diffusible plasma
ASOFT	RSIC	7.97E-05	1.29E-05	Transfer rate from small intestine to upper large intestine
ASOFT	GSCAL	5.87E-05	1.26E-05	Age-scaling factor for GIT transfer
ASOFT	RPLAS	4.96E-06	4.38E-06	Total transfer rate from diffusible plasma to all compartments
ASOFT	RULI	3.04E-05	4.28E-06	Transfer rate from upper large intestine to lower large intestine
ASOFT	RPROT	4.81E-07	1.18E-06	Transfer rate from bound plasma to diffusible plasma
ASOFT	RLLI	3.76E-06	5.16E-07	Transfer rate from lower large intestine to feces

Variable	Parameter	Child	Adult	Parameter Description
ASOFT	SIZEVF	5.87E-07	5.06E-07	Relative volume of the EVF compartment compared to plasma (EVF/Plasma)
ASOFT	RSTMC	5.46E-06	1.73E-07	Transfer rate from stomach to small intestine
ASOFT	TOKDN1	8.53E-09	4.76E-08	Deposition fraction from diffusible plasma to kidney compartment 1
ASOFT	RKDN1	3.29E-11	3.21E-08	Transfer rate from kidney compartment 1 to urinary pathway
ASOFT	TOURIN	6.40E-09	1.19E-08	Deposition fraction from diffusible plasma to urine
ASOFT	TOSWET	1.54E-09	2.88E-09	Deposition fraction from diffusible plasma to sweat
ASOFT	POWER	0.00E+00	0.00E+00	Exponent for RBC deposition
ASOFT	RBCNL	0.00E+00	0.00E+00	Threshold concentration in RBC for non-linear deposition from diffusible plasma to RBC
ASOFT	SATRAT	0.00E+00	0.00E+00	Maximum (saturating) concentration of lead in RBC
ASOFT	RBLAD	0.00E+00	0.00E+00	Age-scaled transfer rate from urinary bladder to urine

1

TABLE 4-9. AALM-OF STANDARDIZED SENSITIVITY COEFFICIENTS FOR BLOOD PB IN CHILDREN (5 YEARS) AND ADULTS (30 YEARS)

Variable	Parameter	Child	Adult	Parameter Description
ABLOOD	C1	2.41E+00	9.34E+00	Constant 1 for urinary clearance of Pb as a fraction of GFR
ABLOOD	C2	1.38E+00	7.54E+00	Constant 2 for urinary clearance of Pb as a fraction of GFR
ABLOOD	BIND	9.92E-01	9.92E-01	Maximum capacity of sites in red cells to bind Pb
ABLOOD	KBIND	9.88E-01	9.89E-01	Half-saturation concentration of Pb for binding by sites in red cells
ABLOOD	P0	5.73E-03	6.19E-02	Permeability constant for diffusion from canaliculi to bone
ABLOOD	R0	4.96E-03	5.58E-02	Permeability constant for diffusion from bone to canaliculi
ABLOOD	RAD8	4.27E-03	3.97E-02	Radius of shell 8 of bone in the canalicular diffusion region of deeper bone
ABLOOD	CON	7.51E-04	2.50E-02	Fraction of bone blood flow to trabecular bone
ABLOOD	D0	9.99E-04	1.07E-02	Diffusion constant
ABLOOD	BASE	1.72E-04	9.01E-03	Base bone formation rate in bone growth algorithm
ABLOOD	C3	4.46E-01	7.10E-03	Constant 3 for urinary clearance of Pb as a fraction of GFR
ABLOOD	S	8.26E-04	6.67E-03	Surface area of canaliculi
ABLOOD	RAD1	6.66E-04	5.09E-03	Radius of shell 1 of bone in the canalicular diffusion region of deeper bone
ABLOOD	G	1.13E-02	3.48E-03	Linear parameter for unbound lead in red cells
ABLOOD	RAD2	3.67E-04	2.85E-03	Radius of shell 2 of bone in the canalicular diffusion region of deeper bone
ABLOOD	RAD3	2.27E-04	2.16E-03	Radius of shell 3 of bone in the canalicular diffusion region of deeper bone
ABLOOD	PL	1.12E-02	2.08E-03	Liver/plasma partition coefficient
ABLOOD	RAD4	1.51E-04	1.88E-03	Radius of shell 4 of bone in the canalicular diffusion region of deeper bone
ABLOOD	RAD5	1.04E-04	1.64E-03	Radius of shell 5 of bone in the canalicular diffusion region of deeper bone
ABLOOD	RAD6	6.93E-05	1.29E-03	Radius of shell 6 of bone in the canalicular diffusion region of deeper bone
ABLOOD	EXPO	7.16E-03	1.12E-03	Exponent constant for bone volume participating in adult-type bone remodeling
ABLOOD	QKC	1.52E-03	1.11E-03	Fraction cardiac output going to kidney
ABLOOD	A1	9.16E-03	1.01E-03	Constant 1 for bone formation rate algorithm
ABLOOD	A3	4.20E-03	9.44E-04	Constant 3 for bone formation rate algorithm

Variable	Parameter	Child	Adult	Parameter Description
ABLOOD	QWC	1.33E-02	9.31E-04	Fraction cardiac output going to other well-perfused tissues
ABLOOD	QLC	1.32E-02	9.16E-04	Fraction cardiac output going to liver
ABLOOD	RAD7	3.62E-05	7.55E-04	Radius of shell 7 of bone in the canalicular diffusion region of deeper bone
ABLOOD	A5	0.00E+00	6.65E-04	Constant 5 for bone formation rate algorithm
ABLOOD	PW	2.64E-03	6.07E-04	Well-perfused/plasma partition coefficient
ABLOOD	A2	3.06E-03	1.98E-04	Constant 2 for bone formation rate algorithm
ABLOOD	QBONEC	7.94E-03	1.62E-04	Fraction cardiac output going to bone
ABLOOD	PP	8.01E-05	1.12E-04	Poorly perfused/plasma partition coefficient
ABLOOD	PK	3.60E-05	2.25E-05	Kidney/plasma partition coefficient
ABLOOD	QCC	0.00E+00	0.00E+00	Cardiac output in the adult

TABLE 4-10. AALM-OF STANDARDIZED SENSITIVITY COEFFICIENTS FOR BONE PB IN CHILDREN (5 YEARS) AND ADULTS (30 YEARS)

Variable	Parameter	Child	Adult	Parameter Description
ABONE	C1	1.99E+00	8.70E+00	Constant 1 for urinary clearance of Pb as a fraction of GFR
ABONE	C2	9.73E-01	7.12E+00	Constant 2 for urinary clearance of Pb as a fraction of GFR
ABONE	R0	2.79E-02	2.14E-01	Permeability constant for diffusion from bone to canaliculi
ABONE	RAD8	2.63E-02	1.64E-01	Radius of shell 8 of bone in the canalicular diffusion region of deeper bone
ABONE	P0	5.73E-03	6.19E-02	Permeability constant for diffusion from canaliculi to bone
ABONE	D0	5.61E-03	4.12E-02	Diffusion constant
ABONE	CON	8.59E-02	3.71E-02	Fraction of bone blood flow to trabecular bone
ABONE	EXPO	2.16E-01	3.07E-02	Exponent constant for bone volume participating in adult-type bone remodeling
ABONE	S	5.50E-03	2.97E-02	Surface area of canaliculi
ABONE	C3	3.78E-01	2.47E-02	Constant 3 for urinary clearance of Pb as a fraction of GFR
ABONE	RAD1	4.42E-03	2.35E-02	Radius of shell 1 of bone in the canalicular diffusion region of deeper bone
ABONE	RAD2	2.28E-03	1.29E-02	Radius of shell 2 of bone in the canalicular diffusion region of deeper bone
ABONE	BASE	4.36E-05	1.08E-02	Base bone formation rate in bone growth algorithm
ABONE	RAD3	1.35E-03	9.01E-03	Radius of shell 3 of bone in the canalicular diffusion region of deeper bone
ABONE	RAD4	8.09E-04	6.94E-03	Radius of shell 4 of bone in the canalicular diffusion region of deeper bone
ABONE	RAD5	4.66E-04	5.34E-03	Radius of shell 5 of bone in the canalicular diffusion region of deeper bone
ABONE	RAD6	2.46E-04	3.78E-03	Radius of shell 6 of bone in the canalicular diffusion region of deeper bone
ABONE	RAD7	1.06E-04	2.07E-03	Radius of shell 7 of bone in the canalicular diffusion region of deeper bone
ABONE	A3	6.95E-03	1.18E-03	Constant 3 for bone formation rate algorithm
ABONE	PL	3.82E-03	1.10E-03	Liver/plasma partition coefficient
ABONE	QKC	4.17E-03	9.41E-04	Fraction cardiac output going to kidney
ABONE	PW	6.23E-03	9.31E-04	Well-perfused/plasma partition coefficient
ABONE	BIND	1.37E-03	8.40E-04	Maximum capacity of sites in red cells to bind Pb
ABONE	KBIND	1.12E-03	8.30E-04	Half-saturation concentration of Pb for binding by sites in red cells

Variable	Parameter	Child	Adult	Parameter Description
ABONE	G	2.96E-03	5.62E-04	Linear parameter for unbound lead in red cells
ABONE	QBONEC	2.66E-03	5.61E-04	Fraction cardiac output going to bone
ABONE	A2	3.42E-03	4.88E-04	Constant 2 for bone formation rate algorithm
ABONE	A5	0.00E+00	2.72E-04	Constant 5 for bone formation rate algorithm
ABONE	QLC	9.11E-03	2.41E-04	Fraction cardiac output going to liver
ABONE	QWC	9.22E-03	2.24E-04	Fraction cardiac output going to other well-perfused tissues
ABONE	PP	1.43E-04	1.36E-04	Poorly perfused/plasma partition coefficient
ABONE	A1	1.50E-02	3.05E-05	Constant 1 for bone formation rate algorithm
ABONE	PK	1.73E-04	1.20E-05	Kidney/plasma partition coefficient
ABONE	QCC	0.00E+00	0.00E+00	Cardiac output in the adult

1

2

TABLE 4-11. AALM-OF STANDARDIZED SENSITIVITY COEFFICIENTS FOR LIVER PB IN CHILDREN (5 YEARS) AND ADULTS (30 YEARS)

Variable	Parameter	Child	Adult	Parameter Description
ALIVER	C1	2.39E+00	9.28E+00	Constant 1 for urinary clearance of Pb as a fraction of GFR
ALIVER	C2	1.38E+00	7.56E+00	Constant 2 for urinary clearance of Pb as a fraction of GFR
ALIVER	PL	1.01E+00	9.98E-01	Liver/plasma partition coefficient
ALIVER	P0	5.73E-03	6.19E-02	Permeability constant for diffusion from canaliculi to bone
ALIVER	R0	4.98E-03	5.60E-02	Permeability constant for diffusion from bone to canaliculi
ALIVER	RAD8	4.29E-03	3.98E-02	Radius of shell 8 of bone in the canalicular diffusion region of deeper bone
ALIVER	CON	7.53E-04	2.51E-02	Fraction of bone blood flow to trabecular bone
ALIVER	D0	1.00E-03	1.07E-02	Diffusion constant
ALIVER	BASE	1.73E-04	9.04E-03	Base bone formation rate in bone growth algorithm
ALIVER	C3	4.48E-01	7.12E-03	Constant 3 for urinary clearance of Pb as a fraction of GFR
ALIVER	S	8.29E-04	6.69E-03	Surface area of canaliculi
ALIVER	RAD1	6.69E-04	5.11E-03	Radius of shell 1 of bone in the canalicular diffusion region of deeper bone
ALIVER	RAD2	3.68E-04	2.85E-03	Radius of shell 2 of bone in the canalicular diffusion region of deeper bone
ALIVER	RAD3	2.28E-04	2.16E-03	Radius of shell 3 of bone in the canalicular diffusion region of deeper bone
ALIVER	RAD4	1.51E-04	1.89E-03	Radius of shell 4 of bone in the canalicular diffusion region of deeper bone
ALIVER	RAD5	1.05E-04	1.65E-03	Radius of shell 5 of bone in the canalicular diffusion region of deeper bone
ALIVER	RAD6	6.96E-05	1.29E-03	Radius of shell 6 of bone in the canalicular diffusion region of deeper bone
ALIVER	EXPO	7.19E-03	1.12E-03	Exponent constant for bone volume participating in adult-type bone remodeling
ALIVER	QKC	1.24E-03	1.12E-03	Fraction cardiac output going to kidney
ALIVER	A1	9.35E-03	1.01E-03	Constant 1 for bone formation rate algorithm
ALIVER	QLC	1.34E-02	9.67E-04	Fraction cardiac output going to liver
ALIVER	A3	4.21E-03	9.38E-04	Constant 3 for bone formation rate algorithm
ALIVER	QWC	1.33E-02	9.34E-04	Fraction cardiac output going to other well-perfused tissues
ALIVER	BIND	8.28E-04	7.63E-04	Maximum capacity of sites in red cells to bind Pb

Variable	Parameter	Child	Adult	Parameter Description
ALIVER	KBIND	8.44E-04	7.58E-04	Half-saturation concentration of Pb for binding by sites in red cells
ALIVER	RAD7	3.63E-05	7.57E-04	Radius of shell 7 of bone in the canalicular diffusion region of deeper bone
ALIVER	A5	0.00E+00	6.67E-04	Constant 5 for bone formation rate algorithm
ALIVER	PW	2.11E-03	6.09E-04	Well-perfused/plasma partition coefficient
ALIVER	A2	3.08E-03	1.98E-04	Constant 2 for bone formation rate algorithm
ALIVER	QBONEC	8.66E-03	1.62E-04	Fraction cardiac output going to bone
ALIVER	G	8.74E-03	1.60E-04	Linear parameter for unbound lead in red cells
ALIVER	PP	8.13E-05	1.14E-04	Poorly perfused/plasma partition coefficient
ALIVER	PK	3.61E-05	2.25E-05	Kidney/plasma partition coefficient
ALIVER	QCC	0.00E+00	0.00E+00	Cardiac output in the adult

1

TABLE 4-12. AALM-OF STANDARDIZED SENSITIVITY COEFFICIENTS FOR KIDNEY PB IN CHILDREN (5 YEARS) AND ADULTS (30 YEARS)

Variable	Parameter	Child	Adult	Parameter Description
AKIDNEY	C1	2.39E+00	9.28E+00	Constant 1 for urinary clearance of Pb as a fraction of GFR
AKIDNEY	C2	1.38E+00	7.56E+00	Constant 2 for urinary clearance of Pb as a fraction of GFR
AKIDNEY	PK	1.00E+00	9.99E-01	Kidney/plasma partition coefficient
AKIDNEY	P0	5.73E-03	6.19E-02	Permeability constant for diffusion from canaliculi to bone
AKIDNEY	R0	4.99E-03	5.60E-02	Permeability constant for diffusion from bone to canaliculi
AKIDNEY	RAD8	4.29E-03	3.98E-02	Radius of shell 8 of bone in the canalicular diffusion region of deeper bone
AKIDNEY	CON	7.53E-04	2.51E-02	Fraction of bone blood flow to trabecular bone
AKIDNEY	D0	1.00E-03	1.07E-02	Diffusion constant
AKIDNEY	BASE	1.73E-04	9.04E-03	Base bone formation rate in bone growth algorithm
AKIDNEY	C3	4.48E-01	7.12E-03	Constant 3 for urinary clearance of Pb as a fraction of GFR
AKIDNEY	S	8.29E-04	6.69E-03	Surface area of canaliculi
AKIDNEY	RAD1	6.69E-04	5.11E-03	Radius of shell 1 of bone in the canalicular diffusion region of deeper bone
AKIDNEY	RAD2	3.68E-04	2.85E-03	Radius of shell 2 of bone in the canalicular diffusion region of deeper bone
AKIDNEY	RAD3	2.28E-04	2.16E-03	Radius of shell 3 of bone in the canalicular diffusion region of deeper bone
AKIDNEY	PL	1.13E-02	2.10E-03	Liver/plasma partition coefficient
AKIDNEY	RAD4	1.51E-04	1.89E-03	Radius of shell 4 of bone in the canalicular diffusion region of deeper bone
AKIDNEY	RAD5	1.05E-04	1.65E-03	Radius of shell 5 of bone in the canalicular diffusion region of deeper bone
AKIDNEY	RAD6	6.96E-05	1.29E-03	Radius of shell 6 of bone in the canalicular diffusion region of deeper bone
AKIDNEY	EXPO	7.19E-03	1.12E-03	Exponent constant for bone volume participating in adult-type bone remodeling
AKIDNEY	QKC	1.47E-03	1.05E-03	Fraction cardiac output going to kidney
AKIDNEY	A1	9.32E-03	1.01E-03	Constant 1 for bone formation rate algorithm
AKIDNEY	A3	4.22E-03	9.37E-04	Constant 3 for bone formation rate algorithm
AKIDNEY	QWC	1.33E-02	9.34E-04	Fraction cardiac output going to other well-perfused tissues
AKIDNEY	QLC	1.32E-02	9.19E-04	Fraction cardiac output going to liver

Variable	Parameter	Child	Adult	Parameter Description
AKIDNEY	RAD7	3.63E-05	7.57E-04	Radius of shell 7 of bone in the canalicular diffusion region of deeper bone
AKIDNEY	A5	0.00E+00	6.67E-04	Constant 5 for bone formation rate algorithm
AKIDNEY	BIND	3.64E-04	6.52E-04	Maximum capacity of sites in red cells to bind Pb
AKIDNEY	KBIND	3.85E-04	6.47E-04	Half-saturation concentration of Pb for binding by sites in red cells
AKIDNEY	PW	2.05E-03	6.09E-04	Well-perfused/plasma partition coefficient
AKIDNEY	A2	3.08E-03	1.98E-04	Constant 2 for bone formation rate algorithm
AKIDNEY	QBONEC	8.68E-03	1.62E-04	Fraction cardiac output going to bone
AKIDNEY	G	8.77E-03	1.60E-04	Linear parameter for unbound lead in red cells
AKIDNEY	PP	8.05E-05	1.13E-04	Poorly perfused/plasma partition coefficient
AKIDNEY	QCC	0.00E+00	0.00E+00	Cardiac output in the adult

1

TABLE 4-13. AALM-OF STANDARDIZED SENSITIVITY COEFFICIENTS FOR POORLY PERFUSED TISSUES PB IN CHILDREN (5 YEARS) AND ADULTS (30 YEARS)

Variable	Parameter	Child	Adult	Parameter Description
APOOR	C1	2.39E+00	9.28E+00	Constant 1 for urinary clearance of Pb as a fraction of GFR
APOOR	C2	1.38E+00	7.56E+00	Constant 2 for urinary clearance of Pb as a fraction of GFR
APOOR	PP	1.00E+00	1.00E+00	Poorly perfused/plasma partition coefficient
APOOR	P0	5.73E-03	6.19E-02	Permeability constant for diffusion from canaliculi to bone
APOOR	R0	4.99E-03	5.60E-02	Permeability constant for diffusion from bone to canaliculi
APOOR	RAD8	4.29E-03	3.98E-02	Radius of shell 8 of bone in the canalicular diffusion region of deeper bone
APOOR	CON	7.54E-04	2.51E-02	Fraction of bone blood flow to trabecular bone
APOOR	D0	1.00E-03	1.07E-02	Diffusion constant
APOOR	BASE	1.73E-04	9.03E-03	Base bone formation rate in bone growth algorithm
APOOR	C3	4.48E-01	7.12E-03	Constant 3 for urinary clearance of Pb as a fraction of GFR
APOOR	S	8.29E-04	6.69E-03	Surface area of canaliculi
APOOR	RAD1	6.69E-04	5.11E-03	Radius of shell 1 of bone in the canalicular diffusion region of deeper bone
APOOR	RAD2	3.68E-04	2.85E-03	Radius of shell 2 of bone in the canalicular diffusion region of deeper bone
APOOR	RAD3	2.28E-04	2.16E-03	Radius of shell 3 of bone in the canalicular diffusion region of deeper bone
APOOR	PL	1.13E-02	2.08E-03	Liver/plasma partition coefficient
APOOR	RAD4	1.51E-04	1.89E-03	Radius of shell 4 of bone in the canalicular diffusion region of deeper bone
APOOR	RAD5	1.05E-04	1.65E-03	Radius of shell 5 of bone in the canalicular diffusion region of deeper bone
APOOR	RAD6	6.96E-05	1.29E-03	Radius of shell 6 of bone in the canalicular diffusion region of deeper bone
APOOR	EXPO	7.19E-03	1.12E-03	Exponent constant for bone volume participating in adult-type bone remodeling
APOOR	QKC	1.55E-03	1.12E-03	Fraction cardiac output going to kidney
APOOR	A1	9.13E-03	1.01E-03	Constant 1 for bone formation rate algorithm
APOOR	A3	4.22E-03	9.48E-04	Constant 3 for bone formation rate algorithm
APOOR	QWC	1.34E-02	9.34E-04	Fraction cardiac output going to other well-perfused tissues
APOOR	QLC	1.33E-02	9.19E-04	Fraction cardiac output going to liver

Variable	Parameter	Child	Adult	Parameter Description
APOOR	RAD7	3.63E-05	7.57E-04	Radius of shell 7 of bone in the canalicular diffusion region of deeper bone
APOOR	BIND	6.34E-04	7.16E-04	Maximum capacity of sites in red cells to bind Pb
APOOR	KBIND	6.52E-04	7.11E-04	Half-saturation concentration of Pb for binding by sites in red cells
APOOR	A5	0.00E+00	6.67E-04	Constant 5 for bone formation rate algorithm
APOOR	PW	2.74E-03	6.15E-04	Well-perfused/plasma partition coefficient
APOOR	A2	3.08E-03	1.98E-04	Constant 2 for bone formation rate algorithm
APOOR	QBONEC	7.84E-03	1.62E-04	Fraction cardiac output going to bone
APOOR	G	7.92E-03	1.60E-04	Linear parameter for unbound lead in red cells
APOOR	PK	3.62E-05	2.25E-05	Kidney/plasma partition coefficient
APOOR	QCC	0.00E+00	0.00E+00	Cardiac output in the adult

1

TABLE 4-14. AALM-OF STANDARDIZED SENSITIVITY COEFFICIENTS FOR WELL-PERFUSED TISSUES PB IN CHILDREN (5 YEARS) AND ADULTS (30 YEARS)

Variable	Parameter	Child	Adult	Parameter Description
AWELL	C1	2.39E+00	9.28E+00	Constant 1 for urinary clearance of Pb as a fraction of GFR
AWELL	C2	1.38E+00	7.56E+00	Constant 2 for urinary clearance of Pb as a fraction of GFR
AWELL	PW	1.00E+00	1.00E+00	Well-perfused/plasma partition coefficient
AWELL	P0	5.73E-03	6.19E-02	Permeability constant for diffusion from canaliculi to bone
AWELL	R0	4.99E-03	5.60E-02	Permeability constant for diffusion from bone to canaliculi
AWELL	RAD8	4.29E-03	3.98E-02	Radius of shell 8 of bone in the canalicular diffusion region of deeper bone
AWELL	CON	7.53E-04	2.51E-02	Fraction of bone blood flow to trabecular bone
AWELL	D0	1.00E-03	1.07E-02	Diffusion constant
AWELL	BASE	1.73E-04	9.05E-03	Base bone formation rate in bone growth algorithm
AWELL	C3	4.48E-01	7.12E-03	Constant 3 for urinary clearance of Pb as a fraction of GFR
AWELL	S	8.29E-04	6.69E-03	Surface area of canaliculi
AWELL	RAD1	6.69E-04	5.11E-03	Radius of shell 1 of bone in the canalicular diffusion region of deeper bone
AWELL	RAD2	3.68E-04	2.85E-03	Radius of shell 2 of bone in the canalicular diffusion region of deeper bone
AWELL	RAD3	2.28E-04	2.16E-03	Radius of shell 3 of bone in the canalicular diffusion region of deeper bone
AWELL	PL	1.11E-02	2.08E-03	Liver/plasma partition coefficient
AWELL	RAD4	1.51E-04	1.89E-03	Radius of shell 4 of bone in the canalicular diffusion region of deeper bone
AWELL	RAD5	1.05E-04	1.65E-03	Radius of shell 5 of bone in the canalicular diffusion region of deeper bone
AWELL	RAD6	6.96E-05	1.29E-03	Radius of shell 6 of bone in the canalicular diffusion region of deeper bone
AWELL	EXPO	7.19E-03	1.12E-03	Exponent constant for bone volume participating in adult-type bone remodeling
AWELL	QKC	1.09E-03	1.12E-03	Fraction cardiac output going to kidney
AWELL	A1	9.45E-03	1.01E-03	Constant 1 for bone formation rate algorithm
AWELL	QWC	1.32E-02	9.34E-04	Fraction cardiac output going to other well-perfused tissues
AWELL	A3	4.21E-03	9.30E-04	Constant 3 for bone formation rate algorithm
AWELL	QLC	1.31E-02	9.19E-04	Fraction cardiac output going to liver

Variable	Parameter	Child	Adult	Parameter Description
AWELL	RAD7	3.63E-05	7.57E-04	Radius of shell 7 of bone in the canalicular diffusion region of deeper bone
AWELL	BIND	6.34E-04	7.16E-04	Maximum capacity of sites in red cells to bind Pb
AWELL	KBIND	6.52E-04	7.11E-04	Half-saturation concentration of Pb for binding by sites in red cells
AWELL	A5	0.00E+00	6.67E-04	Constant 5 for bone formation rate algorithm
AWELL	A2	3.08E-03	1.98E-04	Constant 2 for bone formation rate algorithm
AWELL	QBONEC	9.15E-03	1.64E-04	Fraction cardiac output going to bone
AWELL	G	9.14E-03	1.60E-04	Linear parameter for unbound lead in red cells
AWELL	PP	8.05E-05	1.13E-04	Poorly perfused/plasma partition coefficient
AWELL	PK	3.61E-05	2.25E-05	Kidney/plasma partition coefficient
AWELL	QCC	0.00E+00	0.00E+00	Cardiac output in the adult

1

TABLE 4-15. DOMINANT PARAMETERS INFLUENCING MAJOR DIFFERENCES IN PREDICTIONS FROM AALM-LG AND AALM-OF

Predicted Variable	Model Difference	Dominant Parameters	
		AALM-LG	**AALM-OF**
Child blood Pb	AALM-OF < AALM-LG	TEVF TORBC TOSOF0 RRBC TOLVR1 H1TOBL TBONE	C1 C2 BIND KBIND
Child bone Pb	AALM-OF < AALM-LG	TEVF TORBC TBONE TOSOF0 FLONG RCS2DF TOLVR1 H1TOBL RTS2DF	C1 C2 R0 RAD8
Liver Pb	AALM-OF < AALM-LG	TEVF TORBC TOSOF0 TOLVR1 H1TOH2 RLVR2 H1TOBL RLVR1	C1 C2 PL
Kidney Pb	AALM-OF < AALM-LG	TEVF TORBC TOSOF0 RKDN1 TOKDN1 TOKDN2 RKDN2	C1 C2 PK
Other soft tissues	AALM-OF < AALM-LG	TEVF TORBC TOSOF0 RSOF2 TOSOF2 TOLVR1 H1TOBL TOSOF1 RSOF1	C1 C2 PP PW

TABLE 4-16. STRATEGY USED FOR SEQUENTIAL OPTIMIZATION OF AALM BIOKINETICS MODEL

Step	Objective	Observation Data Sources
1	Unify parameter values for GI absorption and growth	(O'Flaherty, 1995, 1993)
2	Optimize plasma/RBC ratio	(Smith et al., 2002; Bergdahl et al., 1999; Bergdahl et al., 1998; Hernandez-Avila et al., 1998; Bergdahl et al., 1997; Schutz et al., 1996)
3	Optimize plasma(blood)-to-urine clearance	(Rentschler et al., 2012; Dewoskin and Thompson, 2008; Manton and Cook, 1984; Manton and Malloy, 1983; Chamberlain et al., 1978)
4	Optimize soft tissue (kidney, liver, muscle)/bone ratios	(Gerhardsson et al., 1995; Barry, 1981, 1975; Gross et al., 1975)
5	Optimize plasma(blood)/bone ratios	(Hernandez-Avila et al., 1998; Cake et al., 1996)
6	Optimize bone Pb elimination kinetics	(Nilsson et al., 1991)
7	Evaluate blood Pb elimination kinetics – adults	(Rabinowitz et al., 1976)
8	Evaluate blood Pb elimination kinetics – infants	(Sherlock and Quinn, 1986; Ryu et al., 1983)

TABLE 4-17. COMPARISON OF PREDICTED AND OBSERVED PLASMA PB/BONE PB SLOPES

Model	Study	Bone	Predicted Slope	Observed Slope	SE	95%CL	Residual
AALM-LG	CA96	Cortical	0.037	0.052	0.013	0.027, 0.077	-1.16
AALM-LG	CA96	Trabecular	0.040	0.041	0.007	0.027, 0.054	-0.16
AALM-LG	HE98	Cortical	0.037	0.036	0.011	0.014, 0.058	0.12
AALM-LG	HE98	Trabecular	0.040	0.025	0.004	0.017, 0.033	3.67
AALM-OF	CA96	Cortical	0.042	0.052	0.013	0.027, 0.077	-0.81
AALM-OF	CA96	Trabecular	0.060	0.041	0.007	0.027, 0.054	2.70
AALM-OF	HE98	Cortical	0.042	0.036	0.011	0.014, 0.058	0.53
AALM-OF	HE98	Trabecular	0.060	0.025	0.004	0.017, 0.033	8.68

CA96, Cake et al. (1996); HE98, Hernandez-Avila et al. (1998)

TABLE 4-18. CHANGES TO (O'FLAHERTY, 1995, 1993) AND (LEGGETT, 1993) MODELS INCORPORATED INTO AALM

Model Component	Parameter Change	AALM-LG	AALM-OF
Growth	Body and tissue growth as functions of age and body weight	X	
Respiratory tract	Simulation of deposition, mucociliary clearance and absorption of inhaled Pb based on ICRP HRTM	X	X
GI tract	Age-dependent absorption calculated with a continuous function rather than age array variable	X	
GI tract	Infant GI absorption fractions optimized	X	X
GI tract	Absorption fraction adjustable by user-specified media-specific relative bioavailability fractions	X	X
Tissue Pb	Age-dependent values for tissue-blood partition coefficients		X
Tissue Pb	Bone, kidney and liver concentrations calculated from Pb masses and tissue weights	X	
Neonate	Neonatal model which sets Pb masses in blood and tissues at birth as a function of maternal Pb concentration	X	X
RBC	Parameters for plasma-RBC binding and uptake optimized	X	X
GFR	Parameters for GFR adjusted to predict adult GFR of 170 L/day/1.73m^2 (120 mL/min/1.73m^2) and 30% of adult in infants (<1 year)		X
Urine Pb	Parameters for Pb transfer to urine optimized	X	X

GFR, glomerular filtration rate; GI, gastrointestinal; ICRP, International Commission of Radiological Protection; RBC, red blood cell

TABLE 4-19. COMPARISON OF AALM-LG AND AALM-OF PREDICTIONS OF BLOOD AND TISSUE PB CONCENTRATIONS

Dose (µg/day)	Age (year)	Sex	Tissue	Unit	AALM-LG	AALM-OF
5	2	M	Blood	µg/dL	1.86	2.39
5	2	M	Bone	µg/g	0.88	0.43
5	2	M	Kidney	µg/g	0.06	0.08
5	2	M	Liver	µg/g	0.14	0.09
5	40	M	Blood	µg/dL	0.28	0.50
5	40	M	Bone	µg/g	0.14	0.15
5	40	M	Kidney	µg/g	0.005	0.010
5	40	M	Liver	µg/g	0.008	0.012
5	2	F	Blood	µg/dL	1.95	2.39
5	2	F	Bone	µg/g	0.93	0.43
5	2	F	Kidney	µg/g	0.07	0.08
5	2	F	Liver	µg/g	0.15	0.09
5	40	F	Blood	µg/dL	0.36	0.50
5	40	F	Bone	µg/g	0.20	0.15
5	40	F	Kidney	µg/g	0.006	0.010
5	40	F	Liver	µg/g	0.010	0.012

F, female; M, male

TABLE 4-20. COMPARISON OF ADULT LEAD METHODOLOGY, AALM-LG AND AALM-OF PREDICTIONS OF BLOOD PB CONCENTRATIONS IN ADULTS

Parameter	Description	Units	ALM	AALM-LG	AALM-OF
PbS	Soil lead concentration	µg/g or ppm	1000	1000	1000
BKSF	Biokinetic Slope Factor	µg/dL per µg/day	0.4	NA	NA
PbB_0	Baseline Blood Pb	µg/dL	1.5	1.5	1.5
IR_S	Soil Ingestion Rate	g/day	0.050	0.05	0.05
$AF_{S, D}$	Absorption Fraction	--	0.12	0.048	0.048
$EF_{S, D}$	Exposure Frequency	days/yr	219	219	219
$AT_{S, D}$	Averaging Time	days/yr	365	365	365
PbB_{adult}	Blood Pb Concentration	µg/dL	2.9	3.1	4.6

ALM, Adult Lead Methodology

TABLE 4-21. COMPARISON OF AALM-LG AND AALM-OF PREDICTIONS OF BLOOD AND TISSUE PB CONCENTRATIONS AFTER CALIBRATING RBC PARAMETER VALUES TO THE IEUBK MODEL OUTPUT

Dose (µg/day)	Age (year)	Sex	Tissue	Unit	AALM-LG	AALM-OF
5	2	M	Blood	µg/dL	1.6	1.2
5	2	M	Bone	µg/g	1.33	0.43
5	2	M	Kidney	µg/g	0.10	0.08
5	2	M	Liver	µg/g	0.21	0.09
5	40	M	Blood	µg/dL	0.28	0.50
5	40	M	Bone	µg/g	0.15	0.15
5	40	M	Kidney	µg/g	0.005	0.010
5	40	M	Liver	µg/g	0.008	0.012
5	2	F	Blood	µg/dL	1.7	1.2
5	2	F	Bone	µg/g	1.42	0.46
5	2	F	Kidney	µg/g	0.10	0.08
5	2	F	Liver	µg/g	0.23	0.10
5	40	F	Blood	µg/dL	0.36	0.55
5	40	F	Bone	µg/g	0.20	0.14
5	40	F	Kidney	µg/g	0.006	0.012
5	40	F	Liver	µg/g	0.010	0.014

F, female; M, male

TABLE 4-22. CHANGES MADE TO THE (LEGGETT, 1993) MODEL TO CREATE AALM-LG.CSL

LEGGETT	AALM-LG	Output/Functionality Affected
Age-dependent blood volume	Age-dependent blood volume based on O'Flaherty (1995, 1993)	Age-dependent RBC and plasma volumes
Constant hematocrit	Age-dependent hematocrit based on O'Flaherty (1995, 1993)	Age-dependent RBC and plasma volumes
Adult bone mass	Age-dependent bone mass based on O'Flaherty (1995, 1993)	Age-dependent cortical and trabecular bone Pb concentration
Adult kidney mass	Age-dependent kidney mass based on O'Flaherty (1995, 1993)	Age-dependent kidney Pb concentration
NA	Age-dependent liver mass based on O'Flaherty (1995, 1993)	Age-dependent liver Pb concentration
Age-dependent absorption fraction (*FI*): • birth: 0.45 • 0.27 y: 0.45 • 1 y: 0.30 • 5 y: 0.30 • 10 y: 0.30 • 15 y: 0.30 • ≥25 y: 0.15	Age-dependent absorption fraction (*FI*): • birth: 0.39 • 0.27 y: 0.39 • 1 y: 0.38 • 5 y: 0.17 • ≥10 y: 0.12	Absorption fraction for ingested Pb
Absorption fraction for ingested Pb not adjusted for RBA	Absorption fraction adjusted for media-specific RBA	Absorption fraction of ingested Pb
RBC Pb saturation threshold: 60 µg/dL blood) Maximum: 350 µg/dL RBC	RBC Pb saturation threshold: 20 µg/dL blood) Maximum: 350 µg/dL RBC	Plasma-RBC Pb relationship
Transfer rate from (d^{-1}) RBC to diffusible plasma: • birth: 0.462 • 0.27 y: 0.462 • 1 y: 0.462 • 5 y: 0.277 • ≥10 y: 0.139	Transfer rate from (d^{-1}) from RBC to diffusible plasma: • birth: 0.462 • 0.27 y: 0.462 • 1 y: 0.785 • 5 y: 0.499 • 10 y: 0.195 • ≥ 15 y: 0.139	Plasma-RBC Pb relationship
Deposition fraction from diffusible plasma to RBC (0.24)	Deposition fraction from diffusible plasma to RBC (0.25)	Plasma-RBC relationship
Deposition fraction from diffusible plasma to urine (30)	Deposition fraction from diffusible plasma to urine (0)	Plasma to urine clearance

LEGGETT	AALM-LG	Output/Functionality Affected
Transfer rate (d^{-1}) from liver to diffusible plasma: • birth: 0.00693 • 0.27 y: 0.00693 • 1 y: 0.00693 • 5 y: 0.00693 • 10 y: 0.00190 • 15 y: 0.00190 • ≥25 y: 0.00190	Transfer rate (d^{-1}) from liver to diffusible plasma: • birth: 0.00693 • 0.27 y: 0.00693 • 1 y: 0.00693 • 5 y: 0.00139 • 10 y: 0.000570 • 15 y: 0.000570 • 25 y: 0.000570 • 30 y: 0.00142 • 40 y: 0.00304 • 60 y: 0.00342 • 90 y: 0.00380	Plasma to liver Pb kinetics
Deposition fraction from diffusible plasma to kidney (40)	Deposition fraction from diffusible plasma to kidney (50)	Urinary clearance of plasma Pb
Transfer rate (d^{-1}) from kidney to diffusible plasma (RKDN2): • birth: 0.00693 • 0.27 y: 0.00693 • 1 y: 0.00693 • 5 y: 0.00693 • 10 y: 0.00190 • 15 y: 0.00190 • ≥25 y: 0.00190	Transfer rate (d^{-1}) from kidney to diffusible plasma (RKDN2): • birth: 0.000693 • 0.27 y: 0.000693 • 1 y: 0.000693 • 5 y: 0.000693 • 10 y: 0.000190 • 15 y: 0.000190 • 25 y: 0.000190 • 30 y: 0.000950 • ≥40 y: 0.00190	Plasma to kidney Pb kinetics
Fraction of total transfer from exchangeable bone to nonexchangeable bone (0.2)	Fraction of total transfer from exchangeable bone to nonexchangeable bone (0.6)	Bone Pb retention
Transfer rate (d^{-1}) from non-exchangeable cortical bone to diffusible plasma: • birth: 0.00822 • 0.27 y: 0.00822 • 1 y: 0.00288 • 5 y: 0.00154 • 10 y: 0.000890 • 15 y: 0.000512 • ≥25 y: 0.0000822	Transfer rate (d^{-1}) from non-exchangeable cortical bone to diffusible plasma: • birth: 0.0204 • 0.27 y: 0.0164 • 1 y: 0.00576 • 5 y: 0.00308 • 10 y: 0.00178 • 15 y: 0.00102 • ≥25 y: 0.000164	Bone to plasma Pb kinetics

LEGGETT	AALM-LG	Output/Functionality Affected
Transfer rate (d^{-1}) from non-exchangeable trabecular bone to diffusible plasma: • birth: 0.00822 • 0.27 y: 0.00822 • 1 y: 0.00288 • 5 y: 0.00181 • 10 y: 0.00132 • 15 y: 0.000956 • ≥25 y: 0.000493	Transfer rate (d^{-1}) from non-exchangeable trabecular bone to diffusible plasma: • birth: 0.0102 • 0.27 y: 0.01644 • 1 y: 0.00576 • 5 y: 0.00362 • 10 y: 0.00264 • 15 y: 0.00192 • ≥25 y: 0.000986	Bone-to-plasma Pb transfer kinetics

1

2

FIGURE 4-1. DATA FLOW DIAGRAM FOR AALM.

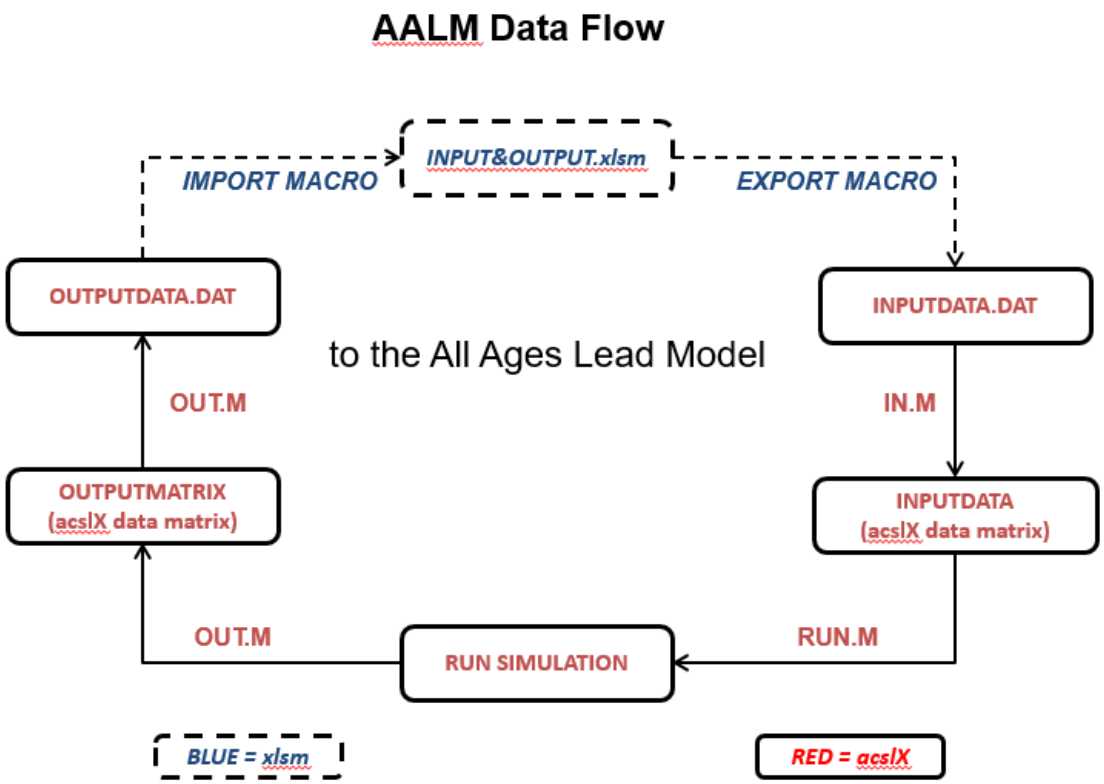

FIGURE 4-2. STRUCTURE OF AALM-LG MODEL.

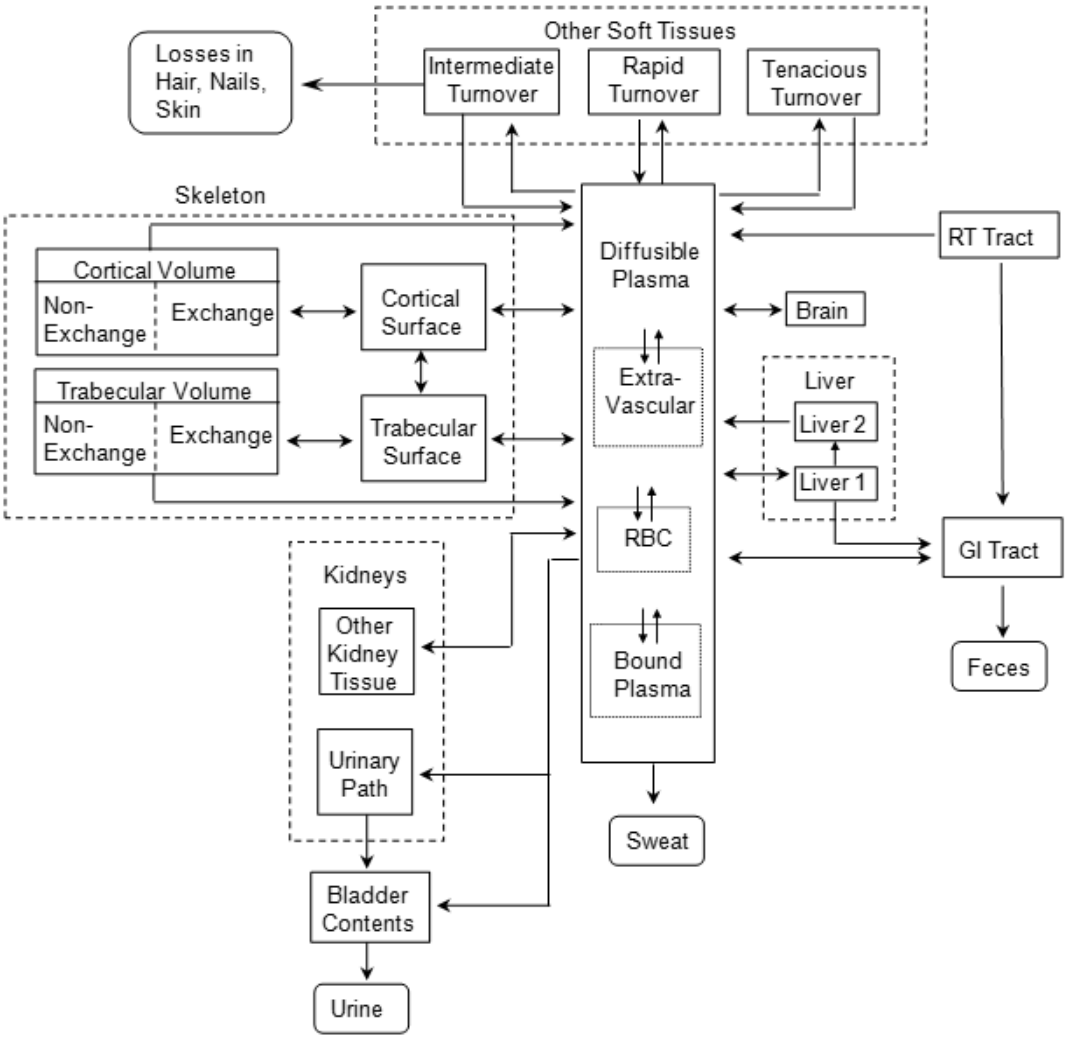

Figure is based on Leggett (1993).

FIGURE 4-3. STRUCTURE OF AALM-OF MODEL.

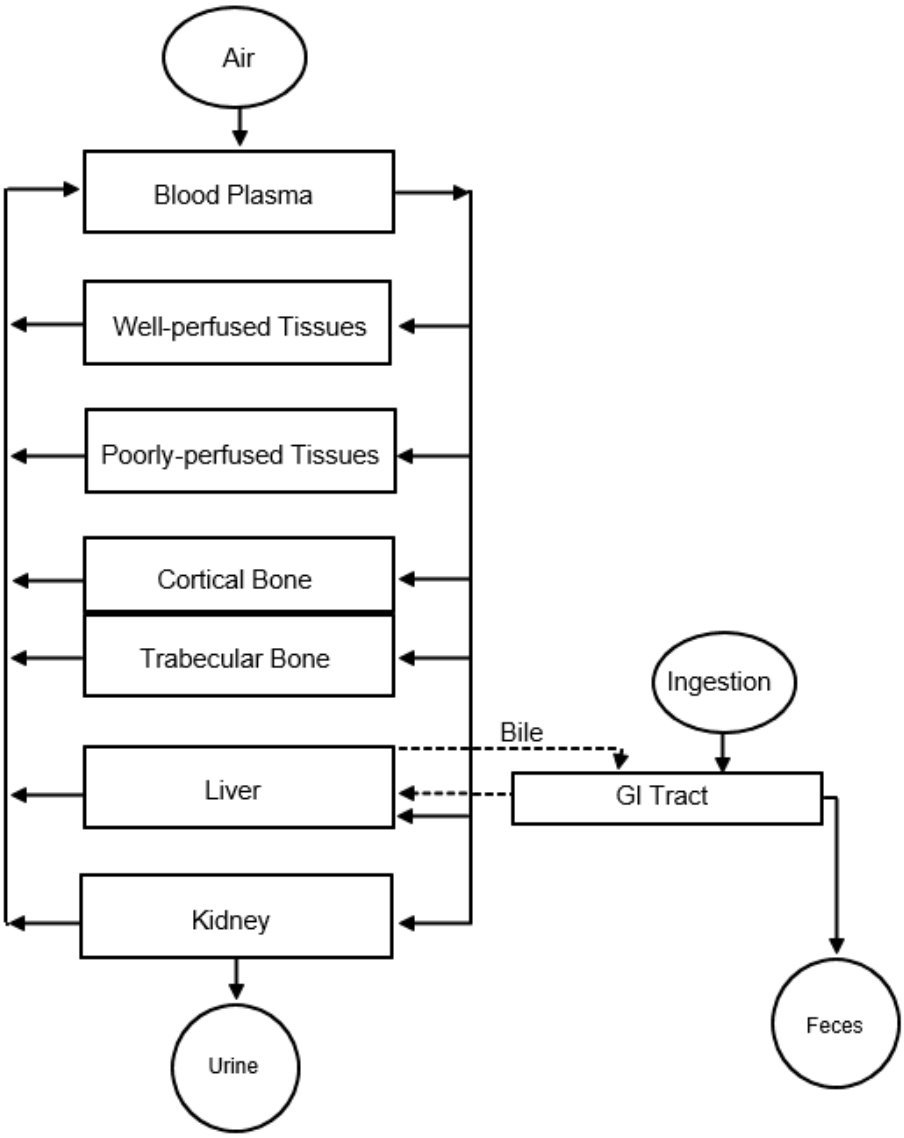

Figure is based on O'Flaherty (1993) .

FIGURE 4-4. STRUCTURE OF AALM-LG BONE MODEL.

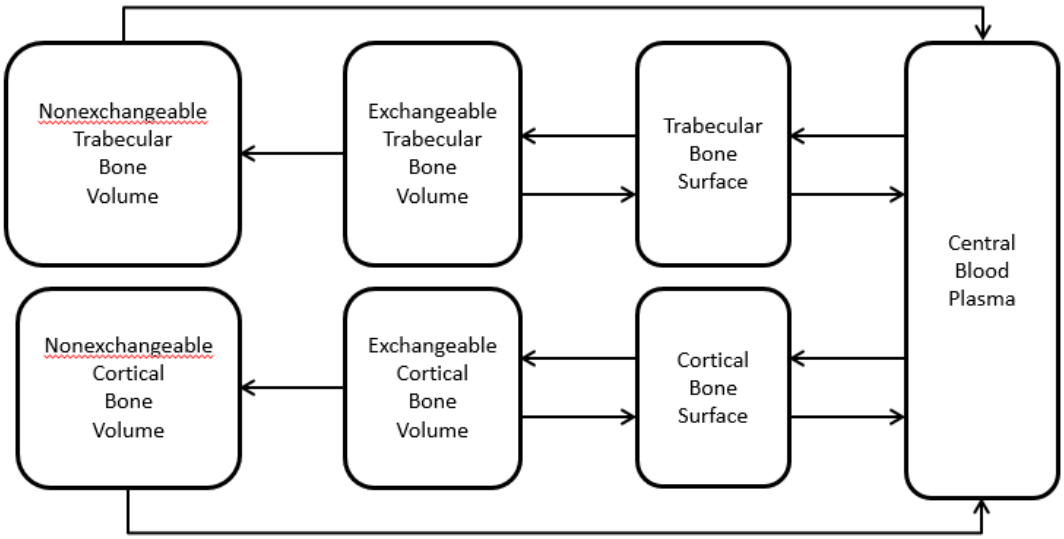

Figure is based on Leggett (1993).

FIGURE 4-5. STRUCTURE OF AALM-OF BONE MODEL.

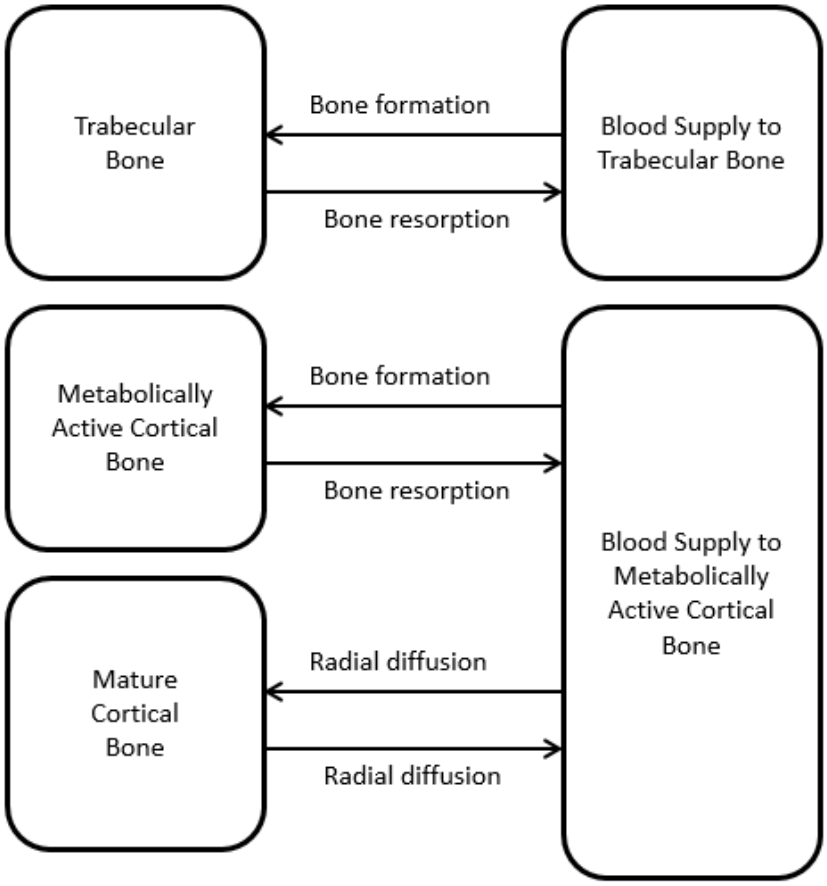

Figure is based on O'Flaherty (1993).

FIGURE 4-6. COMPARISON OF PB (µG) LEVELS PREDICTED FROM AALM-OF AND AALM-LG FOR A CONSTANT INGESTION OF 5 µG PB/DAY FOR AGES 0 TO 30 YEARS.

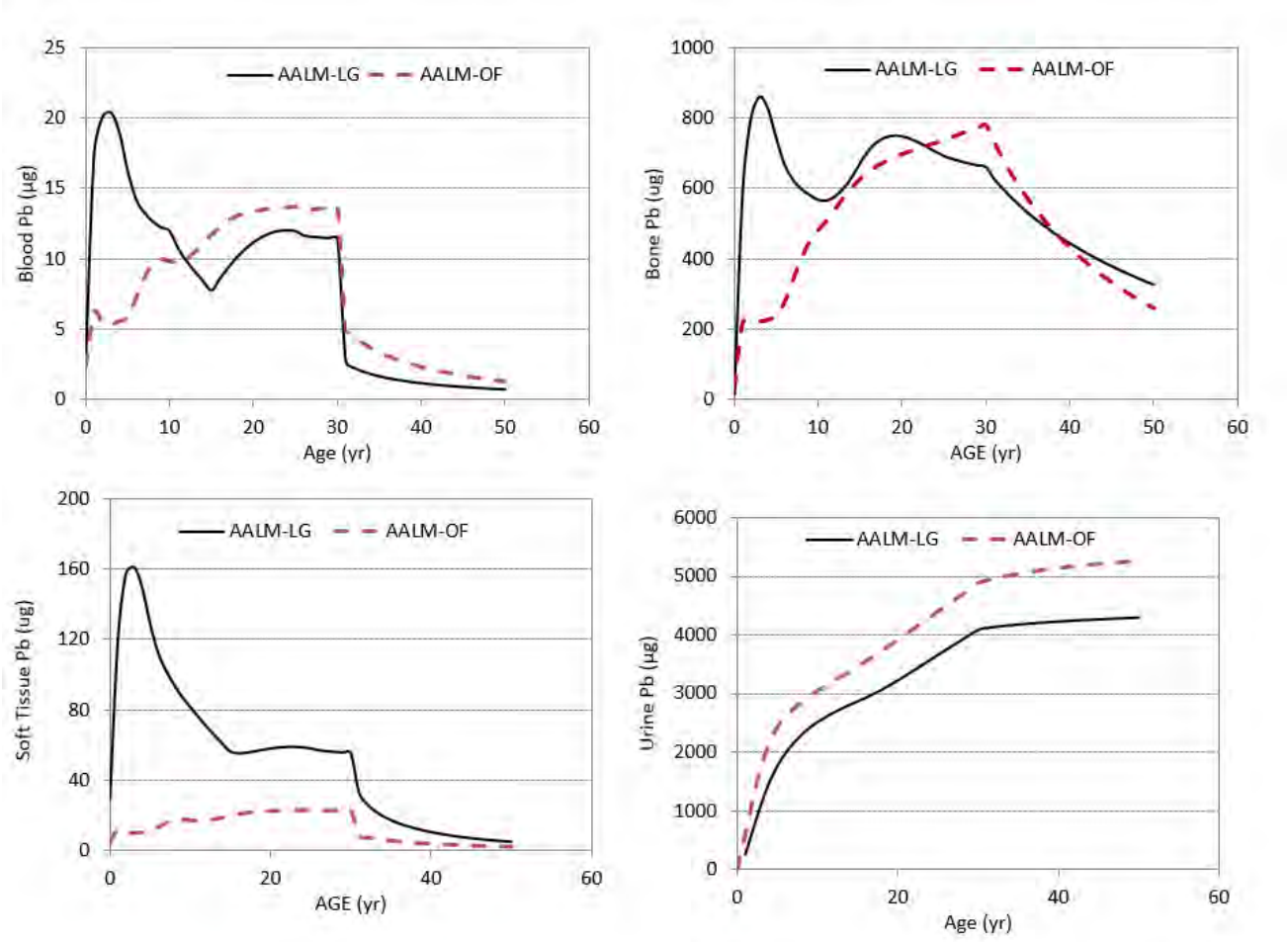

FIGURE 4-7. DIFFERENCES IN PB LEVELS PREDICTED FROM AALM-LG AND AALM-OF.

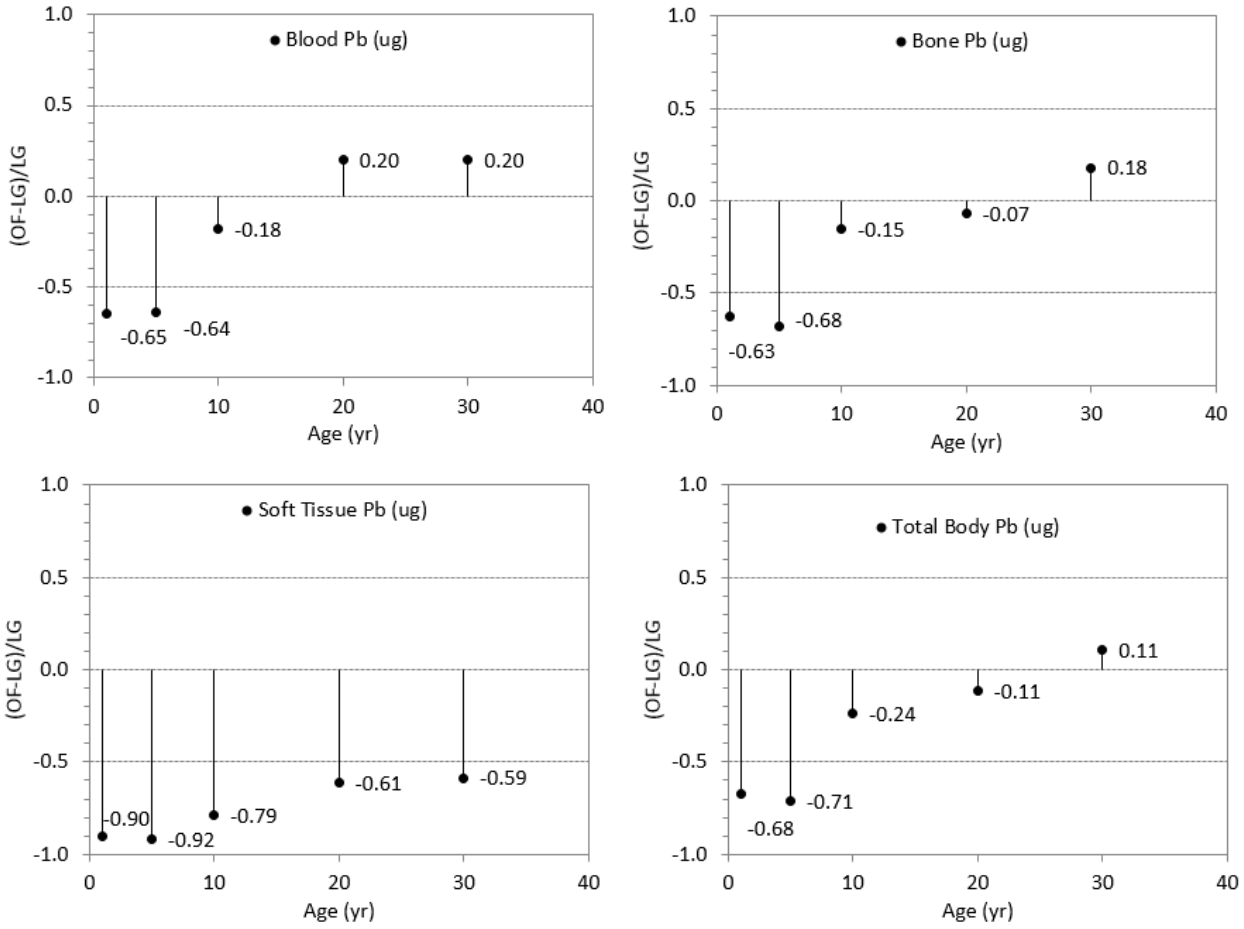

Differences are expressed relative to the prediction from AALM-LG.

FIGURE 4-8. COMPARISON OF CUMULATIVE URINARY AND FECAL PB EXCRETION (µG) LEVELS PREDICTED FROM AALM-OF AND AALM-LG FOR A CONSTANT INGESTION OF 5 µG PB/DAY FOR AGES 0 TO 30 YEARS.

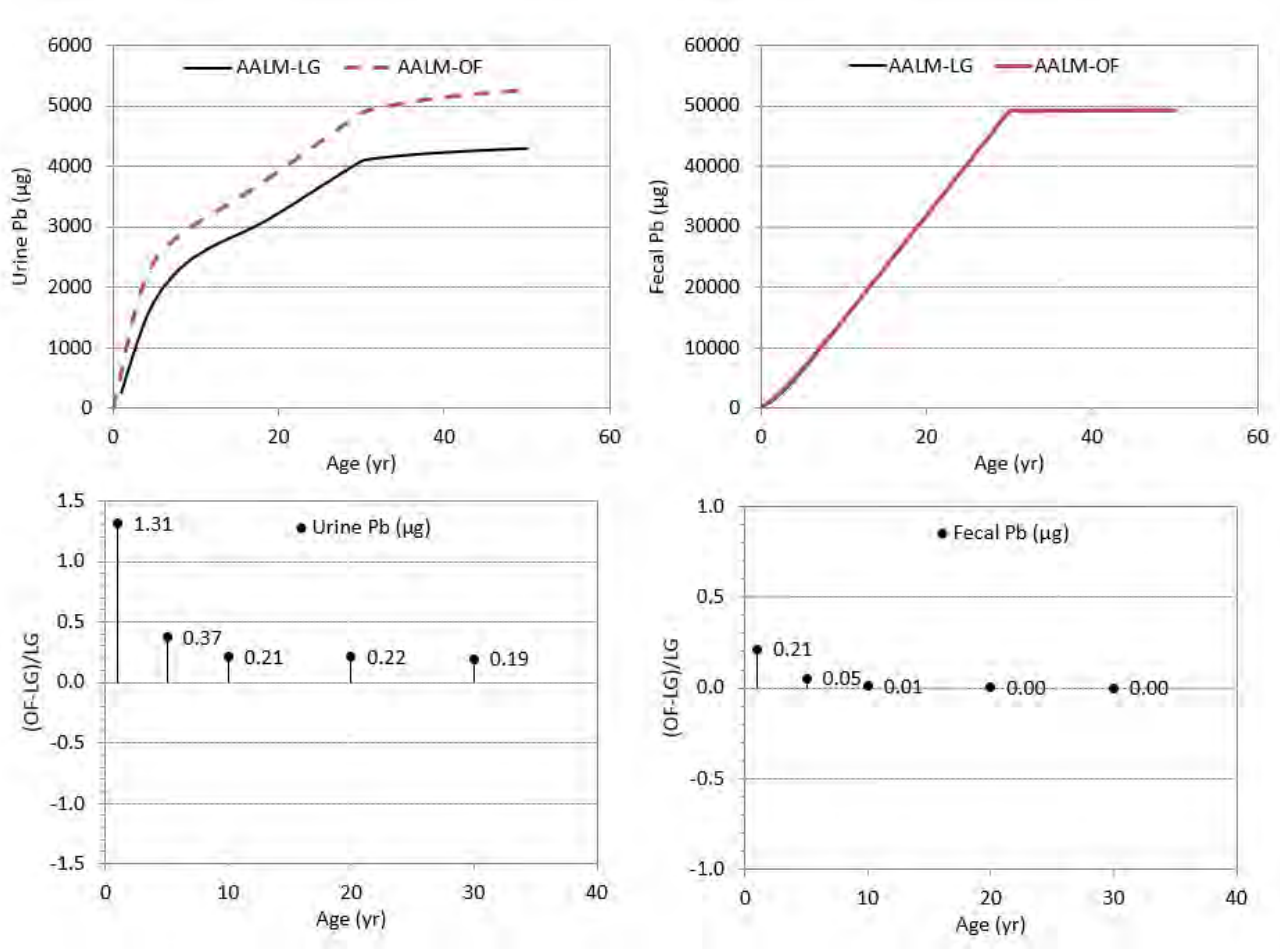

FIGURE 4-9. DECLINE IN PB LEVELS FOLLOWING CESSATION OF EXPOSURE PREDICTED FROM AALM-LG AND AALM-OF FOR AGES 5 AND 30 YEARS.

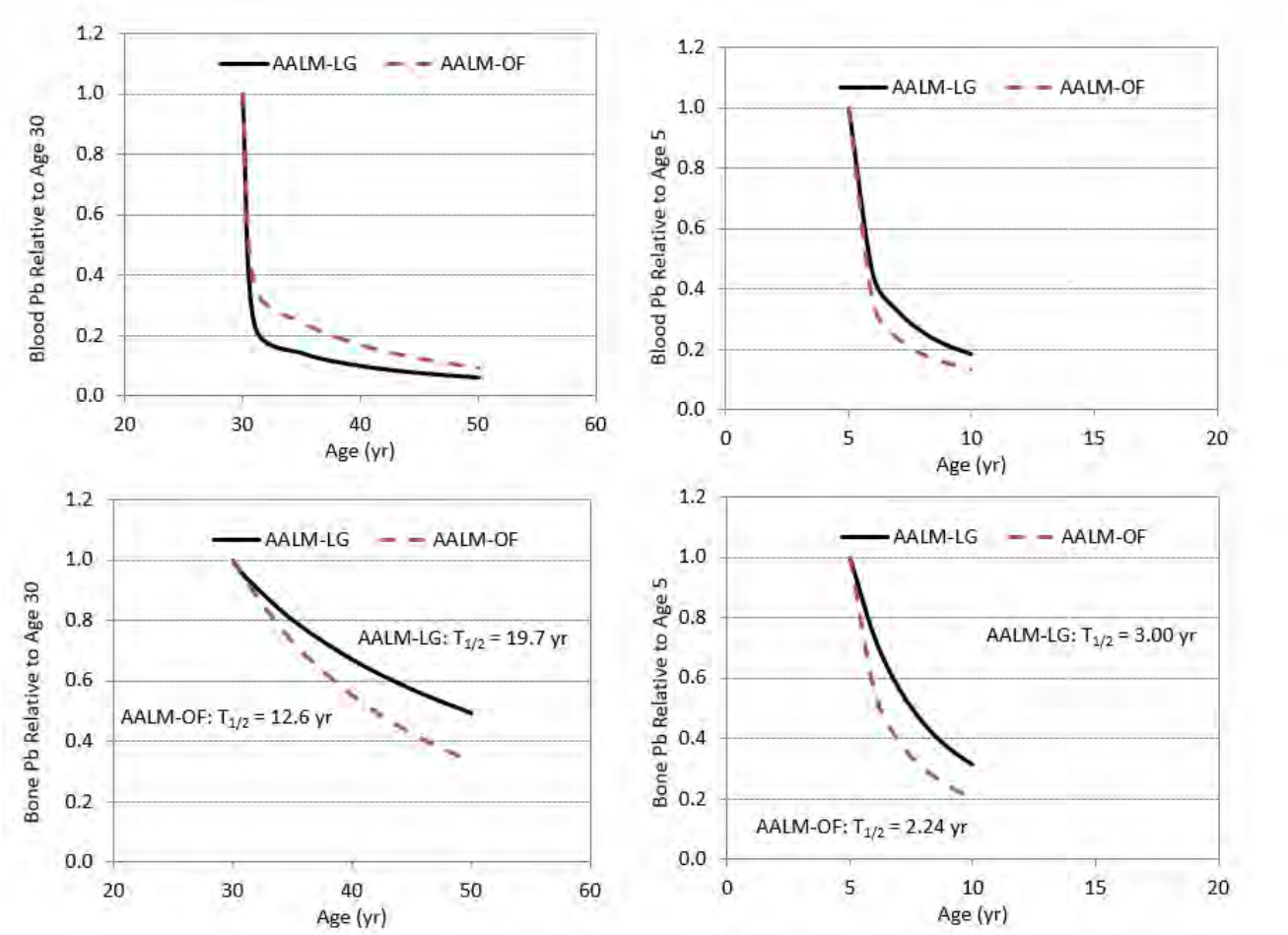

Half-times are based on applying a single exponential model to the predicted time series (i.e., $Pb_{t=i} = Pb_{t=0} \times e^{-kt}$). The decline in blood Pb has multiple rates. In adults, the half-time for the first 50 days following cessation of exposure is approximately 36 days in AALM-LG and 46 days in AALM-OF. The half-time for the period 5–20 years following cessation of exposure is 12.7 years in AALM-LG and 10.9 years in AALM-OF.

FIGURE 4-10. COMPARISON OF PB CONCENTRATIONS PREDICTED FROM AALM-LG AND AALM-OF FOR A CONSTANT INGESTION OF 5 µG PB/DAY FOR AGES 0 TO 30 YEARS.

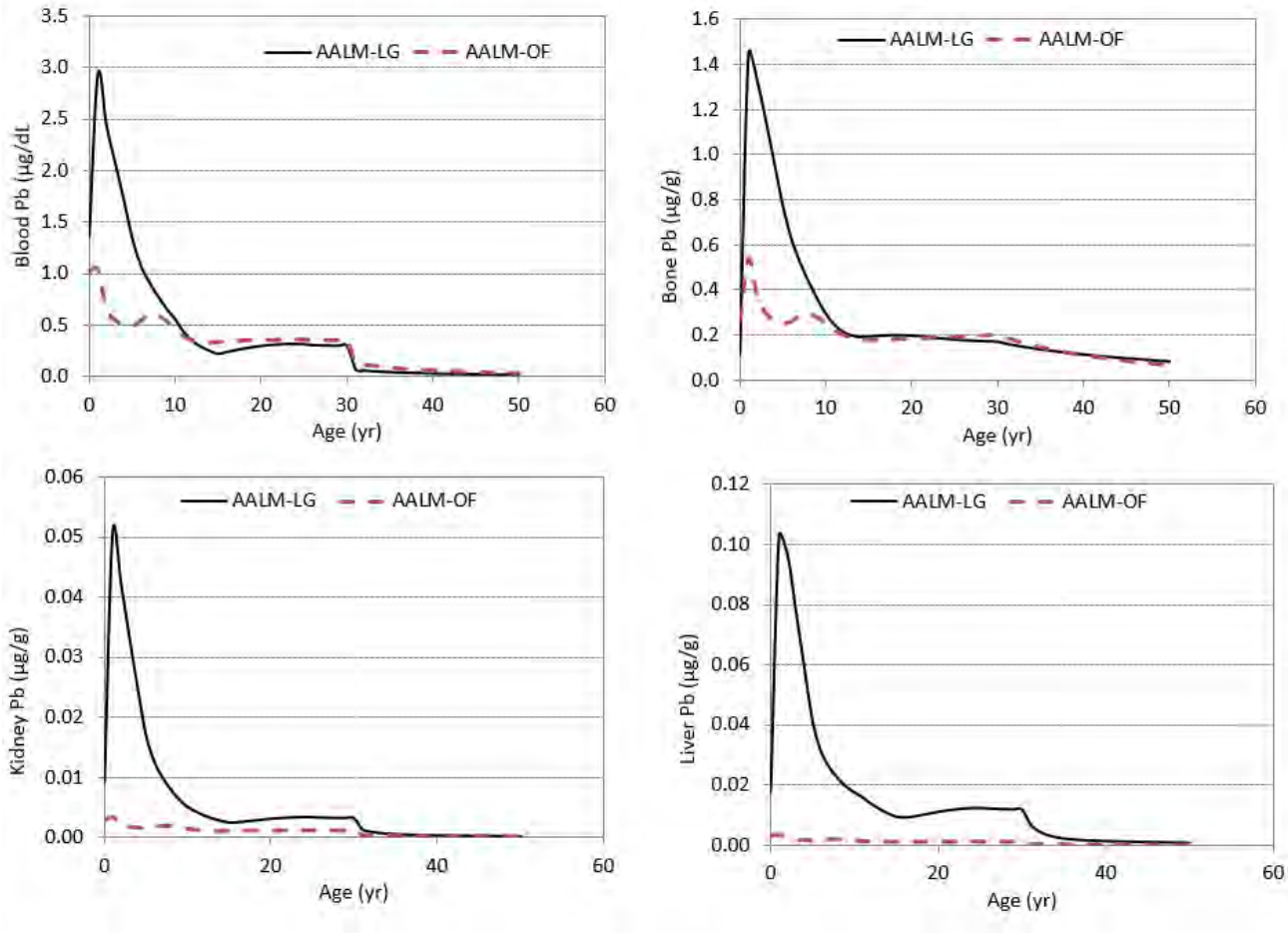

FIGURE 4-11. DOSE-RESPONSE RELATIONSHIP FOR PB LEVELS AT AGE 5 YEARS PREDICTED FROM AALM-LG AND AALM-OF.

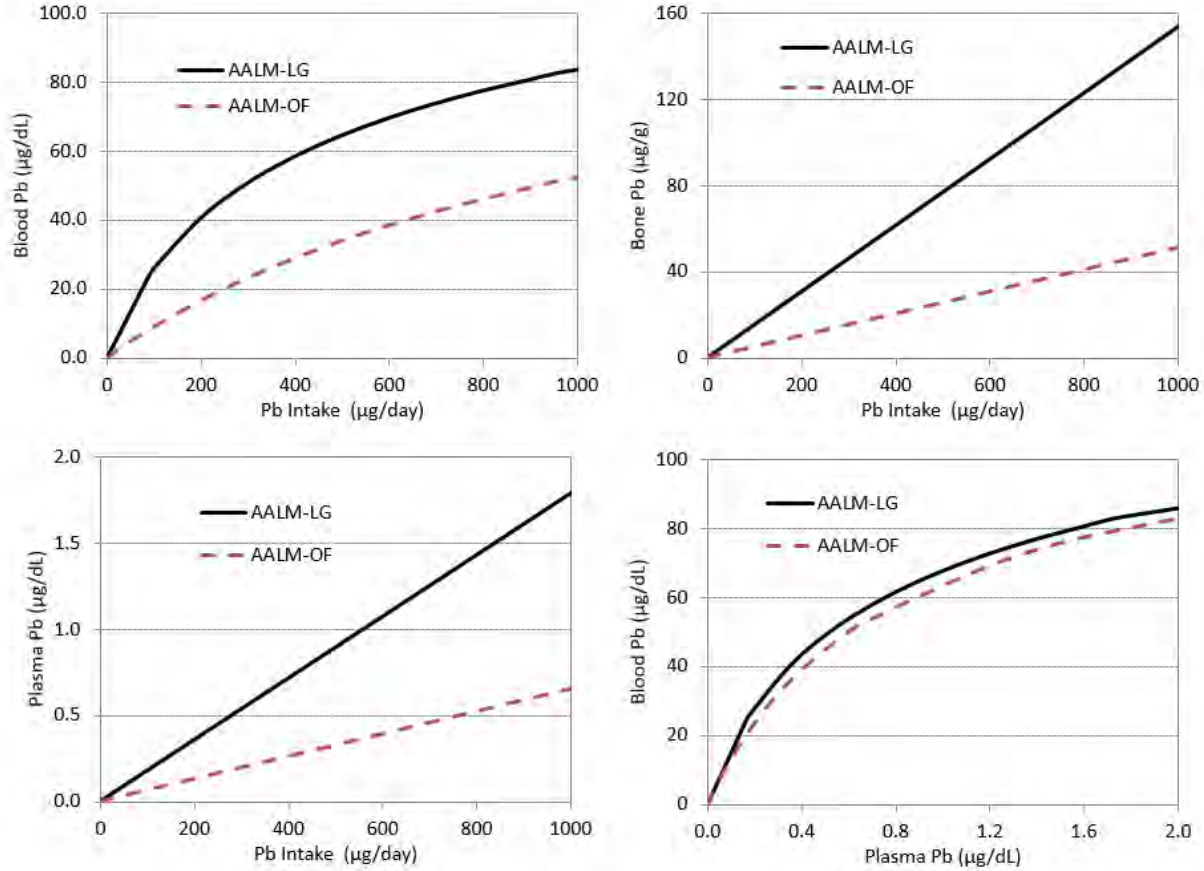

FIGURE 4-12. DOSE-RESPONSE RELATIONSHIP FOR PB LEVELS AT AGE 30 YEARS PREDICTED FROM AALM-LG AND AALM-OF.

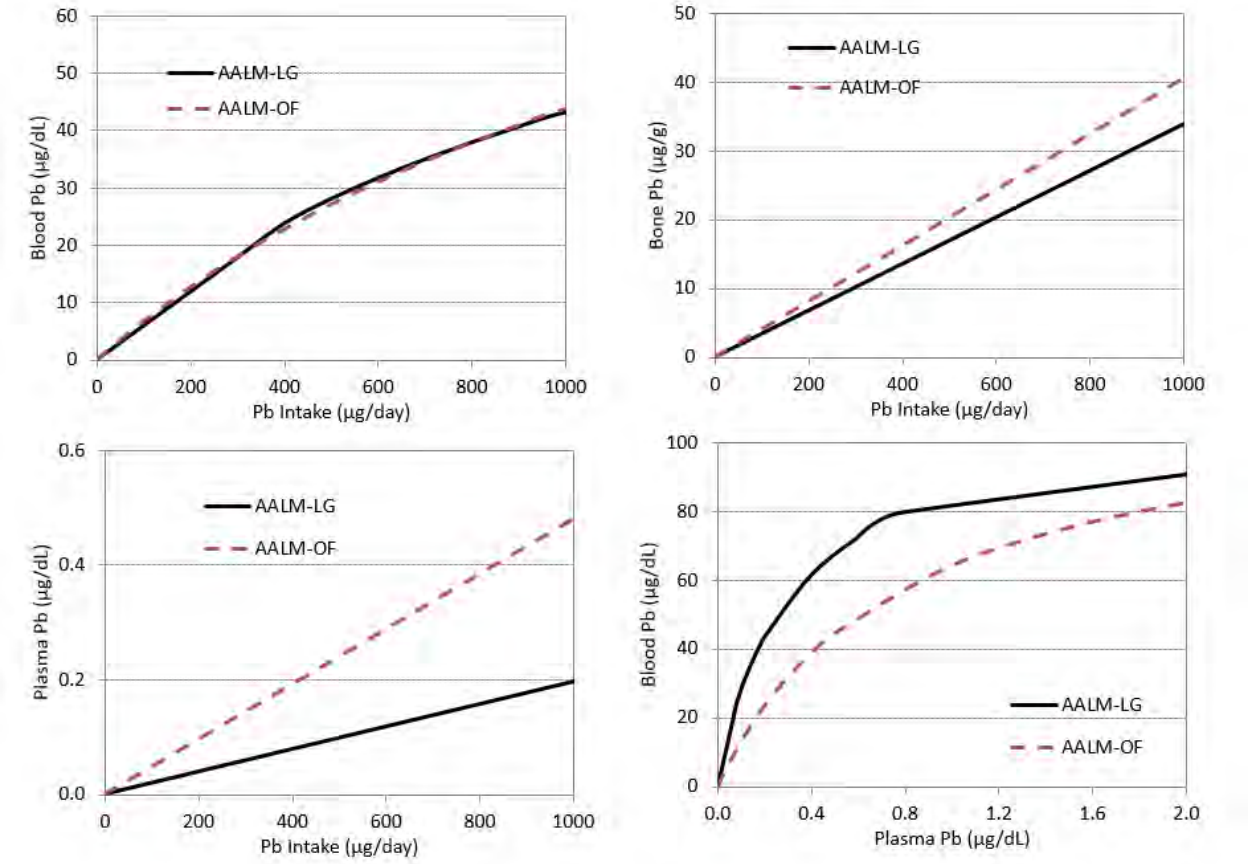

FIGURE 4-13. GASTROINTESTINAL ABSORPTION OF PB IN THE O'FLAHERTY MODEL (OF) AND LEGGETT MODEL (OF) AND AALM, OPTIMIZED TO (RYU ET AL., 1983).

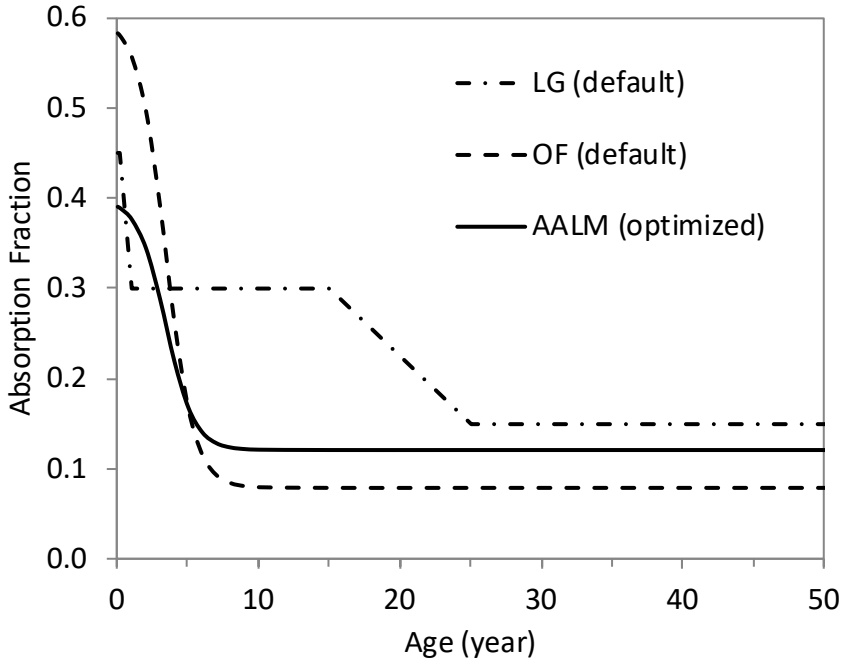

FIGURE 4-14. BODY AND TISSUE GROWTH IN AALM.

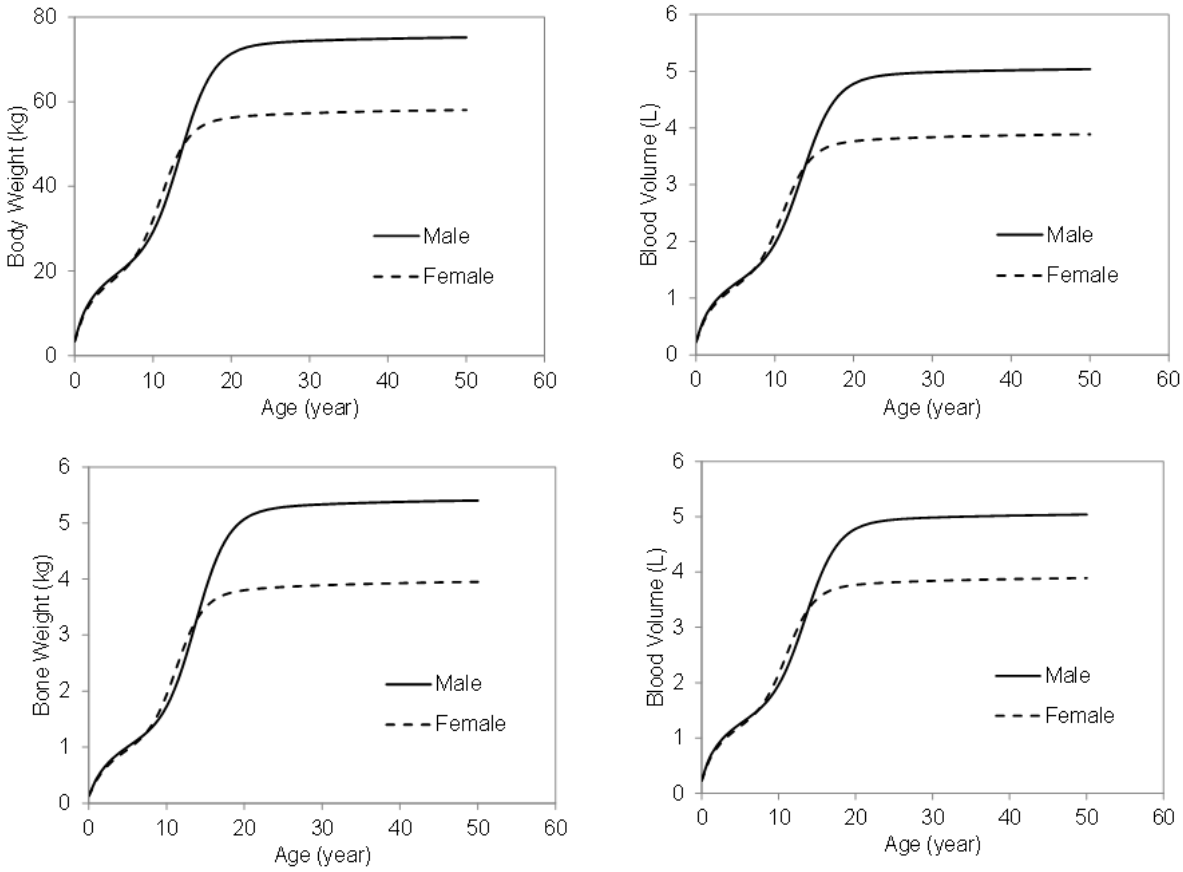

FIGURE 4-15. SIMULATION OF WHOLE BLOOD AND PLASMA PB IN ADULTS (SMITH ET AL., 2002; BERGDAHL ET AL., 1999; BERGDAHL ET AL., 1998; HERNANDEZ-AVILA ET AL., 1998; BERGDAHL ET AL., 1997; SCHUTZ ET AL., 1996).

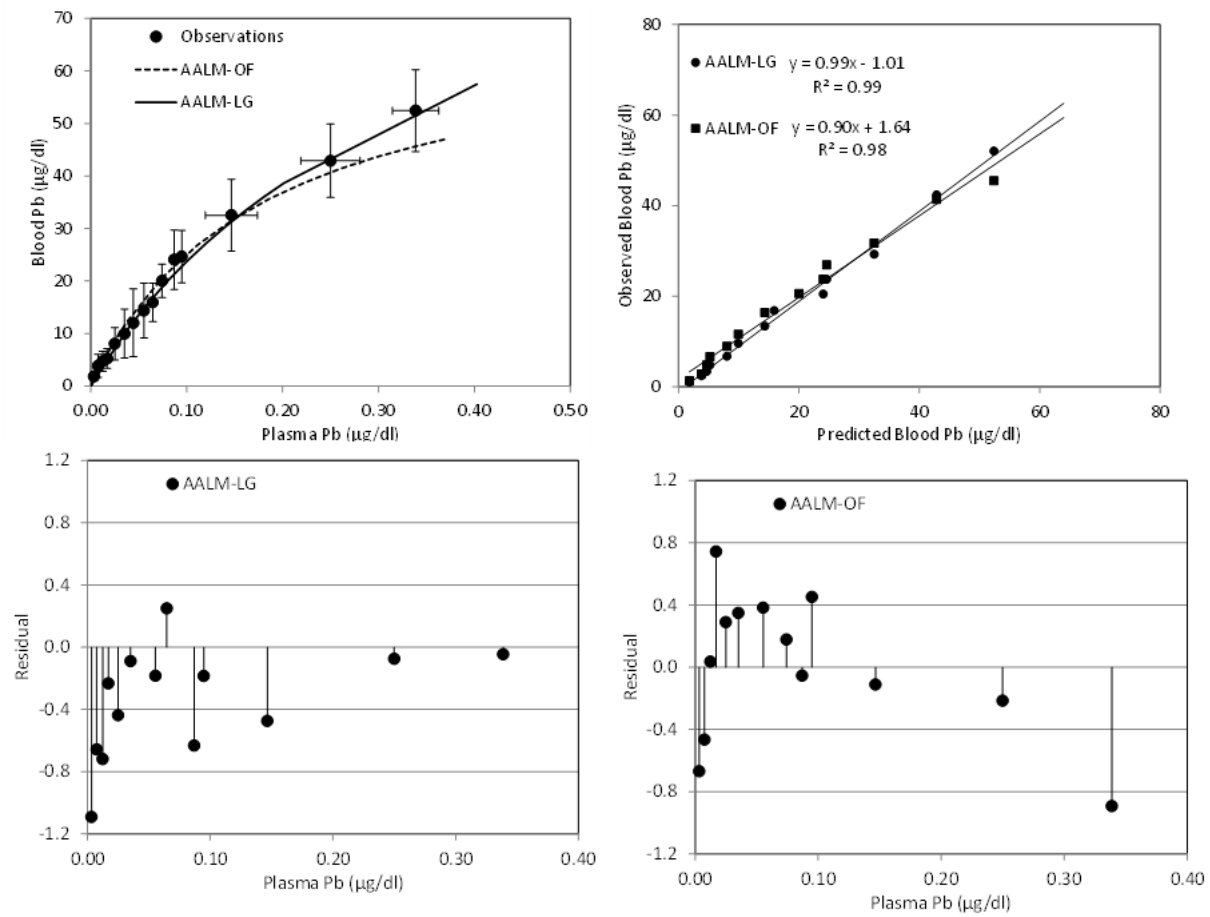

Combined data for individuals (N = 406) from all studies were quantized into ranges of plasma Pb; shown are mean and standard deviations for ranges. Upper right panel shows linear regression for predicted and observed blood Pb concentrations. Lower panels show residuals for predictions ([predicted-observed]/standard deviation).

FIGURE 4-16. SIMULATION OF PLASMA-TO-URINE CLEARANCE.

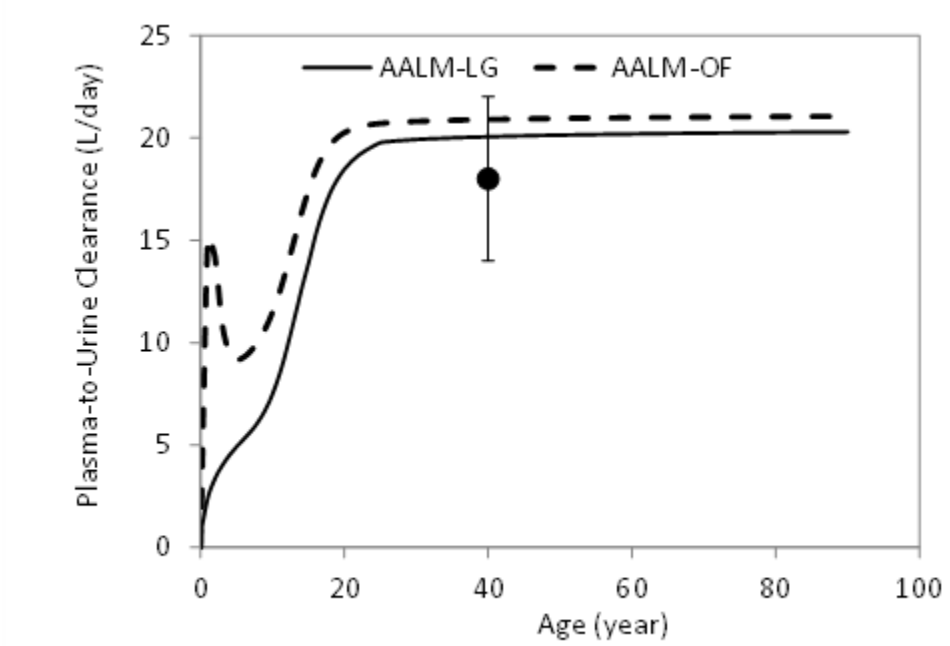

Data point is mean and standard deviation for four estimates based on 32 (normal) adults (Araki et al., 1986; Manton and Cook, 1984; Manton and Malloy, 1983; Chamberlain et al., 1978).

FIGURE 4-17. SIMULATION OF POST-MORTEM SOFT TISSUE/TIBIA PB RATIOS.

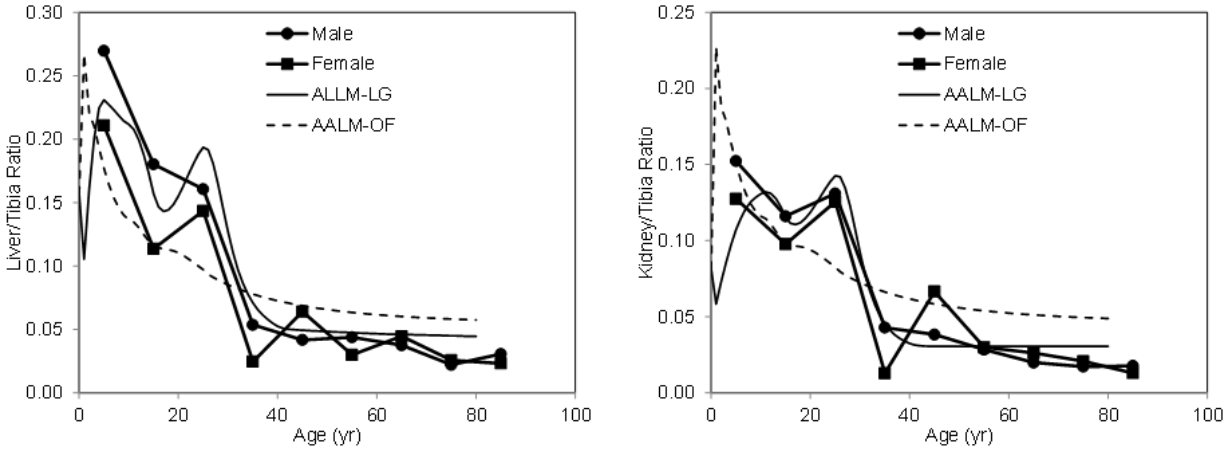

Shown are group means for kidney (n = 8) and for liver (n = 9), based on Barry (1975).

FIGURE 4-18. SIMULATION OF PLASMA PB/BONE PB RATIO IN ADULTS.

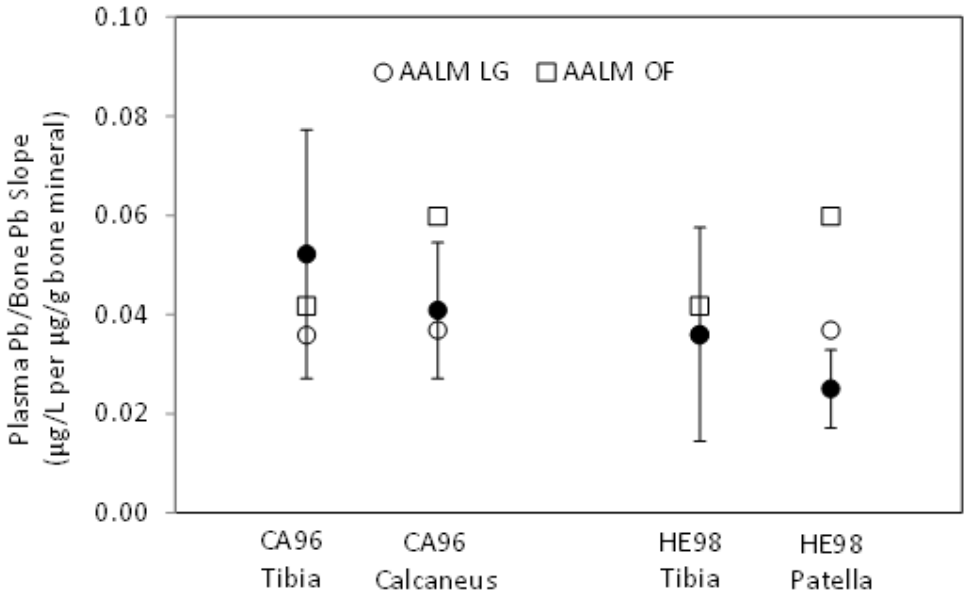

Observations are means and 95% CIs, based onCA96, Cake et al. (1996); and HE98, Hernandez-Avila et al. (1998).

FIGURE 4-19. SIMULATION OF ELIMINATION KINETICS OF PB FROM BLOOD (LEFT PANEL) AND BONE (RIGHT PANEL).

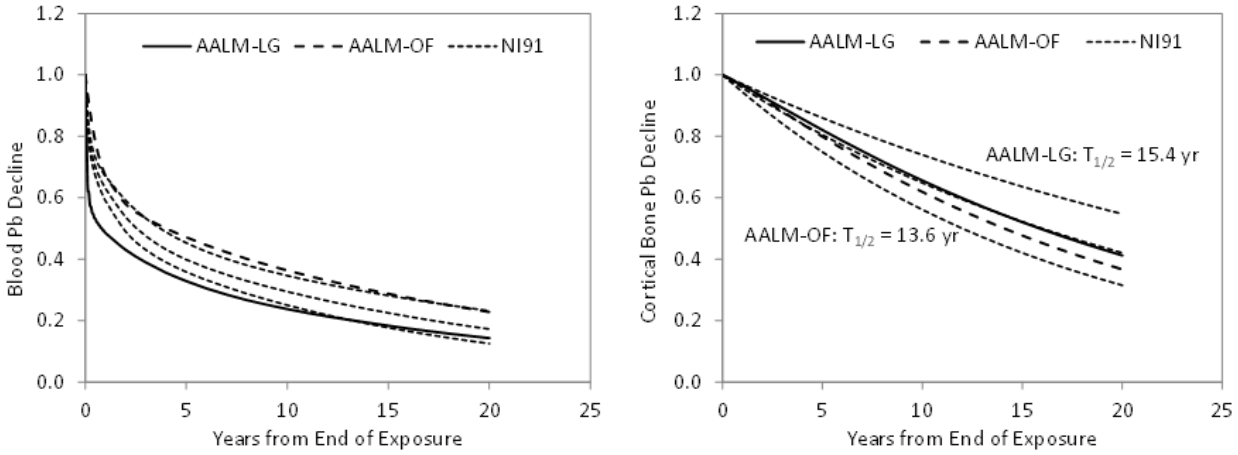

Dotted lines show the elimination from based on the median and upper and lower 95% confidence limits of the tri-exponential model retired Pb workers (n = 14, median age 60 years at time of retirement) reported in Nilsson et al. (1991).

FIGURE 4-20. COMPARISON OF OBSERVED AND PREDICTED BLOOD PB CONCENTRATIONS IN INDIVIDUALS WHO RECEIVED INGESTION DOSES OF [202PB]-NITRATE (RABINOWITZ ET AL., 1976).

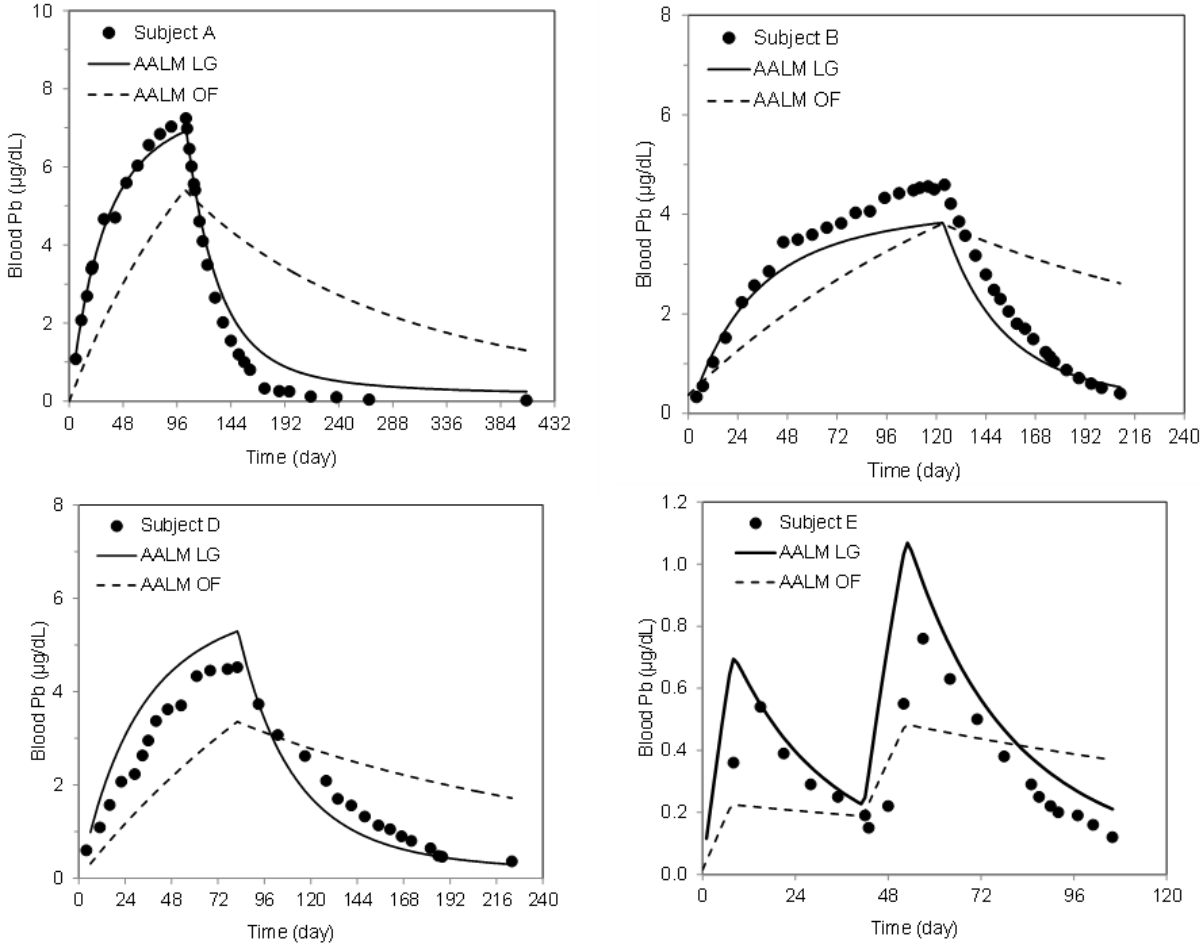

Subject A received 204 µg/day for 104 days, Subject B received 185 µg/day for 124 days, Subject D received 105 µg/day for 83 days, and Subject E received 99 µg/day for on days 1–8 and days 42–51. Estimated absorption fractions were 8.5% for Subject A, 6.5% for Subject B, 10.9% for Subject D and 9.1% for Subject E.

FIGURE 4-21. SIMULATION OF FORMULA-FED INFANTS FROM (RYU ET AL., 1983).

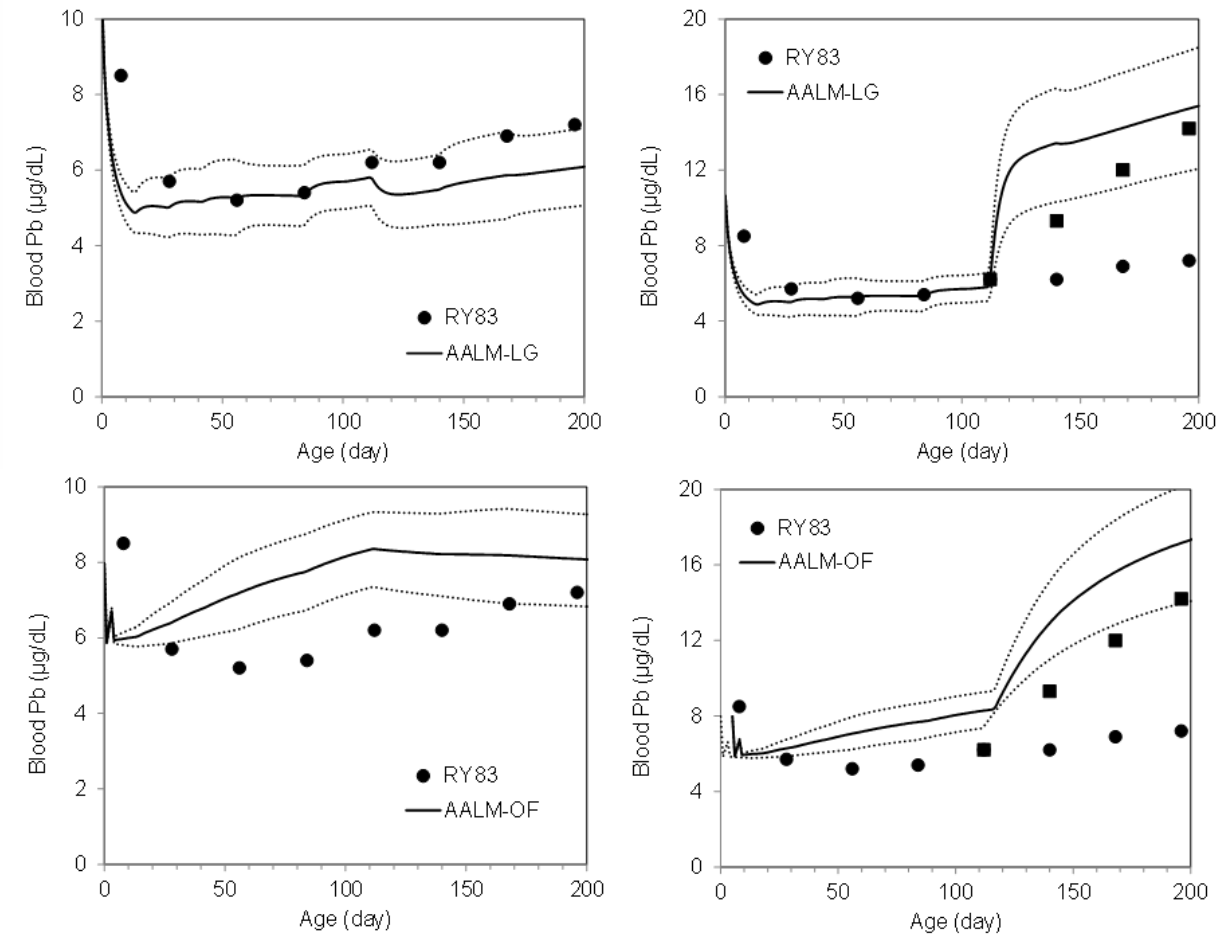

Data in left panels are from 25 infants fed formula from cartons (12–20 µg/day) from age 8–196 days. Data in right panels are show a subset (n = 7) that were switched to formula from cans at age 112 days (60–63 µg/day). Solid lines show simulations of the mean Pb intakes; dotted lines show simulations of ±1 SD of mean intakes.

FIGURE 4-22. SIMULATION OF FORMULA-FED INFANTS (N = 131, AGE 91 DAYS) FROM (SHERLOCK AND QUINN, 1986).

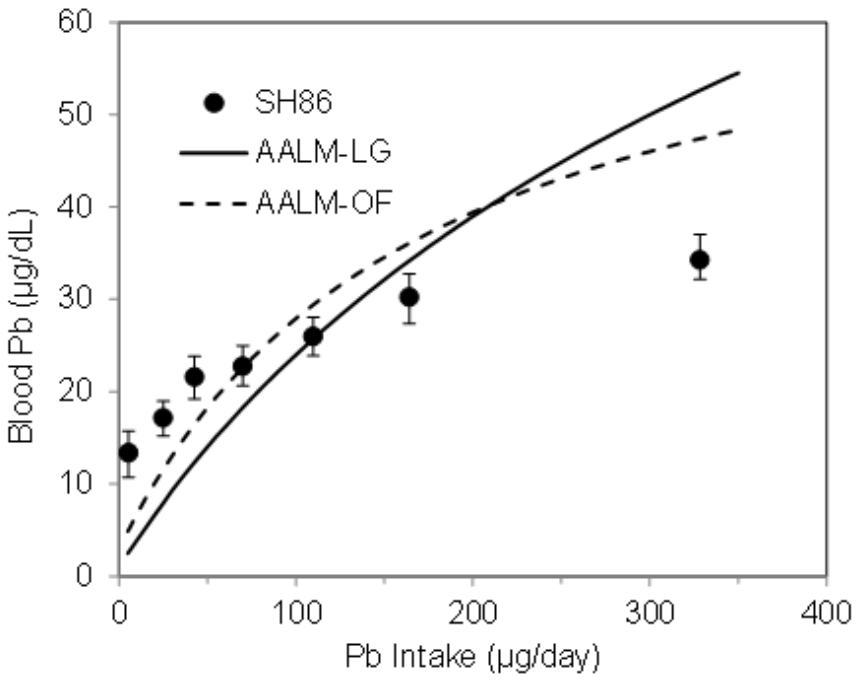

Blood Pb were measured and Pb intakes were estimated from duplicate diets assessed at age 91 days.

FIGURE 4-23. COMPARISON OF INITIAL AND OPTIMIZED AALM-LG AND AALM-OF MODELS FOR CONTINUOUS PB INTAKE OF 5 µG/DAY.

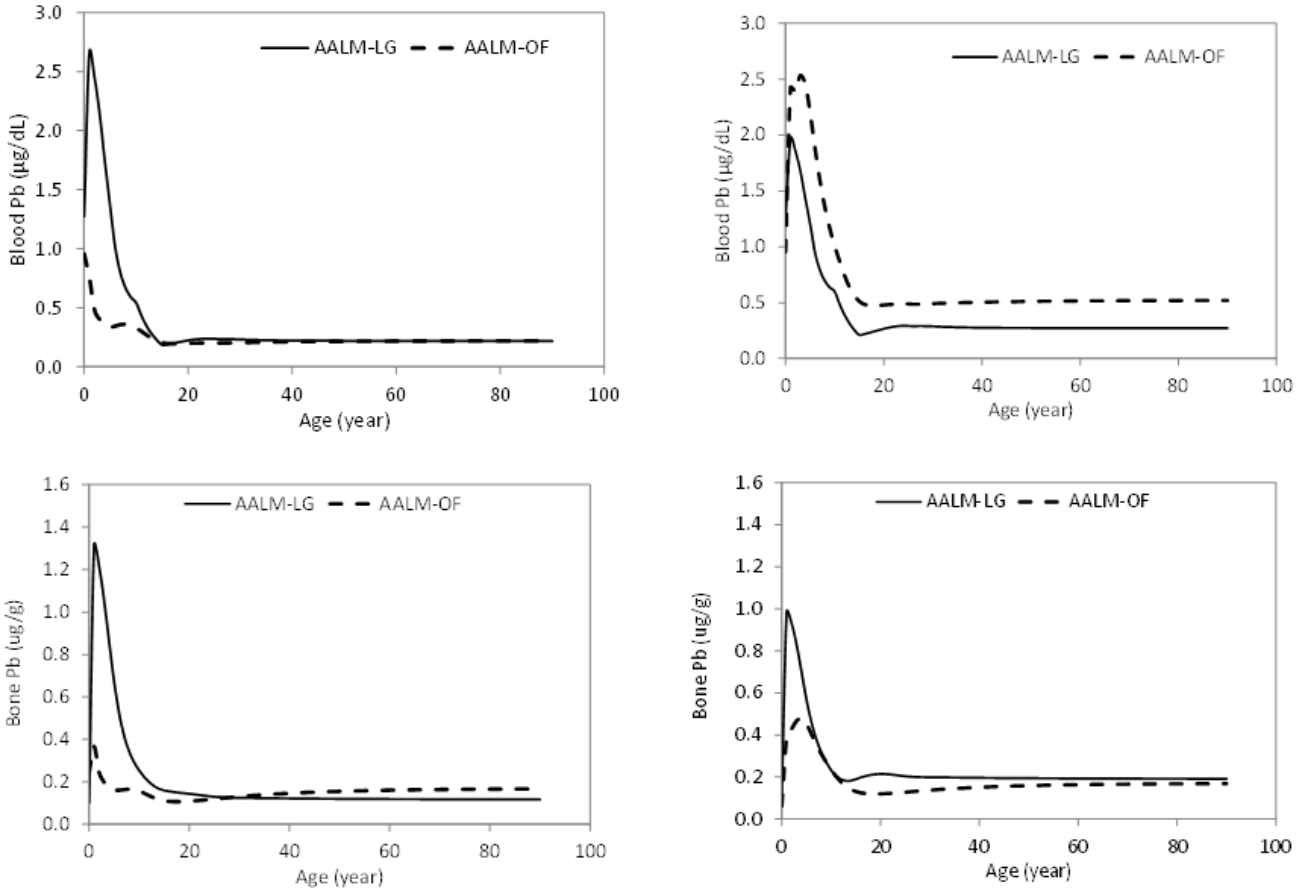

Right panels show optimized models.

FIGURE 4-24. COMPARISON OF INITIAL AND OPTIMIZED AALM-LG AND AALM-OF MODELS FOR CONTINUOUS PB INTAKE OF 5 µG/DAY.

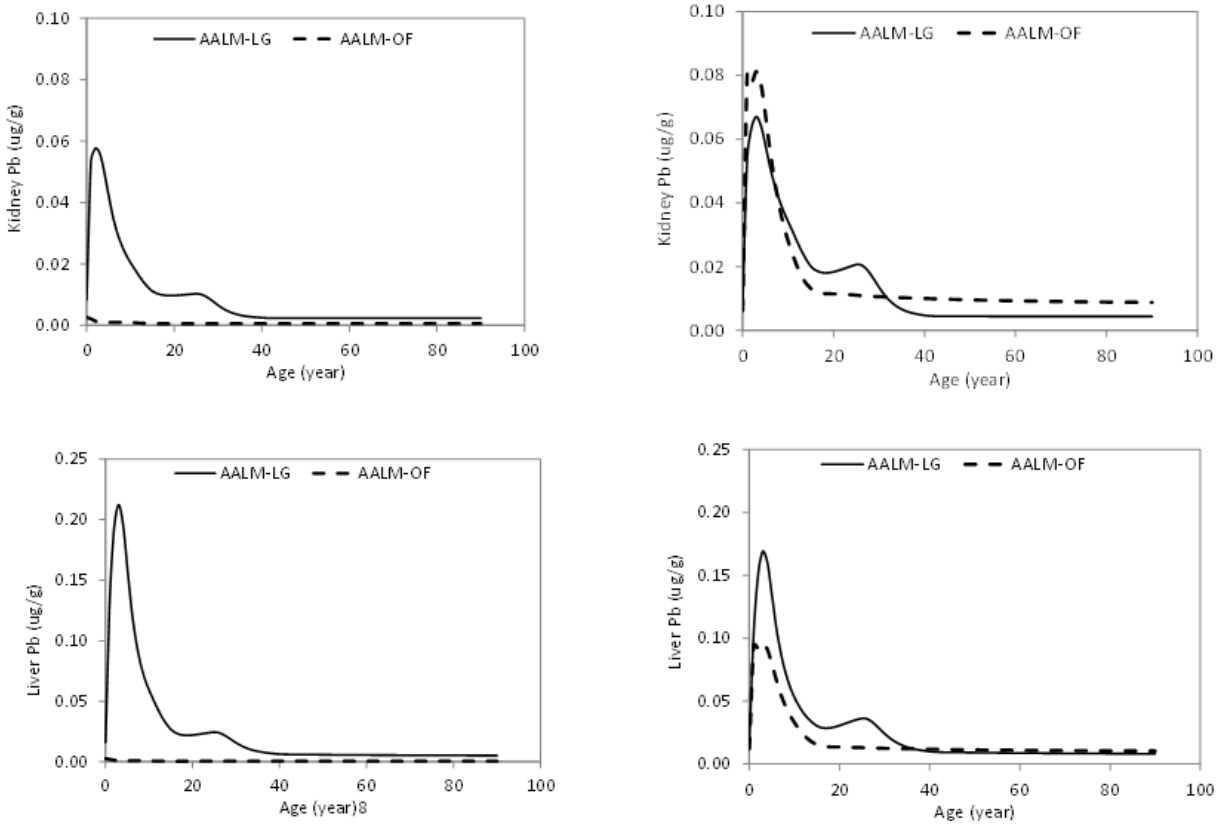

Right panels show optimized models.

FIGURE 4-25. COMPARISON OF BLOOD PB PREDICTIONS OF AALM AND IEUBK MODEL.

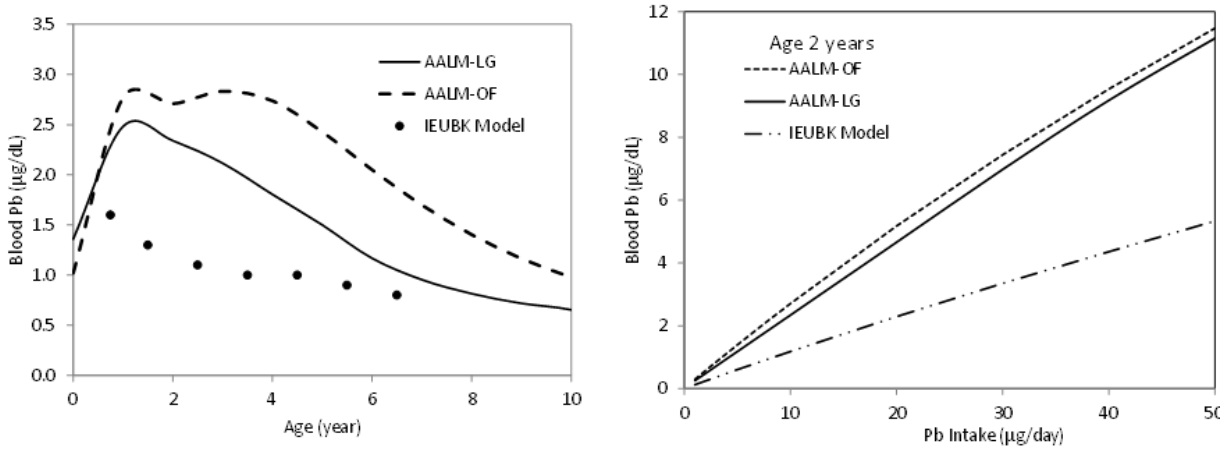

Left panel shows simulations of continuous intake of 10 µg Pb/day in dust. Right panel shows relationship between dust Pb intake and blood Pb concentration at 2 years of age. In both models, the RBA for Pb in dust was assumed to be 60%. This corresponds to an absolute bioavailability of approximately 20% at age 2 years in the AALM and 30% in the IEUBK model.

FIGURE 4-26. COMPARISON OF BLOOD PB PREDICTIONS OF AALM AND IEUBK MODEL AFTER ADJUSTMENT OF RED BLOOD CELL PARAMETERS (RRBC IN AALM-LG, KBIND IN AALM-OF).

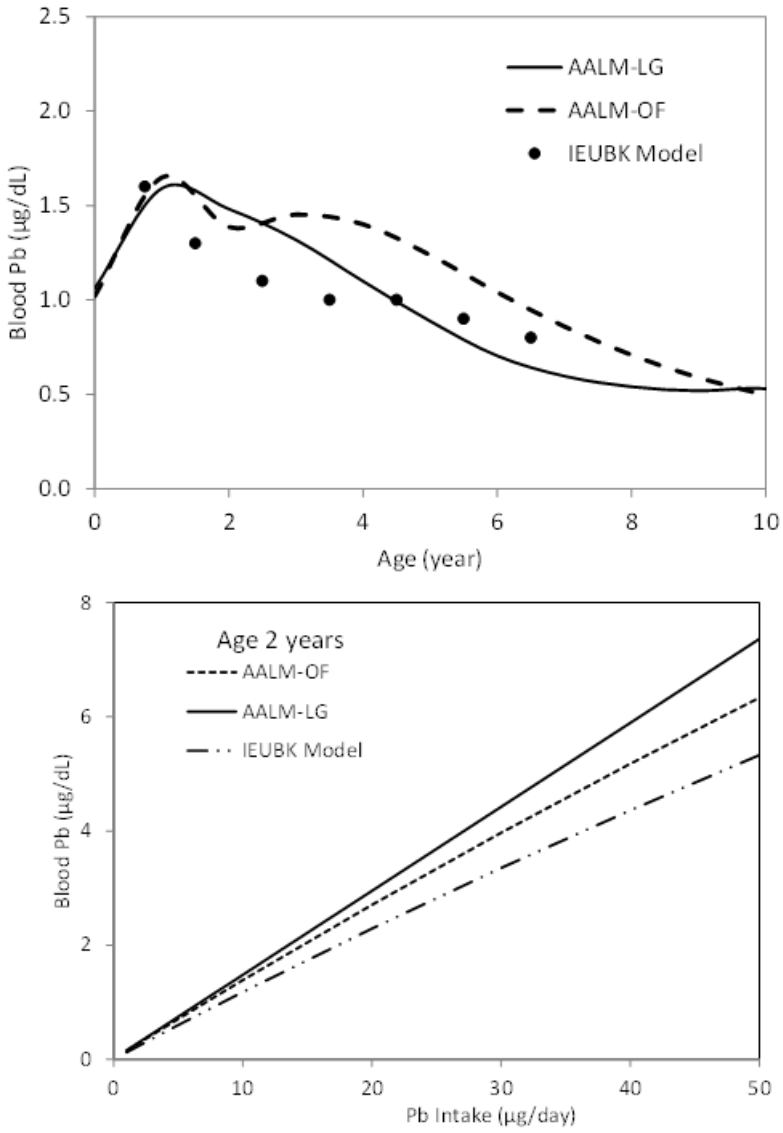

Upper panel shows simulations of continuous intake of 10 µg Pb/day in dust. Lower panel shows relationship between dust Pb intake and blood Pb concentration at 2 years of age. In both models, the RBA for Pb in dust was assumed to be 60%. This corresponds to an absolute bioavailability of approximately 20% at age 2 years in the AALM and 30% in the IEUBK model.

FIGURE 4-27. SIMULATION OF FORMULA-FED INFANTS FROM (RYU ET AL., 1983) AFTER ADJUSTMENT OF RED BLOOD CELL (RRBC IN AALM-LG, KBIND IN AALM-OF).

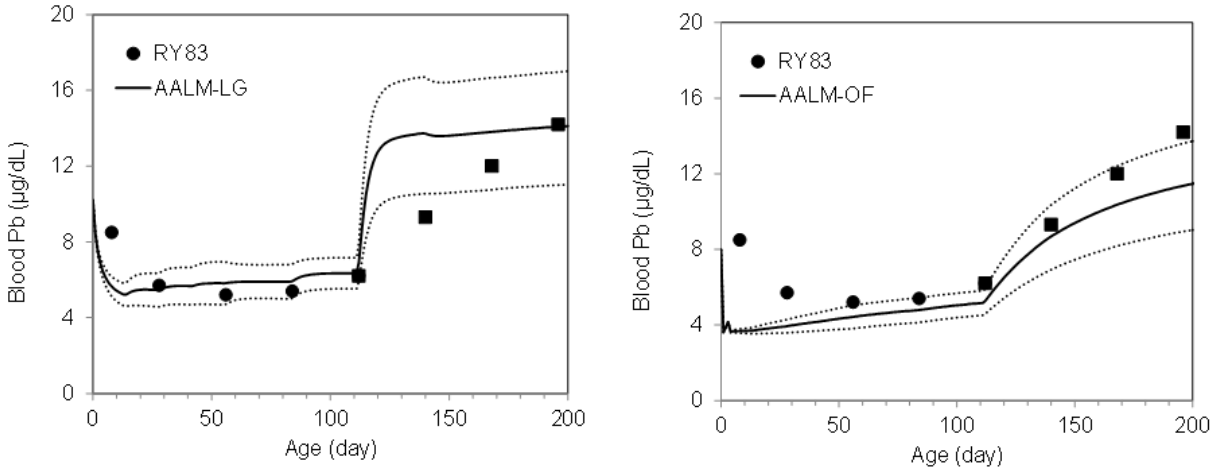

Data in left panels are from 25 infants fed formula from cartons (12–20 µg/day) from age 8–196 days (closed circles) and then a subset (n = 7) that were switched to formula from cans at age 112 days (60–63 µg/day, closed squares). Solid lines show simulations of the mean Pb intakes; dotted lines show simulations of ±1 SD of mean intakes.

FIGURE 4-28. SIMULATION OF FORMULA-FED INFANTS (N = 131, AGE 91 DAYS) FROM (SHERLOCK AND QUINN, 1986) AFTER ADJUSTMENT OF RED BLOOD CELL (RRBC IN AALM-LG, KBIND IN AALM-OF).

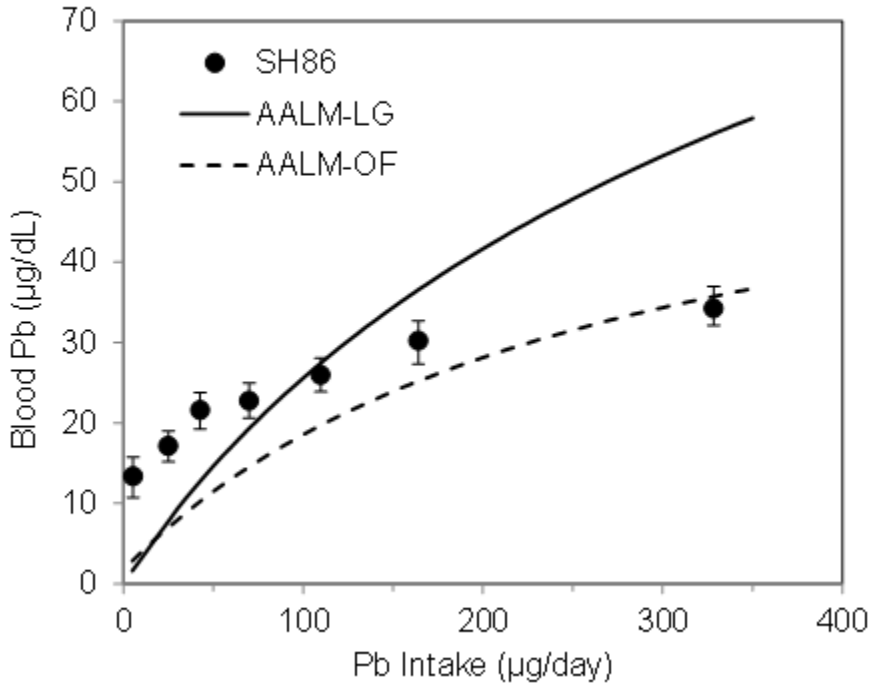

Blood Pb were measured and Pb intakes were estimated from duplicate diets assessed at age 91 days.

5. REFERENCES

Alexander, FW; Clayton, BE; Delves, HT. (1974). Mineral and trace-metal balances in children receiving normal and synthetic diets. Q J Med 43: 89-111.

Araki, S; Aono, H; Yokoyama, K; Murata, K. (1986). Filterable plasma concentration, glomerular filtration, tubular balance, and renal clearance of heavy metals and organic substances in metal workers. Arch Environ Occup Health 41: 216-221. http://dx.doi.org/10.1080/00039896.1986.9938336

Barry, PSI. (1975). A comparison of concentrations of lead in human tissues. Occup Environ Med 32: 119-139.

Barry, PSI. (1981). Concentrations of lead in the tissues of children. Occup Environ Med 38: 61-71.

Bergdahl, IA; Schutz, A; Gerhardsson, L; Jensen, A; Skerfving, S. (1997). Lead concentrations in human plasma, urine and whole blood. Scand J Work Environ Health 23: 359-363.

Bergdahl, IA; Sheveleva, M; Schutz, A; Artamonova, VG; Skerfving, S. (1998). Plasma and blood lead in humans: Capacity-limited binding to delta-aminolevulinic acid dehydratase and other lead-binding components. Toxicol Sci 46: 247-253. http://dx.doi.org/10.1093/toxsci/46.2.247

Bergdahl, IA; Vahter, M; Counter, SA; Schutz, A; Buchanan, LH; Ortega, F; Laurell, G; Skerfving, S. (1999). Lead in plasma and whole blood from lead-exposed children. Environ Res 80: 25-33. http://dx.doi.org/10.1006/enrs.1998.3880

Booker, DV; Chamberlain, AC; Newton, D; Stott, ANB. (1969). Uptake of radioactive lead following inhalation and injection. Br J Radiol 42: 457-466. http://dx.doi.org/10.1259/0007-1285-42-498-457

Bornschein, RL; Succop, P; Dietrich, KN; Clark, CS; S, QH; Hammond, PB. (1985). The influence of social and environmental factors on dust lead, hand lead, and blood lead levels in young children. Environ Res 38: 108-118. http://dx.doi.org/10.1016/0013-9351(85)90076-3

Cake, KM; Bowins, RJ; Vaillancourt, C; Gordon, CL; McNutt, RH; Laporte, R; Webber, CE; Chettle, DR. (1996). Partition of circulating lead between serum and red cells is different for internal and external sources of lead. Am J Ind Med 29: 440-445. http://dx.doi.org/10.1002/(SICI)1097-0274(199605)29:5<440::AID-AJIM2>3.0.CO;2-Q

CalEPA (California Environmental Protection Agency). (2013). Estimating workplace air and worker blood lead concentration using an updated Physiologically-based Pharmacokinetics (PBPK) model. https://oehha.ca.gov/air/document/estimating-workplace-air-and-worker-blood-lead-concentration-using-updated-pbpk-model

CDC (Centers for Disease Control and Prevention). (2013). Fourth national report on human exposure to environmental chemicals, updated tables, September 2013. (CS244702-A). Atlanta, GA. http://www.cdc.gov/exposurereport/pdf/FourthReport_UpdatedTables_Sep2013.pdf

Chamberlain, AC; Heard, MJ; Little, P; Newton, D; Wells, AC; Wiffin, RD. (1978). Investigations into lead from motor vehicles. (AERE-R9198). Berkshire, England: Transportation and Road Research Laboratory.

Cohen, N; Eisenbud, M; Wrenn, ME. (1970). Radioactivity studies. Volume I. The retention and distribution of 210Pb in the adult baboon. Annual progress report, September 1, 1969-August 31, 1970. (AT(30-1)-3086). New York: New York University Medical Center.

Dewoskin, RS; Thompson, CM. (2008). Renal clearance parameters for PBPK model analysis of early lifestage differences in the disposition of environmental toxicants [Review]. Regul Toxicol Pharmacol 51: 66-86. http://dx.doi.org/10.1016/j.yrtph.2008.02.005

Diamond, GL. (1992). Review of default value for lead plasma-to-urine transfer coefficient (TPLUR) in the U.S. EPA uptake/biokinetic model. (SRC TR-92-135). Syracuse, NY: Syracuse Research Corporation.

Dixon, SL; Gaitens, JM; Jacobs, DE; Strauss, W; Nagaraja, J; Pivetz, T; Wilson, JW; Ashley, PJ. (2009). Exposure of US children to residential dust lead, 1999-2004: II. The contribution of lead-

contaminated dust to children's blood lead levels. Environ Health Perspect 117: 468-474. http://dx.doi.org/10.1289/ehp.11918

Gear, CW. (1971). The automatic integration of ordinary differential equations [Magazine]. Association for Computing Machinery Communications, 14, 176-179.

Gerhardsson, L; Englyst, V; Lundstrom, NG; Nordberg, G; Sandberg, S; Steinvall, F. (1995). Lead in tissues of deceased lead smelter worker. J Trace Elem Med Biol 9: 136-143. http://dx.doi.org/10.1016/S0946-672X(11)80037-4

Gross, SB; Pfitzer, EA; Yeager, DW; Kehoe, RA. (1975). Lead in human tissues. Toxicol Appl Pharmacol 32: 638-651. http://dx.doi.org/10.1016/0041-008X(75)90127-1

Harrison, GE; Carr, TEF; Sutton, A. (1967). Distribution of radioactive calcium, strontium, barium and radium following intravenous injection into a healthy man. Int J Radiat Biol 13: 235-247. http://dx.doi.org/10.1080/09553006814550161

Hart, HE; Spencer, H. (1976). Vascular and extravascular calcium interchange in man determined with radioactive calcium. Radiat Res 67: 149-161. http://dx.doi.org/10.2307/3574505

Hattis, D. (1981). Dynamics of medical removal protection for lead--A reappraisal. (CPA-81-25). Cambridge, MA: Massachusetts Institute of Technology, Center for Policy Alternatives.

Heard, MJ; Chamberlain, AC. (1982). Effect of minerals and food on uptake of lead from the gastrointestinal tract in humans. Hum Exp Toxicol 1: 411-415. http://dx.doi.org/10.1177/096032718200100407

Heard, MJ; Chamberlain, AC. (1984). Uptake of Pb by human skeleton and comparative metabolism of Pb and alkaline earth elements. Health Phys 47: 857-865.

Hernandez-Avila, M; Smith, D; Meneses, F; Sanin, LH; Hu, H. (1998). The influence of bone and blood lead on plasma lead levels in environmentally exposed adults. Environ Health Perspect 106: 473-477. http://dx.doi.org/10.1289/ehp.98106473

Hogan, K; Marcus, A; Smith, R; White, P. (1998). Integrated exposure uptake biokinetic model for lead in children: empirical comparisons with epidemiologic data. Environ Health Perspect 106: 1557-1567. http://dx.doi.org/10.1289/ehp.98106s61557

Hu, H; Shih, R; Rothenberg, S; Schwartz, BS. (2007). The epidemiology of lead toxicity in adults: Measuring dose and consideration of other methodologic issues [Review]. Environ Health Perspect 115: 455-462. http://dx.doi.org/10.1289/ehp.9783

Hursh, JB; Mercer, TT. (1970). Measurement of 212Pb loss rate from human lungs. J Appl Physiol (1985) 28: 268-274. http://dx.doi.org/10.1152/jappl.1970.28.3.268

Hursh, JB; Schraub, A; Sattler, EL; Hofmann, HP. (1969). Fate of 212Pb inhaled by human subjects. Health Phys 16: 257-267.

Hursh, JB; Suomela, J. (1968). Absorption of 212Pb from the gastrointestinal tract of man. Acta Radiol 7: 108-120. http://dx.doi.org/10.3109/02841866809133184

ICRP (International Commission on Radiological Protection). (1981). Report of the task group on reference man: A report prepared by a task group of committee 2 of the International Commission on Radiological Protection. New York, NY: Pergamon Press. http://dx.doi.org/10.1016/S0074-2740(75)80015-8

ICRP (International Commission on Radiological Protection). (1993). Appendix A: Age-specific biokinetic models for the alkaline earth elements and lead. Ann ICRP 23(3-4): 95-120. http://dx.doi.org/10.1016/0146-6453(93)90031-3

ICRP (International Commission on Radiological Protection). (1994). Human respiratory tract model for radiological protection: A report of a task group of the International Commission on Radiological Protection. ICRP Publication 66. New York, NY: Pergamon Press.

ICRP (International Commission on Radiological Protection). (2002). Basic anatomical and physiological data for use in radiological protection: Reference values (pp. 1-277). (ISSN 0146-6453

EISSN 1872-969X

ICRP Publication 89). New York, NY: Pergamon Press. http://dx.doi.org/10.1016/S0146-6453(03)00002-2

James, HM; Hilburn, ME; Blair, JA. (1985). Effects of meals and meal times on uptake of lead from the gastrointestinal tract of humans. Hum Exp Toxicol 4: 401-407. http://dx.doi.org/10.1177/096032718500400406

Lanphear, BP; Matte, TD; Rogers, J; Clickner, RP; Dietz, B; Bornschein, RL; Succop, P; Mahaffey, KR; Dixon, S; Galke, W; Rabinowitz, M; Farfel, M; Rohde, C; Schwartz, J; Ashley, P; Jacobs, DE. (1998). The contribution of lead-contaminated house dust and residential soil to children's blood lead levels: A pooled analysis of 12 epidemiologic studies. Environ Res 79: 51-68. http://dx.doi.org/10.1006/enrs.1998.3859

Lanphear, BP; Roghmann, KJ. (1997). Pathways of lead exposure in urban children. Environ Res 74: 67-73.

Leggett, RW. (1985). A model of the retention, translocation and excretion of systemic public health. Health Phys 49: 1115-1137.

Leggett, RW. (1992a). A generic age-specific biokinetic model for calcium-like elements. Radiat Prot Dosimetry 41: 183-198.

Leggett, RW. (1992b). A retention-excretion model for americium in humans. Health Phys 62: 288-310.

Leggett, RW. (1993). An age-specific kinetic model of lead metabolism in humans [Review]. Environ Health Perspect 101: 598-616. http://dx.doi.org/10.1289/ehp.93101598

Leggett, RW; Eckerman, KF; Williams, LR. (1993). An elementary method for implementing complex biokinetic models. Health Phys 64: 260-271.

Lloyd, RD; Mays, CW; Atherton, DR; Bruenger, FW. (1975). 210Pb studies in beagles. Health Phys 28: 575-583. http://dx.doi.org/10.1097/00004032-197505000-00011

Lorenzana, RM; Troast, R; Klotzbach, JM; Follansbee, MH; Diamond, GL. (2005). Issues related to time averaging of exposure in modeling risks associated with intermittent exposures to lead. Risk Anal 25: 169-178. http://dx.doi.org/10.1111/j.0272-4332.2005.00576.x

Maddaloni, M; Ballew, M; Diamond, G; Follansbee, M; Gefell, D; Goodrum, P; Johnson, M; Koporec, K; Khoury, G; Luey, J; Odin, M; Troast, R; Van Leeuwen, P; Zaragoza, L. (2005). Assessing lead risks at non-residential hazardous waste sites. Hum Ecol Risk Assess 11: 967-1003. http://dx.doi.org/10.1080/10807030500257838

Malcoe, LH; Lynch, RA; Kegler, MC; Skaggs, VJ. (2002). Lead sources, behaviors, and socioeconomic factors in relation to blood lead of Native American and white children: A community-based assessment of a former mining area. Environ Health Perspect 110: 221-231. http://dx.doi.org/10.1289/ehp.02110s2221

Manton, WI; Cook, JD. (1984). High accuracy (stable isotope dilution) measurements of lead in serum and cerebrospinal fluid. Occup Environ Med 41: 313-319. http://dx.doi.org/10.1136/oem.41.3.313

Manton, WI; Malloy, CR. (1983). Distribution of lead in body fluids after ingestion of soft solder. Occup Environ Med 40: 51-57. http://dx.doi.org/10.1136/oem.40.1.51

Manton, WI; Rothenberg, SJ; Manalo, M. (2001). The lead content of blood serum. Environ Res 86: 263-273. http://dx.doi.org/10.1006/enrs.2001.4271

Morrow, PE; Beiter, H; Amato, F; Gibb, FR. (1980). Pulmonary retention of lead: An experimental study in man. Environ Res 21: 373-384. http://dx.doi.org/10.1016/0013-9351(80)90040-7

Nie, HL; Chettle, DR; Webber, CE; Brito, JAA; O'Meara, JM; McNeill, FE. (2005). The study of age influence on human bone lead metabolism by using a simplified model and X-ray fluorescence data. J Environ Monit 7: 1069-1073. http://dx.doi.org/10.1039/b507749d

Nilsson, U; Attewell, R; Christoffersson, JO; Schutz, A; Ahlgren, L; Skerfving, S; Mattsson, S. (1991). Kinetics of lead in bone and blood after end of occupational exposure. Basic Clin Pharmacol Toxicol 68: 477-484.

O'Flaherty, EJ. (1991a). Physiologically based models for bone-seeking elements I Rat skeletal and bone growth [Review]. Toxicol Appl Pharmacol 111: 299-312. http://dx.doi.org/10.1016/0041-008X(91)90032-A

O'Flaherty, EJ. (1991b). Physiologically based models for bone-seeking elements. II. Kinetics of lead disposition in rats. Toxicol Appl Pharmacol 111: 313-331. http://dx.doi.org/10.1016/0041-008X(91)90033-B

O'Flaherty, EJ. (1991c). Physiologically based models for bone-seeking elements. III. Human skeletal and bone growth. Toxicol Appl Pharmacol 111: 332-341. http://dx.doi.org/10.1016/0041-008X(91)90034-C

O'Flaherty, EJ. (1993). Physiologically based models for bone-seeking elements: IV. Kinetics of lead disposition in humans. Toxicol Appl Pharmacol 118: 16-29. http://dx.doi.org/10.1006/taap.1993.1004

O'Flaherty, EJ. (1995). Physiologically based models for bone-seeking elements: V. Lead absorption and disposition in childhood [Review]. Toxicol Appl Pharmacol 131: 297-308. http://dx.doi.org/10.1006/taap.1995.1072

O'Flaherty, EJ. (1998). A physiologically based kinetic model for lead in children and adults [Review]. Environ Health Perspect 106: 1495-1503. http://dx.doi.org/10.1289/ehp.98106s61495

O'Flaherty, EJ. (2000). Modeling normal aging bone loss, with consideration of bone loss in osteoporosis. Toxicol Sci 55: 171-188.

O'Flaherty, EJ; Inskip, MJ; Franklin, CA; Durbin, PW; Manton, WI; Baccanale, CL. (1998). Evaluation and modification of a physiologically based model of lead kinetics using data from a sequential isotope study in cynomolgus monkeys. Toxicol Appl Pharmacol 149: 1-16. http://dx.doi.org/10.1006/taap.1997.8328

OMB (U.S. Office of Management and Budget). (2004). Final information quality bulletin for peer review. (Memorandum M-05-03). Washington, DC: US Office of Management and Budget (OMB). http://www.whitehouse.gov/sites/default/files/omb/assets/omb/memoranda/fy2005/m05-03.pdf

Peters, A; Henderson, BL; Lui, D. (2000). Indexed glomerular filtration rate as a function of age and body size. Clin Sci (Lond) 98: 439-444. http://dx.doi.org/10.1042/cs0980439

Peters, AM. (2004). The kinetic basis of glomerular filtration rate measurement and new concepts of indexation to body size [Review]. Eur J Nucl Med Mol Imaging 31: 137-149. http://dx.doi.org/10.1007/s00259-003-1341-8

Pounds, JG; Leggett, RW. (1998). The ICRP age-specific biokinetic model for lead: Validations, empirical comparisons, and explorations [Review]. Environ Health Perspect 106: 1505-1511. http://dx.doi.org/10.1289/ehp.98106s61505

Rabinowitz, MB; Kopple, JD; Wetherill, GW. (1980). Effect of food intake and fasting on gastrointestinal lead absorption in humans. Am J Clin Nutr 33: 1784-1788. http://dx.doi.org/10.1093/ajcn/33.8.1784

Rabinowitz, MB; Wetherill, GW; Kopple, JD. (1976). Kinetic analysis of lead metabolism in healthy humans. J Clin Invest 58: 260-270. http://dx.doi.org/10.1172/JCI108467

Rentschler, G; Broberg, K; Lundh, T; Skerfving, S. (2012). Long-term lead elimination from plasma and whole blood after poisoning. Int Arch Occup Environ Health 85: 311-316. http://dx.doi.org/10.1007/s00420-011-0673-0

Ryu, JE; Ziegler, EE; Nelson, SE; Fomon, SJ. (1983). Dietary intake of lead and blood lead concentration in early infancy. Am J Dis Child 137: 886-891.

Schutz, A; Bergdahl, IA; Ekholm, A; Skerfving, S. (1996). Measurement by ICP-MS of lead in plasma and whole blood of lead workers and controls. Occup Environ Med 53: 736-740. http://dx.doi.org/10.1136/oem.53.11.736

Sherlock, JC; Quinn, MJ. (1986). Relationship between blood and lead concentrations and dietary lead intake in infants: The Glasgow Duplicate Diet Study 1979-1980. Food Addit Contam 3: 167-176. http://dx.doi.org/10.1080/02652038609373579

Smith, D; Hernandez-Avila, M; Tellez-Rojo, MM; Mercado, A; Hu, H. (2002). The relationship between lead in plasma and whole blood in women. Environ Health Perspect 110: 263-268. http://dx.doi.org/10.1289/ehp.02110263

SRC (Syracuse Research Corporation). (2003). Evaluation of the ICRP lead biokinetics model: Empirical comparisons with observations of plasma-blood lead concentration relationships in humans [draft final]. (SRC No. FA332). Washington, DC: U.S. Environmental Protection Agency.

SRC (Syracuse Research Corporation). (2008). Theoretical framework for the All Ages Lead Model. (SRC TR-08-142).

SRC (Syracuse Research Corporation). (2009a). Evidence supporting further refinement of the EPA All Ages Lead Model. (SRC TR-09-178).

SRC (Syracuse Research Corporation). (2009b). Review of lead exposure biokinetics models. (SRC TR-09-139).

Stover, BJ. (1959). Pb212 (ThB) tracer studies in adult beagle dogs. Proc Soc Exp Biol Med 100: 269-272. http://dx.doi.org/10.3181/00379727-100-24596

TerraGraphics Environmental Engineering (TerraGraphics Environmental Engineering Inc). (2004). Human health remedial evaluation report for the Bunker Hill Superfund site box. Moscow, ID.

U.S. EPA (U.S. Environmental Protection Agency). (1989). Review of the national ambient air quality standard for lead: Exposure analysis methodology and validation [EPA Report]. (EPA/450/2-89-011).

U.S. EPA (U.S. Environmental Protection Agency). (1994a). Guidance manual for the integrated exposure uptake biokinetic model for lead in children [EPA Report]. (EPA/540/R-93/081). Washington, DC. http://nepis.epa.gov/Exe/ZyPURL.cgi?Dockey=2000WN4R.txt

U.S. EPA (U.S. Environmental Protection Agency). (1994b). Revised interim soil lead guidance for CERCLA sites and RCRA corrective action facilities [memorandum from EPA's Assistant Administrator for Solid Waste and Emergency Response to regional administrators I-X] [EPA Report]. (OSWER Directive #9355.4-12; EPA/540/F-94/043). Washington, DC. https://semspub.epa.gov/work/HQ/175347.pdf

U.S. EPA (U.S. Environmental Protection Agency). (1994c). Technical support document: Parameters and equations used in integrated exposure uptake biokinetic model for lead in children (v 099d) [EPA Report]. (EPA/54O/R-94/04O). Washington, DC.

U.S. EPA (U.S. Environmental Protection Agency). (1998). Federal guidance report no. 13: Part I - Interim version: Health risks from low level environmental exposures to radionuclides: Radionuclide-specific lifetime radiogenic cancer risk coefficients for the U.S. population, based on age-dependent intake, dosimetry, and risk models [EPA Report]. (EPA 402-R-97-014).

U.S. EPA (U.S. Environmental Protection Agency). (2003). Recommendations of the Technical Review Workgroup for Lead for an approach to assessing risks associated with adult exposures to lead in soil [EPA Report]. (EPA-540-R-03-001). Washington, DC. https://semspub.epa.gov/work/HQ/174559.pdf

U.S. EPA (U.S. Environmental Protection Agency). (2006). Air quality criteria for lead: Volume I of II [EPA Report]. (EPA/600/R-05/144aF). Research Triangle Park, NC. http://cfpub.epa.gov/ncea/CFM/recordisplay.cfm?deid=158823

U.S. EPA (U.S. Environmental Protection Agency). (2007). EPA science advisory board (SAB) ad hoc all-ages lead model review panel's peer review of the "all-ages lead model (AALM) version 1.05 (External review draft) ". (EPA-SAB-07-002). https://cfpub.epa.gov/si/si_public_record_report.cfm?dirEntryId=139314&Lab=NCEA

U.S. EPA (U.S. Environmental Protection Agency). (2013). Integrated science assessment for lead [EPA Report]. (EPA/600/R-10/075F). Research Triangle Park, NC: U.S. Environmental Protection Agency, National Center for Environmental Assessment. http://cfpub.epa.gov/ncea/cfm/recordisplay.cfm?deid=255721

U.S. EPA (U.S. Environmental Protection Agency). (2014a). Appendices to the approach for estimating exposures and incremental health effects from lead due to renovation, repair, and painting activities in public and commercial buildings. Washington, DC. https://www.epa.gov/lead/approach-estimating-exposures-and-incremental-health-effects-lead-due-renovation-repair-and

U.S. EPA (U.S. Environmental Protection Agency). (2014b). Approach for estimating exposures and incremental health effects from lead due to renovation, repair, and painting activities in public and commercial building. Washington, DC. https://www.epa.gov/lead/approach-estimating-exposures-and-incremental-health-effects-lead-due-renovation-repair-and

U.S. EPA (U.S. Environmental Protection Agency). (2014c). Framework for identifying and evaluating lead-based paint hazards from renovation, repair, and painting activities in public and commercial buildings. Washington, DC. https://www.epa.gov/sites/production/files/2014-05/documents/lead_pncb_framework_document.pdf

Versar (Versar Inc.). (2015). Post-meeting peer review summary report: External peer review of EPA's approach for estimating exposures and incremental health effects from lead due to renovation, repair, and painting activities in public and commercial buildings. https://www.regulations.gov/document?D=EPA-HQ-OPPT-2010-0173-0259

Watson, WS; Morrison, J; Bethel, MIF; Baldwin, NM; Lyon, DTB; Dobson, H; Moore, MR; Hume, R. (1986). Food iron and lead absorption in humans. Am J Clin Nutr 44: 248-256.

Wells, AC; Venn, JB; Heard, MJ. (1977). Deposition in the lung and uptake to blood of motor exhaust labelled with 203Pb. In WH Walton; B McGovern (Eds.), Inhaled particles IV: Proceedings of an international symposium organized by the British Occupational Hygiene Society: Part 1 (pp. 175-189). Oxford, UK: Pergamon.

White, PD; Van Leeuwan, P; Davis, BD; Maddaloni, M; Hogan, KA; Marcus, AH; Elias, RW. (1998). The conceptual structure of the integrated exposure uptake biokinetic model for lead in children [Review]. Environ Health Perspect 106: 1513-1530. http://dx.doi.org/10.1289/ehp.98106s61513

Zaragoza, L; Hogan, K. (1998). The integrated exposure uptake biokinetic model for lead in children: Independent validation and verification [Review]. Environ Health Perspect 6: 1551-1556.

Ziegler, EE; Edwards, BB; Jensen, RL; Mahaffey, KR; Fomon, SJ. (1978). Absorption and retention of lead by infants. Pediatr Res 12: 29-34. http://dx.doi.org/10.1203/00006450-197801000-00008

APPENDIX A – EQUATIONS IN AALM.FOR

TABLE A-1. EQUATIONS OF THE ALL AGES LEAD MODEL (AALM.FOR)

Model	Submodel	Equation
Daily lead intake rate from air (µg/day)		
Exposure	Air	For each discrete age: $Air_{TWA_{discrete}} = Air_1 * f_{Air_1} + Air_2 * f_{Air_2} + Air_3 * f_{Air_3}$
Exposure	Air	For each discrete age: $f_{Air_3} = 1 - (f_{Air_1} + f_{Air_2})$
Exposure	Air	For each discrete age: $INair_{discrete} = Air_{TWA_{discrete}} * V_{air}$
Exposure	Air	For each pulse: $INair_{pulse_{sum}} = (Air_{baseline} + Air_{pulse}) \cdot V_{air}$
Exposure	Air	For combined discrete and pulse: $INair_{Total} = INair_{discrete} * (1 - f_{pulse_{air}}) + INair_{pulse} * f_{pulse_{air}}$
Daily lead intake rate from indoor dust (µg/day)		
Exposure	Dust	For each discrete age: $Dust_{TWA_{discrete}} = Dust_1 * f_{Dust_1} + Dust_2 * f_{Dust_2} + Dust_3 * f_{Dust_3}$
Exposure	Dust	For each discrete age: $f_{Dust_3} = 1 - (f_{Dust_1} + f_{Dust_2})$
Exposure	Dust	For each discrete age: $INdust_{discrete} = Dust_{TWA_{discrete}} * IR_{Dust} * RBA_{Dust}$

Model	Submodel	Equation
Exposure	Dust	For each pulse: $INdust_{pulse_{sum}} = (Dust_{baseline} + Dust_{pulse}) * IR_{Dust} * RBA_{Dust}$
Exposure	Dust	For combined discrete and pulse: $INdust_{Total} = INdust_{discrete} * (1 - f_{pulse}) + INdust_{pulse} * f_{pulse}$
Exposure	Dust	For each discrete age: $Dust_{TWA_{discrete}} = Dust_1 * f_{Dust_1} + Dust_2 * f_{Dust_2} + Dust_3 * f_{Dust_3}$
Exposure	Dust	$IR_{Dust} = IR_{SD} * (1 - f_{IR_{Soil}})$
Daily lead intake rate from soil (µg/day)		
Exposure	Soil	For each discrete age: $Soil_{TWA_{discrete}} = Soil_1 * f_{Soil_1} + Soil_2 * f_{Soil_2} + Soil_3 * f_{Soil_3}$
Exposure	Soil	For each discrete age: $f_{Soil_3} = 1 - (f_{Soil_1} + f_{Soil_2})$
Exposure	Soil	For each discrete age: $INsoil_{discrete} = Soil_{TWA_{discrete}} * IR_{Soil} * RBA_{Doil}$
Exposure	Soil	For each pulse: $INsoil_{pulse_{sum}} = (Soil_{baseline} + Soil_{pulse}) * IR_{Soil} * RBA_{Soil}$
Exposure	Soil	For combined discrete and pulse: $INsoil_{Total} = INsoil_{discrete} * (1 - f_{pulse}) + INsoil_{pulse} * f_{pulse}$
Exposure	Soil	$IR_{Soil} = IR_{SD} * f_{IR_{Soil}}$

Model	Submodel	Equation
Daily lead intake rate from water (µg/day)		
Exposure	Water	For each discrete age: $\mathrm{Water}_{\mathrm{TWA}_{\mathrm{discrete}}} = \mathrm{Water}_1 * \mathrm{f}_{\mathrm{Water}_1} + \mathrm{Water}_2 * \mathrm{f}_{\mathrm{Water}_2} + \mathrm{Water}_3 * \mathrm{f}_{\mathrm{Water}_3}$
Exposure	Water	For each discrete age: $\mathrm{f}_{\mathrm{Water}_3} = 1 - (\mathrm{f}_{\mathrm{Water}_1} + \mathrm{f}_{\mathrm{Water}_2})$
Exposure	Water	For each discrete age: $\mathrm{INwater}_{\mathrm{discrete}} = \mathrm{Water}_{\mathrm{TWA}_{\mathrm{discrete}}} * \mathrm{IR}_{\mathrm{water}} * \mathrm{RBA}_{\mathrm{water}}$
Exposure	Water	For each pulse: $\mathrm{INwater}_{\mathrm{pulse}_{\mathrm{sum}}} = (\mathrm{Water}_{\mathrm{baseline}} + \mathrm{Water}_{\mathrm{pulse}}) * \mathrm{IR}_{\mathrm{water}} * \mathrm{RBA}_{\mathrm{water}}$
Exposure	Water	For combined discrete and pulse: $\mathrm{INwater}_{\mathrm{Total}} = \mathrm{INwater}_{\mathrm{discrete}} * (1 - \mathrm{f}_{\mathrm{pulse}_{\mathrm{water}}}) + \mathrm{INwater}_{\mathrm{pulse}} * \mathrm{f}_{\mathrm{pulse}_{\mathrm{water}}}$
Daily lead intake rate from food (µg/day)		
Exposure	Food	For each discrete age: $\mathrm{Food}_{\mathrm{Total}_{\mathrm{discrete}}} = \mathrm{Food}_1 + \mathrm{Food}_2 + \mathrm{Food}_3$
Exposure	Food	For each discrete age: $\mathrm{INfood}_{\mathrm{discrete}} = \mathrm{Food}_{\mathrm{Total}_{\mathrm{discrete}}} * \mathrm{RBA}_{\mathrm{food}}$
Exposure	Food	For each pulse: $\mathrm{INfood}_{\mathrm{pulse}_{\mathrm{sum}}} = (\mathrm{Food}_{\mathrm{baseline}} + \mathrm{Food}_{\mathrm{pulse}}) * \mathrm{RBA}_{\mathrm{food}}$
Exposure	Food	For combined discrete and pulse: $\mathrm{INfood}_{\mathrm{Total}} = \mathrm{INfood}_{\mathrm{discrete}} * (1 - \mathrm{f}_{\mathrm{pulse}}) + \mathrm{INfood}_{\mathrm{pulse}} * \mathrm{f}_{\mathrm{pulse}}$

Model	Submodel	Equation
Daily lead intake rate from other sources (µg/day)		
Exposure	Other	For each discrete age: $\text{Other}_{\text{Total}_{\text{discrete}}} = \text{Other1} + \text{Other}_2 + \text{Other}_3$
Exposure	Other	For each discrete age: $\text{INother}_{\text{discrete}} = \text{Other}_{\text{Total}_{\text{discrete}}} * \text{RBA}_{\text{other}}$
Exposure	Other	For each pulse: $\text{INother}_{\text{pulse}_{\text{sum}}} = (\text{Other}_{\text{baseline}} + \text{Other}_{\text{pulse}}) * \text{RBA}_{\text{other}}$
Exposure	Other	For combined discrete and pulse: $\text{INother}_{\text{Total}} = \text{INother}_{\text{discrete}} * (1 - \text{f}_{\text{pulse}}) + \text{INother}_{\text{pulse}} * \text{f}_{\text{pulse}}$
Daily lead intake from all sources (µg/day)		
Exposure	Inhaled	For input to biokinetics: $\text{BRETH} = \text{INair}_{\text{total}}$
Exposure	Ingested	For combined ingestion pathways: $\text{IN}_{\text{ingestion}_{\text{total}}} = \text{IN}_{\text{water}} + \text{IN}_{\text{dust}} + \text{IN}_{\text{food}} + \text{IN}_{\text{other}}$
Exposure	Ingested	For input to biokinetics: $\text{EAT} = \text{IN}_{\text{ingestion}_{\text{total}}}$
BioKinetics Equations (including absorption processes)		
Growth and tissue volumes (L or dL) and masses (kg)		

Model	Submodel	Equation
Biokinetics	Growth	$\mathrm{WBODY} = \mathrm{WBIRTH} + \frac{\mathrm{WCHILD} * \mathrm{HOWOLD}}{\mathrm{HALF} + \mathrm{HOWOLD}} + \frac{\mathrm{WADULT}}{1 + \mathrm{KAPPA} * \mathrm{e}^{(\mathrm{LAMBDA} * \mathrm{WADULT} * \mathrm{HOWOLD})}}$
Biokinetics	Growth	$\mathrm{AMTBLD} = \mathrm{VBLC} * \mathrm{WBODY} * 10$
Biokinetics	Growth	$\mathrm{PLSVOL} = \mathrm{AMTBLD} * (1 - \mathrm{BLDHCT})$
Biokinetics	Growth	$\mathrm{RBCVOL} = \mathrm{AMTBLD} * \mathrm{BLDHCT}$
Biokinetics	Growth	$\mathrm{BLDHCT}_{\mathrm{HOWOLD} \leq 0.01} = 0.52 + \mathrm{HOWOLD} * 14$ $\mathrm{BLDHCT}_{\mathrm{HOWOLD} > 0.01} = \mathrm{HCTA} * (1 + (0.66 - \mathrm{HCTA}) * \mathrm{e}^{-(\mathrm{HOWOLD} - 0.01) * 13.9})$
Biokinetics	Growth	$\mathrm{VK} = 1000 * \mathrm{VKC} * (\mathrm{WBIRTH} + \mathrm{WCHILD} + \mathrm{WADULT}) * \left(\frac{\mathrm{WBODY}}{\mathrm{WBIRTH} + \mathrm{WCHILD} + \mathrm{WADULT}}\right)^{0.84}$
Biokinetics	Growth	$\mathrm{KIDWT} = \mathrm{VK} * 1.05$
Biokinetics	Growth	$\mathrm{VL} = 1000 * \mathrm{VLC} * (\mathrm{WBIRTH} + \mathrm{WCHILD} + \mathrm{WADULT}) * \left(\frac{\mathrm{WBODY}}{\mathrm{WBIRTH} + \mathrm{WCHILD} + \mathrm{WADULT}}\right)^{0.85}$
Biokinetics	Growth	$\mathrm{LIVWT} = \mathrm{VL} * 1.05$
Biokinetics	Growth	$\mathrm{TSKELWT} = 1000 * 0.058 * \mathrm{WBODY}^{1.21}$
Biokinetics	Growth	$\mathrm{WBONE} = 1000 * 0.029 * \mathrm{WBODY}^{1.21}$

Model	Submodel	Equation
Biokinetics	Growth	$VBONE = 1000 * 0.0168 * WBODY^{1.188}$
Biokinetics	Growth	$CVBONE = 0.8 * VBONE$
Biokinetics	Growth	$TVBONE = VBONE - CVBONE$
Biokinetics	Growth	$CORTWT = \frac{WBONE * CVBONE}{VBONE}$
Biokinetics	Growth	$TRABWT = \frac{WBONE * TVBONE}{VBONE}$
Deposition fractions (DF, unitless) of lead from diffusible plasma to tissue compartments		
Biokinetics	DF	$\mathrm{AGESCL} = \frac{1.0 - \mathrm{TEVF} - \mathrm{TBONE}}{1.0 - \mathrm{TEVF} - \mathrm{ATBONE}}$
Biokinetics	DF	$\mathrm{TURIN} = \mathrm{AGESC} * \mathrm{TOURIN}$
Biokinetics	DF	$\mathrm{TSWET} = \mathrm{AGESCL} * \mathrm{TOSWET}$
Biokinetics	DF	$\mathrm{TSOF0} = \mathrm{AGESCL} * \mathrm{TOSOF0}$
Biokinetics	DF	$\mathrm{TSOF1} = \mathrm{AGESCL} * \mathrm{TOSOF1}$

Model	Submodel	Equation
Biokinetics	DF	$\mathrm{TSOF2} = \mathrm{AGESCL} * \mathrm{TOSOF2}$
Biokinetics	DF	$\mathrm{TBRAN} = \mathrm{AGESCL} * \mathrm{TOBRAN}$
Biokinetics	DF	$\mathrm{TLVR1} = \mathrm{AGESCL} \cdot \mathrm{TOLVR1}$
Biokinetics	DF	$\mathrm{TKDN1} = \mathrm{AGESCL} * \mathrm{TOKDN1}$
Biokinetics	DF	$\mathrm{TKDN2} = \mathrm{AGESCL} * \mathrm{TOKDN2}$
Biokinetics	DF	$\mathrm{TRBC} = \mathrm{AGESCL} * \mathrm{TORBC}$
Biokinetics	DF	$\mathrm{TPROT} = \mathrm{AGESCL} * \mathrm{TOPROT}$
Biokinetics	DF	$\mathrm{TOORBC} = \mathrm{TRBC} * \left(1 - \frac{\mathrm{RBCONC} - \mathrm{RBCNL}}{\mathrm{SATRAT} - \mathrm{RBCNL}}\right)^{\mathrm{POWER}}$
Biokinetics	DF	$\mathrm{TSUM} = \mathrm{TOORBC} + \mathrm{TEVF} + \mathrm{TPROT} + \mathrm{TBONE} + \mathrm{TURIN} + \mathrm{TFECE} + \mathrm{TSWET} + \mathrm{TLVR1} + \mathrm{TKDN1} + \mathrm{TKDN2} + \mathrm{TSOF0} + \mathrm{TSOF1} + \mathrm{TSOF2} + \mathrm{TBRAN}$
Biokinetics	DF	$\mathrm{CF} = \frac{1.0 - \mathrm{TOORBC}}{1.0 - \mathrm{TRBC}}$
Deposition fractions (DF, unitless) of lead from diffusible plasma to tissue compartments during chelation therapy		

Model	Submodel	Equation
Biokinetics	DF	$\mathrm{TEVF} = (1 - \mathrm{CHLEFF}) * \mathrm{TEVF}$
Biokinetics	DF	$\mathrm{TFECE} = (1 - \mathrm{CHLEFF}) * \mathrm{TFECE}$
Biokinetics	DF	$\mathrm{TSWET} = (1 - \mathrm{CHLEFF}) * \mathrm{TSWET}$
Biokinetics	DF	$\mathrm{TSOF0} = (1 - \mathrm{CHLEFF}) * \mathrm{TSOF0}$
Biokinetics	DF	$\mathrm{TSOF1} = (1 - \mathrm{CHLEFF}) * \mathrm{TSOF1}$
Biokinetics	DF	$\mathrm{TSOF2} = (1 - \mathrm{CHLEFF}) * \mathrm{TSOF2}$
Biokinetics	DF	$\mathrm{TBRAN} = (1 - \mathrm{CHLEFF}) * \mathrm{TBRAN}$
Biokinetics	DF	$\mathrm{TLVR1} = (1 - \mathrm{CHLEFF}) * \mathrm{TLVR1}$
Biokinetics	DF	$\mathrm{TKDN1} = (1 - \mathrm{CHLEFF}) * \mathrm{TKDN1}$
Biokinetics	DF	$\mathrm{TPROT} = (1 - \mathrm{CHLEFF}) * \mathrm{TPROT}$
Biokinetics	DF	$\mathrm{TBONE} = (1 - \mathrm{CHLEFF}) * \mathrm{TBONE}$

Model	Submodel	Equation
Biokinetics	DF	$\mathrm{TOORBC} = (1 - \mathrm{CHLEFF}) * \mathrm{TOORBC}$
Biokinetics	DF	$\mathrm{TURIN} = 1 - (\mathrm{TOORBC} + \mathrm{TEVF} + \mathrm{TPROT} + \mathrm{TBONE} + \mathrm{TURIN} + \mathrm{TFECE} + \mathrm{TSWET} + \mathrm{TLVR1} + \mathrm{TKDN1} + \mathrm{TKDN2} + \mathrm{TSOF0} + \mathrm{TSOF1} + \mathrm{TSOF2} + \mathrm{TBRAN})$
Transfer rates (day^{-1})		
Biokinetics	Plasma	$\mathrm{RPLS} = \mathrm{TSUM} * \mathrm{RPLAS}$
Biokinetics	Plasma	$\mathrm{BTEMP} = \mathrm{RPLS} * \mathrm{YPLS_W}$
Biokinetics	Growth	$\mathrm{REVF} = \frac{\mathrm{TEVF} * \mathrm{RPLS}}{\mathrm{SIZEVF}}$
Biokinetics	RBC	$\mathrm{CF} = \frac{1.0 - \mathrm{TOORBC}}{1.0 - \mathrm{TRBC}}$
Amount of lead (µg) in compartment at start of each integration step (Y_0) and amount integrated over the step (Y_W)		

Model	Submodel	Equation
Biokinetics	Lung	IF DELT*OUTRATE >50: $YR1_0 = \frac{INRATE}{RDECAY + BR1}$ IF DELT*OUTRATE ≤50: $YR1_0 = \left(YR1_0 - \left(\frac{INRATE}{OUTRATE}\right)\right) * e^{(-OUTRATE*DELT)} + \frac{INRATE}{OUTRATE}$ $ACUTE: INRATE = 0, \quad YR1_0 = R1$ $CHRONIC: INRATE = R1 * BRTCRN$ $OUTRATE = BR1 + RDECAY$
Biokinetics	Lung	IF DELT*OUTRATE>50: $YR1_W = \frac{1}{OUTRATE} * YR1_0 - \frac{INRATE}{OUTRATE} + \frac{INRATE * DELT}{OUTRATE}$ IF DELT*OUTRATE ≤50: $YR1_W = \left(\frac{1 - e^{(-OUTRATE*DELT)}}{OPUTRATE} * YR1_0 - \frac{INRATE}{OUTRATE}\right) + \frac{INRATE * DELT}{OUTRATE}$ $ACUTE: INRATE = 0, \quad YR1 = R1$ $CHRONIC: INRATE = R1 * BRTCRN$ $OUTRATE = BR1 + RDECAY$

Model	Submodel	Equation
Biokinetics	Lung	IF DELT*OUTRATE >50: $YR2_0 = \frac{INRATE}{OUTRATE}$ IF DELT*OUTRATE ≤50: $YR2_0 = \left(YR2_0 - \left(\frac{INRATE}{OUTRATE}\right)\right) * e^{(-OUTRATE*DELT)} + \frac{INRATE}{OUTRATE}$ $ACUTE: INRATE = 0, \quad YR2 = R2$ $CHRONIC: INRATE = R2 * BRTCRN$ $OUTRATE = BR2 + RDECAY$
Biokinetics	Lung	IF DELT*OUTRATE >50: $YR2_W = \frac{1}{OUTRATE} * YR2_0 - \frac{INRATE}{OUTRATE} + \frac{INRATE * DELT}{OUTRATE}$ IF DELT*OUTRATE ≤50: $YR2_W = \left(\frac{1 - e^{(-OUTRATE*DELT)}}{OUTRATE} * YR2_0 - \frac{INRATE}{OUTRATE}\right) + \frac{INRATE * DELT}{OUTRATE}$ $ACUTE: INRATE = 0, \quad YR2 = R2$ $CHRONIC: INRATE = R2 * BRTCRN$ $OUTRATE = BR2 + RDECAY$

Model	Submodel	Equation
Biokinetics	Lung	IF DELT*OUTRATE >50: $YR3_0 = \frac{INRATE}{OUTRATE}$ IF DELT*OUTRATE ≤50: $YR3_0 = \left(YR3_0 - \left(\frac{INRATE}{OUTRATE}\right)\right) * e^{(-OUTRATE*DELT)} + \frac{INRATE}{OUTRATE}$ $ACUTE: INRATE = 0, \quad YR3 = R3$ $CHRONIC: INRATE = R3 * BRTCRN$ $OUTRATE = BR3 + RDECAY$
Biokinetics	Lung	IF DELT*OUTRATE >50: $YR3_W = \frac{1}{OUTRATE} * YR3_0 - \frac{INRATE}{OUTRATE} + \frac{INRATE * DELT}{OUTRATE}$ IF DELT*OUTRATE ≤50: $YR3_W = \left(\frac{1 - e^{(-OUTRATE*DELT)}}{OUTRATE} * YR3_0 - \frac{INRATE}{OUTRATE}\right) + \frac{INRATE * DELT}{OUTRATE}$ $ACUTE: INRATE = 0, \quad YR3 = R3$ $CHRONIC: INRATE = R3 * BRTCRN$ $OUTRATE = BR3 + RDECAY$

Model	Submodel	Equation
Biokinetics	Lung	IF DELT*OURTATE >50: $YR4_0 = \frac{INRATE}{OUTRATE}$ IF DELT*OUTRATE ≤50: $YR4_0 = \left(YR4_0 - \left(\frac{INRATE}{OUTRATE}\right)\right) * e^{(-OUTRATE*DELT)} + \frac{INRATE}{OUTRATE}$ $ACUTE: INRATE = 0, \quad YR4 = R4$ $CHRONIC: INRATE = R4 * BRTCRN$ $OUTRATE = BR4 + RDECAY$
Biokinetics	Lung	IF DELT*OUTRATE >50: $YR4_W = \frac{1}{OUTRATE} * YR4_0 - \frac{INRATE}{OUTRATE} + \frac{INRATE * DELT}{OUTRATE}$ IF DELT*OUTRATE ≤50: $YR4_W = \left(\frac{1 - e^{(-OUTRATE*DELT)}}{OUTRATE} * YR4_0 - \frac{INRATE}{OUTRATE}\right) + \frac{INRATE * DELT}{OUTRATE}$ $ACUTE: INRATE = 0, \quad YR4 = R4$ $CHRONIC: INRATE = R4 * BRTCRN$ $OUTRATE = BR4 + RDECAY$

Model	Submodel	Equation
Biokinetics	GI Tract	$F_1 = AF_{C1} - \frac{AF_{C2}}{1 + 30 * e^{-HOWOLD}}$ (calculated outside of Fortran code)
Biokinetics	GI Tract	IF DELT*OUTRATE >50: $YRSTMC_0 = \frac{INRATE}{OUTRATE}$ IF DELT*OUTRATE≤50: $YSTMC_0 = \left(YSTMC_0 - \left(\frac{INRATE}{OUTRATE}\right)\right) * e^{(-OUTRATE*DELT)} + \frac{INRATE}{OUTRATE}$ ACUTE: $INRATE = 0, \quad YSTMC_0 = 1$ CHRONIC (no inhalation): $INRATE = EATCRN$ CHRONIC (COMBINATION): $INRATE = EATCRN + CILIAR * \frac{\left(BR1 * YR1_W + BR2 * YR2_W + BR3 * YR3_W + BR4 * YR4_W\right)}{DELT}$ $OUTRATE = GSCALE * RSTMC + RDECAY$

Model	Submodel	Equation
Biokinetics	GI Tract	IF DELT*OUTRATE >50: $\mathrm{YSTMC_W} = \frac{1}{\mathrm{OUTRATE}} * \mathrm{YRSTMC_0} - \frac{\mathrm{INRATE}}{\mathrm{OUTRATE}} + \mathrm{INRATE} * \frac{\mathrm{DELT}}{\mathrm{OUTRATE}}$ IF DELT*OUTRATE ≤50: $\mathrm{YSTMC_W} = \left(\frac{1 - e^{(\mathrm{OUTRATE}*\mathrm{DELT})}}{\mathrm{OUTRATE}} * \mathrm{YSTMC_0} - \frac{\mathrm{INRATE}}{\mathrm{OUTRATE}}\right) + \frac{\mathrm{INRATE} * \mathrm{DELT}}{\mathrm{OUTRATE}}$ ACUTE: $\mathrm{INRATE} = 0, \quad \mathrm{YSTMC_0} = 1$ CHRONIC (no inhalation): $\mathrm{INRATE} = \mathrm{EATCRN}$ CHRONIC (COMBINATION): $\mathrm{INRATE} = \mathrm{EATCRN} + \mathrm{CILIAR} * \frac{\left(\mathrm{BR1} * \mathrm{YR1_W} + \mathrm{BR2} * \mathrm{YR2_W} + \mathrm{BR3} * \mathrm{YR3_W} + \mathrm{BR4} * \mathrm{YR4_W}\right)}{\mathrm{DELT}}$ $\mathrm{OUTRATE} = \mathrm{GSCALE} * \mathrm{RSTMC} + \mathrm{RDECAY}$

Model	Submodel	Equation
Biokinetics	GI Tract	IF DELT*OUTRATE >50: $\mathrm{YSIC_0} = \frac{\mathrm{INRATE}}{\mathrm{OUTRATE}}$ IF DELT*OUTRATE ≤50: $\mathrm{YSIC_0} = \left(\mathrm{YSIC_0} - \left(\frac{\mathrm{INRATE}}{\mathrm{OUTRATE}}\right)\right) * \mathrm{e}^{(-\mathrm{OUTRATE}*\mathrm{DELT})} + \frac{(\mathrm{INRATE})}{\mathrm{OUTRATE}}$ $\mathrm{INRATE} = \frac{(\mathrm{GSCALE} * \mathrm{RSTMC} * \mathrm{YSTMC_W}) + (\mathrm{H1TOSI} * \mathrm{RLVR1} * \mathrm{YRLVR1_W}) + (\mathrm{TFECE} * \mathrm{CF} * \mathrm{BTEMP})}{\mathrm{DELT}}$ $\mathrm{OUTRATE} = \mathrm{GSCALE} * \mathrm{RSIC} + \mathrm{RDECAY}$
Biokinetics	GI Tract	IF DELT*OUTRATE >50: $\mathrm{YSIC_W} = \frac{1}{\mathrm{OUTRATE}} * \mathrm{YSIC_0} - \frac{\mathrm{INRATE}}{\mathrm{OUTRATE}} + \frac{\mathrm{INRATE} * \mathrm{DELT}}{\mathrm{OUTRATE}}$ IF DELT*OUTRATE ≤50: $\mathrm{YSIC_W} = \left(\frac{1 - \mathrm{e}^{(-\mathrm{OUTRATE}*\mathrm{DELT})}}{\mathrm{OUTRATE}} * \mathrm{YSIC_0} - \frac{\mathrm{INRATE}}{\mathrm{OUTRATE}}\right) + \frac{\mathrm{INRATE} * \mathrm{DELT}}{\mathrm{OUTRATE}}$ $\mathrm{INRATE} = \frac{(\mathrm{GSCALE} * \mathrm{RSTMC} * \mathrm{YSTMC_W}) + (\mathrm{H1TOSI} * \mathrm{RLVR1} * \mathrm{YRLVR1_W}) + (\mathrm{TFECE} * \mathrm{CF} * \mathrm{BTEMP})}{\mathrm{DELT}}$ $\mathrm{OUTRATE} = \mathrm{GSCALE} * \mathrm{RSIC} + \mathrm{RSIC}$

Model	Submodel	Equation
Biokinetics	GI Tract	IF DELT*OUTRATE >50: $\mathrm{YULIC}_0 = \frac{\mathrm{INRATE}}{\mathrm{OUTRATE}}$ IF DELT*OUTRATE ≤50: $\mathrm{YULIC}_0 = \left(\mathrm{YULIC}_0 - \left(\frac{\mathrm{INRATE}}{\mathrm{OUTRATE}}\right)\right) * \mathrm{e}^{-\mathrm{OUTRATE}*\mathrm{DELT}} + \frac{\mathrm{INRATE}}{\mathrm{OUTRATE}}$ $\mathrm{INRATE} = \frac{(1.0 - \mathrm{F1}) * \mathrm{GSCALE} * \mathrm{RSIC} * \mathrm{YSIC}_W}{\mathrm{DELT}}$ $\mathrm{OUTRATE} = \mathrm{GSCALE} * \mathrm{RULI} + \mathrm{RDECAY}$

Model	Submodel	Equation
Biokinetics	GI Tract	IF DELT*OUTRATE>50: $\mathrm{YULIC_W} = \frac{1}{\mathrm{OUTRATE}} * \mathrm{YULIC_0} - \frac{\mathrm{INRATE}}{\mathrm{OUTRATE}} + \frac{\mathrm{INRATE} * \mathrm{DELT}}{\mathrm{OUTRATE}}$ IF DELT*OUTRATE≤50: $\mathrm{YULIC_W} = \left(\frac{1 - e^{(-\mathrm{OUTRATE} * \mathrm{DELT})}}{\mathrm{OUTRATE}} * \mathrm{YULIC_0} - \frac{\mathrm{INRATE}}{\mathrm{OUTRATE}}\right) + \frac{\mathrm{INRATE} * \mathrm{DELT}}{\mathrm{OUTRATE}}$ $\mathrm{INRATE} = \frac{(1.0 - \mathrm{F1}) * \mathrm{GSCALE} * \mathrm{RSIC} * \mathrm{YSIC_W}}{\mathrm{DELT}}$ $\mathrm{OUTRATE} = \mathrm{GSCALE} * \mathrm{RULI} + \mathrm{RDECAY}$

Model	Submodel	Equation
Biokinetics	GI Tract	IF DELT*OUTRATE >50: $\mathrm{YLLIC}_0 = \frac{\mathrm{INRATE}}{\mathrm{OUTRATE}}$ IF DELT*OUTRATE ≤50: $\mathrm{YLLIC}_0 = \left(\mathrm{YLLIC}_0 - \left(\frac{\mathrm{INRATE}}{\mathrm{OUTRATE}}\right)\right) * \mathrm{e}^{(-\mathrm{OUTRATE}*\mathrm{DELT})} + \frac{\mathrm{INRATE}}{\mathrm{OUTRATE}}$ $\mathrm{INRATE} = \frac{\mathrm{GSCALE} * \mathrm{RULI} * \mathrm{YULIC}_W}{\mathrm{DELT}}$ $\mathrm{OUTRATE} = \mathrm{GSCALE} * \mathrm{RLLI} + \mathrm{RDECAY}$

Model	Submodel	Equation
Biokinetics	GI Tract	IF DELT*OUTRATE >50: $\mathrm{YLLIC_W} = \frac{1}{\mathrm{OUTRATE}} * \mathrm{YULIC_0} - \frac{\mathrm{INRATE}}{\mathrm{OUTRATE}} + \frac{\mathrm{INRATE} * \mathrm{DELT}}{\mathrm{OUTRATE}}$ IF DELT*OUTRATE ≤50: $\mathrm{YLLIC_W} = \left(\frac{1 - \mathrm{e}^{(-\mathrm{OUTRATE}*\mathrm{DELT})}}{\mathrm{OUTRATE}} * \mathrm{YLLIC_0} - \frac{\mathrm{INRATE}}{\mathrm{OUTRATE}}\right) + \frac{\mathrm{INRATE} * \mathrm{DELT}}{\mathrm{OUTRATE}}$ $\mathrm{INRATE} = \frac{\mathrm{GSCALE} * \mathrm{RULI} * \mathrm{YULIC_W}}{\mathrm{DELT}}$ $\mathrm{OUTRATE} = \mathrm{GSCALE} * \mathrm{RLLI} + \mathrm{RDECAY}$

Model	Submodel	Equation
Biokinetics	Plasma	IF DELT*OUTRATE >50: $\mathrm{YPLS}_0 = \frac{\mathrm{INRATE}}{\mathrm{OUTRATE}}$ IF DELT*OUTRATE ≤50: $\mathrm{YPLS}_0 = \left(\mathrm{YPLS}_0 - \left(\frac{\mathrm{INRATE}}{\mathrm{OUTRATE}}\right)\right) * \mathrm{e}^{(-\mathrm{OUTRATE}*\mathrm{DELT})} + \frac{(\mathrm{INRATE})}{\mathrm{OUTRATE}}$ $\mathrm{INRATE} = \begin{cases} \text{ACUTE: } \mathrm{INRATE}_{\mathrm{TISSUE}} \\ \text{CHRONIC: } \mathrm{INRATE}_{\mathrm{TISSUE}} + \mathrm{CRONIC} \\ \text{INHALATION: } \mathrm{INRATE}_{\mathrm{TISSUE}} + \frac{(1.0 + \mathrm{CILIAR}) * (\mathrm{BR1} * \mathrm{YR1_W} + \mathrm{BR2} * \mathrm{YR2_W} + \mathrm{BR3} * \mathrm{YR3_W} + \mathrm{BR4} * \mathrm{YR4_W})}{\mathrm{DELT}} \end{cases}$ $\mathrm{TISSUE\ RATES} = \mathrm{RPROT} * \mathrm{YPROT_W} + \mathrm{RRBC} * \mathrm{YRBC_W} + \mathrm{REVF} * \mathrm{YEVF_W} + \mathrm{RSOF0} * \mathrm{YSOF0_W} * (1 - \mathrm{S2HAIR}) * \mathrm{RSOF1} * \mathrm{YSOF1_W} + \mathrm{RSOF2} * \mathrm{YSOF2_W} + \mathrm{H1TOBL} * \mathrm{RLVR1} * \mathrm{YLVR1_W} + \mathrm{RLVR2} * \mathrm{YLVR2_W} + \mathrm{RKDN2} * \mathrm{YKDN2_W} + \mathrm{RCS2B} * \mathrm{YCSUR_W} + \mathrm{RTS2B} * \mathrm{YTSUR_W} + \mathrm{RCORT} * \mathrm{YCVOL_W} + \mathrm{RTRAB} * \mathrm{YTVOL_W} + \mathrm{RBRAN} * \mathrm{YBRAN_W} + \mathrm{F1} * \mathrm{GSCALE} * \mathrm{RSIC} * \mathrm{YSIC_W}$ $\mathrm{INRATE}_{\mathrm{TISSUE}} = \frac{\mathrm{TISSUE\ RATES}}{\mathrm{DELT}}$ $\mathrm{OUTRATE} = \mathrm{RPLS} + \mathrm{RDECAY}$

Model	Submodel	Equation
Biokinetic	Plasma	IF DELT*OUTRATE >50: $\mathrm{YPLS_W} = \frac{1}{\mathrm{OUTRATE}} * \mathrm{YPLS_0} - \frac{\mathrm{INRATE}}{\mathrm{OUTRATE}} + \frac{\mathrm{INRATE} * \mathrm{DELT}}{\mathrm{OUTRATE}}$ IF DELT*OUTRATE ≤50: $\mathrm{YPLS_W} = \left(\frac{1 - \mathrm{e}^{(-\mathrm{OUTRATE}*\mathrm{DELT})}}{\mathrm{RDECAY} + \mathrm{RPLS}} * \mathrm{YPLS_0} - \frac{\mathrm{INRATE}}{\mathrm{RDECAY} + \mathrm{RPLS}}\right) + \frac{\mathrm{INRATE} * \mathrm{DELT}}{\mathrm{OUTRATE}}$ $\mathrm{INRATE} = \begin{cases} \text{ACUTE: } \mathrm{INRATE_{TISSUE}} \\ \text{CHRONIC: } \mathrm{INRATE_{TISSUE}} + \mathrm{CRONIC} \\ \text{INHALATION: } \mathrm{INRATE_{TISSUE}} + \frac{(1.0 + \mathrm{CILIAR}) * (\mathrm{BR1} * \mathrm{YR1_W} + \mathrm{BR2} * \mathrm{YR2_W} + \mathrm{BR3} * \mathrm{YR3_W} + \mathrm{BR4} * \mathrm{YR4_W})}{\mathrm{DELT}} \end{cases}$ $\mathrm{TISSUE\ RATES} = \mathrm{RPROT} * \mathrm{YPROT_W} + \mathrm{RRBC} * \mathrm{YRBC_W} + \mathrm{REVF} * \mathrm{YEVF_W} + \mathrm{RSOF0} * \mathrm{YSOF0_W} * (1 - \mathrm{S2HAIR}) * \mathrm{RSOF1} * \mathrm{YSOF1_W} + \mathrm{RSOF2} * \mathrm{YSOF2_W} + \mathrm{H1TOBL} * \mathrm{RLVR1} * \mathrm{YLVR1_W} + \mathrm{RLVER2} * \mathrm{YLVR2_W} + \mathrm{RKDN2} * \mathrm{YKDN2_W} + \mathrm{RCS2B} * \mathrm{YCSUR_W} + \mathrm{RTS2B} * \mathrm{YTSUR_W} + \mathrm{RCORT} * \mathrm{YCVOL_W} + \mathrm{RTRAB} * \mathrm{YTVOL_W} + \mathrm{RBRAN} * \mathrm{YBRAN_W} + \mathrm{F1} * \mathrm{GSCALE} * \mathrm{RSIC} * \mathrm{YSIC_W}$ $\mathrm{INRATE_{TISSUE}} = \frac{\mathrm{TISSUE\ RATES}}{\mathrm{DELT}}$ $\mathrm{OUTRATE} = \mathrm{RPLS} + \mathrm{RDECAY}$

Model	Submodel	Equation
Biokinetics	Plasma Protein	IF DELT*OUTRATE >50: $\mathrm{YPROT}_0 = \frac{\mathrm{INRATE}}{\mathrm{OUTRATE}}$ IF DELT*OUTRATE ≤50: $\mathrm{YPROT}_0 = \left(\mathrm{YPROT}_0 - \left(\frac{\mathrm{INRATE}}{\mathrm{OUTRATE}}\right)\right) * e^{(-\mathrm{OUTRATE}*\mathrm{DELT})} + \frac{\mathrm{INRATE}}{\mathrm{OUTRATE}}$ $\mathrm{INRATE} = \frac{\mathrm{TPROT} * \mathrm{CF} * \mathrm{BTEMP}}{\mathrm{DELT}}$ $\mathrm{OUTRATE} = \mathrm{RPROT} + \mathrm{RDECAY}$

Model	Submodel	Equation
Biokinetics	Plasma Protein	IF DELT*OUTRATE >50: $\mathrm{YPROT_W} = \frac{1}{\mathrm{OUTRATE}} * \mathrm{YPROT_0} - \frac{\mathrm{INRATE}}{\mathrm{OUTRATE}} + \frac{\mathrm{INRATE} * \mathrm{DELT}}{\mathrm{OUTRATE}}$ IF DELT*OUTRATE ≤50: $\mathrm{YPROT_W} = \left(\frac{1 - e^{(-\mathrm{OUTRATE} * \mathrm{DELT})}}{\mathrm{OUTRATE}} * \mathrm{YPROT_0} - \frac{\mathrm{INRATE}}{\mathrm{OUTRATE}}\right) + \frac{\mathrm{INRATE} * \mathrm{DELT}}{\mathrm{OUTRATE}}$ $\mathrm{INRATE} = \frac{\mathrm{TPROT} * \mathrm{CF} * \mathrm{BTEMP}}{\mathrm{DELT}}$ $\mathrm{OUTRATE} = \mathrm{RDECAY} + \mathrm{RPROT}$

Model	Submodel	Equation
Biokinetics	RBC	IF DELT*OUTRATE >50: $\mathrm{YRBC}_0 = \frac{\mathrm{INRATE}}{\mathrm{OUTRATE}}$ IF DELT*OUTRATE ≤50: $\mathrm{YRBC}_0 = \left(\mathrm{YRBC}_0 - \left(\frac{\mathrm{INRATE}}{\mathrm{OUTRATE}}\right)\right) * e^{(-\mathrm{OUTRATE}*\mathrm{DELT})} + \frac{\mathrm{INRATE}}{\mathrm{OUTRATE}}$ $\mathrm{INRATE} = \frac{\mathrm{TOORBC} * \mathrm{BTEMP}}{\mathrm{DELT}}$ $\mathrm{OUTRATE} = \mathrm{RRBC} + \mathrm{RDECAY}$

Model	Submodel	Equation
Biokinetics	RBC	IF DELT*OUTRATE >50: $\mathrm{YRBC_W} = \frac{1}{\mathrm{OUTRATE}} * \mathrm{YRBC_0} - \frac{\mathrm{INRATE}}{\mathrm{OUTRATE}} + \frac{\mathrm{INRATE} * \mathrm{DELT}}{\mathrm{OUTRATE}}$ IF DELT*OUTRATE ≤50: $\mathrm{YRBC_W} = \left(\frac{1 - e^{(-\mathrm{OUTRATE} * \mathrm{DELT})}}{\mathrm{OUTRATE}} * \mathrm{YRBC_0} - \frac{\mathrm{INRATE}}{\mathrm{OUTRATE}}\right) + \frac{\mathrm{INRATE} * \mathrm{DELT}}{\mathrm{OUTRATE}}$ $\mathrm{INRATE} = \frac{\mathrm{TOORBC} * \mathrm{BTEMP}}{\mathrm{DELT}}$ $\mathrm{OUTRATE} = \mathrm{RRBC+RDECAY}$

Model	Submodel	Equation
Biokinetics	EVF	IF DELT*OUTRATE >50: $\mathrm{YEVF}_0 = \frac{\mathrm{INRATE}}{\mathrm{OUTRATE}}$ IF DELT*OUTRATE ≤50: $\mathrm{YEVF}_0 = \left(\mathrm{YEVF}_0 - \left(\frac{\mathrm{INRATE}}{\mathrm{OUTRATE}}\right)\right) * \mathrm{e}^{(-\mathrm{OUTRATE}*\mathrm{DELT})} + \frac{\mathrm{INRATE}}{\mathrm{OUTRATE}}$ $\mathrm{INRATE} = \frac{\mathrm{TEVF} * \mathrm{CF} * \mathrm{BTEMP}}{\mathrm{DELT}}$ $\mathrm{OUTRATE} = \mathrm{REVF} + \mathrm{RDECAY}$

Model	Submodel	Equation
Biokinetics	EVF	IF DELT*OUTRATE >50: $\mathrm{YEVF_W} = \frac{1}{\mathrm{OUTRATE}} * \mathrm{YEVF_0} - \frac{\mathrm{INRATE}}{\mathrm{OUTRATE}} + \frac{\mathrm{INRATE} * \mathrm{DELT}}{\mathrm{OUTRATE}}$ IF DELT*OUTRATE ≤50: $\mathrm{YEVF_W} = \left(\frac{1 - \mathrm{e}^{(-\mathrm{OUTRATE}*\mathrm{DELT})}}{\mathrm{OUTRATE}} * \mathrm{YEVF_0} - \frac{\mathrm{INRATE}}{\mathrm{OUTRATE}}\right) + \frac{\mathrm{INRATE} * \mathrm{DELT}}{\mathrm{OUTRATE}}$ $\mathrm{INRATE} = \frac{\mathrm{TEVF} * \mathrm{CF} * \mathrm{BTEMP}}{\mathrm{DELT}}$ $\mathrm{OUTRATE} = \mathrm{REVF} + \mathrm{RDECAY}$

Model	Submodel	Equation
Biokinetics	Brain	IF DELT*OUTRATE >50: $\mathrm{YBRAN}_0 = \frac{\mathrm{INRATE}}{\mathrm{OUTRATE}}$ IF DELT*OUTRATE ≤50: $\mathrm{YBRAN}_0 = \left(\mathrm{YBRAN}_0 - \left(\frac{\mathrm{INRATE}}{\mathrm{OUTRATE}}\right)\right) * e^{(-\mathrm{OUTRATE}*\mathrm{DELT})} + \frac{\mathrm{INRATE}}{\mathrm{OUTRATE}}$ $\mathrm{INRATE} = \frac{\mathrm{TBRAN} * \mathrm{CF} * \mathrm{BTEMP}}{\mathrm{DELT}}$ $\mathrm{OUTRATE} = \mathrm{RBRAN} + \mathrm{RDECAY}$

Model	Submodel	Equation
Biokinetics	Brain	IF DELT*OUTRATE >50: $\mathrm{YBRAN_W} = \frac{1}{\mathrm{OUTRATE}} * \mathrm{YBRAN_0} - \frac{\mathrm{INRATE}}{\mathrm{OUTRATE}} + \frac{\mathrm{INRATE} * \mathrm{DELT}}{\mathrm{OUTRATE}}$ IF DELT*OUTRATE ≤50: $\mathrm{YBRAN_W} = \left(\frac{1 - e^{(-\mathrm{OUTRATE} * \mathrm{DELT})}}{\mathrm{OUTRATE}} * \mathrm{YBRAN_0} - \frac{\mathrm{INRATE}}{\mathrm{OUTRATE}}\right) + \frac{\mathrm{INRATE} * \mathrm{DELT}}{\mathrm{OUTRATE}}$ $\mathrm{INRATE} = \frac{\mathrm{TBRAN} * \mathrm{CF} * \mathrm{BTEMP}}{\mathrm{DELT}}$ $\mathrm{OUTRATE} = \mathrm{RBRAN} + \mathrm{RDECAY}$

Model	Submodel	Equation
Biokinetics	Kidney	IF DELT*OUTRATE >50: $\mathrm{YKDN1}_0 = \frac{\mathrm{INRATE}}{\mathrm{OUTRATE}}$ IF DELT*OUTRATE ≤50: $\mathrm{YKDN1}_0 = \left(\mathrm{YKDN1}_0 - \left(\frac{\mathrm{INRATE}}{\mathrm{OUTRATE}}\right)\right) * e^{(-\mathrm{OUTRATE}*\mathrm{DELT})} + \frac{\mathrm{INRATE}}{\mathrm{OUTRATE}}$ $\mathrm{INRATE} = \frac{\mathrm{TKDN1} * \mathrm{CF} * \mathrm{BTEMP}}{\mathrm{DELT}}$ $\mathrm{OUTRATE} = \mathrm{RKDN1} + \mathrm{RDECAY}$

Model	Submodel	Equation
Biokinetics	Kidney	IF DELT*OUTRATE >50: $\mathrm{YKDN1_W} = \frac{1}{\mathrm{OUTRATE}} * \mathrm{YKDN1_0} - \frac{\mathrm{INRATE}}{\mathrm{OUTRATE}} + \frac{\mathrm{INRATE} * \mathrm{DELT}}{\mathrm{OUTRATE}}$ IF DELT*OUTRATE ≤50: $\mathrm{YKDN1_W} = \left(\frac{1 - \mathrm{e}^{(-\mathrm{OUTRATE} * \mathrm{DELT})}}{\mathrm{OUTRATE}} * \mathrm{YKDN1_0} - \frac{\mathrm{INRATE}}{\mathrm{OUTRATE}}\right) + \frac{\mathrm{INRATE} * \mathrm{DELT}}{\mathrm{OUTRATE}}$ $\mathrm{INRATE} = \frac{\mathrm{TKDN1} * \mathrm{CF} * \mathrm{BTEMP}}{\mathrm{DELT}}$ $\mathrm{OUTRATE} = \mathrm{RKDN1} + \mathrm{RDECAY}$

Model	Submodel	Equation
Biokinetics	Kidney	IF DELT*OUTRATE >50: $\mathrm{YKDN2}_0 = \frac{\mathrm{INRATE}}{\mathrm{OUTRATE}}$ IF DELT*OUTRATE ≤50: $\mathrm{YKDN2}_0 = \left(\mathrm{YKDN2}_0 - \left(\frac{\mathrm{INRATE}}{\mathrm{OUTRATE}}\right)\right) * e^{(-\mathrm{OUTRATE}*\mathrm{DELT})} + \frac{\mathrm{INRATE}}{\mathrm{OUTRATE}}$ $\mathrm{INRATE} = \frac{\mathrm{TKDN2} * \mathrm{CF} * \mathrm{BTEMP}}{\mathrm{DELT}}$ $\mathrm{OUTRATE} = \mathrm{RKDN2} + \mathrm{RDECAY}$

Model	Submodel	Equation
Biokinetics	Kidney	IF DELT*OUTRATE >50: $\mathrm{YKDN2_W} = \frac{1}{\mathrm{OUTRATE}} * \mathrm{YKDN2_0} - \frac{\mathrm{INRATE}}{\mathrm{OUTRATE}} + \frac{\mathrm{INRATE} * \mathrm{DELT}}{\mathrm{OUTRATE}}$ IF DELT*OUTRATE ≤50: $\mathrm{YKDN2_W} = \left(\frac{1 - e^{(-\mathrm{OUTRATE} * \mathrm{DELT})}}{\mathrm{OUTRATE}} * \mathrm{YKDN2_0} - \frac{\mathrm{INRATE}}{\mathrm{OUTRATE}}\right) + \frac{\mathrm{INRATE} * \mathrm{DELT}}{\mathrm{OUTRATE}}$ $\mathrm{INRATE} = \frac{\mathrm{TKDN2} * \mathrm{CF} * \mathrm{BTEMP}}{\mathrm{DELT}}$ $\mathrm{OUTRATE} = \mathrm{RKDN2} + \mathrm{RDECAY}$

Model	Submodel	Equation
Biokinetics	Bladder	IF DELT*OUTRATE >50: $\mathrm{YBLAD}_0 = \frac{\mathrm{INRATE}}{\mathrm{OUTRATE}}$ IF DELT*OUTRATE ≤50: $\mathrm{YBLAD}_0 = \left(\mathrm{YBLAD}_0 - \left(\frac{\mathrm{INRATE}}{\mathrm{OUTRATE}}\right)\right) * \mathrm{e}^{(-\mathrm{OUTRATE}*\mathrm{DELT})} + \frac{\mathrm{INRATE}}{\mathrm{OUTRATE}}$ $\mathrm{INRATE} = \frac{\mathrm{TURIN} * \mathrm{CF} * \mathrm{BTEMP} + \mathrm{RKDN1} * \mathrm{YKDN1}_{\mathrm{W}}}{\mathrm{DELT}}$ $\mathrm{OUTRATE} = \mathrm{RBLAD} + \mathrm{RDECAY}$

Model	Submodel	Equation
Biokinetics	Bladder	IF DELT*OUTRATE >50: $\mathrm{YBLAD_W} = \frac{1}{\mathrm{OUTRATE}} * \mathrm{YBLAD_0} - \frac{\mathrm{INRATE}}{\mathrm{OUTRATE}} + \frac{\mathrm{INRATE} * \mathrm{DELT}}{\mathrm{OUTRATE}}$ IF DELT*OUTRATE ≤50: $\mathrm{YBLAD_W} = \left(\frac{1 - \mathrm{e}^{(-\mathrm{OUTRATE}*\mathrm{DELT})}}{\mathrm{OUTRATE}} * \mathrm{YBLAD_0} - \frac{\mathrm{INRATE}}{\mathrm{OUTRATE}}\right) + \frac{\mathrm{INRATE} * \mathrm{DELT}}{\mathrm{OUTRATE}}$ $\mathrm{INRATE} = \frac{\mathrm{TURIN} * \mathrm{CF} * \mathrm{BTEMP} + \mathrm{RKDN1} * \mathrm{YKDN1_W}}{\mathrm{DELT}}$ $\mathrm{OUTRATE} = \mathrm{RBLAD} + \mathrm{RDECAY}$

Model	Submodel	Equation
Biokinetics	Liver	IF DELT*OUTRATE >50: $YLVR1_0 = \frac{INRATE}{OUTRATE}$ IF DELT*OUTRATE ≤50: $YLVR1_0 = \left(YLVR1_0 - \left(\frac{INRATE}{OUTRATE}\right)\right) * e^{(-OUTRATE*DELT)} + \frac{INRATE}{OUTRATE}$ $INRATE = \frac{TLVR1 * CF * BTEMP}{DELT}$ $OUTRATE = RLVR1 + RDECAY$

Model	Submodel	Equation
Biokinetics	Liver	IF DELT*OUTRATE >50: $\mathrm{YLVR1_W} = \frac{1}{\mathrm{OUTRATE}} * \mathrm{YLVR1_0} - \frac{\mathrm{INRATE}}{\mathrm{OUTRATE}} + \frac{\mathrm{INRATE} * \mathrm{DELT}}{\mathrm{OUTRATE}}$ IF DELT*OUTRATE ≤50: $\mathrm{YLVR1_W} = \left(\frac{1 - \mathrm{e}^{(-\mathrm{OUTRATE}*\mathrm{DELT})}}{\mathrm{OUTRATE}} * \mathrm{YLVR1_0} - \frac{\mathrm{INRATE}}{\mathrm{OUTRATE}}\right) + \frac{\mathrm{INRATE} * \mathrm{DELT}}{\mathrm{OUTRATE}}$ $\mathrm{INRATE} = \frac{\mathrm{TLVR1} * \mathrm{CF} * \mathrm{BTEMP}}{\mathrm{DELT}}$ $\mathrm{OUTRATE} = \mathrm{RLVR1} + \mathrm{RDECAY}$

Model	Submodel	Equation
Biokinetics	Liver	IF DELT*OUTRATE >50: $\mathrm{YLVR2}_0 = \frac{\mathrm{INRATE}}{\mathrm{OUTRATE}}$ IF DELT*OUTRATE ≤50: $\mathrm{YLVR2}_0 = \left(\mathrm{YLVR2}_0 - \left(\frac{\mathrm{INRATE}}{\mathrm{OUTRATE}}\right)\right) * e^{(-\mathrm{OUTRATE}*\mathrm{DELT})} + \frac{\mathrm{INRATE}}{\mathrm{OUTRATE}}$ $\mathrm{INRATE} = \frac{\mathrm{H1TOH2} * \mathrm{RLVR1} * \mathrm{YLVR1}_W}{\mathrm{DELT}}$ $\mathrm{OUTRATE} = \mathrm{RLVR2} + \mathrm{RDECAY}$

Model	Submodel	Equation
Biokinetics	Liver	IF DELT*OUTRATE >50: $\mathrm{YLVR2_W} = \frac{1}{\mathrm{OUTRATE}} * \mathrm{YLVR2_0} - \frac{\mathrm{INRATE}}{\mathrm{OUTRATE}} + \frac{\mathrm{INRATE} * \mathrm{DELT}}{\mathrm{OUTRATE}}$ IF DELT*OUTRATE ≤50: $\mathrm{YLVR2_W} = \left(\frac{1 - e^{(-\mathrm{OUTRATE} * \mathrm{DELT})}}{\mathrm{OUTRATE}} * \mathrm{YLVR2_0} - \frac{\mathrm{INRATE}}{\mathrm{OUTRATE}}\right) + \frac{\mathrm{INRATE} * \mathrm{DELT}}{\mathrm{OUTRATE}}$ $\mathrm{INRATE} = \frac{\mathrm{H1TOH2} * \mathrm{RLVR1} * \mathrm{YLVR1_W}}{\mathrm{DELT}}$ $\mathrm{OUTRATE} = \mathrm{RLVR2} + \mathrm{RDECAY}$

Model	Submodel	Equation
Biokinetics	Soft Tissue	IF DELT*OUTRATE >50: $\mathrm{YSOF0}_0 = \frac{\mathrm{INRATE}}{\mathrm{OUTRATE}}$ IF DELT*OUTRATE ≤50: $\mathrm{YSOF0}_0 = \left(\mathrm{YSOF0}_0 - \left(\frac{\mathrm{INRATE}}{\mathrm{OUTRATE}}\right)\right) * \mathrm{e}^{(-\mathrm{OUTRATE}*\mathrm{DELT})} + \frac{\mathrm{INRATE}}{\mathrm{OUTRATE}}$ $\mathrm{INRATE} = \frac{\mathrm{TSOF0} * \mathrm{CF} * \mathrm{BTEMP}}{\mathrm{DELT}}$ $\mathrm{OUTRATE} = \mathrm{RSOF0} + \mathrm{RDECAY}$

Model	Submodel	Equation
Biokinetics	Soft Tissue	IF DELT*OUTRATE >50: $\mathrm{YSOF0_W} = \frac{1}{\mathrm{OUTRATE}} * \mathrm{YSOF0_0} - \frac{\mathrm{INRATE}}{\mathrm{OUTRATE}} + \frac{\mathrm{INRATE} * \mathrm{DELT}}{\mathrm{OUTRATE}}$ IF DELT*OUTRATE ≤50: $\mathrm{YSOF0_W} = \left(\frac{1 - \mathrm{e}^{(-\mathrm{OUTRATE}*\mathrm{DELT})}}{\mathrm{OUTRATE}} * \mathrm{YSOF0_0} - \frac{\mathrm{INRATE}}{\mathrm{OUTRATE}}\right) + \frac{\mathrm{INRATE} * \mathrm{DELT}}{\mathrm{OUTRATE}}$ $\mathrm{INRATE} = \frac{\mathrm{TSOF0} * \mathrm{CF} * \mathrm{BTEMP}}{\mathrm{DELT}}$ $\mathrm{OUTRATE} = \mathrm{RSOF0} + \mathrm{RDECAY}$

Model	Submodel	Equation
Biokinetics	Soft Tissue	IF DELT*OUTRATE >50: $\mathrm{YSOF1}_0 = \frac{\mathrm{INRATE}}{\mathrm{OUTRATE}}$ IF DELT*OUTRATE ≤50: $\mathrm{YSOF1}_0 = \left(\mathrm{YSOF1}_0 - \left(\frac{\mathrm{INRATE}}{\mathrm{OUTRATE}}\right)\right) * \mathrm{e}^{(-\mathrm{OUTRATE}*\mathrm{DELT})} + \frac{\mathrm{INRATE}}{\mathrm{OUTRATE}}$ $\mathrm{INRATE} = \frac{\mathrm{TSOF01} * \mathrm{CF} * \mathrm{BTEMP}}{\mathrm{DELT}}$ $\mathrm{OUTRATE} = \mathrm{RSOF1} + \mathrm{RDECAY}$

Model	Submodel	Equation
Biokinetics	Soft Tissue	IF DELT*OUTRATE >50: $\mathrm{YSOF1_W} = \frac{1}{\mathrm{OUTRATE}} * \mathrm{YSOF1_0} - \frac{\mathrm{INRATE}}{\mathrm{OUTRATE}} + \frac{\mathrm{INRATE} * \mathrm{DELT}}{\mathrm{OUTRATE}}$ IF DELT*OUTRATE ≤50: $\mathrm{YSOF1_W} = \left(\frac{1 - \mathrm{e}^{(-\mathrm{OUTRATE}*\mathrm{DELT})}}{\mathrm{OUTRATE}} * \mathrm{YSOF1_0} - \frac{\mathrm{INRATE}}{\mathrm{OUTRATE}}\right) + \frac{\mathrm{INRATE} * \mathrm{DELT}}{\mathrm{OUTRATE}}$ $\mathrm{INRATE} = \frac{\mathrm{TSOF1} * \mathrm{CF} * \mathrm{BTEMP}}{\mathrm{DELT}}$ $\mathrm{OUTRATE} = \mathrm{RSOF1} + \mathrm{RDECAY}$

Model	Submodel	Equation
Biokinetics	Soft Tissue	IF DELT*OUTRATE >50: $\mathrm{YSOF2}_0 = \frac{\mathrm{INRATE}}{\mathrm{OUTRATE}}$ IF DELT*OUTRATE ≤50: $\mathrm{YSOF2}_0 = \left(\mathrm{YSOF2}_0 - \left(\frac{\mathrm{INRATE}}{\mathrm{OUTRATE}}\right)\right) * \mathrm{e}^{(-\mathrm{OUTRATE}*\mathrm{DELT})} + \frac{\mathrm{INRATE}}{\mathrm{OUTRATE}}$ $\mathrm{INRATE} = \frac{\mathrm{TSOF02} * \mathrm{CF} * \mathrm{BTEMP}}{\mathrm{DELT}}$ $\mathrm{OUTRATE} = \mathrm{RSOF2} + \mathrm{RDECAY}$

Model	Submodel	Equation
Biokinetics	Soft Tissue	IF DELT*OUTRATE >50: $\mathrm{YSOF2_W} = \frac{1}{\mathrm{OUTRATE}} * \mathrm{YSOF2_0} - \frac{\mathrm{INRATE}}{\mathrm{OUTRATE}} + \frac{\mathrm{INRATE} * \mathrm{DELT}}{\mathrm{OUTRATE}}$ IF DELT*OUTRATE ≤50: $\mathrm{YSOF2_W} = \left(\frac{1 - e^{(-\mathrm{OUTRATE}*\mathrm{DELT})}}{\mathrm{OUTRATE}} * \mathrm{YSOF2_0} - \frac{\mathrm{INRATE}}{\mathrm{OUTRATE}}\right) + \frac{\mathrm{INRATE} * \mathrm{DELT}}{\mathrm{OUTRATE}}$ $\mathrm{INRATE} = \frac{\mathrm{TSOF2} * \mathrm{CF} * \mathrm{BTEMP}}{\mathrm{DELT}}$ $\mathrm{OUTRATE} = \mathrm{RSOF2} + \mathrm{RDECAY}$

Model	Submodel	Equation
Biokinetics	Bone	IF DELT*OUTRATE >50: $\mathrm{YCDIF}_0 = \frac{\mathrm{INRATE}}{\mathrm{OUTRATE}}$ IF DELT*OUTRATE ≤50: $\mathrm{YCDIF}_0 = \left(\mathrm{YCDIF}_0 - \left(\frac{\mathrm{INRATE}}{\mathrm{OUTRATE}}\right)\right) * e^{(-\mathrm{OUTRATE}*\mathrm{DELT})} + \frac{\mathrm{INRATE}}{\mathrm{OUTRATE}}$ $\mathrm{INRATE} = \frac{\mathrm{RCS2DF} * \mathrm{YCSUR}_W}{\mathrm{DELT}}$ $\mathrm{OUTRATE} = \mathrm{RDF2CS} + \mathrm{RDF2DC} + \mathrm{RDECAY}$

Model	Submodel	Equation
Biokinetics	Bone	IF DELT*OUTRATE >50: $\mathrm{YCDIF_W} = \frac{1}{\mathrm{OUTRATE}} * \mathrm{YCDIF_0} - \frac{\mathrm{INRATE}}{\mathrm{OUTRATE}} + \frac{\mathrm{INRATE} * \mathrm{DELT}}{\mathrm{OUTRATE}}$ IF DELT*OUTRATE ≤50: $\mathrm{YCDIF_W} = \left(\frac{1 - \mathrm{e}^{(-\mathrm{OUTRATE}*\mathrm{DELT})}}{\mathrm{OUTRATE}} * \mathrm{YCDIF_0} - \frac{\mathrm{INRATE}}{\mathrm{OUTRATE}}\right) + \frac{\mathrm{INRATE} * \mathrm{DELT}}{\mathrm{OUTRATE}}$ $\mathrm{INRATE} = \frac{\mathrm{RCS2DF} * \mathrm{YCSUR_W}}{\mathrm{DELT}}$ $\mathrm{OUTRATE} = \mathrm{RDF2CS} + \mathrm{RDF2DC} + \mathrm{RDECAY}$

Model	Submodel	Equation
Biokinetics	Bone	IF DELT*OUTRATE >50: $\mathrm{YCSUR_0} = \frac{\mathrm{INRATE}}{\mathrm{OUTRATE}}$ IF DELT*OUTRATE ≤50: $\mathrm{YCSUR_0} = \left(\mathrm{YCSUR_0} - \left(\frac{\mathrm{INRATE}}{\mathrm{OUTRATE}}\right)\right) * \mathrm{e}^{(-\mathrm{OUTRATE}*\mathrm{DELT})} + \frac{\mathrm{INRATE}}{\mathrm{OUTRATE}}$ $\mathrm{INRATE} = \frac{(\mathrm{TBONE} * (1.0 - \mathrm{TFRAC}) * \mathrm{CF} * \mathrm{BTEMP} * \mathrm{RDF2CS} * \mathrm{YCDIF_W}}{\mathrm{DELT}}$ $\mathrm{OUTRATE} = \mathrm{RCS2B} + \mathrm{RCS2DF} + \mathrm{RDECAY}$

Model	Submodel	Equation
Biokinetics	Bone	IF DELT*OUTRATE >50: $\mathrm{YCSUR_W} = \frac{1}{\mathrm{OUTRATE}} * \mathrm{YCSUR_0} - \frac{\mathrm{INRATE}}{\mathrm{OUTRATE}} + \frac{\mathrm{INRATE} * \mathrm{DELT}}{\mathrm{OUTRATE}}$ IF DELT*OUTRATE ≤50: $\mathrm{YCSUR_W} = \left(\frac{1 - e^{(-\mathrm{OUTRATE} * \mathrm{DELT})}}{\mathrm{OUTRATE}} * \mathrm{YCSUR_0} - \frac{\mathrm{INRATE}}{\mathrm{OUTRATE}}\right) + \frac{\mathrm{INRATE} * \mathrm{DELT}}{\mathrm{OUTRATE}}$ $\mathrm{INRATE} = \frac{(\mathrm{TBONE} * (1.0 - \mathrm{TFRAC}) * \mathrm{CF} * \mathrm{BTEMP} * \mathrm{RDF2CS} * \mathrm{YCDIF_W}}{\mathrm{DELT}}$ $\mathrm{OUTRATE} = \mathrm{RCS2B} + \mathrm{RCS2DF} + \mathrm{RDECAY}$

Model	Submodel	Equation
Biokinetics	Bone	IF DELT*OUTRATE >50: $YCVOL_0 = \frac{INRATE}{OUTRATE}$ IF DELT*OUTRATE ≤50: $YCVOL_0 = \left(YCVOL_0 - \left(\frac{INRATE}{OUTRATE}\right)\right) * e^{(-OUTRATE*DELT)} + \frac{INRATE}{OUTRATE}$ $INRATE = \frac{RDF2DC * YCDIF_W}{DELT}$ $OUTRATE = RCORT + RDECAY$

Model	Submodel	Equation
Biokinetics	Bone	IF DELT*OUTRATE >50: $\mathrm{YCVOL_W} = \frac{1}{\mathrm{OUTRATE}} * \mathrm{YCVOL_0} - \frac{\mathrm{INRATE}}{\mathrm{OUTRATE}} + \frac{\mathrm{INRATE} * \mathrm{DELT}}{\mathrm{OUTRATE}}$ IF DELT*OUTRATE ≤50: $\mathrm{YCVOL_W} = \left(\frac{1 - e^{(-\mathrm{OUTRATE} * \mathrm{DELT})}}{\mathrm{OUTRATE}} * \mathrm{YCVOL_0} - \frac{\mathrm{INRATE}}{\mathrm{OUTRATE}}\right) + \frac{\mathrm{INRATE} * \mathrm{DELT}}{\mathrm{OUTRATE}}$ $\mathrm{INRATE} = \frac{\mathrm{RDF2DC} * \mathrm{YCDIF_W}}{\mathrm{DELT}}$ $\mathrm{OUTRATE} = \mathrm{RCORT} + \mathrm{RDECAY}$

Model	Submodel	Equation
Biokinetics	Bone	IF DELT*OUTRATE >50: $\mathrm{YTDIF}_0 = \frac{\mathrm{INRATE}}{\mathrm{OUTRATE}}$ IF DELT*OUTRATE ≤50: $\mathrm{YTDIF}_0 = \left(\mathrm{YTDIF}_0 - \left(\frac{\mathrm{INRATE}}{\mathrm{OUTRATE}}\right)\right) * \mathrm{e}^{(-\mathrm{OUTRATE}*\mathrm{DELT})} + \frac{\mathrm{INRATE}}{\mathrm{OUTRATE}}$ $\mathrm{INRATE} = \frac{\mathrm{RTS2DF} * \mathrm{YTSUR}_W}{\mathrm{DELT}}$ $\mathrm{OUTRATE} = \mathrm{RDF2TS} + \mathrm{RDF2DT} + \mathrm{RDECAY}$

Model	Submodel	Equation
Biokinetics	Bone	IF DELT*OUTRATE >50: $\mathrm{YTDIF_W} = \frac{1}{\mathrm{OUTRATE}} * \mathrm{YTDIF_0} - \frac{\mathrm{INRATE}}{\mathrm{OUTRATE}} + \frac{\mathrm{INRATE} * \mathrm{DELT}}{\mathrm{OUTRATE}}$ IF DELT*OUTRATE ≤50: $\mathrm{YTDIF_W} = \left(\frac{1 - \mathrm{e}^{(-\mathrm{OUTRATE}*\mathrm{DELT})}}{\mathrm{OUTRATE}} * \mathrm{YTDIF_0} - \frac{\mathrm{INRATE}}{\mathrm{OUTRATE}}\right) + \frac{\mathrm{INRATE} * \mathrm{DELT}}{\mathrm{OUTRATE}}$ $\mathrm{INRATE} = \frac{\mathrm{RTS2DF} * \mathrm{YTSUR_W}}{\mathrm{DELT}}$ $\mathrm{OUTRATE} = \mathrm{RDF2TS} + \mathrm{RDF2DT} + \mathrm{RDECAY}$

Model	Submodel	Equation
Biokinetics	Bone	IF DELT*OUTRATE >50: $\mathrm{YTSUR}_0 = \frac{\mathrm{INRATE}}{\mathrm{OUTRATE}}$ IF DELT*OUTRATE ≤50: $\mathrm{YTSUR}_0 = \left(\mathrm{YTSUR}_0 - \left(\frac{\mathrm{INRATE}}{\mathrm{OUTRATE}}\right)\right) * \mathrm{e}^{(-\mathrm{OUTRATE}*\mathrm{DELT})} + \frac{\mathrm{INRATE}}{\mathrm{OUTRATE}}$ $\mathrm{INRATE} = \frac{\mathrm{TBONE} * \mathrm{TFRAC} * \mathrm{CF} * \mathrm{BTEMP} * \mathrm{RDF2TS} * \mathrm{YTDIF}_\mathrm{W}}{\mathrm{DELT}}$ $\mathrm{OUTRATE} = \mathrm{RTS2B} + \mathrm{RTS2DF} + \mathrm{RDECAY}$

Model	Submodel	Equation
Biokinetics	Bone	IF DELT*OUTRATE >50: $\mathrm{YTSUR_W} = \frac{1}{\mathrm{OUTRATE}} * \mathrm{YTSUR_0} - \frac{\mathrm{INRATE}}{\mathrm{OUTRATE}} + \frac{\mathrm{INRATE} * \mathrm{DELT}}{\mathrm{OUTRATE}}$ IF DELT*OUTRATE ≤50: $\mathrm{YTSUR_W} = \left(\frac{1 - e^{(-\mathrm{OUTRATE} * \mathrm{DELT})}}{\mathrm{OUTRATE}} * \mathrm{YTSUR_0} - \frac{\mathrm{INRATE}}{\mathrm{OUTRATE}}\right) + \frac{\mathrm{INRATE} * \mathrm{DELT}}{\mathrm{OUTRATE}}$ $\mathrm{INRATE} = \frac{\mathrm{TBONE} * \mathrm{TFRAC} * \mathrm{CF} * \mathrm{BTEMP} * \mathrm{RDF2TS} * \mathrm{YTDIF_W}}{\mathrm{DELT}}$ $\mathrm{OUTRATE} = \mathrm{RTS2B} + \mathrm{RTS2DF} + \mathrm{RDECAY}$

Model	Submodel	Equation
Biokinetics	Bone	IF DELT*OUTRATE >50: $\mathrm{YTVOL}_0 = \frac{\mathrm{INRATE}}{\mathrm{OUTRATE}}$ IF DELT*OUTRATE ≤50: $\mathrm{YTVOL}_0 = \left(\mathrm{YTVOL}_0 - \left(\frac{\mathrm{INRATE}}{\mathrm{OUTRATE}}\right)\right) * \mathrm{e}^{(-\mathrm{OUTRATE}*\mathrm{DELT})} + \frac{\mathrm{INRATE}}{\mathrm{OUTRATE}}$ $\mathrm{INRATE} = \frac{\mathrm{RDF2DT} * \mathrm{YTDIF}_W}{\mathrm{DELT}}$ $\mathrm{OUTRATE} = \mathrm{RTRAB} + \mathrm{RDECAY}$

Model	Submodel	Equation
Biokinetics	Bone	IF DELT*OUTRATE >50: $\mathrm{YTVOL_W} = \frac{1}{\mathrm{OUTRATE}} * \mathrm{YTVOL_0} - \frac{\mathrm{INRATE}}{\mathrm{OUTRATE}} + \frac{\mathrm{INRATE} * \mathrm{DELT}}{\mathrm{OUTRATE}}$ IF DELT*OUTRATE ≤50: $\mathrm{YTVOL_W} = \left(\frac{1 - \mathrm{e}^{(-\mathrm{OUTRATE}*\mathrm{DELT})}}{\mathrm{OUTRATE}} * \mathrm{YTVOL_0} - \frac{\mathrm{INRATE}}{\mathrm{OUTRATE}}\right) + \frac{\mathrm{INRATE} * \mathrm{DELT}}{\mathrm{OUTRATE}}$ $\mathrm{INRATE} = \frac{\mathrm{RDF2DT} * \mathrm{YTDIF_W}}{\mathrm{DELT}}$ $\mathrm{OUTRATE} = \mathrm{RTRAB} + \mathrm{RDECAY}$
Lead Masses in Tissues at Birth		
Biokinetics	Blood	$\mathrm{YRBC} = \mathrm{RBCIN} * \frac{\mathrm{BLDMOT} * \mathrm{BRATIO} * 3}{\mathrm{RBCIN}}$
Biokinetics	Brain	$\mathrm{YBRAN} = \mathrm{BRANIN} * \frac{\mathrm{BLDMOT} * \mathrm{BRATIO} * 3}{\mathrm{RBCIN}}$

Model	Submodel	Equation
Biokinetics	Kidney	$YKDN2 = RENIN * \frac{BLDMOT * BRATIO * 3}{RBCIN}$
Biokinetics	Liver	$YLVR2 = HEPIN * \frac{BLDMOT * BRATIO * 3}{RBCIN}$
Biokinetics	Soft Tissue	$YSOF2 = SOFIN * \frac{BLDMOT * BRATIO * 3}{RBCIN}$
Biokinetics	Bone	$YCVOL = 0.8 * \frac{BLDMOT * BRATIO * 3}{RBCIN}$
Biokinetics	Bone	$YTVOL = 0.2 * \frac{BLDMOT * BRATIO * 3}{RBCIN}$
Composite lead masses in tissues		
Biokinetics	Blood	$YBLUD = YPLAS + YRBC$
Biokinetics	Plasma	$YPLAS = YPLS + YPROT$

Model	Submodel	Equation
Biokinetics	Plasma	$\mathrm{YPLAS_W} = \mathrm{YPLS_W} + \mathrm{YPROT_W}$
Biokinetics	RBC	$\mathrm{SUMRBC} = \mathrm{SUMRBC} + \mathrm{YRBC_W}$
Biokinetics	Kidney	$\mathrm{YKDNE} = \mathrm{YKDNI} + \mathrm{YKDN2}$
Biokinetics	Liver	$\mathrm{YLIVR} = \mathrm{YLVR1} + \mathrm{YLVR2}$
Biokinetics	Lung	$\mathrm{YLUNG} = \mathrm{YR1} + \mathrm{YR2} + \mathrm{YR3} + \mathrm{YR4}$
Biokinetics	Soft Tissue	$\mathrm{YSOFT} = \mathrm{YSOF0} + \mathrm{YSOF1} + \mathrm{YSOF2}$
Biokinetics	Bone	$\mathrm{YCORT} = \mathrm{YCSUR} + \mathrm{YCDIF} + \mathrm{YCVOL}$
Biokinetics	Bone	$\mathrm{YTRAB} = \mathrm{YRSUR} + \mathrm{YTDIF} + \mathrm{YTVOL}$
Biokinetics	Bone	$\mathrm{YSKEL} = \mathrm{YCVOL} + \mathrm{YTVOL} + \mathrm{YCSUR} + \mathrm{YTSUR} + \mathrm{YCDIF} + \mathrm{YTDIF}$
Biokinetics	Body	$\mathrm{TBODY1} = \mathrm{YPLAS} + \mathrm{YRBC} + \mathrm{YEVF} + \mathrm{YSOF0} + \mathrm{YSOF1} + \mathrm{YSOF2} + \mathrm{YBRAN} + \mathrm{YCVOL} + \mathrm{YTVOL} + \mathrm{YCSUR} + \mathrm{YTSUR} + \mathrm{YCDIF} + \mathrm{YTDIF} + \mathrm{YKDNE} + \mathrm{YLIVR}$
Biokinetics	Body	$\mathrm{TBODY2} = \mathrm{TBODY1} + \mathrm{YR1} + \mathrm{YR2} + \mathrm{YR3} + \mathrm{YR4} + \mathrm{YBLAD} + \mathrm{YSTMC} + \mathrm{YSIC} + \mathrm{YULIC} + \mathrm{YLLIC}$

Model	Submodel	Equation
Fraction of lead in tissues relative to total body burden or blood		
Biokinetics	Blood	$\mathrm{BLDFRC} = \frac{\mathrm{YBLUD}}{\mathrm{TBODY1}}$
Biokinetics	Plasma	$\mathrm{PLSRBC} = \frac{\mathrm{YPLAS}}{\mathrm{YBLUD}}$
Biokinetics	Plasma	$\mathrm{PCENT} = \frac{100 * \mathrm{YPLAS}}{\mathrm{YBLUD}}$
Biokinetics	Brain	$\mathrm{BRNFRC} = \frac{\mathrm{YBRN}}{\mathrm{TBODY1}}$
Biokinetics	Kidney	$\mathrm{RENFRC} = \frac{\mathrm{YKDNE}}{\mathrm{TBODY1}}$
Biokinetics	Liver	$\mathrm{HEPFRC} = \frac{\mathrm{YLIVR}}{\mathrm{TBODY1}}$
Biokinetics	Soft Tissue	$\mathrm{OTHFRC} = \frac{\mathrm{YSOFT}}{\mathrm{TBODY1}}$
Biokinetics	Bone	$\mathrm{BONFRC} = \frac{YSKEL}{\mathrm{TBODY1}}$
Tissue-specific lead concentrations (µg/g or µg/dL)		
Biokinetics	Blood	$\mathrm{BLCONC} = \frac{\mathrm{YBLUD}}{\mathrm{AMTBLD}}$
Biokinetics	Plasma	$\mathrm{DECPLS} = \frac{\mathrm{YPLAS}}{\mathrm{PLSVOL}}$

Model	Submodel	Equation
Biokinetics	RBC	$\mathrm{RBCONC} = \frac{\mathrm{YRBC}}{\mathrm{BLDHCT} * \mathrm{AMTBLD}}$
Biokinetics	Kidney	$\mathrm{RENCON} = \frac{\mathrm{YKDNE}}{\mathrm{KIDWT}}$
Biokinetics	Liver	$\mathrm{LIVCON} = \frac{\mathrm{YLIVR}}{\mathrm{LIVWT}}$
Biokinetics	Bone	$\mathrm{CRTCON} = \frac{\mathrm{YCORT}}{\mathrm{CORTWT}}$
Biokinetics	Bone	$\mathrm{TRBCON} = \frac{\mathrm{YTRAB}}{\mathrm{TRABWT}}$
Biokinetics	Bone	$\mathrm{ASHCON} = \frac{\mathrm{YSKEL}}{\mathrm{TSKELWT}}$
Biokinetics	Bone	$\mathrm{CRTCONBM} = \frac{\mathrm{CRTCON}}{0.55}$
Biokinetics	Bone	$\mathrm{TRBCONBM} = \frac{\mathrm{TRBCON}}{0.5}$
Lead excretion (µg or µg/day)		
Biokinetics	Urine	$\mathrm{YURIN} = \mathrm{YURIN}_0 + \mathrm{INRATE} * \mathrm{DELT}$ $\mathrm{INRATE} = \frac{\mathrm{RBLAD} * \mathrm{YBLAD}_W}{\mathrm{DELT}}$ $\mathrm{URIN} = \mathrm{YURIN} - \mathrm{YURIN}_0$

Model	Submodel	Equation
Biokinetics	Feces	$\mathrm{YFECE} = \mathrm{YFECE}_0 + \mathrm{INRATE} * \mathrm{DELT}$ $\mathrm{INRATE} = \frac{\mathrm{GSCALE} * \mathrm{RLLI} * \mathrm{YLLIC}_W}{\mathrm{DELT}}$
Biokinetics	Sweat	$\mathrm{YSWET} = \mathrm{YSWET}_0 + \mathrm{INRATE} * \mathrm{DELTT}$ $\mathrm{INRATE} = \frac{\mathrm{TSWET} * \mathrm{CF} * \mathrm{BTEMP}}{\mathrm{DELT}}$
Biokinetics	Other	$\mathrm{YHAIR} = \mathrm{YHAIR}_0 + \mathrm{INRATE} * \mathrm{DELT}$ $\mathrm{INRATE} = \frac{\mathrm{S2HAIR} * \mathrm{RSOF1} * \mathrm{YSOF1}_W}{\mathrm{DELT}}$
Biokinetics	Total	$\mathrm{TOTEXC} = \mathrm{YURIN} + \mathrm{YFECE} + \mathrm{YSWET} + \mathrm{YHAIR}$
Clearance (day^{-1})		
Biokinetics	Urine	$\mathrm{CLEAR} = \frac{\mathrm{URINE}}{\mathrm{DELT}} * \frac{1}{\mathrm{YPLAS}}$
Biokinetics	Blood	$\mathrm{BCLEAR} = 100 * \frac{\mathrm{URIN}}{\mathrm{DELT}} * \frac{1}{\mathrm{YBLUD}}$

1

APPENDIX B – ALL AGES LEAD MODEL (AALM.FOR) PARAMETERS

TABLE B-1. ALL AGES LEAD MODEL PARAMETER DESCRIPTIONS

Variable	Units	Form	Type	Explanation
EXPOSURE MODEL PARAMETERS				
Age_air_discrete	day	A	F	Age for discrete air Pb concentration
Age_air_V	day	A	F	Age for air ventilation rate
Age_dust_discrete	day	A	F	Age for discrete dust Pb concentration
Age_dust_IR	day	A	F	Age for dust ingestion rate
Age_food_discrete	day	A	F	Age for discrete food Pb concentration
Age_other_discrete	day	A	F	Age for discrete other Pb concentration
Age_soil_discrete	day	A	F	Age for discrete soil Pb concentration
Age_soil_IR	day	A	F	Age for indoor soil ingestion rate
Age_water_discrete	day	A	F	Age for discrete water Pb concentration
Age_water_IR	day	A	F	Age for water ingestion rate
Air_baseline	µg/m^3	C	F	Baseline air Pb concentration used in exposure pulse train
Air_i; i= 1, 2,3	µg/m^3	A	F	Air Pb concentrations for discrete exposures
Air_pulse	µg/m^3	C	F	Air Pb concentration used in exposure pulse train
Air_discrete_weighted	µg/m^3	V	F	Weighted average air Pb concentrations for discrete exposures
Dust_baseline	µg/g	C	F	Baseline dust Pb concentration used in exposure pulse train
Dust_i; i= 1, 2,3	µg/g	A	F	Dust Pb concentrations for discrete exposures
Dust_pulse	µg/g	C	F	Dust Pb concentration used in exposure pulse train
Dust_discrete_weigted	µg/g	V	F	Weighted average dust Pb concentrations for discrete exposures
f_Air_i; i= 1,2,3	unitless	A	F	Fraction of discrete Air_i contributing to daily air Pb exposure
f_Dust_i; i= 1,2	unitless	A	F	Fraction of discrete Dust_i contributing to daily dust Pb exposure
f_IR_soil	unitless	C	F	Soil fraction of soil and dust ingestion rate (IR_sd)
f_Other_i; i= 1,2,3	unitless	A	F	Fraction of discrete Other_i contributing to daily other Pb exposure
f_pulse_air	unitless	C	F	Fraction of air daily air exposure from pulse train
f_pulse_dust	unitless	C	F	Fraction of daily dust exposure from pulse train
f_pulse_other	unitless	C	F	Fraction of daily other exposure from pulse train

Variable	Units	Form	Type	Explanation
f_pulse_soil	unitless	C	F	Fraction of daily soil exposure from pulse train
f_pulse_water	unitless	C	F	Fraction of daily water exposure from pulse train
f_Soil_i; i= 1,2	unitless	A	F	Fraction of discrete Soil_i contributing to daily soil Pb exposure
f_Water_i; i= 1,2,3	unitless	A	F	Fraction of discrete Water_i contributing to daily water Pb exposure
Food_baseline	µg/day	C	F	Baseline food Pb intake used in exposure pulse train
Food_i; i= 1, 2,3	µg/day	A	F	Food Pb intakes for discrete exposures
Food_pulse	µg/day	C	F	Food Pb intake used in exposure pulse train
Food_total_discrete	µg/day	V	F	Total food Pb intakes for discrete exposures
IN_air_discrete	µg/day	V	F	Pb intake from discrete exposures to air
IN_air_pulse	µg/day	V	F	Pb intake from pulse train exposures to air
IN_air_total	µg/day	V	F	Pb intake from combined discrete and pulse train exposures to air
IN_dust_discrete	µg/day	V	F	Pb intake from discrete exposures to dust
IN_dust_pulse	µg/day	V	F	Pb intake from pulse train exposures to dust
IN_dust_total	µg/day	V	F	Pb intake from combined discrete and pulse train exposures to dust
IN_food_discrete	µg/day	V	F	Pb intake from discrete exposures to food
IN_food_pulse	µg/day	V	F	Pb intake from pulse train intakes from food
IN_food_total	µg/day	V	F	Pb intake from combined discrete and pulse train exposures to food
IN_ingestion_total	µg/day	V	F	Pb intake from all ingestion exposures combined (dust, soil, food, water, other)
IN_other_discrete	µg/day	V	F	Pb intake from discrete exposures to other sources
IN_other_pulse	µg/day	V	F	Pb intake from pulse train intakes from other sources
IN_other_total	µg/day	V	F	Pb intake from combined discrete and pulse train exposures to other sources
IN_soil_discrete	µg/day	V	F	Pb intake from discrete exposures to soil
IN_soil_pulse	µg/day	V	F	Pb intake from pulse train exposures to soil
IN_soil_total	µg/day	V	F	Pb intake from combined discrete and pulse train exposures to soil
IN_water_discrete	µg/day	V	F	Pb intake from discrete exposures to water
IN_water_pulse	µg/day	V	F	Pb intake from pulse train exposures to water
IN_water_total	µg/day	V	F	Pb intake from combined discrete and pulse train exposures to water

Variable	Units	Form	Type	Explanation
IR_dust	g/day	C	F	Dust ingestion rate for dust Pb exposures
IR_soil	g/day	C	F	Dust ingestion rate for soil Pb exposures
IR_sd	g/day	A	F	Combined soil and dust ingestion rate for Pb exposures
IR_water	L/day	C	F	Dust ingestion rate for water Pb exposures
Other_baseline	µg/day	C	F	Baseline other Pb intake used in exposure pulse train
Other_i; i= 1, 2,3	µg/day	A	F	Food Pb intakes for discrete exposures
Other_pulse	µg/day	C	F	Other Pb intake used in exposure pulse train
Other_total_discrete	µg/day	V	F	Total other Pb intakes for discrete exposures
Pulse_i_period_air; i=1,2	day	C	F	Period for pulse train exposure to air
Pulse_i_period_dust; i=1,2	day	C	F	Period for pulse train exposure to dust
Pulse_i_period_food; i=1,2	day	C	F	Period for pulse train exposure to food
Pulse_i_period_other; i=1,2	day	C	F	Period for pulse train exposure to other
Pulse_i_period_soil; i=1,2	day	C	F	Period for pulse train exposure to soil
Pulse_i_period_water; i=1,2	day	C	F	Period for pulse train exposure to water
Pulse_i_width_air; i=1,2	day	C	F	Width for pulse train exposure to air
Pulse_i_width_dust; i=1,2	day	C	F	Width for pulse train exposure to dust
Pulse_i_width_food; i=1,2	day	C	F	Width for pulse train exposure to food
Pulse_i_width_other; i=1,2	day	C	F	Width for pulse train exposure to other
Pulse_i_width_soil; i=1,2	day	C	F	Width for pulse train exposure to indoor soil
Pulse_i_width_water; i=1,2	day	C	F	Width for pulse train exposure to water
Pulse_start_air	day	C	F	Start age for pulse train exposure to air
Pulse_start_dust	day	C	F	Start age for pulse train exposure to dust
Pulse_start_food	day	C	F	Start age for pulse train exposure to food
Pulse_start_other	day	C	F	Start age for pulse train exposure to other
Pulse_start_soil	day	C	F	Start age for pulse train exposure to indoor soil

Variable	Units	Form	Type	Explanation
Pulse_start_water	day	C	F	Start age for pulse train exposure to water
Pulse_stop_air	day	C	F	Stop age for pulse train exposure to air
Pulse_stop_dust	day	C	F	Stop age for pulse train exposure to dust
Pulse_stop_food	day	C	F	Stop age for pulse train exposure to food
Pulse_stop_other	day	C	F	Stop age for pulse train exposure to other
Pulse_stop_soil	day	C	F	Stop age for pulse train exposure to soil
Pulse_stop_water	day	C	F	Stop age for pulse train exposure to water
RBA_dust	unitless	C	F	Relative bioavailability of dust Pb
RBA_food	unitless	C	F	Relative bioavailability of food Pb
RBA_other	unitless	C	F	Relative bioavailability of other Pb
RBA_soil	unitless	C	F	Relative bioavailability of soil Pb
RBA_water	unitless	C	F	Relative bioavailability of water Pb
Sex	unitless	C	S	Female of male
Soil_baseline	µg/g	C	F	Baseline dust Pb concentration used in exposure pulse train
Soil_i; i= 1, 2,3	µg/g	A	F	Soil Pb concentrations for discrete exposures
Soil_pulse	µg/g	C	F	Soil Pb concentration used in exposure pulse train
Soil_discrete_weigted	µg/g	V	F	Weighted average soil Pb concentrations for discrete exposures
Water_baseline	µg/L	C	F	Baseline water Pb concentration used in exposure pulse train
Water_i; i= 1, 2,3	µg/L	A	F	Water Pb concentrations for discrete exposures
Water_pulse	µg/L	C	F	Water Pb concentration used in exposure pulse train
Water_discrete_weighted	µg/L	V	F	Weighted average water Pb concentrations for discrete exposures
V_air	m^3/day	A	F	Ventilation rate for air Pb exposures
BIOKINETIC MODEL PARAMETERS				
AF1	unitless	A	F	Fractional absorption of Pb from small intestine – age array (see F1)
AGESCAL	unitless	A	F	Age scaling factor for gastrointestinal transfers – age array (see GSCALE)
AGEYEAR	year	V	F	Age from birth in years
AMTBLD	dL	V	F	Amount of blood at time(t)
ARBLAD	day^{-1}	A	F	Rate coefficient for Pb transfer from urinary bladder to urine – age array (see RBLAD)

Variable	Units	Form	Type	Explanation
ARBRAN	day^{-1}	A	F	Rate coefficient for Pb transfer from brain to diffusible plasma – age array (see RBRAN)
ARCORT	day^{-1}	A	F	Rate coefficient for Pb transfer from non-exchangeable cortical bone to diffusible plasma – age array (see RCORT)
ARCS2B	day^{-1}	A	F	Rate coefficient for Pb transfer from cortical bone surface to diffusible plasma – age array (see RCS2B)
ARCSDF	day^{-1}	A	F	Rate coefficient for Pb transfer from cortical bone surface to exchangeable cortical bone – age array (see RCS2DF)
ARD2CS	day^{-1}	A	F	Rate coefficient for Pb transfer from exchangeable cortical bone to cortical bone surface – age array (see RDF2CS)
ARD2DC	day^{-1}	A	F	Rate coefficient for Pb transfer from exchangeable cortical bone to non-exchangeable cortical bone – age array (see RDF2DC)
ARD2DT	day^{-1}	A	F	Rate coefficient for Pb transfer from exchangeable trabecular bone to non-exchangeable trabecular bone – age array (see RDF2DT)
ARD2TS	day^{-1}	A	F	Rate coefficient for Pb transfer from exchangeable trabecular bone to trabecular bone surface – age array (see RDF2DS)
ARKDN2	day^{-1}	A	F	Rate coefficient for transfer from kidney compartment 2 to diffusible plasma – age array (see RKDN2)
ARLVR2	day^{-1}	A	F	Rate coefficient for Pb transfer from the slow liver compartment 2 to diffusible plasma – age array (see RLVR2)
ARRBC	day^{-1}	A	F	Rate coefficient for Pb transfer from RBC to diffusible plasma – age array (see RRBC)
ARTRAB	day^{-1}	A	F	Rate coefficient for Pb transfer from non-exchangeable trabecular bone to diffusible plasma – age array (see RTRAB)
ARTS2B	day^{-1}	A	F	Rate coefficient for Pb transfer from trabecular bone surface to diffusible plasma – age array (see RTS2B)
ARTSDF	day^{-1}	A	F	Rate coefficient for Pb transfer from surface trabecular bone to exchangeable trabecular bone – age array (see RTS2DF)
ASHCON	µg/g	V	F	Pb concentration in skeletal mineral

Variable	Units	Form	Type	Explanation
ATBONE	unitless	A	F	Deposition fraction for Pb from diffusible plasma to surface bone – age array (see TBONE)
ATBRAN	unitless	A	F	Deposition fraction for Pb from diffusible plasma to brain – age array (see RBRAN)
ATFRAC	unitless	A	F	Fraction of diffusible plasma-to-bone deposition that goes to trabecular surface bone – age array (see TFRAC)
ATOSOF0	unitless	A	F	Deposition fraction for Pb from diffusible plasma to soft tissue compartment 0 – age array (see TOSOF0)
ATOSOF1	unitless	A	F	Deposition fraction for Pb from diffusible plasma to soft tissue compartment 1 – age array (see TOSOF1)
ATOSOF2	unitless	A	F	Deposition fraction for Pb from diffusible plasma to soft tissue compartment 2 – age array (see TOSOF2)
BCLEAR	day^{-1}	V	F	Clearance of Pb from blood to urine
BLCONC	µg/dL	V	D	Pb concentration in whole blood
BLDFRC	unitless	V	F	Amount of Pb in blood as a fraction of total body Pb
BLDHCT	unitless	V	F	Blood hematocrit
BLDMOT	µg/dL	C	F	Maternal blood Pb concentration
BLDVOL	dL	V	F	Blood volume as the sum of RBC and plasma volume
BONFRC	unitless	V	F	Amount of Pb in bone as a fraction of total body Pb
BR1	day^{-1}	C	F	Rate coefficient for Pb transfer from RT compartment 1 to diffusible plasma
BR2	day^{-1}	C	F	Rate coefficient for Pb transfer from RT compartment 2 to diffusible plasma
BR3	day^{-1}	C	F	Rate coefficient for Pb transfer from RT compartment 3 to diffusible plasma
BR4	day^{-1}	C	F	Rate coefficient for Pb transfer from RT compartment 4 to diffusible plasma
BRATIO	unitless	C	F	Child (at birth):maternal blood Pb concentration ratio
BRETH	µg/day	V	A	Pb intake rate age array from inhalation of Pb in air (see IN_air_total)
BRNFRC	unitless	V	F	Amount of Pb in brain as a fraction of total body Pb

Variable	Units	Form	Type	Explanation
BRTCRN	µg/day	V	F	Pb intake from inhalation exposure at each age range
BTEMP	µg/day	V	F	Total outflow of Pb from diffusible plasma to all compartments
CF	unitless	V	F	Factor for adjusting Pb deposition fractions from diffusible plasma to account for non-linear uptake of Pb in RBC
CHAGE	day	A	F	Ages at which biokinetics parameters are specified (for each NUMAGE)
CHEL1	unitless	C	I	First day of chelation therapy
CHEL2	unitless	C	I	Last day of chelation therapy
CHLEFF	unitless	C	I	Deposition change factor due to chelation therapy
CHR	µg	A	F	Chronic injection uptakes for each NCHRON
CILIAR	unitless	C	F	Fraction of inhaled Pb transferred to gastrointestinal tract
CORTWT	g	V	F	cortical bone weight
CRONIC	µg	V	F	Chronic injection intake at current integration time step
CRTCON	µg/g	V	F	Pb concentration in cortical bone
CRTCONBM	µg/g	V	F	Pb concentration in cortical bone mineral
CVBONE	mL	V	F	cortical bone volume
DECLTR	µg/dL	V	D	Pb concentration in total blood
DECPLS	µg/dL	V	D	Pb concentration in diffusible plasma
DECRBC	µg/dL	V	D	Pb concentration in RBCs
DELT0	day	C	F	Initial integration time step
DELTA	unitless	A	F	Numerical integration cycle lengths – age array
DELT_i	day	A	F	Array of integration step sizes for each NDELT
EAT	µg/day	A	F	Pb intake rate age array from ingestion of Pb (see IN_ingestion_total)
EATCRN	µg/day	V	F	Pb intake from oral exposure at each age range
ENDDAY	day	C	F	Age and end of simulation
ENDPT	day	A	F	End days for chronic intakes for each NCHRON
EXPAGE	day	C	F	Age at start exposure
F1	unitless	V	F	Fractional absorption of Pb from small intestine at time(t) (see AF1)
FLONG	unitless	A	F	Fraction of total Pb transfer from the exchangeable bone to non-exchangeable bone

Variable	Units	Form	Type	Explanation
GSCALE	unitless	V	F	Age scaling factor for gastrointestinal transfers at time(t) (see AGSCL)
HALF	year	C	F	Age at which body weight is half of WCHILD
HCTA	unitless	C	F	Adult hematocrit
H1TOBL	unitless	C	F	Fraction of Pb transfer out of liver compartment 1 that goes to diffusible plasma
H1TOH2	unitless	C	F	Fraction of Pb transfer out of liver compartment 1 that goes to liver compartment 2
H1TOSI	unitless	C	F	Fraction of Pb transfer out of liver compartment 1 that goes to the small intestine
HEPFRC	unitless	V	F	Amount of Pb in liver as a fraction of total body Pb
IACUTE	unitless	C	I	Switch for acute (1) or chronic array (2) uptakes
ICHEL	unitless	C	I	Switch for chelation simulation off (0) or on (1)
ICYC_i	unitless	A	F	Number of numerical integration cycles for each NDELT
IFETAL	unitless	C	I	Switch for fetal simulation on (1) or off (0)
INMODE	unitless	C	I	Switch for injection (0), inhalation (1), ingestion (2), or combination (3)
IRBC	unitless	C	I	Switch for linear (0) or non-linear (1) RBC uptake
ISKIP	day	C	F	Communication interval
KAPPA	unitless	C	F	Logistic body growth parameter
KIDWT	g	V	F	Kidney weight
LAMBDA	unitless	C	F	Logistic body growth parameter
LINPUT	unitless	C	I	Switch for manual input (0) or array input (1)
LIVCON	µg/g	V	F	Pb concentration in liver
LIVWT	g	V	F	Liver weight
NCHRON	unitless	C	F	Number of different chronic intakes
NCYCLE	unitless	C	F	Maximum number of numerical integration cycles
NDELT	unitless	C	F	Number of times the integration step changes
NUMAGE	unitless	C	F	Number of ages at which biokinetics parameter values are specified
OTHFRC	unitless	V	F	Amount of Pb in other soft tissue as a fraction of total body Pb
PCENT	percent	V	F	Percent of whole blood Pb in plasma
PLSRBC	unitless	V	F	Plasma fraction of Pb in whole blood
PLSVOL	dL	V	F	Plasma volume
POWER	unitless	C	F	Exponent for non-linear deposition of Pb from diffusible plasma to RBC

Variable	Units	Form	Type	Explanation
R1	unitless	C	F	Fraction of inhaled Pb deposited in RT compartment 1
R2	unitless	C	F	Fraction of inhaled Pb deposited in RT compartment 2
R3	unitless	C	F	Fraction of inhaled Pb deposited in RT compartment 3
R4	unitless	C	F	Fraction of inhaled Pb deposited in RT compartment 4
RBCIN	unitless	V	F	Amount of Pb in RBC as a fraction of body Pb, at birth
RBCNL	µg/dL	C	F	Threshold Pb concentration in RBC for non-linear deposition of Pb from diffusible plasma to RBC
RBCON	µg/dL	V	F	Concentration of Pb in RBC
RBCVOL	dL	V	F	RBC volume
RBLAD	day^{-1}	V	F	Rate coefficient for Pb transfer from urinary bladder to urine at time(t) (see ARBLAD)
RBRAN	day^{-1}	V	F	Rate coefficient for Pb transfer from brain to diffusible plasma at time(t) (see ABRAN)
RCORT	day^{-1}	V	F	Rate coefficient for Pb transfer from non-exchangeable cortical bone to diffusible plasma at time(t) (see ACORT)
RCS2B	day^{-1}	V	F	Rate coefficient for Pb transfer from cortical bone surface to diffusible plasma at time(t) (see ARCS2B)
RCS2DF	day^{-1}	V	F	Rate coefficient for Pb transfer from cortical bone surface to exchangeable cortical bone at time(t) (see ARCSDF)
RDECAY	day^{-1}	C	F	Rate coefficient for radioactive decay
RDF2CS	day^{-1}	V	F	Rate coefficient for Pb transfer from exchangeable cortical bone to cortical bone surface at time(t) (see ARD2CS)
RDF2DC	day^{-1}	V	F	Rate coefficient for Pb transfer from exchangeable cortical bone to non-exchangeable cortical bone at time(t) (see ARD2DC)
RDF2DT	day^{-1}	V	F	Rate coefficient for Pb transfer from exchangeable trabecular bone to non-exchangeable trabecular bone at time(t) (see ARD2DT)
RDF2TS	day^{-1}	V	F	Rate coefficient for Pb transfer from exchangeable trabecular bone to trabecular bone surface at time(t) (see ARD2TS)

Variable	Units	Form	Type	Explanation
RDIFF	day^{-1}	A	F	Rate coefficient for Pb transfer from exchangeable bone (cortical or trabecular) to surface and non-exchangeable bone – age array (see FLONG for fraction to non-exchangeable)
RENCON	µg/g	V	F	Pb concentration in kidney
RENFRC	unitless	V	F	Amount of Pb in kidney as a fraction of total body Pb
REVF	day^{-1}	V	F	Rate coefficient for transfer from diffusible plasma to the extravascular fluid
RKDN1	day^{-1}	C	F	Rate coefficient for transfer from kidney compartment 1 to urinary pathway
RKDN2	day^{-1}	V	F	Rate coefficient for transfer from kidney compartment 2 to diffusible plasma at time(t) (see ARKDN2)
RLLI	day^{-1}	C	F	Rate coefficient for Pb transfer from lower large intestine to feces
RLVR1	day^{-1}	C	F	Rate coefficient for Pb transfer from liver compartment 1 to small intestine or diffusible plasma
RLVR2	day^{-1}	V	F	Rate coefficient for Pb transfer from the slow liver compartment 2 to diffusible plasma at time(t) (see ARLVR2)
RPLAS	day^{-1}	C	F	Rate coefficient for Pb transfer from diffusible plasma to all compartments; Note: scaled to bone surface deposition (see RPLS)
RPLS	day^{-1}	V	F	Rate coefficient for Pb transfer from diffusible plasma scaled to bone surface deposition (see RPLAS)
RPROT	day^{-1}	C	F	Rate coefficient for Pb transfer from bound plasma to diffusible plasma
RRBC	day^{-1}	V	F	Rate coefficient for Pb transfer from RBC to diffusible plasma at time(t) (see ARRBC)
RSIC	day^{-1}	C	F	Rate coefficient for Pb transfer from small intestine to upper large intestine
RSOF0	day^{-1}	C	F	Rate coefficient for Pb transfer from soft tissue compartment 0 to diffusible plasma
RSOF1	day^{-1}	C	F	Rate coefficient for Pb transfer from soft tissue compartment 1 to diffusible plasma
RSOF2	day^{-1}	C	F	Rate coefficient for Pb transfer from soft tissue compartment 2 to diffusible plasma
RSTMC	day^{-1}	C	F	Rate coefficient for Pb transfer from stomach to small intestine

Variable	Units	Form	Type	Explanation
RTRAB	day^{-1}	V	F	Rate coefficient for Pb transfer from non-exchangeable trabecular bone to diffusible plasma at time(t) (see ARTRAB)
RTS2B	day^{-1}	V	F	Rate coefficient for Pb transfer from trabecular bone surface to diffusible plasma at time(t) (see ARTS2B)
RTS2DF	day^{-1}	V	F	Rate coefficient for Pb transfer from surface trabecular bone to exchangeable trabecular bone at time(t) (see ARTSDF)
RULI	day^{-1}	C	F	Rate coefficient for Pb transfer from upper large intestine to lower large intestine
S2HAIR	unitless	C	F	Deposition fraction for Pb from soft tissue compartment 1 to other excreta
SATRAT	µg/dL	C	F	Maximum (saturating) concentration of Pb in RBC
SIGMA	µg	V	F	Amount of Pb in all compartments
SIZEVF	unitless	C	F	Relative volume of the EVF compartment compared to plasma (EVF/Plasma)
SOFIN	unitless	C	F	Amount of Pb in other soft tissue as a fraction of total body Pb, at birth
SUMRBC	µg	V	F	Cumulative amount of Pb in RBC over the simulation
TBODY1	µg	V	F	Pb mass in body, excluding bladder, GIT and RT
TBODY2	µg	V	F	Pb mass in body, including bladder, gastrointestinal tract, and RT
TBONE	unitless	V	F	Deposition fraction for Pb from diffusible plasma to surface bone at time(t) (see ATBONE)
TBRAN	unitless	V	F	Deposition fraction for Pb from diffusible plasma to brain at time(t) scaled to bone surface deposition (see TOBRAN)
TEVF	unitless	C	F	Deposition fraction for Pb from diffusible plasma to extravascular fluid
TFECE	unitless	V	F	Deposition fraction for Pb from diffusible plasma directly to the small intestine at time(t) scaled bone surface deposition (not including the transfer from biliary secretion, specified by RLVR1) (see TOFECE)
TFRAC	unitless	V	F	Fraction of diffusible plasma-to-bone deposition that goes to trabecular surface bone at time(t); 1-TFRAC is the fraction that goes to cortical surface bone

Variable	Units	Form	Type	Explanation
TKDN1	unitless	V	F	Deposition fraction for Pb from diffusible plasma to kidney compartment 1 scaled to bone surface deposition (see TOKDN1)
TKDN2	unitless	V	F	Deposition fraction for Pb from diffusible plasma to liver compartment 2 scaled to bone surface deposition (see TOKDN2)
TLVR1	unitless	V	F	Deposition fraction for Pb from diffusible plasma to liver compartment 1 scaled to bone surface deposition (see TOLVR1)
TOBRAN	unitless	A	F	Deposition fraction for Pb from diffusible plasma to brain at time(t) (not scaled for bone surface deposition – see TBRAN)
TOEVF	unitless	C	F	Deposition fraction for Pb from diffusible plasma to extravascular fluid
TOFECE	unitless	C	F	Deposition fraction for Pb from diffusible plasma directly to the small intestine (not including the transfer from biliary secretion, specified by RLVR1, not scaled to bone surface deposition – see TFECE)
TOKDN1	unitless	C	F	Deposition fraction for Pb from diffusible plasma to kidney compartment 1 not scaled to bone surface deposition (see TKDN1)
TOKDN2	unitless	C	F	Deposition fraction for Pb from diffusible plasma to kidney compartment 2 not scaled to bone surface deposition (see TKDN2)
TOLVR1	unitless	C	F	Deposition fraction for Pb from diffusible plasma to liver compartment 2 not scaled to bone surface deposition (see TLVR1)
TOORBC	unitless	V	F	Deposition fraction for Pb from diffusible plasma to RBC adjusted for capacity-limited deposition in RBC and scaled to bone surface deposition
TOPROT	unitless	C	F	Deposition fraction for Pb from diffusible plasma to protein-bound plasma not scaled to bone surface deposition (see TPROT)
TORBC	unitless	C	F	Deposition fraction from diffusible plasma to RBC not scaled to bone surface (see TRBC)
TOSOF0	unitless	A	F	Deposition fraction for Pb from diffusible plasma to soft tissue compartment 0 at time (t), not scaled to bone surface deposition (see TSOF0)
TOSOF1	unitless	A	F	Deposition fraction for Pb from diffusible plasma to soft tissue compartment 1 at time (t), not scaled to bone surface deposition (see TSOF1)

Variable	Units	Form	Type	Explanation
TOSOF2	unitless	A	F	Deposition fraction from diffusible plasma to soft tissue compartment 2 at time (t), not scaled to bone surface deposition (see TSOF2)
TOSWET	unitless	C	F	Deposition fraction for Pb from diffusible plasma to sweat not scaled to bone surface deposition (see TSWET)
TOTEXC	µg	V	F	Pb mass in urine, feces, sweat, hair, nails, and skin
TOURIN	unitless	C	F	Deposition fraction for Pb from diffusible plasma to urine not scaled to bone surface deposition (see TURIN)
TPROT	unitless	V	F	Deposition fraction for Pb from diffusible plasma to protein-bound plasma scaled to bone surface deposition (see TOPROT)
TRABWT	g	F	F	Trabecular bone weight
TRBC	unitless	V	F	Deposition fraction for Pb from diffusible plasma to RBCs, below non-linear threshold, scaled to bone surface deposition (see TORBC)
TRBCON	µg/g	V	F	Pb concentration in trabecular bone
TRBCONBM	µg/g	V	F	Pb concentration in trabecular bone mineral
TSKELWT	g	V	F	Skeleton weight
TSOF0	unitless	V	F	Deposition fraction for Pb from diffusible plasma to soft tissue compartment 0 at time (t), scaled to bone surface deposition (see TOSF0)
TSOF1	unitless	V	F	Deposition fraction for Pb from diffusible plasma to soft tissue compartment 1 at time (t), scaled to bone surface deposition (see TOSOF1)
TSOF2	unitless	V	F	Deposition fraction from diffusible plasma to soft tissue compartment 2 at time (t), scaled to bone surface deposition (see TOSF2)
TSUM	unitless	V	F	Sum of deposition fractions (TOORBC,TEVF,TPROT,TBONE,TURIN,TFECE,TSWET,TLVR1,TKDN1,TKDN2,TSOF0,TSOF1,TSOF2,TBRAN)
TSWET	unitless	V	F	Deposition fraction for Pb from diffusible plasma to sweat, scaled to bone surface deposition (see TOSWET)
TURIN	unitless	V	F	Deposition fraction for Pb from diffusible plasma to urine, scaled to bone surface deposition (see TOURIN)
TVBONE	mL	V	F	trabecular bone volume
URIN	µg	V	F	Amount of Pb excreted in urine during the integration time step

Variable	Units	Form	Type	Explanation
VBL	L	V	F	Whole blood volume
VBLC	L/kg	C	F	Blood volume fraction of body weight
VBONE	mL	V	F	bone volume
VK	mL	V	F	Kidney volume
VKC	L/kg	C	F	Kidney volume fraction of body weight
VL	mL	V	F	Liver volume
VLC	L/kg	C	F	Liver volume fraction of body weight
VLUC	L/kg	C	F	Lung volume fraction of body weight
VP	mL	V		Lung tissue volume
WADULT	kg	C	F	Maximum body weight
WBIRTH	kg	C	F	Weight at birth
WBODY	kg	V	F	Age-dependent body weight
WBONE	g	V	F	Bone weight
WCHLD	kg	C	F	Maximum body weight achieved during early hyperbolic growth phase.
XMXAGE	day	C	F	End age for biokinetics parameter values array (max NUMAGE)
YBLOOD	µg	V	F	Amount of Pb in blood
$YBRAN_0$	µg	V	F	Amount of Pb in brain at the beginning of each integration cycle
$YBRAN_W$	µg	V	F	Amount of Pb in the brain integrated over the time interval DELT
$YCDIF_0$	µg	V	F	Amount of Pb in the exchangeable volume of cortical bone at the beginning of each integration cycle
$YCDIF_W$	µg	V	F	Amount of Pb in the exchangeable volume of cortical bone integrated over the time interval DELT
YCORT	µg	V	F	Amount of Pb in cortical bone
$YCSUR_0$	µg	V	F	Amount of Pb in cortical bone surface at the beginning of each integration cycle
$YCSUR_W$	µg	V	F	Amount of Pb in the cortical bone surface integrated over the time interval DELT
$YCVOL_0$	µg	V	F	Amount of Pb in non-exchangeable volume of cortical bone at the beginning of each integration cycle
$YCVOL_W$	µg	V	F	Amount of Pb in the non-exchangeable volume of cortical bone over the time interval DELT

Variable	Units	Form	Type	Explanation
$YEVF_0$	µg	V	F	Amount of Pb in extravascular fluid at the beginning of each integration cycle
$YEVF_W$	µg			Amount of extravascular fluid in the brain integrated over the time interval DELT
YFECE	µg	V	F	Amount of Pb excreted in feces
YHAIR	µg	V	F	Amount of Pb excreted by routes other than feces, sweat and urine (e.g., hair, nails, and desquamated skin)
$YKDN1_0$	µg	V	F	Amount of Pb in fast-turnover kidney at the beginning of each integration cycle
$YKDN2_0$	µg	V	F	Amount of Pb in slow-turnover kidney at the beginning of each integration cycle
$YKDN2_W$	µg	V	F	Amount of Pb in the slow-turnover over kidney the time interval DELT
$YKIDN1_W$	µg	V	F	Amount of fast-turnover kidney in the brain integrated over the time interval DELT
$YLLIC_0$	µg	V	F	Amount of Pb in lower portion of large intestine at the beginning of each integration cycle
$YLLIC_W$	µg	V	F	Amount of Pb in the lower portion of large intestine integrated over the time interval DELT
$YLVR1_0$	µg	V	F	Amount of Pb in fast-turnover liver at the beginning of each integration cycle
$YLVR1_W$	µg	V	F	Amount of fast-turnover liver in the brain integrated over the time interval DELT
$YLVR_{20}$	µg	V	F	Amount of Pb in slow-turnover liver at the beginning of each integration cycle
$YLVR2_W$	µg			Amount of slow-turnover liver in the brain integrated over the time interval DELT
YPLAS	µg	V	F	Amount of Pb in plasma (diffusible plus protein bound)
$YPLAS_W$	µg	V	F	Amount of Pb in plasma (diffusible plus protein bound) integrated over the time interval DELT
YPLS0	µg	V	F	Amount of Pb in diffusible plasma (0.69 × YPLAS) at the beginning of each integration cycle
$YPLS_W$	µg	V	F	Amount of Pb in diffusible plasma (0.69 × YPLAS) integrated over the time interval DELT
$YPROT_0$	µg	V	F	Amount of Pb in plasma protein at the beginning of each integration cycle
$YPROT_W$	µg	V	F	Amount of Pb in the plasma protein integrated over the time interval DELT

Variable	Units	Form	Type	Explanation
$YR0_0$	µg	V	F	Amount of Pb in RT region 1 at the beginning of each integration cycle
$YR0_W$	µg	V	F	Amount of Pb in the RT region 1 integrated over the time interval DELT
$YR1_0$	µg	V	F	Amount of Pb in RT region 2 at the beginning of each integration cycle
$YR1_W$	µg	V	F	Amount of Pb in the RT region 2 integrated over the time interval DELT
$YR2_0$	µg	V	F	Amount of Pb in RT region 3 at the beginning of each integration cycle
$YR2_W$	µg	V	F	Amount of Pb in the RT region 3 integrated over the time interval DELT
$YR3_0$	µg	V	F	Amount of Pb in RT region 4 at the beginning of each integration cycle
$YR3_W$	µg	V	F	Amount of Pb in the RT region 4 integrated over the time interval DELT
$YRBC_0$	µg	V	F	Amount of Pb in RBCs at the beginning of each integration cycle
$YRBC_W$	µg	V	F	Amount of Pb in RBCs integrated over the time interval DELT
$YSIC_0$	µg	V	F	Amount of Pb in small intestine at the beginning of each integration cycle
$YSIC_W$	µg	V	F	Amount of Pb in the small intestine integrated over the time interval DELT
YSKEL	µg	V	F	Amount of Pb in bone
$YSOF0_0$	µg	V	F	Amount of Pb in fast-turnover soft tissue at the beginning of each integration cycle
$YSOF0_W$	µg	V	F	Amount of Pb in the fast-turnover soft tissue integrated over the time interval DELT
$YSOF1_0$	µg	V	F	Amount of Pb in intermediate-turnover soft tissue at the beginning of each integration cycle
$YSOF1_W$	µg	V	F	Amount of Pb in the intermediate-turnover soft tissue integrated over the time interval DELT
$YSOF2_0$	µg	V	F	Amount of Pb in slow-turnover soft tissue at the beginning of each integration cycle
$YSOF2_W$	µg	V	F	Amount of Pb in the slow-turnover soft tissue integrated over the time interval DELT
YSOFT	µg	V	F	Amount of Pb in soft tissues
$YSTMC_0$	µg	V	F	Amount of Pb in stomach at the beginning of each integration cycle

Variable	Units	Form	Type	Explanation
$YSTMC_W$	µg	V	F	Amount of Pb in the stomach integrated over the time interval DELT
YSWET	µg	V	F	Amount of Pb excreted in sweat
$YTDIF_0$	µg	V	F	Amount of Pb in exchangeable trabecular bone surface at the beginning of each integration cycle
$YTDIF_W$	µg	V	F	Amount of Pb in the exchangeable trabecular bone surface integrated over the time interval DELT
YTRAB	µg	V	F	Amount of Pb in brain at the beginning of each integration cycle
$YTSUR_0$	µg	V	F	Amount of Pb in trabecular bone surface at the beginning of each integration cycle
$YTSUR_W$	µg	V	F	Amount of Pb in the trabecular bone surface integrated over the time interval DELT
$YTVOL_0$	µg	V	F	Amount of Pb in non-exchangeable volume of trabecular bone at the beginning of each integration cycle
$YTVOL_W$	µg	V	F	Amount of Pb in the non-exchangeable volume of trabecular bone integrated over the time interval DELT
$YULIC_0$	µg	V	F	Amount of Pb in upper portion of lower intestine at the beginning of each integration cycle
$YULIC_W$	µg	V	F	Amount of Pb in the upper portion of lower intestine integrated over the time interval DELT
YURIN	µg	V	F	Amount of Pb in excreted in urine

Abbreviations: A=array; C=constant; F=floating point; I=integer; S=switch; V=variable

1

APPENDIX C – ALL AGES LEAD MODEL (AALM.FOR) EXPOSURE PARAMETER VALUES

The AALM.FOR exposure model includes parameters that are variables (i.e., computed in mathematical expressions), and parameters that are assigned constants or are represented by age arrays. A list of parameters that are assigned constants or are represented by age arrays are presented in Table C-1. The bases for values assigned to each parameter are summarized below. Parameters are presented in alphabetical order, according to the parameter name.

Exposure variables include variables that represent the concentration of Pb in air, indoor dust, soil, food and water, and activity factors that represent the intensity of exposure to contaminated environmental media (e.g., water consumption rates). All exposure variables that are accessible to the user are included in Table C-1. Default values are intended to be central tendency estimates that are representative of the U.S. population. Sources for the default values are provided along with a brief summary of the sources. Some exposure variables were not assigned default values. Some of these variables were considered to be inherently site-specific and assigning default values to them would therefore be arbitrary. For others, reliable sources of data upon which to base a default value were not identified.

In general, the activity factors were taken from the Exposure Factors Handbook (EFH; U.S. EPA, 2011). The EFH recommendations for default values for activity factors are based on thorough reviews of the exposure science literature and independent analyses of exposure data from surveys performed by others. The use of the EFH-recommended default values in the AALM.FOR, when appropriate, also promotes consistency in risk assessments performed by or for the Agency. In some cases, default values were based on recent studies that were not included in the EFH when the studies were deemed to be sufficiently reliable.

A strong preference was placed on basing default values for environmental concentration variables and activity factors on data from statistical surveys that were designed to provide data representative of the entire U.S. Equally important was ensuring that analyses of data from these surveys were done properly to produce unbiased estimates (i.e., properly used the sampling weights in calculating estimates and considered the complex sampling design when calculating standard errors).

AIR CONCENTRATION

AALM Variables: Air_baseline, Air_i, Air_pulse

The AALM.FOR allows the user to define multiple exposures to Pb in air. These can include up to three discrete (i.e., age-specific) exposure concentrations, a constant baseline concentration and up to two pulse trains in which air Pb concentration can vary at inputted durations and periods. Multiple exposures could be used to represent exposures to air Pb in various settings such as outdoor and indoor air; air at the home, school, workplace, or recreational sites; or continuous exposure or intermittent exposures.

Concentrations of Pb in air can be expected to vary considerably by location, depending on proximity to local sources (U.S. EPA, 2013). Based on analysis of data from U.S. national monitoring networks collected during the period 2008-2010, air Pb concentrations were as follows (U.S. EPA, 2013):

	Source Oriented	Non-source Oriented
Mean	0.21	0.012
Median	0.079	0.010
95th percentile	0.88	0.037

Units: µg/m^3

3-month rolling average, 2008-2010

Source-oriented monitors are within one mile of ≥0.5 ton/year emission non-airport source or near airports in which use of leaded aviation fuels are estimated to result in >1 tone/year emissions.

A detailed description the national monitoring networks and related data can be found in U.S. EPA (2013).

Recommendations. Based on these data, 0.01 µg/m^3 is recommended as a default value for the parameter *Air_baseline* to represent average U.S. exposure concentrations distant from substantial emissions sources. For simulations of populations living near emissions sources, the source-oriented average could be used as a default for average air concentrations, however, it should be recognized that air Pb concentrations near emission sources could vary considerably depending on the strength of the source and other geographic and weather factors that would affect dispersion and deposition of emissions.

Although, the default values are based on measurements made of outdoor air, indoor and outdoor air Pb concentrations are expected to be similar if indoor environments that do not have substantial indoor sources of Pb (Clayton et al., 1999; Robertson et al., 1999).

INDOOR DUST LEAD CONCENTRATION

AALM Variables: Dust_baseline, Dust_i, Dust_pulse

The AALM.FOR allows the user to define multiple exposures to Pb in indoor dusts. These can include up to three discrete (i.e., age-specific) exposure concentrations, a constant baseline concentration and up to three pulse trains in which dust Pb concentration can vary at inputted durations and periods. These could be used to represent exposures to Pb in various sources of dust such dusts at various locations (e.g., at the home, school, workplace, or recreational sites); or continuous exposure or intermittent exposures.

The National Human Exposure Assessment Surveys (NHEXAS) provides data on indoor dust Pb concentrations in statistical samples from various locations. Based on data for approximately 250 residences in EPA Region 5 (Great Lakes region), the mean Pb concentrations were as follows (Clayton et al., 1999):

Surface	Window Sill
463	954
(188, 738)	(481, 3164)

Units: µg/g (95% CL)

Based on NHEXAS data for approximately 119 residences in Arizona, the median Pb concentration (XRF) was 21 µg/g (90th percentile: 122; Robertson et al., 1999).

Concentrations of Pb in dusts can be expected to vary considerably by location, depending on proximity to local sources, presence in lead-based paint, and dust cleaning practices (U.S. EPA, 2013). The National

Survey of Lead and Allergens (NSLAH) conducted by the Department of Housing and Urban Development; (Clickner et al., 2002) provides data in Table 5.7 of their report on Pb in residential indoor dusts for a statistical sample of U.S. residences. Based on a sample of approximately 2000 homes, the mean Pb loading (µg/ft^2) were as follows:

Floors (n = 3,894	Window Sills (n = 2,302)	Window Troughs (n = 1,607)
13.6±484	195±1683	1991±12,086

Units: µg/ft^2

Data on dust Pb loading on indoor surfaces (µg Pb/ft^2) provide additional sources estimated of indoor dust Pb concentration (U.S. EPA, 2019). An analysis of data on Pb loading collected as part of the American Healthy Housing Survey (AHHS, Cox et al., 2011) provided the following central estimates for residential Pb loading and concentration (U.S. EPA, 2019):

Loading (µg/ft^2)		Concentration (µg/g)	
Median	Mean	Median	Mean
0.8	1.2	107.8	175.0

Recommendations. Based on the above data, 175 µg/g is recommended as a default value for the parameter *Dust_baseline* to represent average U.S. exposure concentrations distant from substantial current or historical emission sources (e.g., background) that could impact the indoor environment (e.g. track in from contaminated soil). A value of equal to the soil Pb concentration (see section on *Soil Lead Concentration*) is recommended for *Dust_baseline* for simulating residences where soil derived dust is the major source of indoor dust Pb (e.g. no other significant indoor sources such as paint or hobbies). Indoor dust Pb concentrations in residences impacted by Pb-based paint can be expected to vary considerably within and between residences and local exposure conditions should be considered to establish a representative estimate.

SOIL LEAD CONCENTRATION

AALM Variables: Soil_baseline, Soil_i, Soil_pulse

The AALM.FOR allows the user to define multiple exposures to Pb in soil. These can include up to three discrete (i.e., age-specific) exposure concentrations, a constant baseline concentration and up to three pulse trains in which dust Pb concentration can vary at inputted durations and periods. These could be used to represent exposures to Pb in various sources of surface soil such soils at various locations (e.g., at the home, school, workplace, or recreational sites); or continuous exposure or intermittent exposures.

Concentrations of Pb in soils can be expected to vary considerably by location, depending on proximity to local sources (U.S. EPA, 2013). A study conducted by the U.S. Geological Survey measured soil Pb concentrations along a 4000 km east-west transect of the U.S. (Smith et al., 2013; Reimann et al., 2011). Sampling locations were selected to avoid local sources, including roads, buildings, power plants and smelters. The mean concentrations for samples collected a depth of 0–5 cm depth (sieved at 2 mm) were as follows:

Full Transect (n = 4841)	Statewide Average (n = 48)
25	30
(8, 44)[a]	(14, 68)[b]

Units: µg/g.
Statewide average is the average of state means.
[a]5th-95th percentile range
[b]range

Data for individual U.S. states and physiographic provinces are provided in Smith et al. (2013).

NSLAH conducted by the Department of Housing and Urban Development; Clickner et al. (2002) provide data in Table 6.3 of their report on Pb in residential soil for a statistical sample of U.S. residences. Based on a sample of approximately 700 residential yards, the mean Pb concentrations (µg/g) were as follows:

Main Entryway	Dripline 1	Dripline 2	Midyard 1	Midyard 2
235±1094	243±818	404±1613	87±195	123±360

µg/g, mean ± SD

Based on data from the AHHS (Cox et al., 2011; Clickner et al., 2002), the following central estimates for soil Pb concentration were estimated (U.S. EPA, 2019):

Housing Stock	GM	GSD	Median	Mean
Pre-1940	113.4	3.58	113.4	246.8
1940-1977	28.6	2.9	28.6	50.0
Pre-1978	26.3	3.8	26.3	64.1

GM, geometric mean, µg/g; GSD, geometric standard deviation

Recommendations. Based on the above data, 25 µg/g is recommended as a default value for the parameter *Soil_baseline* to represent average U.S. exposure concentrations distant from substantial current or historical emission sources (e.g., background). Means for individual U.S. states ranged 6 to 80 µg/g. These estimates are based on measurements made in soils sieved to <2 mm and which may have underestimated Pb concentration in the fine fraction (e.g. <250 µm or <150 µm) that is typically used to represent the exposure term for the adherence to hand-to-mouth pathway used in risk assessment. The value 50 µg/g is recommended as a value for yard soils associated with post 1940 housing stock and 250 µg/g for older housing stock.

WATER CONCENTRATION

AALM Variables: Water_baseline, Water_i, Water_pulse

The AALM.FOR allows the user to define multiple exposures to Pb in drinking water. These can include up to three discrete (i.e., age-specific) exposure concentrations, a constant baseline concentration and up to two pulse trains in which water Pb concentration can vary at inputted durations and periods. These could be used to represent exposures to Pb in various exposure settings such: home, school, workplace, or recreational sites; or continuous exposure or intermittent exposures.

Concentrations of Pb in drinking water can be expected to vary considerably by location, depending on water source, Pb in service lines and extent of plumbing corrosion (U.S. EPA, 2007a). In residences served by lines containing Pb, first-draw water that has been stagnant in plumbing will tend to have a higher Pb concentration than after the system has been flushed. The NHEXAS provides data on drinking water Pb concentrations in statistical samples from various locations. Based on data for approximately 250 residences in EPA Region 5 (Great Lakes region), the mean Pb concentrations were as follows (Clayton et al., 1999):

First draw	Flushed
3.92	0.84
(3.06, 4.79)	(0.6, 1.07)

Units: µg/L (95% CL)

Based on NHEXAS data for approximately 82 residences in Arizona, median, 75th and 90th percentile of Pb concentrations in flushed unfiltered tap water were 0.4, 0.9, and 1.3 µg/L, respectively (O'Rourke et al., 1999).

The EPA TRW analysed data tap water concentrations reported for the Six-Year Review-ICR dataset. This survey conducted during the period 1998-2005 measured first-draw tap water concentration in residences supplied by approximately 883 public water suppliers in the U.S. Based on this analysis, the mean tap water concentrations were as follows:

Sample Mean	Population Weighted Mean
4.89	0.89
(4.38, 5.39)	(0.78, 1.01)

Units: µg/L (95% CL)
Population weighted mean is weighted for number of people served by each supplier.

Based on data in Supplemental Information from Zartarian et al. (2017), the average, 95th percentile and 99th percentile values from this dataset are 0.89, 2.25 and 13.27 µg/L, respectively. The following central estimates for water Pb concentration were estimated (U.S. EPA, 2019):

GM	GSD	Median	Mean
0.69	2.1	0.69	0.89

GM, geometric mean, µg/g; GSD, geometric standard deviation

Recommendations. Based on the above data, 0.9 µg/L is recommended as a default value for the parameter *Water_baseline* to represent average U.S. exposure concentrations to tap water from public water supplies. This default value may not apply to local conditions that contribute to leaching of Pb into tap water (e.g. Pb service lines, Pb solder, corrosion).

FOOD LEAD INTAKE

AALM Variables: Food_baseline, Food_i, Food_pulse

The AALM.FOR allows the user to define multiple exposures to Pb in food. These can include up to three discrete (i.e., age-specific) food Pb intakes (µg/day), a constant baseline intake and up to two pulse trains

in which food Pb intake can vary at inputted durations and periods. These could be used to represent exposures to Pb in various diets or sources of food (e.g., market basket, home grown produce, local fish or game); or continuous exposure or intermittent exposures.

The rate of Pb intake from food can be expected to vary considerably depending on the diet and age. The NHEXAS provides data on food Pb intakes in statistical samples from various locations (Clayton et al., 1999; Thomas et al., 1999). Based on a sample for 159 residences (children and adults), the mean food Pb intakes was 7.96 µg/day (95% CL: 4.2, 11.6; Clayton et al., 1999).

The EPA TRW estimated food Pb intakes in children based on data from the U.S. Food and Drug Administration Total Diet Studies performed between 1995–2005 (FDA, 2007, 2006) and food consumption data from the National Food Consumption Survey (NCFS) that was performed as part of the Third National Health and Nutrition Examination Survey (NHANES 2003–2006). Age category mean Pb intakes were as follows:

Age Category (months)	Dietary Pb Intake (µg/day)
0 to <12	2.26
12 to <24	1.96
24 to <36	2.13
36 to <48	2.04
40 to <60	1.95
60 to <72	2.05
72 to <84	2.22

Recommendations. Based on the above data, 10 µg/day is recommended as a default value for *Food_baseline* the food Pb intake in adults. This corresponds to an intake of approximately 0.14 µg/kg bw/day which, if extrapolated to children, yield estimates that are similar to those recommended by the EPA TRW, if AALM.FOR growth is assumed:

Age (year)	Female BW (kg)	Male BW (kg)	Female Pb Intake (µg/day)	Male Pb Intake (µg/day)
1	8.9	9.4	1.2	1.3
2	12.3	12.9	1.7	1.8
3	14.6	15.3	2.0	2.1
4	16.4	17.2	2.3	2.4
5	18.0	18.8	2.5	2.6
6	19.7	20.2	2.8	2.8
7	21.7	21.8	3.0	3.1
8	24.2	23.7	3.4	3.3
9	27.7	26.1	3.9	3.7
10	32.1	29.3	4.5	4.1
15	52.5	56.4	7.3	7.9

Age (year)	Female BW (kg)	Male BW (kg)	Female Pb Intake (µg/day)	Male Pb Intake (µg/day)
≥20	56.2	71.4	7.9	10.0

For intake 0.14 µg/kg bw/day.
BW, body weight

The above age array of food Pb intakes are recommended default values for *Food_i*, where *i* would represent age category baseline intakes for the average U.S. diet.

DUST AND SOIL INGESTION RATES

AALM Variables: IR_sd, f_IR_s, IR_dust, IR_soil

The EPA Exposure Factors Handbook (U.S. EPA, 2017) provides the following recommendations for dust and soil ingestion rates to be used in U.S. EPA risk assessments.

Age Category	Dust (g/day)	Soil (g/day)	Dust + Soil (g/day)
<6 months	0.020	0.020	0.040
6 months to 1 year	0.040	0.030	0.070
1 to <2 years	0.050	0.040	0.090
2 to <6 years	0.030	0.030	0.060
1 to 6 years	0.040	0.040	0.080
6 to <12 years	0.030	0.030	0.060
>12 years	0.020	0.010	0.030

The EPA TRW estimated combined soil and dust ingestion rates in children based on the best fit model from von Lindern et al. (2016) and supported by modelled estimates from Ozkaynak et al. (2011) and Wilson et al. (2013). Age category mean ingestion rates were as follows:

Age Category (months)	Soil + Dust (g/day)
0 to 12	0.086
13 to 24	0.094
25 to 36	0.067
37 to 48	0.063
49 to 60	0.067
61 to 72	0.052
73 to 84	0.055

Recommendations. Based on the Exposure Factors Handbook (U.S. EPA, 2017), the following values are recommended as default values for the parameters *IR_dust* and *IR_soil* to represent average U.S. ingestion rates in children and adults. The default values for adults may not represent activities that result in intensive dermal contact with surface dusts, such as construction or excavation.

Age (days)	Dust Ingestion *IR_dust* (g/day)	Soil Ingestion *IR_soil* (g/day)	Combined Dust and Soil *IR_sd* (g/day)	Soil Fraction *f_IR_soil*
0	0.022	0.018	0.040	0.45
90	0.039	0.032	0.070	0.45
365	0.050	0.041	0.090	0.45
1825	0.044	0.036	0.080	0.45
3650	0.033	0.027	0.060	0.45
5475	0.017	0.014	0.030	0.45
9125	0.017	0.014	0.030	0.45
≥18250	0.017	0.014	0.030	0.45

WATER INTAKE RATE

AALM Variables *IR_water*

Water ingestion rate can be expected to vary with age, activity level and environmental factors (e.g. temperature, humidity). U.S. EPA (2011) has recommended the following age-specific water ingestion rates for use in EPA risk assessments of the general population:

Age	Mean Intake (mL/day)	95th Percentile (mL/day)
Birth to <1 mo	184	839
1 to <3 mo	227	896
3 to < 6 mo	362	1056
6 to <12 mo	360	1055
1 to <2 yr	271	837
2 to <3yr	317	877
3 to <6 yr	327	959
6 to <11 yr	414	1316
11 to <16 yr	520	1821
16 to <21 yr	573	1783
18 to <21 yr	681	2368
≥21 yr	1043	2958
≥65 yr	1046	2733
All ages	869	2717

The EPA TRW estimated drinking water intakes rates in children based on and analysis of data from the e 1994–1996 and 1998 Continuing Survey of Food Intakes by Individuals (CSFII; USDA, 2000) as reported by Kahn and Stralka (2009). Age category mean ventilation rates were as follows:

Age Category (months)	Water Intake (L/day)
0 to <12	0.40
12 to <24	0.43
24 to <36	0.51
36 to <48	0.54
40 to <60	0.57
60 to <72	0.60
72 to <84	0.63

Recommendations. Based on the above data, the following values are recommended as default values for the parameter *IR_water* to represent average U.S. drinking water ingestion rates in children and adults:

Age (days)	Water Intake (L/day)
0	0.20
90	0.30
365	0.35
1825	0.35
3650	0.45
5475	0.55
9125	0.70
≥18250	1.04

VENTILATION RATE

AALM Variable: *V_air*

The AALM.FOR assigns values for regional deposition of inhaled Pb (see parameters *B1*, *B2*, *B3*, *B4*; Appendix D and clearance in the RT (see parameter *CILIAR*; Appendix D). Values for these parameters were based on experimental studies conducted adults who inhaled submicron particles from automobile exhausts while they were sedentary. However, regional deposition and clearance in the RT (will depend on numerous factors, including age and particle size, as well as various factors that affect ventilation rates (m^3/day) which vary with age and physical activity. The interrelationships between particle size, clearance, regional deposition and ventilation rate should be considered in assigning values to these parameters for simulating specific populations and exposure settings. these subjects are treated in depth in ICRP (1994).

The ICRP (1994) has recommended the following age-specific activity weighted ventilation rates for use in radiation dosimetry assessments of the general population:

Age	Ventilation (m^3/day) Male	Ventilation (m^3/day) Female	Ventilation (m^3/day) Average
3 mo	2.86	2.86	2.86
1 yr	5.2	5.2	5.2
5 yr	8.76	8.76	8.76
10 yr	15.28	15.28	15.28
15 yr	20.1	15.72	17.91
>17 yr	22.18	17.68	19.93

From ICRP (1994).
Values for children are from Table B.16A
Values for >17 yr are for sedentary workers (Table B.16B)

The above ventilation rates can be matched to corresponding regional deposition rates, also provided in ICRP (1994).

U.S. EPA (2011) has recommended the following age-specific activity weighted ventilation rates for use in EPA risk assessments of the general population:

Age Category	Mean Ventilation (m^3/day)	95th Percentile (m^3/day)
Birth to <1 mo	3.6	7.1
1 to <3 mo	3.5	5.8
3 to < 6 mo	4.1	6.1
6 to <12 mo	5.4	8.0
Birth to <1 yr	5.4	9.2
1 to <2 yr	8.0	12.8
2 to <3yr	8.9	13.7
3 to <6 yr	10.1	13.8
6 to <11 yr	12.0	16.6
11 to <16 yr	15.2	21.9
16 to <21 yr	16.3	24.6
21 to <31 yr	15.7	21.3
31 to <41 yr	16.0	21.4
41 to 51 yr	16.0	21.2
51 to 61 yr	15.7	21.3
61 to 71 yr	14.2	18.1
71 to <81 yr	12.9	16.6
≥ 81 yr	12.2	15.7

The EPA TRW estimated ventilation rates in children based on and analysis of data on total energy expenditure (estimated from doubly labeled water studies) and relationships between energy expenditure

and ventilation rate (Stifelman, 2007; Brochu et al., 2006; IOM, 2005; Layton, 1993). Age category mean ventilation rates were as follows:

Age Category (months)	Ventilation Rate (m^3/day)
0 to <12	3.22
12 to <24	4.97
24 to <36	6.09
36 to <48	6.95
40 to <60	7.68
60 to <72	8.32
72 to <84	8.89

Recommendations. Based on the above data, the following values are recommended as default values for the parameter *V_air* to represent average U.S. ventilation rates in children and adults:

Age (days)	Ventilation (m^3/day)
0	2.9
90	2.9
365	5.2
1825	8.8
3650	15.3
5475	17.9
9125	19.9
≥18250	19.9

RBA_dust. A discussion of available data on RBA of Pb in indoor dust can be found in U.S. EPA (2013). RBA of Pb in house dusts has not been rigorously evaluated quantitatively in humans or in experimental animal models, unlike soil (see section on *RBA_soil*). As with soil, RBA of dust Pb can be expected to vary depending on the Pb mineralogy, physical characteristics of the Pb in the dust (e.g., encapsulated or exposed) and size of the Pb-bearing particles. The RBA for paint Pb mixed with soil (relative to lead acetate) was reported to be approximately 0.72 (95% CI: 0.44, 0.98) in juvenile swine, suggesting that paint Pb dust reaching the gastrointestinal tract maybe highly bioavailable (Casteel et al., 2006). Several studies have measured in vitro bioaccessibility (IVBA) of Pb in residential indoor dust; however, with few exceptions, these have not used IVBA methods for from which RBA can be reliably predicted (Juhasz et al., 2011; Lu et al., 2011; Smith et al., 2011; Roussel et al., 2010; Yu et al., 2006). A study conducted at two sites in EPA Region 7 compared Pb RBA predicted from IVBA using a prediction method that had been validated for soil as described in U.S. EPA (2013). At the Herculaneum site, mean RBA was 0.47 (SD 0.07, 10 samples) for indoor dust and 0.69 (SD 0.03, 12 samples) for soil. At the Omaha site, mean Pb RBA was 0.73 (SD 0.10, 90 samples) for indoor dust and 0.70 (SD 0.10, 45 samples) for soil.

RBA_soil. A discussion of available data on RBA of Pb in soil can be found in U.S. EPA (2013). RBA of soil Pb can be expected to vary depending on the Pb mineralogy, physical characteristics of the Pb in the soil (e.g., encapsulated or exposed) and size of the Pb-bearing particles. The EPA TRW has recommended a value of 60% for RBA for ingested soil Pb based on analysis of data on soil Pb RBA estimated in bioassays of juvenile swine (Bannon et al., 2009; Smith et al., 2009; Casteel et al., 2006; Marschner et al., 2006); and other unpublished data collected as part of site risk assessments. The soil RBA measured in the swine assay is equivalent to the ratio of the absorbed fraction of an ingested dose of soil Pb to that of water-soluble Pb acetate. Analysis of 31 soils (excluding galena-enriched soil, soils from firing ranges, and soils sieved at >250 µm) resulted in a median RBA estimate of 60% with the 5th–95th percentile range from 11–97%; the mean RBA is 54% ±32 SD. RBA estimates for soils collected from eight firing ranges were approximately 100% (mean =108% ± 18; Bannon et al., 2009). The relatively high RBA for the firing range soils may reflect the high abundance of relatively un-encapsulated lead carbonate (30-90% abundance) and lead oxide (1–60%) in these soils. Similarly, a soil sample (low Pb concentration) mixed with a National Institute of Standards and Technology paint standard (55% lead carbonate, 44% lead oxide) also had a relatively high bioavailability (72%; Casteel et al., 2006). Samples of smelter slag, or soils contaminated with slag, had relatively low RBA (14–40%, n = 3) as did a sample from a mine tailings pile (RBA = 6%), and a sample of finely ground galena mixed with soil (1%; Casteel et al., 2006). A single estimate for RBA of interior dust was 51% for a sample collected at the Herculaneum site.

RBA_food. RBA of water-soluble Pb dissolved in food is assumed to be 1. RBA of Pb in foods has not been studied and it is possible that certain exposure settings could result in ingestion of Pb that has and TBA <1 in association with food. For example, adherence of surface dust, soil or sediments to consumed foods.

RBA_water. RBA of Pb dissolved in water is assumed to be 1. This is based on evidence that dissolution of Pb from the soil/mineralogical matrix in the stomach appears to be the major process that renders soil Pb bioaccessible for absorption in the GI tract (U.S. EPA, 2013, 2007b). However, his may not apply to Pb-bearing particles suspended in surface water and this may be relevant to certain exposure settings (e.g., incidental ingestion of suspended sediments during activities such as swimming or play near shorelines).

Recommendations. Based on the above data, the following values are recommended as default values for the parameters *RBA_dust, RBA_soil, RBA_food, RBA_water*:

Medium	RBA
Dust_paint[a]	1
Dust_soil[b]	0.6
Soil	0.6
Food	1
Water	1

[a]Indoor dust derived from Pb-based paint
[b]Indoor dust derived from soil

TABLE C-1. LIST OF PARAMETERS THAT ARE ASSIGNED CONSTANTS OR ARE REPRESENTED BY AGE ARRAYS

Variable	Units	Form	Type	Explanation	Value		Reference
Air_baseline	µg/m^3	C	F	Baseline air Pb concentration used in exposure pulse train	0.01–0.2		(U.S. EPA, 2013)
Air_i; i= 1, 2,3	µg/m^3	A	F	Air Pb concentrations for discrete exposures	User defined		
Air_pulse	µg/m^3	C	F	Air Pb concentration used in exposure pulse train	User defined		
Dust_baseline	µg/g	C	F	Baseline indoor dust Pb concentration used in exposure pulse train	Residential	175	(U.S. EPA, 2019)
Dust_i; i= 1, 2,3	µg/g	A	F	Dust Pb concentrations for discrete exposures	User defined		
Dust_pulse	µg/g	C	F	Dust Pb concentration used in exposure pulse train	User defined		
f_Air_i; i= 1,2,3	unitless	A	F	Fraction of discrete Air_i contributing to daily air Pb exposure	User defined		See Chapter 16 of U.S. EPA (2011)
f_Dust_i; i= 1,2	unitless	A	F	Fraction of discrete Dust_i contributing to daily dust Pb exposure	User defined		See Chapter 16 of U.S. EPA (2011)
f_IR_soil	unitless	C	F	Soil fraction of combined dust and soil ingestion rate	0.45		Based Table 5-1 of U.S. EPA (2017)

Variable	Units	Form	Type	Explanation	Value	Reference
f_Other_i; i= 1,2,3	unitless	A	F	Fraction of discrete Other_i contributing to daily other Pb exposure	User defined	See Chapter 16 of U.S. EPA (2013)
f_pulse_air	unitless	C	F	Fraction of air daily air exposure from pulse train	User defined	
f_pulse_dust	unitless	C	F	Fraction of daily dust exposure from pulse train	User defined	
f_pulse_other	unitless	C	F	Fraction of daily other exposure from pulse train	User defined	
f_pulse_soil	unitless	C	F	Fraction of daily soil exposure from pulse train	User defined	
f_pulse_water	unitless	C	F	Fraction of daily water exposure from pulse train	User defined	(Clayton et al., 1999)
f_Water_i; i= 1,2,3	unitless	A	F	Fraction of discrete Water_i contributing to daily water Pb exposure	User defined	See Chapter 16 of U.S. EPA (2011)
Food_baseline	µg/day	C	F	Baseline food Pb intake used in exposure pulse train	10 µg/kg bw/day	(Clayton et al., 1999)
Food_i; i= 1, 2,3	µg/day	A	F	Food Pb intakes for discrete exposures	User defined	See Chapter 16 of U.S. EPA (2011)
Food_pulse	µg/day	C	F	Food Pb intake used in exposure pulse train	User defined	

Variable	Units	Form	Type	Explanation	Value		Reference
IR_sd	µg/day	A	F	Combined dust and soil ingestion rate	Age-day	Value	Based Table 5-1 of U.S. EPA (2017)
					0	0.040	
					90	0.070	
					365	0.090	
					1825	0.080	
					3650	0.060	
					5475	0.030	
					9125	0.030	
					18250	0.030	
					25550	0.030	
					32850	0.030	
IR_water	L/day	C	F	Water ingestion rate for water Pb exposures	Age-day	Value	Based on U.S. EPA (2011), Table 3-1, per capita; values are interpolated between ages
					0	0.20	
					90	0.30	
					365	0.35	
					1825	0.35	
					3650	0.45	
					5475	0.55	
					9125	0.70	
					18250	1.04	
					25550	1.04	
					32850	1.04	
Other_baseline	µg/day	C	F	Baseline other Pb intake used in exposure pulse train	User defined		

Variable	Units	Form	Type	Explanation	Value	Reference
Other_i; i= 1, 2,3	µg/day	A	F	Food Pb intakes for discrete exposures	User defined	
Other_pulse	µg/day	C	F	Other Pb intake used in exposure pulse train	User defined	
Pulse_i_period_air; i=1,2	day	C	F	Period for pulse train exposure to air	User defined	
Pulse_i_period_dust; i=1,2	day	C	F	Period for pulse train exposure to dust	User defined	
Pulse_i_period_food; i=1,2	day	C	F	Period for pulse train exposure to food	User defined	
Pulse_i_period_other; i=1,2	day	C	F	Period for pulse train exposure to other	User defined	
Pulse_i_period_soil; i=1,2	day	C	F	Period for pulse train exposure to soil	User defined	
Pulse_i_period_water; i=1,2	day	C	F	Period for pulse train exposure to water	User defined	
Pulse_i_width_air; i=1,2	day	C	F	Width for pulse train exposure to air	User defined	
Pulse_i_width_dust; i=1,2	day	C	F	Width for pulse train exposure to dust	User defined	
Pulse_i_width_food; i=1,2	day	C	F	Width for pulse train exposure to food	User defined	
Pulse_i_width_other; i=1,2	day	C	F	Width for pulse train exposure to other	User defined	
Pulse_i_width_soil; i=1,2	day	C	F	Width for pulse train exposure to soil	User defined	
Pulse_i_width_water; i=1,2	day	C	F	Width for pulse train exposure to water	User defined	

Variable	Units	Form	Type	Explanation	Value	Reference
Pulse_start_air	day	C	F	Start age for pulse train exposure to air	User defined	
Pulse_start_dust	day	C	F	Start age for pulse train exposure to dust	User defined	
Pulse_start_food	day	C	F	Start age for pulse train exposure to food	User defined	
Pulse_start_other	day	C	F	Start age for pulse train exposure to other	User defined	
Pulse_start_soil	day	C	F	Start age for pulse train exposure to soil	User defined	
Pulse_start_water	day	C	F	Start age for pulse train exposure to water	User defined	
Pulse_stop_air	day	C	F	Stop age for pulse train exposure to air	User defined	
Pulse_stop_dust	day	C	F	Stop age for pulse train exposure to dust	User defined	
Pulse_stop_food	day	C	F	Stop age for pulse train exposure to food	User defined	
Pulse_stop_other	day	C	F	Stop age for pulse train exposure to other	User defined	
Pulse_stop_soil	day	C	F	Stop age for pulse train exposure to soil	User defined	
Pulse_stop_water	day	C	F	Stop age for pulse train exposure to water	User defined	

Variable	Units	Form	Type	Explanation	Value		Reference
RBA_dust	unitless	C	F	Relative bioavailability of dust Pb	0.6		(U.S. EPA, 1994)
RBA_food	unitless	C	F	Relative bioavailability of food Pb	1		Assumed to be water soluble (U.S. EPA, 1994)
RBA_other	unitless	C	F	Relative bioavailability of other Pb	User defined		
RBA_soil	unitless	C	F	Relative bioavailability of soil Pb	0.6		(U.S. EPA, 1994)
RBA_water	unitless	C	F	Relative bioavailability of water Pb	1		Assumed to be water soluble (U.S. EPA, 1994)
Soil_baseline	µg/g	C	F	Baseline indoor Soil Pb concentration used in exposure pulse train	Background	25	(U.S. EPA, 2019; Smith et al., 2013)
					Residential (>1940)	50	
					Residential (<1940)	250	
Soil_i; i= 1, 2,3	µg/g	A	F	Soil Pb concentrations for discrete exposures	User defined		
Soil_pulse	µg/g	C	F	Soil Pb concentration used in exposure pulse train	User defined		
Water_baseline	µg/L	C	F	Baseline water Pb concentration used in exposure pulse train	0.9		(U.S. EPA, 2019; Zartarian et al., 2017)

Variable	Units	Form	Type	Explanation	Value		Reference
Water_i; i= 1, 2,3	µg/L	A	F	Water Pb concentrations for discrete exposures	User defined		See Chapter 16 of U.S. EPA (2011)
Water_pulse	µg/L	C	F	Water Pb concentration used in exposure pulse train	User defined		
V_air	m^3/day	A	F	Ventilation rate for air Pb exposures	Age-day	Value	Based on ICRP (1994); also see Chapter 6 of U.S. EPA (2011)
					0	2.9	
					90	2.9	
					365	5.2	
					1825	8.8	
					3650	15.3	
					5475	17.9	
					9125	19.9	
					18250	19.9	
					25550	19.9	
					32850	19.9	

1

APPENDIX C REFERENCES – EXPOSURE VARIABLES (PRIMARY ONLY)

Bannon, DI; Drexler, JW; Fent, GM; Casteel, SW; Hunter, PJ; Brattin, WJ; Major, MA. (2009). Evaluation of small arms range soils for metal contamination and lead bioavailability. Environ Sci Technol 43: 9071-9076. http://dx.doi.org/10.1021/es901834h

Brochu, P; Ducré-Robitaille, JF; Brodeur, J. (2006). Physiological daily inhalation rates for free-living individuals aged 1 month to 96 years, using data from doubly labeled water measurements: A proposal for air quality criteria, standard calculations and health risk assessment. Hum Ecol Risk Assess 12: 675-701. http://dx.doi.org/10.1080/10807030600801550

Casteel, SW; Weis, CP; Henningsen, GM; Brattin, WJ. (2006). Estimation of relative bioavailability of lead in soil and soil-like materials using young swine. Environ Health Perspect 114: 1162-1171. http://dx.doi.org/10.1289/ehp.8852

Clayton, CA; Pellizzari, ED; Whitmore, RW; Perritt, RL; Quackenboss, JJ. (1999). National Human Exposure Assessment Survey (NHEXAS): distributions and associations of lead, arsenic and volatile organic compounds in EPA region 5. J Expo Anal Environ Epidemiol 9: 381-392.

Clickner, RP; Marker, D; Viet, SM; Rogers, J; Broene, P. (2002). National Survey of Lead and Allergens in Housing. Volume I: Analysis of lead hazards. Final report. Revision 7.1. Washington, DC: U.S. Department of Housing and Urban Development.

Cox, DC; Dewalt, G; O'Haver, R; Salatino, B. (2011). American Healthy Homes Survey: Lead and arsenic findings. Washington, DC: U.S. Department of Housing and Urban Development. http://portal.hud.gov/hudportal/documents/huddoc?id=AHHS_REPORT.pdf

FDA (U.S. Food and Drug Administration). (2006). Total diet study. Available online at https://www.fda.gov/Food/FoodScienceResearch/TotalDietStudy/default.htm

FDA (U.S. Food and Drug Administration). (2007). Total diet study statistics on element results, Revision 4.1, Market baskets 1991–3 through 2004–5.

ICRP (International Commission on Radiological Protection). (1994). Human respiratory tract model for radiological protection: A report of a task group of the International Commission on Radiological Protection. ICRP Publication 66. New York, NY: Pergamon Press.

IOM (Institute of Medicine). (2005). Doubly Labeled water data set-Used to establish the estimated average requirement for energy.

Juhasz, AL; Weber, J; Smith, E. (2011). Impact of soil particle size and bioaccessibility on children and adult lead exposure in peri-urban contaminated soil. J Hazard Mater 186: 1870-1879. http://dx.doi.org/10.1016/j.jhazmat.2010.12.095

Kahn, HD; Stralka, K. (2009). Estimated daily average per capita water ingestion by child and adult age categories based on USDA's 1994-1996 and 1998 continuing survey of food intakes by individuals. J Expo Sci Environ Epidemiol 19: 396-404. http://dx.doi.org/10.1038/jes.2008.29

Layton, DW. (1993). Metabolically consistent breathing rates for use in dose assessments. Health Phys 64: 23-36.

Lu, Y; Yin, W; Huang, L; Zhang, G; Zhao, Y. (2011). Assessment of bioaccessibility and exposure risk of arsenic and lead in urban soils of Guangzhou City, China. Environ Geochem Health 33: 93-102. http://dx.doi.org/10.1007/s10653-010-9324-8

Marschner, B; Welge, P; Hack, A; Wittsiepe, J; Wilhelm, M. (2006). Comparison of soil Pb in vitro bioaccessibility and in vivo bioavailability with Pb pools from a sequential soil extraction. Environ Sci Technol 40: 2812-2818. http://dx.doi.org/10.1021/es051617p

O'Rourke, MK; Van De Water, PK; Jin, S; Rogan, SP; Weiss, AD; Gordon, SM; Moschandreas, DM; Lebowitz, MD. (1999). Evaluations of primary metals from NHEXAS Arizona: distributions and preliminary exposures. National Human Exposure Assessment Survey. J Expo Anal Environ Epidemiol 9: 435-445.

Ozkaynak, H; Xue, J; Zartarian, VG; Glen, G; Smith, L. (2011). Modeled estimates of soil and dust ingestion rates for children. Risk Anal 31: 592-608. http://dx.doi.org/10.1111/j.1539-6924.2010.01524.x

Reimann, C; Smith, DB; Woodruff, LG; Flem, B. (2011). Pb-concentrations and Pb-isotope ratios in soils collected along an east-west transect across the United States. Appl Geochem 26: 1623-1631. http://dx.doi.org/10.1016/j.apgeochem.2011.04.018

Robertson, GL; Lebowitz, MD; O'Rourke, MK; Gordon, S; Moschandreas, D. (1999). The National Human Exposure Assessment Survey (NHEXAS) study in Arizona--introduction and preliminary results. J Expo Anal Environ Epidemiol 9: 427-434.

Roussel, H; Waterlot, C; Pelfrene, A; Pruvot, C; Mazzuca, M; Douay, F. (2010). Cd, Pb and Zn oral bioaccessibility of urban soils contaminated in the past by atmospheric emissions from two lead and zinc smelters. Arch Environ Contam Toxicol 58: 945-954. http://dx.doi.org/10.1007/s00244-009-9425-5

Smith, DB; Cannon, WF; Woodruff, LG; Solano, F; Kilburn, JE; Fey, DL. (2013). Geochemical and mineralogical data for soils of the conterminous United States: U.S. Geological Survey data series 801 (pp. 19). (Data Series 801). Reston, VA: U.S. Department of the Interior, U.S. Geological Survey. http://pubs.usgs.gov/ds/801/

Smith, DM; Mielke, HW; Heneghan, JB. (2009). Subchronic lead feeding study in male rats and micropigs. Environ Toxicol 24: 453-461. http://dx.doi.org/10.1002/tox.20448

Smith, E; Weber, J; Naidu, R; Mclaren, RG; Juhasz, AL. (2011). Assessment of lead bioaccessibility in peri-urban contaminated soil. J Hazard Mater 186: 300-305. http://dx.doi.org/10.1016/j.jhazmat.2010.10.111

Stifelman, M. (2007). Using doubly-labeled water measurements of human energy expenditure to estimate inhalation rates. Sci Total Environ 373: 585-590. http://dx.doi.org/10.1016/j.scitotenv.2006.11.041

Thomas, K; Pellizzari, E; Berry, M. (1999). Population-based dietary intakes and tap water concentrations for selected elements in the EPA region V National Human Exposure Assessment Survey (NHEXAS). J Expo Anal Environ Epidemiol 9: 402-413. http://dx.doi.org/10.1038/sj.jea.7500051

U.S. EPA (U.S. Environmental Protection Agency). (1994). Technical support document: Parameters and equations used in integrated exposure uptake biokinetic model for lead in children (v 099d) [EPA Report]. (EPA/54O/R-94/04O). Washington, DC.

U.S. EPA (U.S. Environmental Protection Agency). (2007a). EPA science advisory board (SAB) ad hoc all-ages lead model review panel's peer review of the "all-ages lead model (AALM) version 1.05 (External review draft) ". (EPA-SAB-07-002). https://cfpub.epa.gov/si/si_public_record_report.cfm?dirEntryId=139314&Lab=NCEA

U.S. EPA (U.S. Environmental Protection Agency). (2007b). National primary drinking water regulations for lead and copper: Short-term regulatory revisions and clarifications. Fed Reg 72: 57782-57820.

U.S. EPA (U.S. Environmental Protection Agency). (2011). Exposure factors handbook: 2011 edition (final) [EPA Report]. (EPA/600/R-090/052F). Washington, DC: U.S. Environmental Protection Agency, Office of Research and Development, National Center for Environmental Assessment. http://cfpub.epa.gov/ncea/cfm/recordisplay.cfm?deid=236252

U.S. EPA (U.S. Environmental Protection Agency). (2013). Integrated science assessment for lead [EPA Report]. (EPA/600/R-10/075F). Research Triangle Park, NC: U.S. Environmental Protection Agency, National Center for Environmental Assessment. http://cfpub.epa.gov/ncea/cfm/recordisplay.cfm?deid=255721

U.S. EPA (U.S. Environmental Protection Agency). (2017). Update for chapter 5 of the Exposure Factors Handbook. Soil and dust ingestion. (EPA/600R-17/384F). Washington, DC: National Center for Environmental Assessment, Office of Research and Development.

U.S. EPA (U.S. Environmental Protection Agency). (2019). Technical support document for residential dust-lead hazard standards rulemaking. Title Page. (EPA TSD LDHS).

USDA (U.S. Department of Agriculture). (2000). 1994–1996, and 1998 continuing survey of food intakes by individuals and 1994–1996 diet and health knowledge survey.

von Lindern, I; Spalinger, S; Stifelman, ML; Stanek, LW; Bartrem, C. (2016). Estimating Children's Soil/Dust Ingestion Rates through Retrospective Analyses of Blood Lead Biomonitoring from the Bunker Hill Superfund Site in Idaho. Environ Health Perspect 124: 1462-1470. http://dx.doi.org/10.1289/ehp.1510144

Wilson, R; Jones-Otazo, H; Petrovic, S; Mitchell, I, an; Bonvalot, Y; Williams, D; Richardson, GM. (2013). Revisiting Dust and Soil Ingestion Rates Based on Hand-to-Mouth Transfer. Hum Ecol Risk Assess 19: 158-188. http://dx.doi.org/10.1080/10807039.2012.685807

Yu, CH; Yiin, LM; Lioy, PJ. (2006). The bioaccessibility of lead (Pb) from vacuumed house dust on carpets in urban residences. Risk Anal 26: 125-134. http://dx.doi.org/10.1111/j.1539-6924.2006.00710.x

Zartarian, V; Xue, J; Tornero-Velez, R; Brown, J. (2017). Children’s Lead Exposure: A Multimedia Modeling Analysis to Guide Public Health Decision-Making. Environ Health Perspect 125: n/a. http://dx.doi.org/10.1289/EHP1605

APPENDIX D – ALL AGES LEAD MODEL (AALM.FOR) BIOKINETICS PARAMETER VALUES

AALM biokinetics parameters and values are listed in Table D-1. The bases for values assigned to each parameter are summarized below. Parameters are presented in alphabetical order, according to the parameter name.

AFC1, AFC2: Parameters used calculating age-specific absorption fraction of Pb from small intestine (see variable *F1* in Biokinetics GI Tract, Appendix A). The absorption fraction is calculated based on an expression from O'Flaherty (1995, 1993). AF_{C1} and AF_{C2} were assigned values of 0.40 and 0.28, respectively, based on fitting simulations to data on blood Pb concentration in children (Sherlock and Quinn, 1986; Ryu et al., 1983) and adults (Rabinowitz et al., 1976) as described in Chapter 4. The values for *AFC1* and *AFC2* of 0.40 and 0.28, respectively, produce absorption fractions of 30-40% in infants and during early childhood (Ziegler et al., 1978; Alexander et al., 1974) and 12% in adults (Maddaloni et al., 2005; U.S. EPA, 2003).

AGSCAL: Age-scaling factor for gastrointestinal transfer rates. Age-dependent values assigned to *AGSCAL* are the same as those in Leggett (1993). The value of 1is assigned to adults and higher values for infants and children. This results in a slower removal kinetics in children compared to adults (Corazziari et al., 1985).

ARBLAD: Rate coefficient for Pb transfer from urinary bladder to urine. The value assigned to *ARBLAD* is from Leggett (1993). The value of 5 d^{-1} for adults is based on a removal $t_{1/2}$ of 0.1 days for Pb being voided from the bladder (ICRP, 1975), which approximates a transfer rate of 0.693/0.1 d = 7 d^{-1}. The rate coefficients for children are 7, 8, 11, 15, 12, and 12 d^{-1} for 15, 10, 5, and 1 year old, 3 months old, and birth, respectively.

ARBRAN: Rate coefficient for Pb transfer from brain to diffusible plasma. The value assigned to *ARBRAN* is from Leggett (1993). The value of 0.00095 d^{-1} derives from a removal $t_{1/2}$ of 2 years (0.693/2 yrs = 9.5×10^{-4} d^{-1}). The values for *ABRAN* and *TOBRAN* (deposition of 0.015% of Pb from diffusible plasma), are based on comparison of predicted and observed brain Pb in dogs and baboons (Lloyd et al., 1975; Cohen et al., 1970) and human autopsy observations (Grandjean, 1978; Niyogi, 1974).

ARCORT: Rate coefficient for Pb transfer from non-exchangeable cortical bone to diffusible plasma. Leggett (1993) assigned a value of 0.000082 d^{-1} for *ACORT* in adults based on the assumption that removal of Pb from the non-exchangeable bone volume is occurs at same rate as bone resorption. Childhood and adult rates were adopted from ICRP (1990) for bone-seeking radionuclides, based on histomorphometric measurements taken of human ribs, iliac crest, and various long bones. By adulthood, trabecular bone resorption is about 6-fold higher than in cortical bone. As discussed in Chapter 4, values for children and adults were increased by a factor of 2, based on calibration of simulations of bone Pb elimination kinetics in retired Pb workers (Nilsson et al., 1991).

ARCS2B: Rate coefficient for Pb transfer from cortical bone surface to diffusible plasma. The value assigned to *ARCS2B* is from Leggett (1993). The value of 0.5 d^{-1} for adults was based on model fit of skeletal Pb data for humans (Heard and Chamberlain, 1984), baboons (Cohen et al., 1970), and dogs (Lloyd et al., 1975), assuming a transfer rate of 1 d^{-1} from bone surface and 0.5 d^{-1} each to plasma or exchangeable bone volume. For children, the rate coefficient 0.65 d^{-1} was assigned to *ARCS2B* based on the assumption that, in children, a larger fraction of Pb leaving bone surfaces goes to plasma. By analogy

to strontium, approximately 1.25-fold more Pb transfers from bone surface to plasma in children, compared to adults (1.25×0.5 d^{-1} = 0.65 d^{-1}).

ARCS2DF: Rate coefficient for Pb transfer from cortical bone surface to exchangeable cortical bone volume. The value assigned to *ARCS2DF* is from Leggett (1993). The value of 0.5 d^{-1} in adults was based on model fits to skeletal Pb data for humans (Heard and Chamberlain, 1984), baboons (Cohen et al., 1970), and dogs (Lloyd et al., 1975) assuming transfer rate of 1 d^{-1} from bone surface and 0.5 d^{-1} each to plasma or exchangeable bone volume. For children to age 15, the rate coefficient is 0.35 d^{-1}. By analogy to strontium, approximately 1.25-fold more Pb transfers from bone surface to plasma in children, compared to adults (1.25×0.5 d^{-1} = 0.65 d^{-1}). The remaining Pb transfers to exchangeable bone volume at a rate of 0.35 d^{-1}.

ARKDN2: Rate coefficient for transfer from kidney compartment 2 to diffusible plasma. Leggett (1993) assigned a value of 0.0019 d^{-1} for adults. After parameter values for *TOKDN1* and *RKDN1* were set, 0.02% deposition from diffusible plasma and a removal $t_{1/2}$ of 1 year (rate coefficient: 0.693/1 yrs = 0.0019 d^{-1}) replicated and overestimated slow renal Pb loss in humans (Heard and Chamberlain, 1984) and animals (Lloyd et al., 1975; Cohen et al., 1970), respectively. Rate coefficients for children ages 10-15 years were assigned the adult value, while 0.00693 d^{-1} was used to represent birth to 5 years of age, assuming a removal $t_{1/2}$ of 100 days. This assumption was needed to keep predicted Pb levels from overly accumulating in long-term kidney compartments. These values were revised downward in the AALM.FOR based on calibration of simulations (see Chapter 4) of post-mortem soft tissue-bone Pb concentrations in children and adults reported by Barry (1975). The adjustments were a factor of ×0.1 for ages ≤25 years, increasing to 0.5 at age 30 ears and 1 by age 40 years.

ARLVR2: Rate coefficient for Pb transfer from the slow liver compartment 2 to diffusible plasma. Leggett (1993) assigned a value of 0.0019 d^{-1} for adults and children ≥10 years of age to reproduce observations of 2% fraction of body Pb in liver of chronically exposed humans. For children ages 10–15 years, the rate coefficient was the same as adults, while 0.00693 d^{-1} was used for birth to 5 years of age, assuming a removal $t_{1/2}$ of 100 days. This assumption was made to keep predicted Pb levels from overly accumulating in long-term compartments. Values for children and adults were revised downward in the AALM.FOR based on calibration of simulations (see Chapter 4) of post-mortem soft tissue-bone Pb concentration ratios in children and adults reported by Barry (1975). The adjustments were a factor of 0.1 for ages ≤1 year, increasing progressively to 0.3 at age 10 years, 0.75 at age 30 years, 1.6 at age 40 years, and 1.8 at 60 years.

ARRBC: Rate coefficient for Pb transfer from RBC to diffusible plasma. Leggett (1993) assigned a value of 0.0019 for adults and children ≥10 years of age, based on a removal $t_{1/2}$ from RBCs to plasma of 5 days [0.693/5 days = 0.0019 d^{-1}; (Chamberlain et al., 1978)]. For children from birth to 5 years of age, 0.00693 d^{-1} was assigned to provide reasonable agreement with the reference distributions of RBC levels derived by Leggett (1993). Values for ages 1–10 years were revised upward in the AALM.FOR to achieve alignment of Pb uptake-blood Pb concentration relationships in children predicted by the AALM and IEUBK model (Chapter 4). The adjustments were a factor of ×1.7 at age 1 year, ×1.4 at age 5 years and ×1.4 at age 10 years.

ARTRAB: Rate coefficient for Pb transfer from non-exchangeable trabecular bone volume to diffusible plasma. Leggett assigned a value of 0.000493 d^{-1} to adults (assuming that removal of Pb from the non-exchangeable bone volume occurs at same rate as bone resorption). Childhood and adult rates were

adopted from ICRP (1990) for bone-seeking radionuclides, based on histomorphometric measurements taken of human ribs, iliac crest, and various long bones. By adulthood, trabecular bone resorption is about 6-fold higher than in cortical bone. Values for children and adults were increased by a factor of ×3, based on calibration of simulations (see Chapter 4) of bone Pb elimination kinetics in retired Pb workers (Nilsson et al., 1991).

ARTS2B: Rate coefficient for Pb transfer from trabecular bone surface to diffusible plasma. Values for *ARTS2B* are from Leggett (1993). For adults, the value 0.5 d^{-1} was based on model fit to skeletal Pb data for humans (Heard and Chamberlain, 1984), baboons (Cohen et al., 1970), and dogs (Lloyd et al., 1975). Assuming a total transfer rate of 1 d^{-1} from bone surface, a rate of 0.5 d^{-1} each transfers Pb to plasma or exchangeable bone volume. The rate coefficient for children (≤15 years) is 0.65 d^{-1}, based on the assumption that, in children, a larger fraction of Pb leaves bone surfaces and goes to plasma. By analogy to strontium, approximately 1.25-fold more Pb transfers from bone surface to plasma in children, compared to adults (1.25×0.5 d^{-1} = 0.65 d^{-1}).

ARTS2DF: Rate coefficient for Pb transfer from surface trabecular bone to exchangeable trabecular bone volume. Values for *ARTS2DF* are from Leggett (1993). For adults, the value 0.5 d^{-1} was based on model fit to skeletal Pb data for humans (Heard and Chamberlain, 1984), baboons (Cohen et al., 1970), and dogs (Lloyd et al., 1975). Assuming a total transfer rate of 1d^{-1} from bone surface, a rate of 0.5 d^{-1} each transfers Pb to plasma or exchangeable bone volume. the rate coefficient for children ≤15 years is 0.35 d^{-1}. By analogy to strontium, approximately 1.25-fold more Pb transfers from bone surface to plasma in children, compared to adults (1.25×0.5 d^{-1} = 0.65 d^{-1}). The remaining Pb transfers to exchangeable bone volume at a rate of 0.35 d^{-1}.

ATBONE: Deposition fraction for Pb from diffusible plasma to surface bone. The value of 8% for adults reproduces observations of Pb deposition to total bone of humans (Heard and Chamberlain, 1984), baboons (Cohen et al., 1970), and dogs (Lloyd et al., 1975). For children, the following deposition fractions were used: 23.7% at 15 years, 17.9% at 10 years, 12.8% at 5 years, 14.4% at year, and 24% at birth and 3 months. These values arise from the assumption that Pb deposits to bone surfaces proportional to the rate of calcium addition, as described by Leggett (1992).

ATBRAN: Deposition fraction for Pb from diffusible plasma to brain. Values for *ATBRAN* are from Leggett (1993). For children ≥5 years old and adults, the value of 0.015%, combined with a removal $t_{1/2}$ of 2 years (0.693/2 yrs = 9.49×10^{-4} d^{-1}) were assigned based on model fit to observations of brain Pb levels in dogs (Lloyd et al., 1975) and baboons (Cohen et al., 1970) and human autopsy observations (Grandjean, 1978; Niyogi, 1974). For children from birth to 1 year, the a 3-fold higher value of 0.045% was assigned to account for the relatively larger brain mass:body weight ratio in this age range.

ATFRAC: Fraction of diffusible plasma-to-bone deposition that goes to trabecular surface bone. Values for *ATFRAC* are from Leggett (1993). For adults, the value of 55.6% was assigned based on an approximate 4-fold larger trabecular bone mass than cortical bone in humans (ICRP, 1975), and that calcium deposits in trabecular bone are 5- to 6-fold greater than in cortical bone in humans (Leggett, 1992; Leggett et al., 1982). The fraction transferring from diffusible plasma to cortical bone is 1-*TFRAC*, or 0.444. For children, the following values were assigned: 27.95% for 15 years, 25% for 10 years, 22.2% for 5 years, or 20% for birth to 3 months.

ATOSOF0: Deposition fraction for Pb from diffusible plasma to the fast soft tissue compartment 0. Values for *ATOSOF0* are from Leggett (1993). For adults, the value of 8.88%, and a removal $t_{1/2}$ of 8 hours (RSOF0) was assumed in order to replicate Pb reappearance in blood from extravascular fluid after the first day following Pb injections in animals (Gregus and Klaassen, 1986; Victery et al., 1979; Lloyd et al., 1975; Potter et al., 1971; Cohen et al., 1970; Lloyd et al., 1970). For children, values of 8.38 and 8.35% were assigned to ages 5 to 15 years and birth to 1 year, respectively.

ATOSOF1: Deposition fraction for Pb from diffusible plasma to the intermediate soft tissue compartment 1. Values for *ATOSOF1* are from Leggett (1993). For adults, the value of 0.5% produced an intermediate-rate loss of Pb from soft tissues and that aligned with blood Pb and excretion kinetics (hair, nails, and skin) in humans (Rabinowitz et al., 1976). A value of 1% was assigned children up to 15 years of age (Leggett, 1993).

ATOSOF2: Deposition fraction for Pb from diffusible plasma to the slow soft tissue compartment 2. Values for *ATOSOF2* are from Leggett (1993). The value of 0.1% for adults and children, along with a retention time of at ≥5 years was based on comparisons of predicted and observed post-mortem soft tissue Pb levels in chronically exposed humans (Grandjean, 1978; Niyogi, 1974).

BLDMOT: Maternal blood Pb concentration. The value 0.6 µg/dL is based on an analysis of blood Pb concentration data for U.S. females age 17–45 years reported in the NHANES 2009–2014 and assessed by U.S. EPA (2017).

BR1: Rate coefficient for Pb transfer from RT compartment 1 to the gastrointestinal tract (*CILIAR*) or diffusible plasma (1-*CILIAR*). The value assigned to *BR1* is from Leggett (1993). The value of 16.6 is based on observations of clearance of ^{203}PbO, $^{203}Pb(NO_3)_2$, or ^{203}Pb-labeled exhaust aerosols in humans (Chamberlain et al., 1978), in which 22% of deposited Pb was cleared from lungs with a $t_{1/2}$ of 0.8 hours. The rate of clearance is calculated as 0.693/0.04167 days = 16.6 d^{-1}.

BR2: Rate coefficient for Pb transfer from RT compartment 2 to the gastrointestinal tract (*CILIAR*) or diffusible plasma (1-*CILIAR*). The value assigned to BR2 is from Leggett (1993) . The value of 5.54 is based on observations of clearance of ^{203}PbO, $^{203}Pb(NO_3)_2$, or ^{203}Pb-labeled exhaust aerosols in humans (Chamberlain et al., 1978), in which 34% of deposited Pb was cleared from lungs with a $t_{1/2}$ of 2.5 hours. The rate of clearance is calculated as 0.693/0.125 days = 5.54 d^{-1}.

BR3: Rate coefficient for Pb transfer from RT compartment 3 to the gastrointestinal tract (CILIAR) or diffusible plasma (1-CILIAR). The value assigned to *BR3* is from Leggett (1993). The value of 1.66 d^{-1} was chosen based on observations of clearance of ^{203}PbO, $^{203}Pb(NO_3)_2$, or ^{203}Pb-labeled exhaust aerosols in humans (Chamberlain et al., 1978), in which 33% of deposited Pb was cleared from lungs with a $t_{1/2}$ of 9 hours. The rate of clearance is calculated as 0.693/0.375 days = 1.66 d^{-1}.

BR4: Rate coefficient for Pb transfer from RT compartment 4 to the gastrointestinal tract (CILIAR) or diffusible plasma (1-CILIAR). The value assigned to *BR4* is from Leggett (1993). The value of 0.347 d^{-1} is based on observations of clearance of ^{203}PbO, $^{203}Pb(NO_3)_2$, or ^{203}Pb-labeled exhaust aerosols in humans (Chamberlain et al., 1978), in which 12% of deposited Pb was cleared from lungs with a $t_{1/2}$ of 44 hours. The rate coefficient is calculated as 0.693/2 days = 0.347 d^{-1}.

BRATIO: Child (at birth):maternal blood Pb concentration ratio. The value assigned to BRATIO is from Leggett (1993). The value of 0.85 is based on studies that have compared maternal and fetal cord blood

Pb concentrations which have observed cord-maternal ratios ranging from 0.7 to 1 (Baranowska-Bosiacka et al., 2016; Gulson et al., 2016; Kayaalti et al., 2015; Kim et al., 2015; Baeyens et al., 2014; Chen et al., 2014; Kazi et al., 2014; Reddy et al., 2014; Amaral et al., 2010; Kordas et al., 2009; Patel and Prabhu, 2009; Carbone et al., 1998; Goyer, 1990; Graziano et al., 1990).

BRETH: Pb deposition in RT (µg/day). Values are assigned by the user in AALM Fortran.xlsm (see parameters *IN_air_total,* Appendix B).

CHAGE: Age years for parameters that are assigned values at specific ages. Values assigned to *CHAGE* are from Leggett (1993).

CHR: Pb intake to blood (µg/day), for simulating injection. This parameter is in the Fortran code; however, injection intakes are not simulated in the AALM.FOR.

CILIAR: Fraction of inhaled Pb transferred to gastrointestinal tract. A value of 4% was assigned by Leggett (1993) to the fraction of total deposited Pb deposited cleared from the lung via mucociliary escalation. This value is based observations that in adults approximately 95% of Pb deposited in the RT was absorbed directly to blood (Wells et al., 1977; Hursh et al., 1969). Assuming a total deposition of 40% of inhaled Pb, the value for *CILIAR* is 1.6% (0.016 = 0.04×0.40).

DELT0: Starting value for numerical integration time step. The default value is 0.1 day is intended to limit integration error in the calculation of blood Pb concentration to less than 5%

DELTi: Array of numerical integration time steps if the time step varies in the simulation. The default for the AALM.FOR is to use a single time step for the simulation (0.1 day).

EAT: Pb ingestion (µg/day) for each exposure time step (*NCHRON*). Values are assigned by the user in AALM Fortran.xlsm (see parameters *IN_ingestion_total*, Appendix B).

ENDAY: Ending day of simulation. For example, for a simulation from birth to age 60 years, *ENDAY*=60 * 365=21900.

EXPAGE: Age at start of the simulation. The default value for *EXPAGE* is zero in the AALM.FOR which simulates Pb biokinetics beginning at birth, with a pre-existing body Pb burden based on maternal blood Pb (*BLDMOT*).

FLONG: Fraction of total Pb transfer from the exchangeable bone volume to non-exchangeable bone volume. The fraction of total Pb transfer from the exchangeable bone volume to bone surface (cortical or trabecular) is 1.0-FLONG. The value of 20% from Leggett (1993) was revised to 0.6, based on calibration of simulations (see Chapter 4) of bone Pb elimination kinetics in retired Pb workers (Nilsson et al., 1991).

H1TOBL: Fraction of Pb transfer from liver compartment 1 to diffusible plasma. The value assigned to *H1TOBL* is from Leggett (1993). Transfer out of liver compartment 1 includes 45% to diffusible plasma (*H1TOBL*), 45% to small intestine (*H1TOSI*) and 10% to liver compartment 2 (*H1TOH2*). These assumptions based on estimates of hepatic uptake and retention in humans and animals, and biliary secretion in humans (Heard and Chamberlain, 1984; Lloyd et al., 1975; Cohen et al., 1970).

H1TOH2: Fraction of Pb transfer from liver compartment 1 to liver compartment 2. The value assigned to *H1TOH2* is from Leggett (1993). Transfer out of liver compartment 1 includes 45% to diffusible plasma (*H1TOBL*), 45% to small intestine (*H1TOSI*) and 10% to liver compartment 2 (*H1TOH2*). These

assumptions based on estimates of hepatic uptake and retention in humans and animals, and biliary secretion in humans (Heard and Chamberlain, 1984; Lloyd et al., 1975; Cohen et al., 1970).

H1TOSI: Fraction of Pb transfer from liver compartment 1 to the small intestine. The value assigned to *H1TOSI* is from Leggett (1993). Transfer out of liver compartment 1 includes 45% to diffusible plasma (*H1TOBL*), 45% to small intestine (*H1TOSI*) and 10% to liver compartment 2 (*H1TOH2*). These assumptions based on estimates of hepatic uptake and retention in humans and animals, and biliary secretion in humans (Heard and Chamberlain, 1984; Lloyd et al., 1975; Cohen et al., 1970).

HALF: Age at which body weight is half of *WCHILD*. This parameter is used in body weight and tissue volume growth equations (see variables *WBODY*, *VK*, *VL*, Appendix A). The value assigned to *WCHILD* is from O'Flaherty (1995, 1993).

HCTA: Adult hematocrit. Sex-specific values assigned to *HCTA* are from O'Flaherty (1995, 1993).

IACUTE: Switch for acute (1) or chronic array (2) uptakes. The default value is 2 in the AALM.FOR which simulates chronic (i.e., repeated) daily exposures. Acute (e.g. single day exposures) can be simulated with discrete exposure inputs or pulse train inputs (see Exposure Model Parameters, Appendix C).

ICHEL: Switch for chelation simulation off (0) or on (1). The default value is 0 (no chelation). The AALM Fortran.xlsm user interface does not support the chelation option.

IFETAL: Switch for fetal simulation on (1) or off (0). The default value is 1 which turns on calculations of Pb body burden at birth based on maternal blood Pb (*BLDMOT*, see variables for Pb Masses at Birth, Appendix A).

INMODE: Switch for injection (0), inhalation (1), ingestion (2), or combination (3). The default value is 3 which allows combined ingestion and inhalation exposures. Injection intakes are not supported in the AALM.FOR.

IRBC: Switch for linear (0) or non-linear (1) RBC uptake. The default value is 1 which implements a threshold-specified RBC uptake of Pb from plasma.

KAPPA: Logistic parameter for calculation of body weight (see variable *WBODY* in Appendix A). The parameters *KAPPA* and *LAMBDA* determine the pre-adult rate of increase of body weight. The default value for *KAPPA* is 600 (O'Flaherty, 1995, 1993).

LAMBDA: Logistic parameter in calculation of body weight (see variable *WBODY* in Appendix A). The parameters *KAPPA* and *LAMBDA* determine the pre-adult rate of increase of body weight during. The default value for *LAMBDA* is 0.017 for females and 0.0095 for males (O'Flaherty, 1995, 1993).

NCHRON: Number of exposure time steps, where the exposure time step is an age-day range within which ingestion intake (**EAT**) or inhalation intake (**BRETH**) remains constant.

NCYCLE: Number of numerical integration steps for the simulation. If the numerical integration step size is 0.1 day, *NCYCLE* is the day length of the simulation (*ENDDAY*)/0.1 day.

NDELT: Number of times the numerical integration time step changes during the simulation. The default is 1 which applies the same time step throughout the simulation

NUMAGE: Number of ages (*CHAGE*) at which age-dependent parameters are assigned specific values.

OUTPUTS: Variable identity numbers selected for output. This parameter is in the Fortran code; however, is it not used in the implementation of AALM.FOR, which specifies output variables in the AALM Fortran.xlsm file.

POWER: Exponent factor for non-linear expression for RBC deposition. The value assigned to *POWER* is from Leggett (1993). The value of 1.5 was empirically derived based on data on Pb in human urine, plasma, and blood (Minoia et al., 1990; Iyengar and Woittiez, 1988; Somervaille et al., 1988; Skerfving et al., 1985; Manton and Cook, 1984; DeSilva, 1981; Chamberlain et al., 1978; Schütz and Skerfving, 1976; Cooper et al., 1973).

R1: Fraction of inhaled Pb deposited in the RT compartment 1. Leggett (1993) assigned values for the regional distribution of deposited Pb based on observations of clearance of ^{203}PbO, $^{203}Pb(NO_3)_2$, or ^{203}Pb-labeled exhaust aerosols in humans (Chamberlain et al., 1978), with 22% of deposited Pb cleared from lungs. Leggett (1993) equated cleared Pb with deposited dose and rounded up to 25% for the regional distribution to compartment 1. Assuming a total deposition of 40% of inhaled Pb (Leggett, 1993), the value for R1 is 10% (0.08 = 0.20×0.40).

R2: Fraction of inhaled Pb deposited in the RT compartment 1, representing the tracheobronchial region. Leggett (1993) assigned values for the regional distribution of deposited Pb based on observations of clearance of ^{203}PbO, $^{203}Pb(NO_3)_2$, or ^{203}Pb-labeled exhaust aerosols in humans (Chamberlain et al., 1978), with 34% of deposited Pb cleared from lungs. Leggett (1993) equated cleared Pb with deposited dose and rounded up to 35% for the regional distribution to compartment 2. Assuming a total deposition of 40% of inhaled Pb, the value for R2 is 14% (0.14 = 0.35×0.40).

R3: Fraction of inhaled Pb deposited in the RT compartment 1, representing the tracheobronchial region. Leggett (1993) assigned values for the regional distribution of deposited Pb based on observations of clearance of ^{203}PbO, $^{203}Pb(NO_3)_2$, or ^{203}Pb-labeled exhaust aerosols in humans (Chamberlain et al., 1978), with 33% of deposited Pb was cleared from lungs. Leggett (1993) equated cleared Pb with deposited dose and rounded down to 30% for the regional distribution to compartment 3. Assuming a total deposition of 40% of inhaled Pb, the value for R3 is 12% (0.14 = 0.35×0.40).

R4: Fraction of inhaled Pb deposited in the RT compartment 1, representing the tracheobronchial region. Leggett (1993) assigned values for the regional distribution of deposited Pb based on observations of clearance of ^{203}PbO, $^{203}Pb(NO_3)_2$, or ^{203}Pb-labeled exhaust aerosols in humans (Chamberlain et al., 1978), with 12% of deposited Pb was cleared from lungs. Leggett (1993) equated cleared Pb with deposited dose and rounded down to 10% for the regional distribution to compartment 4. Assuming a total deposition of 40% of inhaled Pb, the value for R4 is 4% (0.04 = 0.10×0.40).

RBCNL: Threshold Pb concentration in RBCs at which non-linear deposition of Pb from diffusible plasma to RBC occurs. Leggett (1993) assigned a value of 60 µg dL^{-1} based on an observed RBC Pb concentration threshold above which non-linear kinetics of Pb in the body were observed (Chamberlain, 1985). The value was revised to 20 µg/dL based on calibration to data on plasma-whole blood Pb concentrations measured in adults (Smith et al., 2002; Manton et al., 2001; Bergdahl et al., 1999; Bergdahl et al., 1998; Hernandez-Avila et al., 1998; Bergdahl et al., 1997; Schutz et al., 1996).

RDECAY: Rate coefficient for radioactive decay of unstable Pb isotope. This parameter is set to 0 by default in the AALM.FOR which simulates biokinetics of stable isotopes of Pb.

RDIFF: Rate coefficient for Pb transfer from exchangeable bone (cortical or trabecular) volume to surface or non-exchangeable bone volume (see FLONG for fraction to non-exchangeable). The value assigned to *RDIFF* is from Leggett (1993). The value of 0.0231 d^{-1} was based on observed rates of removal of Pb from bone of dogs, baboons, and chronically exposed humans appears, which were similar to removal of radium, which has a removal $t_{1/2}$ of 30 days (Leggett, 1992), resulting in a rate coefficient of 0.693/30 days = 0.00231 d^{-1}.

RKDN1: Rate coefficient for transfer from kidney compartment 1 to urinary pathway. The value assigned to *RKDN1* is from Leggett (1993). The value of 0.139 d^{-1} was chosen based on a removal $t_{1/2}$ of 5 days (transfer rate of 0.693/5 days = 0.139 d^{-1}) and a deposition fraction of 2%, which predicts kidney levels in rats and baboons (Cohen et al., 1970) and is also consistent with human excretion data (Campbell et al., 1984; Chamberlain et al., 1978; Hursh and Mercer, 1970; Booker et al., 1969; Hursh and Suomela, 1968).

RLLI: Rate coefficient for Pb transfer from lower large intestine to feces. The value assigned to *RLLI* is from Leggett (1993). The value of 1 d^{-1} is from the ICRP (1979) gastrointestinal tract model.

RLVR1: Rate coefficient for Pb transfer from liver compartment 1 to small intestine or diffusible plasma. The value assigned to *RLVR1* (0.693 d^{-1}) is from Leggett (1993). The removal $t_{1/2}$ for liver compartment 1 is assumed to be 10 days, resulting in a rate coefficient of 0.693/10 days = 0.693 d^{-1}. A relatively short $t_{1/2}$ is needed to reproduce hepatic uptake and loss in humans (Chamberlain et al., 1978), baboons (Cohen et al., 1970), and dogs (Lloyd et al., 1975) for the first weeks following intravenous Pb injection.

RPLAS: Rate coefficient for Pb transfer from diffusible plasma to all compartments, scaled to bone surface deposition. The value assigned to *RPLAS* is from Leggett (1993). The value of 2000 d^{-1} reflects the removal of radio-Pb from plasma at about 1 minute (Campbell et al., 1984; Wells et al., 1977; Booker et al., 1969). Adjusting for rapid uptake in to RBCs and EVF, the rate becomes 1.3–1.4 min^{-1}, rounded to 2000 d^{-1}.

RPROT: Rate coefficient for Pb transfer from bound plasma to diffusible plasma. The value assigned to *RPROT* is from Leggett (1993). The value of 0.139 d^{-1} (0.693/5 days = 0.139 d^{-1}) is based on a removal $t_{1/2}$ of approximately 5 days, the same as observed for plasma proteins (Orten and Neuhaus, 1982).

RSIC: Rate coefficient for Pb transfer from small intestine to upper large intestine. The value assigned to *RSIC* is from Leggett (1993). The value of 6 d^{-1} is from the first-order transfer rate in the ICRP (1979) gastrointestinal tract model.

RSOF0: Rate coefficient for Pb transfer from soft tissues with fast Pb clearance to diffusible plasma. The value assigned to *RSOF0* is from Leggett (1993). The value of 2.079 d^{-1}, based on a removal $t_{1/2}$ of 8 hours (0.693/8 hours = 2.079 d^{-1}) and a deposition fraction of 8.875% from diffusible plasma, reproduces Pb reappearance in blood from EVF after the first day following Pb injections in animals (Gregus and Klaassen, 1986; Victery et al., 1979; Lloyd et al., 1975; Potter et al., 1971; Cohen et al., 1970; Lloyd et al., 1970).

RSOF1: Rate coefficient for Pb transfer from soft tissues with medium Pb clearance to diffusible plasma. The value assigned to *RSOF1* is from Leggett (1993). The value of 0.00693 d^{-1}, based on an removal $t_{1/2}$ of 100 days (0.693/100 days = 0.00693 d^{-1}) and a deposition fraction of 0.5% from diffusible plasma, reproduces Pb reappearance in blood from EVF after the first day following Pb injections in animals

(Gregus and Klaassen, 1986; Victery et al., 1979; Lloyd et al., 1975; Potter et al., 1971; Cohen et al., 1970; Lloyd et al., 1970).

RSOF2: Rate coefficient for Pb transfer from soft tissues with slow Pb clearance to diffusible plasma. The value assigned to *RSOF2* (0.00038 d^{-1}) is from Leggett (1993). Assuming no more than 0.1% of diffusible plasma Pb is deposited into soft tissue having tenacious Pb retention, and the retention time is at least 5 years, consistent with autopsy data for chronically exposed humans (Grandjean, 1978; Niyogi, 1974).

RSTMC: Rate coefficient for Pb transfer from stomach to small intestine. The value assigned to *RSTMC* is from Leggett (1993). The value of 24 d^{-1} is from the ICRP (1979) gastrointestinal tract model.

RULI: Rate coefficient for Pb transfer from upper large intestine to lower large intestine. The value assigned to *RULI* is from Leggett (1993). The value of 1.85 d^{-1} is from the ICRP (1979) gastrointestinal tract model.

S2HAIR: Fraction of Pb transfer from intermediate soft tissue (*SOF2*) to hair, nails, and desquamated skin. The value assigned to *S2HAIR* is from Leggett (1993). The value of40% is based on observations of 3% of the Pb body burden in soft tissues and the remainder in pelt of animals at 28 days after injection (Lloyd et al., 1975, 1970). The remaining fraction leaving *SOF2* (1-*S2HAIR* = 60%) returns to diffusible plasma.

SATRAT: Maximum (saturating) concentration of Pb in RBCs. The value assigned to *SATRAT* is from Leggett (1993). The concentration of 350 µg dL^{-1} was assigned based on the observed upward inflection of ratios of urinary:blood Pb and plasma:blood Pb at RBC concentrations above this level (Minoia et al., 1990; Iyengar and Woittiez, 1988; Somervaille et al., 1988; Skerfving et al., 1985; Manton and Cook, 1984; DeSilva, 1981; Chamberlain et al., 1978; Schütz and Skerfving, 1976; Cooper et al., 1973).

SIZEVF: Relative volume of the EVF compartment compared to plasma (EVF/Plasma). The value assigned to *SIZEVF* is from Leggett (1993). The value of 3-fold was chosen because plasma Pb is about three times that of EVF at equilibrium.

TOEVF: Deposition fraction for Pb from diffusible plasma to extravascular fluid. The value assigned to *STOEVF* is from Leggett (1993). The value of 50% was based on observations of rapid return of Pb to blood from extravascular spaces (Heard and Chamberlain, 1984; Booker et al., 1969; Hursh and Suomela, 1968; Stover, 1959).

TOFECE: Deposition fraction for Pb from diffusible plasma directly to the small intestine (not including the transfer from biliary secretion, specified by *RLVR1*). The value assigned to *TOFECE* is from Leggett (1993). The value of 0.6%, as well as Pb entering from biliary excretion (*H1TOSI*) was based on observations of fecal excretion and the feces-to-urine Pb ratios in adults (Heard and Chamberlain, 1984; Chamberlain et al., 1978; Wells et al., 1977).

TOKDN1: Deposition fraction for Pb from diffusible plasma to kidney compartment 1. Leggett (1993) assigned a value of 2% and a removal $t_{1/2}$ of 5 days (*RKDN1*) based on observed kidney levels in rats and baboons (Cohen et al., 1970) that were also consistent with human excretion data (Campbell et al., 1984; Chamberlain et al., 1978; Hursh and Mercer, 1970; Booker et al., 1969; Hursh and Suomela, 1968). Values for children and adults were revised upward in the AALM.FOR by a factor of ×1.25 based on

calibration of simulations of plasma-to-urine clearance estimated for adults from data reported in (Araki et al., 1986; Manton and Cook, 1984; Manton and Malloy, 1983; Chamberlain et al., 1978).

TOKDN2: Deposition fraction for Pb from diffusible plasma to kidney compartment. The value of 0.02% was chosen. Leggett (1993) assigned a value of 0.02% and a removal $t_{1/2}$ of 1 year (*RKDN2*), after values for *TOKDN1* and *RKND1* were set, based on observations of a slow component for loss of Pb from kidney in humans (Heard and Chamberlain, 1984) and animals (Lloyd et al., 1975; Cohen et al., 1970), respectively. Values for children and adults were revised upward in the AALM.FOR by a factor of ×2 based on calibration of simulations (see Chapter 4) of post-mortem soft tissue-bone Pb concentrations in children and adults reported by Barry (1975).

TOLVR1: Deposition fraction for Pb from diffusible plasma to liver compartment 2. The value assigned to *TOLVR1* is from Leggett (1993). The value of 4% was assigned based on observed uptake and retention of Pb in liver in humans and animals, and biliary secretion in humans (Heard and Chamberlain, 1984; Lloyd et al., 1975; Cohen et al., 1970).

TOPROT: Deposition fraction for Pb from diffusible plasma to protein-bound plasma. The value assigned to *TOPROT* is from Leggett (1993). The value of 0.04% was selected to achieve (1) early bifurcation of tracer Pb between plasma and RBCs, (2) observed urinary clearance of plasma Pb, (3) plasma containing 0.2% of blood Pb at equilibrium, and (4) 15% ultrafilterable plasma Pb at equilibrium.

TORBC: Deposition fraction from diffusible plasma to RBCs. The value assigned to *TORBC* is from Leggett (1993). The value of 24% was based on the observation that approximately one quarter of Pb depositing to RBCs provides good fits to data of Hursh et al. (1969).

TOSWET: Deposition fraction for Pb from diffusible plasma to sweat. The value assigned to *TOSWET* is from Leggett (1993). The value of 0.35% was assigned based on observations of Pb excretion in sweat and which was approximately 10% of urinary excretion for chronic exposure (Rabinowitz et al., 1976).

TOURIN: Deposition fraction for Pb from diffusible plasma to urine. Leggett (1993) assigned a value of 1.5% for *TOURIN*, in addition to 2% being removed from urinary path to bladder (*TOKDN1*), based on observations of human urinary clearance (Minoia et al., 1990; Iyengar and Woittiez, 1988; Somervaille et al., 1988; Skerfving et al., 1985; Chamberlain et al., 1978; Schütz and Skerfving, 1976; Cooper et al., 1973). This parameter was set to zero in the AALM.FOR after calibration of parameter *TOKDN1* to data on plasma-to-urine clearance adults (Araki et al., 1986; Manton and Cook, 1984; Manton and Malloy, 1983; Chamberlain et al., 1978).

VBLC: Blood volume fraction of body weight. The value assigned to *VBLC* is from O'Flaherty (1995, 1993).

VKC: Blood volume fraction of body weight. The value assigned to *VKC* is from O'Flaherty (1995, 1993).

VLC: Liver volume fraction of body weight. The value assigned to *VLC* is from O'Flaherty (1995, 1993).

VLUC: Lung volume fraction of body weight. The value assigned to *VLC* is from O'Flaherty (1995, 1993).

WADULT: Adult maximum weight used in calculation of body weight growth (see variable *WBODY* in Appendix A). The value assigned to *WADULT* is from O'Flaherty (1995, 1993).

WBIRTH: Weight at birth used in calculation of body weight growth (see variable *WBODY* in Appendix A). The value assigned to *WBIRTH* is from O'Flaherty (1995, 1993).

WCHILD: Maximum body weight achieved during early hyperbolic growth phase, used in calculation of body weight growth (see variable *WBODY* in Appendix A). The value assigned to *WCHILD* is from O'Flaherty (1995, 1993).

TABLE D-1. AALM BIOKINETICS PARAMETERS AND VALUES

Parameter	Unit	Form	Type	Description	Value		Source
AFC1	unitless	C	F	Parameter used in calculating age-specific absorption fraction (*F1*)	0.40		(Ziegler et al., 1978; Alexander et al., 1974)
AFC2	unitless	C	F	Parameter used in calculating age-specific absorption fraction (*F1*)	0.28		(Maddaloni et al., 2005)
AGSCAL	unitless	A	F	Age scaling factor for gastrointestinal transfer rates	Age	Value	(Leggett, 1993)
					≥25 yr	1	
					15 yr	1.33	
					10 yr	1.67	
					5 yr	1.67	
					1 yr	1.67	
					0.274 yr	1.67	
					Birth	1.67	
ARBRAN	d^{-1}	A	F	Rate coefficient for Pb transfer from brain to diffusible plasma	9.5E04		(Leggett, 1993)
ARCORT	d^{-1}	A	F	Rate coefficient for Pb transfer from non-exchangeable cortical bone to diffusible plasma	Age	Value	(Leggett, 1993; Nilsson et al., 1991) Also see Chapter 4
					≥25 yr	1.644 E-04	
					15 yr	1.024 E-03	
					10 yr	1.780 E-03	
					5 yr	3.080 E-03	
					1 yr	5.760 E-03	
					0.274 yr	1.644 E-02	

Parameter	Unit	Form	Type	Description	Value		Source
					Birth	2.040 E-02	
ARCS2B	d^{-1}	A	F	Rate coefficient for Pb transfer from cortical bone surface to diffusible plasma.	Age	Value	(Leggett, 1993)
					≥25 yr	0.50	
					15 yr	0.35	
					10 yr	0.35	
					5 yr	0.35	
					1 yr	0.35	
					0.274 yr	0.35	
					Birth	0.35	
ARCS2DF	d^{-1}	A	F	Rate coefficient for Pb transfer from cortical bone surface to exchangeable cortical bone volume	Age	Value	(Leggett, 1993)
					≥25 yr	0.50	
					15 yr	0.65	
					10 yr	0.65	
					5 yr	0.65	
					1 yr	0.65	
					0.274 yr	0.65	
					Birth	0.65	
ARKDN2	d^{-1}	A	F	Rate coefficient for transfer from kidney compartment 2 to diffusible plasma	Age	Value	(Leggett, 1993; Barry, 1975) Also see Chapter 4
					≥40 yr	1.90E-03	
					30 yr	9.50E-04	
					25 yr	1.90E-04	
					15 yr	1.90E-04	
					10 yr	1.90E-04	
					5 yr	6.93E-04	
					1 yr	6.93E-04	
					0.274 yr	6.93E-04	
					Birth	6.93E-04	

Parameter	Unit	Form	Type	Description	Value		Source
ARLVR2	d^{-1}	A	F	Rate coefficient for Pb transfer from the slow liver compartment 2 to diffusible plasma	Age	Value	
					90 yr	3.800 E-03	
					60 yr	3.420 E-03	
					40 yr	3.040 E-03	
					30 yr	1.425 E-03	
					25 yr	5.700 E-04	
					15 yr	5.700 E-04	
					10 yr	5.700 E-04	
					5 yr	1.386 E-03	
					1 yr	6.930 E-04	
					0.274 yr	6.930 E-04	
					Birth	6.930 E-04	
ARRBC	d^{-1}	A	F	Rate coefficient for Pb transfer from RBC to diffusible plasma	Age	Value	(Leggett, 1993) Also see Chapter 4
					≥15 yr	1.390 E-01	
					10 yr	1.946 E-01	
					5 yr	4.986 E-01	
					1 yr	7.854 E-01	
					0.274 yr	4.620 E-01	
					Birth	4.620 E-01	
ARTRAB	d^{-1}	A	F	Rate coefficient for Pb transfer from non-exchangeable trabecular bone volume to diffusible plasma	Age	Value	(Leggett, 1993; Nilsson et al., 1991)
					≥25 yr	9.860 E-04	
					15 yr	1.912 E-03	

Parameter	Unit	Form	Type	Description	Value		Source
					10 yr	2.640 E-03	Also see Chapter 4
					5 yr	3.620 E-03	
					1 yr	5.760 E-03	
					0.274 yr	1.644 E-02	
					≥25 yr	2.040 E-02	
ARTS2B	d^{-1}	A	F	Rate coefficient for Pb transfer from trabecular bone surface to diffusible plasma	Age	Value	(Leggett, 1993)
					≥25 yr	0.50	
					15 yr	0.35	
					10 yr	0.35	
					5 yr	0.35	
					1 yr	0.35	
					0.274 yr	0.35	
					Birth	0.35	
ARTS2DF	d^{-1}	A	F	Rate coefficient for Pb transfer from surface trabecular bone to exchangeable trabecular bone volume	Age	Value	(Leggett, 1993)
					≥25 yr	0.50	
					15 yr	0.65	
					10 yr	0.65	
					5 yr	0.65	
					1 yr	0.65	
					0.274 yr	0.65	
					Birth	0.65	
ATBONE	unitless	A	F	Deposition fraction for Pb from diffusible plasma to surface bone	Age	Value	(Leggett, 1993)
					≥25 yr	8.00E-02	
					15 yr	2.37E-01	
					10 yr	1.79E-01	
					5 yr	1.28E-01	
					1 yr	1.44E-01	

Parameter	Unit	Form	Type	Description	Value		Source
					0.274 yr	2.40E-01	
					Birth	2.40E-01	
ATBRAN	unitless	A	F	Deposition fraction for Pb from diffusible plasma to brain	Age	Value	(Leggett, 1993)
					≥5 yr	1.5E094	
					1 yr	4.5E-04	
					0.274 yr	4.5E-04	
					Birth	4.5E-04	
ATFRAC	unitless	A	F	Fraction of diffusible plasma-to-bone deposition that goes to trabecular surface bone	Age	Value	(Leggett, 1993)
					≥25 yr	0.556	
					15 yr	0.279	
					10 yr	0.250	
					5 yr	0.222	
					1 yr	0.200	
					0.274 yr	0.200	
					Birth	0.200	
ATOSOF0	unitless	A	F	Deposition fraction for Pb from diffusible plasma to the fast soft tissue compartment 0	Age	Value	(Leggett, 1993)
					≥25 yr	8.875 E-02	
					15 yr	8.375 E-02	
					10 yr	8.375 E-02	
					5 yr	8.375 E-02	
					1 yr	8.345 E-02	
					0.274 yr	8.345 E-02	
					Birth	8.345 E-02	
ATOSOF1	unitless	A	F	Deposition fraction for Pb from diffusible plasma to the	Age	Value	(Leggett, 1993)
					≥25 yr	0.005	
					15 yr	0.010	

Parameter	Unit	Form	Type	Description	Value		Source
				intermediate soft tissue compartment 1	10 yr	0.010	
					5 yr	0.010	
					1 yr	0.010	
					0.274 yr	0.010	
					Birth	0.010	
ATOSOF2	unitless	A	F	Deposition fraction for Pb from diffusible plasma to the slow soft tissue compartment 2	0.001		(Leggett, 1993)
BLDMOT	µg/dL	C	F	Maternal blood Pb concentration	0.6		NHANES 2009–2014; (U.S. EPA, 2017)
BR1	d^{-1}	C	F	Rate coefficient for Pb transfer from RT compartment 1 to the gastrointestinal tract (CILIAR) or diffusible plasma (1-CILIAR)	16.6		(Leggett, 1993)
BR2	d^{-1}	C	F	Rate coefficient for Pb transfer from RT compartment 2 to the gastrointestinal tract (CILIAR) or diffusible plasma (1-CILIAR)	5.54		(Leggett, 1993)
BR3	d^{-1}	C	F	Rate coefficient for Pb transfer from RT compartment 3 to the gastrointestinal tract (CILIAR) or diffusible plasma (1-CILIAR)	1.66		(Leggett, 1993)
BR4	d^{-1}	C	F	Rate coefficient for Pb transfer from RT compartment 4 to the gastrointestinal tract (CILIAR) or diffusible plasma (1-CILIAR)	0.347		(Leggett, 1993)
BRATIO	unitless	C	F	Child (at birth):maternal blood Pb concentration ratio	0.85		Multiple references, see summary for BRATIO in this Appendix

Parameter	Unit	Form	Type	Description	Value	Source
BRETH	µg/day	A	F	Pb deposition to respiratory tract	User defined in exposure model	NA
CHAGE	day	A	F	Age years for parameters that are assigned values at specific ages	0 100 365 1825 3650 5475 9125 10950 14600 21900 32850	(Leggett, 1993) Also see Chapter 4
CHR	µg/day	A	F	Pb intake to blood from injection	Not supported in AALM.FOR	NA
CILIAR	unitless	C	F	Fraction of inhaled Pb transferred to gastrointestinal tract	0.04	(Leggett, 1993; Wells et al., 1977; Hursh et al., 1969)
DELT0	day	C	F	Starting value for numerical integration time step	0.25	Chapter 3
DELTi	day	A	F	Array of numerical integration time steps if the time step varies in the simulation	0.25	Chapter 3
EAT	µg/day	A	F	Pb ingestion (µg/day) for each exposure time step (*NCHRON*)	User defined in exposure model	NA
EXPAGE	day	C	F	Age at start of the simulation	0 (birth)	Chapter 3
FLONG	unitless	A	F	Fraction of total Pb transfer from the exchangeable bone volume to non-exchangeable bone volume; the fraction of total Pb transfer from the exchangeable bone volume to bone surface (cortical or trabecular) is 1.0-FLONG	0.6	(Leggett, 1993, 1992; Nilsson et al., 1991; Leggett et al., 1982) Also see Chapter 4

Parameter	Unit	Form	Type	Description	Value	Source
H1TOBL	unitless	C	F	Fraction of Pb transfer out of liver compartment 1 that goes to diffusible plasma	0.45	(Leggett, 1993)
H1TOH2	unitless	C	F	Fraction of Pb transfer out of liver compartment 1 that goes to liver compartment 2	0.1	(Leggett, 1993)
H1TOSI	unitless	C	F	Fraction of Pb transfer out of liver compartment 1 that goes to the small intestine	0.45	(Leggett, 1993)
HALF	year	C	F	Age at which body weight is half of *WCHILD*	3	(O'Flaherty, 1995, 1993)
HCTA	unitless	C	F	Adult hematocrit	0.41 (female) 0.46 (male)	(O'Flaherty, 1995, 1993)
IACUTE	unitless	C	I	Switch for acute (1) or chronic array (2) uptakes1	2	NA
ICHEL	unitless	C	I	Switch for chelation simulation off (0) or on (1)	0 chelation option not supported in AALM.FOR	NA
IFETAL	unitless	C	I	Switch for fetal simulation on (1) or off (0)	1	NA
INMODE	unitless	C	I	Switch for injection (0), inhalation (1), ingestion (2), or combination (3)	3	NA
IRBC	unitless	C	I	Switch for linear (0) or non-linear (1) RBC uptake	1	NA
KAPPA	unitless	C	F	Logistic parameter for calculation of body weight (see variable WBODY)	600	(O'Flaherty, 1995, 1993)
LAMBDA	unitless	C	F	Logistic parameter for calculation of body weight (see variable WBODY)	0.017 (female) 0.0095 (male)	(O'Flaherty, 1995, 1993)

Parameter	Unit	Form	Type	Description	Value	Source
NCHRON	unitless	C	I	Number of exposure time steps	Specified by user in exposure model	NA
NCYCLE	unitless	C	I	Number of numerical integration steps for the simulation	Specified by user based on length of simulation and step size	NA
NDELT	unitless	C	I	Number of times the numerical integration time step changes during the simulation	1	NA
NUMAGE	untless	C	I	Number of ages (CHAGE) at which age-dependent parameters are assigned specific values.	1	NA
OUTPUTS	unitless	C	I	Variable identity numbers selected for output.-	Not supported in AALM.FOR	NA
POWER	unitless	C	F	Exponent factor for non-linear expression for RBC deposition.	1.5	(Leggett, 1993)
R1	unitless	C	F	Fraction of inhaled Pb deposited in RT compartment 1	0.08	(Leggett, 1993)
R2	unitless	C	F	Fraction of inhaled Pb deposited in RT compartment 2	0.14	(Leggett, 1993)
R3	unitless	C	F	Fraction of inhaled Pb deposited in RT compartment 3	014	(Leggett, 1993)
R4	unitless	C	F	Fraction of inhaled Pb deposited in RT compartment 4	0.04	(Leggett, 1993)
RBCNL	µg/dL	C	F	Threshold Pb concentration in RBC for non-linear deposition of Pb from diffusible plasma to RBC	20	(Leggett, 1993) Also see Chapter 4
RDECAY	d^{-1}	C	F	Rate coefficient for radioactive decay of unstable Pb isotope	Not supported in AALM.FOR	NA

Parameter	Unit	Form	Type	Description	Value	Source
RDIFF	d^{-1}	C	F	Rate coefficient for Pb transfer from exchangeable bone (cortical or trabecular) volume to surface or non-exchangeable bone volume (see FLONG for fraction to non-exchangeable)	0.0231	(Leggett, 1993)
RKDN1	d^{-1}	C	F	Rate coefficient for transfer from kidney compartment 1 to urinary pathway	0.139	(Leggett, 1993)
RLLI	d^{-1}	C	F	Rate coefficient for Pb transfer from lower large intestine to feces	1	(Leggett, 1993)
RLVR1	d^{-1}	C	F	Rate coefficient for Pb transfer from liver compartment 1 to small intestine or diffusible plasma	0.0693	(Leggett, 1993)
RPLAS	d^{-1}	C	F	Rate coefficient for Pb transfer from diffusible plasma to all compartments, scaled to bone surface deposition	2000	(Leggett, 1993)
RPROT	d^{-1}	C	F	Rate coefficient for Pb transfer from bound plasma to diffusible plasma	0.139	(Leggett, 1993)
RSIC	d^{-1}	C	F	Rate coefficient for Pb transfer from small intestine to upper large intestine	6	(Leggett, 1993)
RSOF0	d^{-1}	C	F	Rate coefficient for Pb transfer from soft tissues with fast Pb clearance to diffusible plasma	2.079	(Leggett, 1993)
RSOF1	d^{-1}	C	F	Rate coefficient for Pb transfer from soft tissues with medium Pb clearance to diffusible plasma	0.00693	(Leggett, 1993)

Parameter	Unit	Form	Type	Description	Value	Source
RSOF2	d^{-1}	C	F	Rate coefficient for Pb transfer from soft tissues with slow Pb clearance to diffusible plasma	0.00038	(Leggett, 1993)
RSTMC	d^{-1}	C	F	Rate coefficient for Pb transfer from stomach to small intestine	24	(Leggett, 1993)
RULI	d^{-1}	C	F	Rate coefficient for Pb transfer from upper large intestine to lower large intestine	1.85	(Leggett, 1993)
S2HAIR	unitless	C	F	Fraction of Pb transfer from intermediate soft tissue to hair, nails, and desquamated skin	0.4	(Leggett, 1993)
SATRAT	$\mu g\ dL^{-1}$	C	F	Maximum (saturating) concentration of Pb in RBC	350	(Leggett, 1993)
SIZEVF	unitless	C	F	Relative volume of the EVF compartment compared to plasma (EVF/Plasma)	3	(Leggett, 1993)
TOEVF	unitless	C	F	Deposition fraction for Pb from diffusible plasma to extravascular fluid	0.5	(Leggett, 1993)
TOFECE	unitless	C	F	Deposition fraction for Pb from diffusible plasma directly to the small intestine (not including the transfer from biliary secretion, specified by *RLVR1*) not scaled to bone surface deposition	0.006	(Leggett, 1993)
TOKDN1	unitless	C	F	Deposition fraction for Pb from diffusible plasma to kidney compartment 1, not scaled to bone surface deposition	0.02	(Leggett, 1993)

Parameter	Unit	Form	Type	Description	Value	Source
TOKDN2	unitless	C	F	Deposition fraction for Pb from diffusible plasma to kidney compartment 2, not scaled to bone surface deposition	0.0002	(Leggett, 1993)
TOLVR1	unitless	C	F	Deposition fraction for Pb from diffusible plasma to liver compartment 2, not scaled to bone surface deposition	0.04	(Leggett, 1993)
TOPROT	unitless	C	F	Deposition fraction for Pb from diffusible plasma to protein-bound plasma, not scaled to bone surface deposition	0.0004	(Leggett, 1993)
TORBC	unitless	C	F	Deposition fraction from diffusible plasma to RBC, not scaled to bone surface deposition	0.24	(Leggett, 1993)
TOSWET	–	C	F	Deposition fraction for Pb from diffusible plasma to sweat not scaled to bone surface deposition, not scaled to bone surface deposition	0.0035	(Leggett, 1993)
TOURIN	–	C	F	Deposition fraction for Pb from diffusible plasma to urine, not scaled to bone surface deposition	0.015	(Leggett, 1993) Also see Chapter 4
VBLC	unitless	C	F	Blood volume fraction of body weight.	0.067	(O'Flaherty, 1995, 1993)
VKC	unitless	C	F	Kidney volume fraction of body weight.	0.0085	(O'Flaherty, 1995, 1993)
VLC	unitless	C	F	Liver volume fraction of body weight.	0.025	(O'Flaherty, 1995, 1993)
VLUC	unitless	C	F	Lung volume fraction of body weight.	0.015	(O'Flaherty, 1995, 1993)

Parameter	Unit	Form	Type	Description	Value	Source
WADULT	kg	C	F	Adult maximum weight used in calculation of body weight growth (see variable WBODY)	34 (female) 50 (male)	(O'Flaherty, 1995, 1993)
WBIRTH	kg	C	F	Weight at birth used in calculation of body weight growth (see variable WBODY)	3.5	(O'Flaherty, 1995, 1993)
WCHILD	kg	C	F	Maximum body weight achieved during early hyperbolic growth phase, used in calculation of body weight growth (see variable *WBODY)*	22 (female) 23 (male)	(O'Flaherty, 1995, 1993)

1 A, array; C, constant; F, floating point, I, integer, NA, not applicable.

APPENDIX D REFERENCES

Alexander, FW; Clayton, BE; Delves, HT. (1974). Mineral and trace-metal balances in children receiving normal and synthetic diets. Q J Med 43: 89-111.

Amaral, JH; Rezende, VB; Quintana, SM; Gerlach, RF; Barbosa, F, Jr; Tanus-Santos, JE. (2010). The relationship between blood and serum lead levels in peripartum women and their respective umbilical cords. Basic Clin Pharmacol Toxicol 107: 971-975. http://dx.doi.org/10.1111/j.1742-7843.2010.00616.x

Araki, S; Aono, H; Yokoyama, K; Murata, K. (1986). Filterable plasma concentration, glomerular filtration, tubular balance, and renal clearance of heavy metals and organic substances in metal workers. Arch Environ Occup Health 41: 216-221. http://dx.doi.org/10.1080/00039896.1986.9938336

Baeyens, W; Vrijens, J, an; Gao, Y, ue; Croes, K, im; Schoeters, G; Den Hond, E; Sioen, I; Bruckers, L; Nawrot, T, im; Nelen, V; Van Den Mieroop, E, ls; Morrens, B; Loots, I; Van Larebeke, N; Leermakers, M. (2014). Trace metals in blood and urine of newborn/mother pairs, adolescents and adults of the Flemish population (2007-2011). Int J Hyg Environ Health 217: 878-890. http://dx.doi.org/10.1016/j.ijheh.2014.06.007

Baranowska-Bosiacka, I; Listos, J; Gutowska, I; Machoy-Mokrzyńska, A; Kolasa-Wołosiuk, A; Tarnowski, M; Puchałowicz, K; Prokopowicz, A; Talarek, S; Listos, P; Wąsik, A; Chlubek, D. (2016). Effects of perinatal exposure to lead (Pb) on purine receptor expression in the brain and gliosis in rats tolerant to morphine analgesia. Toxicology 339: 19-33. http://dx.doi.org/10.1016/j.tox.2015.10.003

Barry, PSI. (1975). A comparison of concentrations of lead in human tissues. Occup Environ Med 32: 119-139.

Bergdahl, IA; Schutz, A; Gerhardsson, L; Jensen, A; Skerfving, S. (1997). Lead concentrations in human plasma, urine and whole blood. Scand J Work Environ Health 23: 359-363.

Bergdahl, IA; Sheveleva, M; Schutz, A; Artamonova, VG; Skerfving, S. (1998). Plasma and blood lead in humans: Capacity-limited binding to delta-aminolevulinic acid dehydratase and other lead-binding components. Toxicol Sci 46: 247-253. http://dx.doi.org/10.1093/toxsci/46.2.247

Bergdahl, IA; Vahter, M; Counter, SA; Schutz, A; Buchanan, LH; Ortega, F; Laurell, G; Skerfving, S. (1999). Lead in plasma and whole blood from lead-exposed children. Environ Res 80: 25-33. http://dx.doi.org/10.1006/enrs.1998.3880

Booker, DV; Chamberlain, AC; Newton, D; Stott, ANB. (1969). Uptake of radioactive lead following inhalation and injection. Br J Radiol 42: 457-466. http://dx.doi.org/10.1259/0007-1285-42-498-457

Campbell, BC; Meredith, PA; Moore, MR; Watson, WS. (1984). Kinetics of lead following intravenous administration in man. Toxicol Lett 21: 231-235.

Carbone, R; Laforgia, N; Crollo, E; Mautone, A; Iolascon, A. (1998). Maternal and neonatal lead exposure in southern Italy. Neonatology 73: 362-366. http://dx.doi.org/10.1159/000013998

Chamberlain, AC. (1985). Prediction of response of blood lead to airborne and dietary lead from volunteer experiments with lead isotopes. 224: 149-182. http://dx.doi.org/10.1098/rspb.1985.0027

Chamberlain, AC; Heard, MJ; Little, P; Newton, D; Wells, AC; Wiffin, RD. (1978). Investigations into lead from motor vehicles. (AERE-R9198). Berkshire, England: Transportation and Road Research Laboratory.

Chen, Z; Myers, R; Wei, T; Bind, E; Kassim, P; Wang, G; Ji, Y; Hong, X; Caruso, D; Bartell, T; Gong, Y; Strickland, P; Navas-Acien, A; Guallar, E; Wang, X. (2014). Placental transfer and concentrations of cadmium, mercury, lead, and selenium in mothers, newborns, and young children. J Expo Sci Environ Epidemiol 24: 537-544. http://dx.doi.org/10.1038/jes.2014.26

Cohen, N; Eisenbud, M; Wrenn, ME. (1970). Radioactivity studies. Volume I. The retention and distribution of 210Pb in the adult baboon. Annual progress report, September 1, 1969-August 31, 1970. (AT(30-1)-3086). New York: New York University Medical Center.

Cooper, WC; Tabershaw, IR; Nelson, KW. (1973). Laboratory studies of workers in lead smelting and refining.

Corazziari, E; Cucchiara, S; Staiano, A; Romaniello, G; Tamburrini, O; Torsoli, A; Auricchio, S. (1985). Gastrointestinal transit time, frequency of defecation, and anorectal manometry in healthy and constipated children. J Pediatr 106: 379-382.

DeSilva, PE. (1981). Determination of lead in plasma and studies on its relationship to lead in erythrocytes. Br J Ind Med 38: 209-217.

Goyer, RA. (1990). Transplacental transport of lead [Review]. Environ Health Perspect 89: 101-105. http://dx.doi.org/10.2307/3430905

Grandjean, P. (1978). Regional distribution of lead in human brains. Toxicol Lett 2: 65-69. http://dx.doi.org/10.1016/0378-4274(78)90065-6

Graziano, JH; Popovac, D; Factor-Litvak, P; Shrout, P; Kline, J; Murphy, MJ; Zhao, YH; Mehmeti, A; Ahmedi, X; Rajovic, B; Zvicer, Z; Nenezic, DU; Lolacono, NJ; Stein, Z. (1990). Determinants of elevated blood lead during pregnancy in a population surrounding a lead smelter in Kosovo, Yugoslavia. Environ Health Perspect 89: 95-100. http://dx.doi.org/10.1289/ehp.908995

Gregus, Z; Klaassen, CD. (1986). Disposition of metals in rats: a comparative study of fecal, urinary, and biliary excretion and tissue distribution of eighteen metals. Toxicol Appl Pharmacol 85: 24-38. http://dx.doi.org/10.1016/0041-008X(86)90384-4

Gulson, B; Mizon, K; Korsch, M; Taylor, A. (2016). Revisiting mobilisation of skeletal lead during pregnancy based on monthly sampling and cord/maternal blood lead relationships confirm placental transfer of lead. Arch Toxicol 90: 805-816. http://dx.doi.org/10.1007/s00204-015-1515-8

Heard, MJ; Chamberlain, AC. (1984). Uptake of Pb by human skeleton and comparative metabolism of Pb and alkaline earth elements. Health Phys 47: 857-865.

Hernandez-Avila, M; Smith, D; Meneses, F; Sanin, LH; Hu, H. (1998). The influence of bone and blood lead on plasma lead levels in environmentally exposed adults. Environ Health Perspect 106: 473-477. http://dx.doi.org/10.1289/ehp.98106473

Hursh, JB; Mercer, TT. (1970). Measurement of 212Pb loss rate from human lungs. J Appl Physiol (1985) 28: 268-274. http://dx.doi.org/10.1152/jappl.1970.28.3.268

Hursh, JB; Schraub, A; Sattler, EL; Hofmann, HP. (1969). Fate of 212Pb inhaled by human subjects. Health Phys 16: 257-267.

Hursh, JB; Suomela, J. (1968). Absorption of 212Pb from the gastrointestinal tract of man. Acta Radiol 7: 108-120. http://dx.doi.org/10.3109/02841866809133184

ICRP (International Commission on Radiological Protection). (1975). Report of the task group on reference man. Oxford, UK: Pergamon Press. http://ani.sagepub.com/site/includefiles/icrp_publications_collection.xhtml

ICRP (International Commission on Radiological Protection). (1979). Limits for intakes of radionuclides by workers: Part 1. Oxford, United Kingdom: Pergamon Press.

ICRP (International Commission on Radiological Protection). (1990). Age-dependent doses to members of the public from intake of radionuclides: Part 1. (ICRP Publication 56). Oxford, UK: Pergamon.

Iyengar, V; Woittiez, J. (1988). Trace Elements in Human Clinical Specimens: Evaluation of Literature Data to Identify Reference Values [Review]. Clin Chem 34: 474-481.

Kayaalti, Z; Kaya-Akyüzlü, D; Söylemez, E; Söylemezoğlu, T. (2015). Maternal hemochromatosis gene H63D single-nucleotide polymorphism and lead levels of placental tissue, maternal and umbilical cord blood. Environ Res 140: 456-461. http://dx.doi.org/10.1016/j.envres.2015.05.004

Kazi, TG; Shah, F; Shaikh, HR; Afridi, HI; Shah, A; Naeemullah, A; Arain, SS. (2014). Exposure of lead to mothers and their new born infants, residents of industrial and domestic areas of Pakistan. Environ Sci Pollut Res Int 21: 3021-3030. http://dx.doi.org/10.1007/s11356-013-2223-7

Kim, YM; Chung, JY; An, HS; Park, SY; Kim, BG; Bae, JW; Han, M; Cho, YJ; Hong, YS. (2015). Biomonitoring of Lead, Cadmium, Total Mercury, and Methylmercury Levels in Maternal Blood and in Umbilical Cord Blood at Birth in South Korea. Int J Environ Res Public Health 12: 13482-13493. http://dx.doi.org/10.3390/ijerph121013482

Kordas, K; Ettinger, AS; Lamadrid-Figueroa, H; Tellez-Rojo, MM; Hernandez-Avila, M; Hu, H; Wright, RO. (2009). Methylenetetrahydrofolate reductase (MTHFR) C677T, A1298C and G1793A genotypes, and the relationship between maternal folate intake, tibia lead and infant size at birth. Br J Nutr 102: 907-914. http://dx.doi.org/10.1017/s0007114509318280

Leggett, RW. (1992). A generic age-specific biokinetic model for calcium-like elements. Radiat Prot Dosimetry 41: 183-198.

Leggett, RW. (1993). An age-specific kinetic model of lead metabolism in humans [Review]. Environ Health Perspect 101: 598-616. http://dx.doi.org/10.1289/ehp.93101598

Leggett, RW; Eckerman, KF; Williams, LR. (1982). Strontium-90 in bone: a case study in age-dependent dosimetric modeling. Health Phys 43: 307-322.

Lloyd, RD; Mays, CW; Atherton, DR; Bruenger, FW. (1970). Distribution and retention of Pb-210 in the beagle. In Retention and dosimetry of some injected radionuclides in beagles (pp. 105-177). (COO-241). Salt Lake City, UT: University of Utah College of Medicine.

Lloyd, RD; Mays, CW; Atherton, DR; Bruenger, FW. (1975). 210Pb studies in beagles. Health Phys 28: 575-583. http://dx.doi.org/10.1097/00004032-197505000-00011

Maddaloni, M; Ballew, M; Diamond, G; Follansbee, M; Gefell, D; Goodrum, P; Johnson, M; Koporec, K; Khoury, G; Luey, J; Odin, M; Troast, R; Van Leeuwen, P; Zaragoza, L. (2005). Assessing lead risks at non-residential hazardous waste sites. Hum Ecol Risk Assess 11: 967-1003. http://dx.doi.org/10.1080/10807030500257838

Manton, WI; Cook, JD. (1984). High accuracy (stable isotope dilution) measurements of lead in serum and cerebrospinal fluid. Occup Environ Med 41: 313-319. http://dx.doi.org/10.1136/oem.41.3.313

Manton, WI; Malloy, CR. (1983). Distribution of lead in body fluids after ingestion of soft solder. Occup Environ Med 40: 51-57. http://dx.doi.org/10.1136/oem.40.1.51

Manton, WI; Rothenberg, SJ; Manalo, M. (2001). The lead content of blood serum. Environ Res 86: 263-273. http://dx.doi.org/10.1006/enrs.2001.4271

Minoia, C; Sabbioni, E; Apostoli, P; Pietra, R; Pozzoli, L; Gallorini, M; Nicolaou, G; Alessio, L; Capodaglio, E. (1990). Trace element reference values in tissues from inhabitants of the European Community I A study of 46 elements in urine, blood and serum of Italian subjects. Sci Total Environ 95: 89-105.

Nilsson, U; Attewell, R; Christoffersson, JO; Schutz, A; Ahlgren, L; Skerfving, S; Mattsson, S. (1991). Kinetics of lead in bone and blood after end of occupational exposure. Basic Clin Pharmacol Toxicol 68: 477-484.

Niyogi, SK. (1974). Tissue distribution of lead in cases of poisoning in children. Forensic Sci 3: 199-202.

O'Flaherty, EJ. (1993). Physiologically based models for bone-seeking elements: IV. Kinetics of lead disposition in humans. Toxicol Appl Pharmacol 118: 16-29. http://dx.doi.org/10.1006/taap.1993.1004

O'Flaherty, EJ. (1995). Physiologically based models for bone-seeking elements: V. Lead absorption and disposition in childhood [Review]. Toxicol Appl Pharmacol 131: 297-308. http://dx.doi.org/10.1006/taap.1995.1072

Orten, JM; Neuhaus, OW. (1982). Human biochemistry (10th ed.). London, UK: Mosby.

Patel, AB; Prabhu, AS. (2009). Determinants of lead level in umbilical cord blood. Indian Pediatr 46: 791-793.

Potter, GD; Mcintyre, DR; Vattuone, GM. (1971). The fate and implications of 203 Pb ingestion in a dairy cow and a calf. Health Phys 20: 650-653.
Rabinowitz, MB; Wetherill, GW; Kopple, JD. (1976). Kinetic analysis of lead metabolism in healthy humans. J Clin Invest 58: 260-270. http://dx.doi.org/10.1172/JCI108467
Reddy, YS; Y, A; Ramalaksmi, BA; Kumar, BD. (2014). Lead and trace element levels in placenta, maternal and cord blood: a cross-sectional pilot study. Journal of Obstetrics and Gynaecology Research (Online) 40: 2184-2190. http://dx.doi.org/10.1111/jog.12469
Ryu, JE; Ziegler, EE; Nelson, SE; Fomon, SJ. (1983). Dietary intake of lead and blood lead concentration in early infancy. Am J Dis Child 137: 886-891.
Schutz, A; Bergdahl, IA; Ekholm, A; Skerfving, S. (1996). Measurement by ICP-MS of lead in plasma and whole blood of lead workers and controls. Occup Environ Med 53: 736-740. http://dx.doi.org/10.1136/oem.53.11.736
Schütz, A; Skerfving, S. (1976). Effect of a short, heavy exposure to lead dust upon blood lead level, erythrocyte delta-aminolevulinic acid dehydratase activity and urinary excretion of lead delta-aminolevulinic acid coproporphyrin. Results of a 6-month follow-up of two male subjects. Scand J Work Environ Health 2: 176-184.
Sherlock, JC; Quinn, MJ. (1986). Relationship between blood and lead concentrations and dietary lead intake in infants: The Glasgow Duplicate Diet Study 1979-1980. Food Addit Contam 3: 167-176. http://dx.doi.org/10.1080/02652038609373579
Skerfving, S; Ahlgren, L; Christoffersson, JO; Haeger-Aronson, B; Mattsson, S; Schutz, A; Lindberg, G. (1985). Metabolism of inorganic lead in man. Adv Food Nutr Res 1: 601-607.
Smith, D; Hernandez-Avila, M; Tellez-Rojo, MM; Mercado, A; Hu, H. (2002). The relationship between lead in plasma and whole blood in women. Environ Health Perspect 110: 263-268. http://dx.doi.org/10.1289/ehp.02110263
Somervaille, LJ; Chettle, DR; Scott, MC; Tennant, DR; Mckiernan, MJ; Skilbeck, A; Trethowan, WN. (1988). In vivo tibia lead measurements as an index of cumulative exposure in occupationally exposed subjects. Occup Environ Med 45: 174-181.
Stover, BJ. (1959). Pb212 (ThB) tracer studies in adult beagle dogs. Proc Soc Exp Biol Med 100: 269-272. http://dx.doi.org/10.3181/00379727-100-24596
U.S. EPA (U.S. Environmental Protection Agency). (2003). Recommendations of the Technical Review Workgroup for Lead for an approach to assessing risks associated with adult exposures to lead in soil [EPA Report]. (EPA-540-R-03-001). Washington, DC. https://semspub.epa.gov/work/HQ/174559.pdf
U.S. EPA (U.S. Environmental Protection Agency). (2017). Transmittal of update to the adult lead methodology's default baseline blood lead concentration and geometric standard deviation. OLEM directive 9285: 6–56.
Victery, W; Vander, AJ; Mouw, DR. (1979). Renal handling of lead in dogs: stop-flow analysis. Am J Physiol 237: F408-F414. http://dx.doi.org/10.1152/ajprenal.1979.237.5.F408
Wells, AC; Venn, JB; Heard, MJ. (1977). Deposition in the lung and uptake to blood of motor exhaust labelled with 203Pb. In WH Walton; B McGovern (Eds.), Inhaled particles IV: Proceedings of an international symposium organized by the British Occupational Hygiene Society: Part 1 (pp. 175-189). Oxford, UK: Pergamon.
Ziegler, EE; Edwards, BB; Jensen, RL; Mahaffey, KR; Fomon, SJ. (1978). Absorption and retention of lead by infants. Pediatr Res 12: 29-34. http://dx.doi.org/10.1203/00006450-197801000-00008